Natural braneworlds in six dimensions and the cosmological constant problem

Florian Niedermann

München 2016

Natural braneworlds in six dimensions and the cosmological constant problem

Florian Niedermann

Dissertation
an der Fakultät für Physik
der Ludwig–Maximilians–Universität
München

vorgelegt von
Florian Niedermann
aus Überlingen

München, den 23.03.2016

Erstgutachter: Prof. Dr. Stefan Hofmann
Zweitgutachter: Prof. Dr. Georgi Dvali
Tag der mündlichen Prüfung: 09.05.2016

Table of contents

Zusammenfassung

Die beobachtete beschleunigte Ausdehnung unseres Universums kann erfolgreich durch eine kosmologische Konstante beschrieben werden. Da dieser Parameter der Einstein-Gleichungen nicht vor Quantenkorrekturen geschützt ist, weichen der gemessene und der theoretisch erwartbare Wert stark voneinander ab. Diese Beobachtung gibt Anlass zum Problem der kosmologischen Konstante. Diese Arbeit verfolgt den Ansatz, das Problem durch eine Einbettung unseres Universums, repräsentiert durch eine *Brane*, in eine sechsdimensionale Raumzeit, den *Bulk*, zu adressieren. Hierbei übernimmt die kosmologische Konstante die Rolle einer Branenspannung, die keine Ausdehnung der drei sichtbaren räumlichen Richtungen zur Folge haben muss; vielmehr führt sie zu einer Krümmung des extradimensionalen Raumes und ist folglich unsichtbar für einen Branenbeobachter. In diesem Zusammenhang lautet die entscheidende Frage, ob dieser sogenannte Degravitationsmechanismus auf eine phänomenologisch verträgliche und im 't Hooft-Sinne natürliche Weise eingeführt werden kann. Eine entsprechende Antwort wird im Falle von vier verschiedenen Modellen gegeben werden.

Der Hauptteil der Arbeit befasst sich mit dem 6D "brane induced gravity"-Modell, das eine Verallgemeinerung des Dvali-Gabadadze-Porrati-Modells darstellt. Hier verformt eine Brane mit subkritischer Spannung den Bulk zu einem unendlich ausgedehnten Kegel. Zu Beginn wird gezeigt, dass das Modell nur dann keine Geistinstabilitäten aufweist, wenn die Branenspannung nicht unnatürlich klein ist. Dieses Resultat eröffnet neue Möglichkeiten, theoretisch konsistente und gleichzeitig modifizierte Kosmologien zu untersuchen. Nachfolgend wird aufgezeigt, dass eine homogene und isotrope Brane als eine Antenne agiert, die zylindrisch symmetrische Einstein-Rosen-Wellen aussendet und absorbiert. Zwei interessante Lösungstypen werden hergeleitet – subkritische, die eine dynamische Form von Degravitation aufweisen aber nicht vereinbar mit Beobachtungen sind, sowie superkritische, die zwar phänomenologisch verträglich sein können aber nicht technisch natürlich sind. Während dies klar zeigt, dass das Problem der kosmologischen Konstante nicht in einer 6D Variante des Modells gelöst werden kann, deuten unsere Resultate auf höherdimensionale Konstruktionen als die verbleibende Spielwiese hin.

Anschließend wird ein neues Zwei-Branen-Modell eingeführt. Hier verformt eine dicke, superkritische Brane den extradimensionalen Raum zu einer Zigarre, die ihrerseits in einer mikroskopisch dünnen, subkritischen Brane, die unser Universum repräsentiert, endet. Falls beide Branen nur eine Spannung aber keine anderen lokalisierten Materieformen aufweisen, können vollständig analytische Lösungen abgeleitet werden, die phänomenologisch vielversprechend sind, weil sie einem de-Sitter-Universum auf der Brane entsprechen. Da hierzu leider eine Feinjustierung der Branenspannung erforderlich ist, entspricht dies keiner technisch natürlichen Konfiguration. Dieser Misserfolg kann mit der Kompaktheit der

Extradimension in Verbindung gebracht werden.

Um die Vorzüge unendlich großer Extradimensionen aufzuzeigen, wird ein Hybridmodell entwickelt, dem zufolge die Brane um einen unendlich langen und mikroskopisch dünnen Zylinder gewickelt wird. Es zeigt sich, dass diese Konstruktion dem minimalen Aufbau entspricht, der Gravitationswellen im Bulk als ein dynamisches Element einer modifizierten Kosmologie aufweist. Es wird gezeigt, dass das System aufgrund der Existenz einer unendlichen Extradimension eine degravitierende Attraktorlösung zulässt. Die zugehörige 4D Kosmologie ist zwar konzeptionell interessant, aber ein Supernovafit zeigt, dass unser Universum nicht durch sie beschrieben werden kann.

Zuletzt wird das "supersymmetric large extra dimensions"-Modell betrachtet. Von diesem wurde behauptet, dass es das Problem der kosmologischen Konstante erfolgreich adressiert. Hier stabilisiert ein Maxwell-Fluss den extradimensionalen Raum, der die Form eines Rugbyballes hat. Der Mechanismus wird hier genau durchleuchtet, wobei sich zeigt, dass eine verschwindende Branenkrümmung – wie sie für Degravitation benötigt wird – nur dann gewährleistet ist, wenn der Branensektor skaleninvariant ist. Dies jedoch führt aufgrund einer Flussquantisierungsbedingung zu einer unvermeidlichen Feinjustierung der Modellparameter. Anschließend wird die Analyse auf eine Lösungsklasse, die eine de-Sitter-Geometrie auf der Brane zulässt, ausgedehnt. Vorausgesetzt die Modellparameter sind generisch gewählt, ergibt sich entweder ein Extradimensionsvolumen oder eine Branenkrümmung, die die phänomenologischen Schranken um viele Größenordnungen übersteigt.

Unsere Resultate schränken die Suche nach einer Extradimensionslösung des Problems der kosmologischen Konstante maßgeblich ein. Insbesondere weisen Modelle mit unendlich großen Extradimensionen einen funktionsfähigen Mechanismus auf, der allerdings verbessert werden muss, um mit Beobachtungen verträglich zu sein.

Abstract

The observed accelerated expansion of the universe is successfully parameterized by a cosmological constant. However, since this parameter in Einstein's equations is not protected against quantum corrections, the observed and theoretically expected value vastly differ, thus giving rise to the cosmological constant problem. In this thesis, the issue is addressed by embedding our universe—represented by a brane—in a six-dimensional bulk spacetime, where the cosmological constant plays the role of a brane tension, which then no longer needs to imply an expansion of the three apparent spatial dimensions; rather, it curves the extra space and hence stays hidden from a brane observer. In this context, the crucial question is whether this so-called degravitation mechanism may be implemented in a phenomenologically viable *and* 't Hooft natural way. Corresponding answers will be given in the case of four different models.

The main part of this thesis has its focus on the 6D brane induced gravity model—a higher-dimensional generalization of the Dvali-Gabadadze-Porrati model—according to which a brane with sub-critical tension curves the bulk into a cone of infinite spatial extent. First, it is shown that the model is free of ghost instabilities only if the tension is not unnaturally small. This in turn opens a window of opportunity to study theoretically consistent modified cosmologies. In this context, it is shown that a homogeneous and isotropic brane acts as an antenna that emits and absorbs cylindrically symmetric Einstein-Rosen waves. We encounter two interesting types of solutions—sub-critical ones, which feature dynamical degravitation but are incompatible with observations, as well as compact super-critical ones, which still might be phenomenologically viable but certainly not technically natural. While this clearly shows that the cosmological constant problem cannot be solved in a 6D version of the model, our results point towards higher-dimensional constructions as the remaining playground for future research.

Next, we introduce a new two-brane model where a thick super-critical brane curves the extra space into a cigar that closes in a microscopically thin sub-critical brane, representing our universe. In the case both branes only host a tension, we derive fully analytic solutions, which correspond to a de Sitter phase on our brane and are hence phenomenologically promising. Unfortunately, as a fine-tuning of the brane tension is required, they are not technically natural. The failure is attributed to the compactness of the extra space.

To further exemplify the virtue of infinite volume extra dimensions, we devise a hybrid model where the brane is wrapped around an infinitely long cylinder of microscopic width. This construction turns out to be the minimal setup that features bulk waves as a dynamical ingredient of a modified cosmology. We find that, due to the existence of an infinitely large dimension, the system admits a degravitating solution. While being conceptually interesting, a supernova fit shows that the corresponding 4D cosmology cannot describe

our universe.

Finally, we turn to the model of supersymmetric large extra dimensions that had been claimed to successfully address the cosmological constant problem. Here, a Maxwell flux stabilizes the extra space that has the shape of a rugby ball. We critically review the corresponding mechanism, and find that a vanishing brane curvature—as required by the degravitation idea—is only ensured by a scale invariant brane sector, which however leads to an unavoidable parameter constraint due to a flux quantization condition. In a second step, we generalize our analysis to solutions that admit a de Sitter phase on the brane. Provided the model parameters are not tuned, we find that either the brane curvature or the volume of the extra space exceeds its phenomenological bound by many orders of magnitude.

Our results significantly narrow down the search for solutions of the cosmological constant problem in the realm of extra-dimensional scenarios. In particular, models with infinite volume extra dimensions are found to offer a working mechanism, which yet requires refinement to comply with the observational bounds.

Acronyms

We make frequent use of the following acronyms:

BIG	Brane induced gravity
BLF	Brane localized flux
CC	Cosmological constant
DGP	Dvali-Gabadadze-Porrati
DOF	Degree of freedom
EFT	Effective field theory
ER	Einstein-Rosen
FLRW	Friedmann-Lemaître-Robertson-Walker
EMT	Energy momentum tensor
FQC	Flux quantization condition
GGP	Gibbons-Gueven-Pope
GR	General relativity
IR	Infrared
KK	Kaluza-Klein
ΛCDM	Λ cold dark matter
LED	Large extra dimensions
NEC	Null energy condition
ODE	Ordinary differential equation
PDE	Partial differential equation
SI	Scale invariance
SLED	Supersymmetric large extra dimensions
SM	Standard Model
UV	Ultraviolet

Conventions

The following conventions are employed throughout this thesis (if not stated otherwise):

- We work in units in which $\hbar = c = 1$.
- The bulk spacetime dimension is denoted by D, and the brane dimension by d. We define $n := D - 4$ as the codimension with respect to a three-brane.
- Tensor fields, if not represented in a specific coordinate basis, are written in boldface, e.g. $\boldsymbol{g}$ for the 4D metric.
- The metric signature is mostly plus, i.e. the four-dimensional Minkowski metric reads $\boldsymbol{\eta} := \mathrm{diag}(-1, 1, 1, 1)$.
- Dimensional subscripts and superscripts are usually omitted in 4D, e.g. $\boldsymbol{g}$ instead of $\boldsymbol{g}_4$.
- We denote the D-dimensional Planck mass with M_D. In 4D we use the conventional notation $M_{\mathrm{Pl}} := M_4$.
- Bulk and 4D brane coordinates are denoted by X^A and x^μ, respectively. Induced coordinates on branes with dimension $d > 4$ are denoted by $\tilde{x}^\alpha$, see Tab. 1 for the corresponding index ranges.
- The Einstein-Hilbert action in D spacetime dimensions reads

$$\mathcal{S}^{(D)}_{\mathrm{EH}}[\boldsymbol{g}_D] := \frac{M_D^{D-2}}{2} \int \mathrm{d}^D X \, \sqrt{-g_D} \, \mathcal{R}_D \,, \tag{C1}$$

  where g_D is the determinant of the metric $\boldsymbol{g}_D$.

$A, B, \ldots$	0, 1, 2, 3, 5, 6 …, D
$a, b, \ldots$	5, 6, …, D
$\alpha, \beta, \gamma, \delta$	0, 1, 2, 3, 5, 6, …, d
μ, ν, ρ, σ	0, 1, 2, 3
$i, j, \ldots$	1, 2, 3

Table 1: Index ranges. Deviations, if they occur due to specific coordinate choices, are specified in the respective chapter.

- The 4D energy momentum tensor is defined as

$$T_{\mu\nu} := -\frac{2}{\sqrt{-g}} \frac{\partial \left(\sqrt{-g}\, \mathcal{L}_{\mathrm{m}}\right)}{\partial g^{\mu\nu}} \,. \tag{C2}$$

- The 4D brane tension is denoted by λ and follows from the action

$$\mathcal{S}_{\lambda}[\boldsymbol{g}] := -\lambda \int \mathrm{d}^4x \, \sqrt{-g} \,. \tag{C3}$$

  It is related to the 4D CC via $\lambda = M_{\mathrm{Pl}}^2 \lambda_4$, we also use $\bar{\lambda} := \lambda/(2\pi M_6^4)$.

- For symmetrization we use the convention $\partial_{(i} V_{j)} = \left(\partial_i V_j + \partial_j V_i\right)/2$.

Chapter 1

Introduction

1.1 Overview

General relativity (GR) was developed a century ago [76], and yet its full theoretical and phenomenological richness is still explored with great success. Indeed, the recent detection of gravitational waves is an impressive example of its predictive power and empirical superiority [1]. Let us thus start with its dynamical equations,

$$\mathcal{R}_{\mu\nu} - \frac{1}{2} g_{\mu\nu} \mathcal{R}^{\gamma}{}_{\gamma} + \lambda_4 \, g_{\mu\nu} = \frac{1}{M_{\rm Pl}^2} T_{\mu\nu} \,, \tag{1.1}$$

where the Ricci tensor $\boldsymbol{\mathcal{R}}$ is a function of the metric $\boldsymbol{g}$ and characterizes the curvature of spacetime, generated by the presence of energy and momentum $\boldsymbol{T}$.

Although the phenomenological achievements of GR are indisputable, there is an unsettling theoretical flaw, intimately related to the size of the two dimensionful parameters appearing in (1.1), namely the Planck mass $M_{\rm Pl}$ and the cosmological constant (CC) λ_4. Their respective values are inferred observationally. To be precise, the Planck mass is related to the gravitational constant G via $M_{\rm Pl}^2 \equiv 1/8\pi G$, and hence can be derived by measuring the attraction between to masses.[1] To be specific, $M_{\rm Pl}$ is found to be 15 orders of magnitude larger than the TeV scale, i.e. the typical energy scale of processes described by the electroweak theory. Thus, in contrast to other fundamental scales of the Standard Model (SM), $M_{\rm Pl}$ is astonishingly large.[2] Since the gravitational coupling is proportional to $1/M_{\rm Pl}^2$, this is equivalent to saying that the gravitational interaction is exceptionally weak.

The CC, on the other hand, can be interpreted as a spacetime homogeneous energy density (of size $M_{\rm Pl}^2 \lambda_4$), and as such it leads to a constant curvature affecting the whole of our universe. Specifically, in the absence of other matter components Einstein's equations relate it to a de Sitter geometry, characterized by a (constant) Hubble parameter $H^2 = \lambda_4/3$; physically, it corresponds to the rate at which space expands. In fact, a measurement of today's curvature radius H_0 yields an upper bound on λ_4 (spatial curvature is assumed

[1] Typically, Cavendish is credited with the first accurate (to about 1 %) measurement of G over two centuries ago [39].

[2] That discrepancy gives rise to the electroweak hierarchy problem.

to be sub-dominant),[3]

$$\frac{\lambda_4}{M_{\rm Pl}^2} \lesssim \frac{H_0^2}{M_{\rm Pl}^2} \sim 10^{-120}\,, \tag{1.2}$$

Note that it is only recently, due to significant advances in observational cosmology, that it became possible to measure the value of λ_4, showing that it contributes about 70 % to the energy budget of our universe;[4] hence, the bound is even saturated.[5] In summary, Einstein's equations are governed by two parameters that are separated by ~ 120 orders of magnitude. While $M_{\rm Pl}$ represents the UV energy scale at which a classical description of gravity certainly ceases to exist, λ_4 is linked to the size of our observable universe, and hence represents an extreme IR energy scale. This rather simple observation sets the stage for this thesis.

From a purely classical perspective, the hierarchy between $M_{\rm Pl}$ and λ_4, even though unexpected, does not pose any conceptual problem. To put it differently, as long as all observations are described consistently, there is no need to question the correctness of (1.1). However, once we turn on quantum mechanics, the situation changes dramatically and we arrive at a famous puzzle: Since standard model (SM) particles contribute to $M_{\rm Pl}^2\lambda_4$ via quantum loops, we expect (renormalized) contributions to be of order of the heaviest known particle masses, i.e. of order TeV.

How is it then possible that λ_4 is off by ~ 60 orders of magnitude?

This reasoning is based on a theoretical bias demanding parameter values like the CC to arise generically, i.e. without imposing any sort of tuning. This so-called *cosmological constant problem* is one of the major quantum puzzles arising from Einstein's equations. Although the problem was formulated only shortly after the discovery of (1.1), we still lack a comprehensive answer. We will discuss its origin and significance extensively in Sec. 1.2. Here, let us start by sketching a specific direction towards its resolution.

In principle, there are two ways of addressing the problem. First, we may ask whether there is a way of avoiding quantum contributions to λ_4 in the first place. This, for example, can be achieved by introducing a new symmetry like supersymmetry.[6] Second, we may accept the existence of huge quantum corrections and try to deal with its effects. This thesis has its focus on the second approach.

The CC problem is a direct consequence of Einstein's equations, which—due to the equivalence principle—are sensitive to every type of energy. In other words, provided

[3] Back in 1929, Hubble obtained a first estimate for H_0 [99] (still too large by almost an order of magnitude).

[4] Among different probes, let us explicitly refer to recent supernova and CMB observations [109, 2]. This sector of the budget is normally referred to as "dark energy"—a reference to its unclear physical origin.

[5] This assumes that "dark energy" is exclusively described by a CC; instead, it might also be explained by new physics. However, note that for the CC problem (as we phrase it) to arise, the existence of an upper bound is sufficient.

[6] We will see that resolving the problem would demand supersymmetry to kick in already at the meV scale which is of course unacceptable from a phenomenological point of view.

GR holds without restrictions, a CC has to curve our spacetime. This leads us to the idea that a resolution of the problem may also reside in the gravitational sector. To be precise, by modifying Einstein's equations, we can try to relax the rigid relation between H_0 and λ_4 in such a way that $M_{\rm Pl}^2\lambda_4$ is allowed to be of order TeV even though H_0 is phenomenologically small. In general, there exist two corresponding mechanisms in 4D: First, the *self-tuning* mechanism (cf. [168] for a summary), based on the idea to dynamically cancel the CC by means of additional degrees of freedom, and second, the *degravitation* mechanism, which diminishes the gravitational effect of a CC by effectively promoting G to a high pass filter [12, 70, 50].[7] In the past, both ideas brought forth a plethora of different modifications of GR (for recent reviews see [46, 103, 49]). For several reasons, though, it was soon realized to be a quite difficult endeavor:

1. The theory has to be consistent both classically and quantum mechanically. In particular, it turned out to be notoriously difficult to come up with ghost-free modifications.

2. The model's phenomenology has to compete with the success of GR both on solar system size and cosmological scales.

3. The system has to adapt to changes of the CC—which could for example occur during a phase transition in the early universe—in such a way that the smallness of H_0 is preserved. Accordingly, we look for a dynamical mechanism.

4. The mechanism has to evade a famous no-go theorem by Weinberg [168].

With respect to these issues, braneworld models turned out to be a promising arena. Accordingly, our universe is given by a microscopically thin hypersurface embedded in a higher-dimensional bulk. Then, the CC plays the role of a localized energy density—the brane tension $\lambda := M_{\rm Pl}^2\lambda_4$—and H_0 measures the brane curvature scale. There is a simple geometrical picture explaining the potential of these models with respect to the CC problem [154, 16, 41, 12]:

> *Instead of producing brane curvature, λ_4 curves the extra space directions, and therefore stays hidden from a brane observer.*[8]

In the more recent past two models in 6D were deemed to be particularly promising: The *brane induced gravity model*[9] (BIG) [63, 61, 71, 65, 66] with infinite volume extra dimensions and the model of *supersymmetric large extra dimensions* (SLED) [33, 34, 35] based on two supersymmetric and sub-millimeter sized extra dimensions. In addition to that, we come up with two further extra-dimensional models, one combines a (microscopic)

[7] In this thesis, we will use the term degravitation whenever the gravitational impact of a CC is diminished compared to standard GR.

[8] With regard to the 4D perspective: For infinite volume extra dimensions this corresponds to the degravitation idea, whereas models with finite extra dimensions normally aim for the "self-tuning" mechanism.

[9] The higher-dimensional version of the well-known Dvali-Gabadadze-Porrati (DGP) model in 5D.

compact with an infinite extra dimension, dubbed the *cosmic ring*, and the other one relies on two (large) compact extra dimensions that close in two different branes, dubbed the *cigar model*. Both constructions constitute modifications of the established models in 6D, and hence further exemplify the challenges that need to be overcome when we want to solve the CC problem.

In anticipation of our results, we will be able to significantly constrain all of these models. In particular, we clarify their status with respect to the CC problem and assess their consistency and phenomenological potential. To achieve this, we closely follow the four qualifications stated above and scrutinize their viability. In the course of these investigations, we shed further light on the prospects of extra-dimensional models as a solution to the CC problem. Moreover, we carve out a specific direction in the class of infinite volume models, which we consider particularly promising with respect to future research.

1.2 A quantum puzzle of general relativity

The main motivation for extra-dimensional models is provided by the CC problem. Here, we review the problem in detail with particular focus on the aspect of 't Hooft naturalness. A lot of attempts towards its resolution can be ruled out by virtue of Weinberg's famous no-go theorem [168]. We recapitulate his argument and sketch potential loopholes, which in turn will lead us towards the realm of extra-dimensional models.

To set the stage for our subsequent discussions, we specify the action giving rise to (1.1),

$$\mathcal{S} = \mathcal{S}_{\rm EH}[\boldsymbol{g}] - M_{\rm Pl}^2 \lambda_4 \int \mathrm{d}^4x \, \sqrt{-g} + \mathcal{S}_{\rm m} \,, \tag{1.3}$$

where the first term is the 4D Einstein-Hilbert action, as originally defined in [95, 77] and here in (C1), the second term represents a spacetime homogeneous energy density (or CC equivalently) and the last one describes the matter sector [corresponding to $T_{\mu\nu}$ via (C2)].

1.2.1 The cosmological constant problem

One of the first extensive discussions of the CC problem was provided by Zel'dovich in the late sixties [173, 174].[10] To illustrate the essence of the problem, let us consider the theory (1.3) with $\lambda_4 = 0$ and supplemented with a single (minimally coupled) scalar field ϕ of mass M. First, we ask whether the classical Minkowski vacuum is stable under quantum corrections. To that end, we calculate the one-loop correction $\lambda^{(1)}$ to the (a priori vanishing) CC. Provided it does not vanish after proper renormalization, this contribution is expected to destabilize the classical background, thus leading to a de Sitter (instead of Minkowski)

[10] Awareness of the problem seems to be much older, though: Back in the twenties, Pauli is often credited with the observation that the radius of the universe "nicht einmal bis zum Mond reichen würde " [would not even reach to the moon] if the classical electron radius would set the cutoff in the calculation of the zero-point energy.

vacuum. Its value then gives an estimate of how large a quantum mechanically consistent (or technically natural) CC should be.

Specifically, we use a flat space expansion of the metric, i.e. $\boldsymbol{g} = \boldsymbol{\eta} + \boldsymbol{h}$. This in turn fixes the graviton-scalar interaction vertex, and hence allows us to identify the relevant diagrams, contributing to the quantum effective action:[11]

(1-loop) = 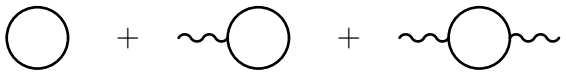 (1.4)

Before calculating them (which can be done by using standard techniques, cf. [37]), we state our expectation: As a consequence of diffeomorphism invariance, we expect them to give rise to a series of terms that can be resummed according to

$$\lambda^{(1)}\sqrt{-g} \quad = \lambda^{(1)}\left[1 + \frac{1}{2}h^{\gamma}{}_{\gamma} + \frac{1}{4}h_{\mu\nu}h^{\mu\nu} - \frac{1}{8}\left(h^{\gamma}{}_{\gamma}\right)^2 + \dots\right], \tag{1.5}$$

where the linear and quadratic terms in $\boldsymbol{h}$ correspond to the tadpole and two-graviton diagram in (1.4), respectively. We end up with two logical possibilities: Either the Minkowski vacuum is stable under quantum corrections, and hence $\lambda^{(1)} = 0$, or the non-vanishing value of $\lambda^{(1)}$ plays the role of a (quantum induced) CC which drives the geometry towards de Sitter (unless we tune it to zero by means of a counter term).

Since we expect $\lambda^{(1)}$ to factor out like it did in (1.5) (otherwise the resummation could not work and diffeomorphism invariance would be violated), it is sufficient to solely calculate one of the diagrams to infer the value of $\lambda^{(1)}$. A rather simple choice is the tadpole (because it couples to a zero momentum graviton).[12] Accordingly, we identify

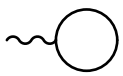 $= \frac{1}{2}h^{\mu\nu}\int \frac{\mathrm{d}^4q}{(2\pi)^4}\frac{q_\mu q_\nu - \frac{1}{2}\eta_{\mu\nu}\left(q^2+M^2\right)}{q^2+M^2} \equiv \mathrm{i}\,\lambda^{(1)}h^{\gamma}{}_{\gamma}\,,$ (1.6)

where the one-loop contribution to the CC can be explicitly calculated,

$$\begin{aligned}\lambda^{(1)} &= -\frac{M^4}{(8\pi)^2}\left[\frac{2}{\epsilon} + \text{finite} - \log M^2\right] \\ &\to -\frac{M^4}{(8\pi)^2}\left[\text{finite} + \log\frac{\mu^2}{M^2}\right].\end{aligned} \tag{1.7}$$

[11] The first diagram represents the sum of all zero point energies in the absence of gravity, see [169, 7] for an explicit calculation.

[12] To cross-check the validity of our reasoning we also evaluated the two-graviton amplitude, which indeed yields the same result.

Here, dimensional regularization with $D := 4-\epsilon$ was used. The divergent term $2/\epsilon$ is of no particular importance; in fact, from an EFT point of view, it parametrizes our ignorance about the UV sector of the theory. We can dispose of it by applying a minimal subtraction scheme, as done in the second line. Technically this amounts to include a bare CC in the action,

$$M_{\rm Pl}^2 \lambda_4^{(\rm bare)} = -\frac{M^4}{(8\pi)^2}\left[-\frac{2}{\epsilon} + \log \mu^2\right] \tag{1.8}$$

where we introduced the arbitrary mass parameter μ to make the final expression dimensionally correct. As usual, it parametrizes a sequence of possible renormalization conditions and is ultimately fixed by a measurement.

The total quantum contribution also contains higher loop effects, i.e. $\lambda = \lambda^{(1)} + \lambda^{(2)} + \ldots$, which are expected to be of similar size.[13] Therefore, it is difficult to predict the precise value of λ as there are significant contributions at each order in perturbation theory (cf. the CC discussion in [105]). However, the crucial observation is that the finite contribution to $M_{\rm Pl}^2\lambda_4$ is of order of the particle mass M. This is bad news for two reasons:

1. It shows that the value of the CC is extremely sensitive to unknown UV physics. Unless we assume supersymmetry to kick in beyond the TeV scale, every new massive particle to be found will yield a significant contribution to the CC. In that sense, the problem is very similar to the problem of the Higgs mass (except that the Higgs mass has a quadratic and the CC a quartic dependence on the UV scale).

2. It is not even necessary to speculate about unknown UV physics to infer a problem: If we consider the contribution of known particles like the electron, we already find a mismatch between the observed value (1.2) and $m_{\rm e}^4/M_{\rm Pl}^2$ (the electron contribution to the CC) of ~ 36 orders of magnitude. Of course, heavier particles even worsen the problem, leading to a mismatch of ~ 60 orders of magnitude if the whole SM particle spectrum is taken into account.

The second observation is really the essence of the CC problem and the reason why it is more severe than the problem of the Higgs mass. To put it differently:

There is no natural understanding of the smallness of λ_4 within the SM.

To get a better understanding of the problem, let us first state the simplest, yet least satisfactory, resolution. It would consist in assuming that $\lambda_4^{(\rm bare)}$ cancels the quantum contribution down to the observed value (1.2) [technically, this corresponds to fixing the scale μ in (1.8)]. However, given our previous discussion, such a resolution would require a tremendous amount of fine-tuning: We would need to specify $\lambda_4^{(\rm bare)}$ up to 60 decimal

[13] The reason is that higher loop diagrams contain more SM vertices, which merely implies a moderate suppression (compared to gravitational interactions). Thus, these contributions remain competitive with the leading order terms.

places to consistently take care of all SM contributions. Even worse, we would need to adapt that tuning at every order in perturbation theory since higher loop contributions, viz. $\lambda^{(n)}$ with $n > 1$, are not hierarchically suppressed. This is exactly what we consider not to be *technically natural*. In fact, it would imply that the unknown UV theory includes a mechanism that tunes all particle masses (including the ones in the low energy EFT) in such a way that their combined contribution to the CC is tremendously small. To put it differently, for physics to be consistent with observations at cosmological scales, we would have to rely on unknown UV physics to come to the rescue at low energies. While being a logical possibility, this is opposed to the way nature is usually organized.

The discussion illustrates why the CC problem is rightly considered a fine-tuning problem. In this thesis, instead of relying on a tuning of model parameters, we will look for a technically natural resolution of the problem. A prominent example of a stable parameter is provided by the electron mass, which is natural in the 't Hooft sense [161]: In the limit $m_\mathrm{e} \to 0$ there is an enhanced symmetry, hence implying that quantum corrections must be proportional to the electron mass itself. As a result, m_e can be chosen arbitrarily small in a radiatively stable way. Note that no such enhanced symmetry exists in the limit $\lambda_4 \to 0$.

We should stress that the above calculations were performed on a Minkowski background although we know that our universe has a non-vanishing curvature on cosmological scales. Thus, a complete discussion would need to include these curvature effects, which are in turn expected to modify the result for $\lambda^{(n)}$. However, as the Compton wavelength of typical SM particles is much smaller than $1/H_0$, we expect these corrections to be suppressed by $H_0^2/M^2 \ll 1$. As a matter of fact, the main contribution to the loop integral in (1.2.1) stems from momenta $\boldsymbol{p} \sim M$, for which we can always assume to be within a patch of local normal coordinates, hence implying suppressed curvature effects (compared to the Minkowski contribution). To summarize, we learn from our considerations that a Minkowski background (or a de Sitter background with phenomenologically large curvature radius) is destabilized by quantum corrections (if we do not assume some sort of fine tuning).[14]

1.2.2 Weinberg's no-go theorem

An important paper on the CC problem was written by Weinberg in the late eighties [168]. There, he not only phrased the problem, but also came up with a powerful no-go theorem that rules out a broad class of simple models. Because of its generality, it turned out to be an important touchstone for aspirant theories trying to address the problem. Here, let us briefly summarize its reasoning.

The initial question is whether there is a dynamical *adjustment mechanism* to completely cancel the CC. It is clear that, ultimately, we need some residual CC (or some type of matter

[14] Note that this reasoning relies on a semiclassical treatment according to which fluctuations on a *classical* de Sitter background are quantized. Albeit it seems conceivable that a spacetime as large as our universe can be treated classically, there might occur collective effects related to the quantum constituency of the background itself, which might change the picture (see [68, 67] and also [98, 92] for a bound state formalism).

that mimics a CC) to account for the observed accelerated expansion of our universe; here instead, we first consider the idealized problem of having a stable Minkowski vacuum. The generalization to de Sitter is discussed afterwards.

We assume that the adjustment is realized in terms of some *local* degree of freedom, which we denote by ϕ and which couples to 4D Einstein gravity in a minimal way. To demonstrate the essence of the argument it is sufficient to consider this simple spin-two plus spin-zero setup.[15]

An adjustment mechanism requires that the system is able to dynamically react to changes in the CC. In other words, the ϕ theory has to be constructed in such a way that the vacuum configuration is one where the CC is exactly canceled. This is realized by the condition[16]

$$\frac{\partial V(\phi)}{\partial \phi} = 4M_{\rm Pl}^2\lambda_4 - T^{\gamma}{}_{\gamma}(\phi)\,, \tag{1.9}$$

where $V(\phi)$ is the scalar potential. And indeed, once the field has settled to its (4D maximally symmetric) vacuum configuration $\phi_0 = \text{const}$, defined by

$$\left.\frac{\partial V(\phi)}{\partial \phi}\right|_{\phi=\phi_0} = 0\,, \tag{1.10}$$

Eq. (1.9) together with Einstein's equations imply

$$M_{\rm Pl}^2\mathcal{R} = 4M_{\rm Pl}^2\lambda_4 - T^{\gamma}{}_{\gamma}(\phi_0) = 0\,. \tag{1.11}$$

In other words, the classical vacuum of a theory that admits (1.9) corresponds to a flat Minkowski geometry despite the presence of a non-vanishing tension.

At first sight, this looks very promising because it seems to be a fully dynamical mechanism: When the tension changes its value, the field ϕ, due to (1.9), will start to evolve towards a Minkowski vacuum again. However, we have to be cautious because so far it is not clear whether the mechanism relies on some sort of parameter constraint and hence is threatened by quantum corrections (which would generically violate the constraint). In fact, this can already be suspected by counting the equations: ϕ and the metric $g_{\mu\nu}$ are determined by their respective equations of motions; but then (1.9) constitutes an additional equation that might turn out to be a parameter constraint.

To answer that question, let us evaluate (1.9) for the vacuum configuration ϕ_0, which yields $V(\phi_0) + M_{\rm Pl}^2\lambda_4 = 0$, where $T^{\gamma}{}_{\gamma}(\phi_0) = -4V(\phi_0)$ was used. This equation has to be understood as parameter constraint [since the value of ϕ_0 is already fixed via (1.10)]. In other words, the minimum of the scalar potential has to be chosen such that it cancels the (quantum corrected) CC. It is clear that this cannot solve the problem because it involves again an unacceptable amount of tuning.

[15] Weinberg is even more general and allows for an arbitrary (but finite) number of additional degrees of freedom, as well as a more general metric theory that does not need to be minimally coupled.

[16] We use a normalization for which the field variable ϕ is dimensionless.

To forge a bridge to Weinberg's discussion (which becomes relevant in the main part of this thesis), consider (1.9) for generic field value $\phi \neq \phi_0$ but vanishing derivatives, i.e. $\partial_\alpha \phi = 0$. Under these assumptions, we obtain a differential equation for $V(\phi)$ that can be solved explicitly by

$$V(\phi) = V_0 \, \mathrm{e}^{4\phi} - M_{\mathrm{Pl}}^2 \lambda_4 \, . \tag{1.12}$$

This potential implies a runaway, which can only be avoided by setting the parameter $V_0 = 0$. Then ϕ corresponds to a flat direction in fields space and can be understood as the Goldstone boson of a spontaneously broken scale invariance. However, the corresponding potential is not stable under quantum corrections and hence requires an unacceptable amount of tuning. Alternatively, we can set $\lambda_4 = 0$ and allow $V_0 \neq 0$, so the Minkowski vacuum is reached asymptotically at $\phi = -\infty$. In that case, the theory is scale invariant and the choice $\lambda_4 = 0$ is indeed stable under quantum corrections (or technically natural equivalently). The problem is that the runaway is incompatible with having a static Minkowski vacuum. Moreover, the theory does not allow to generate particle masses. This can be seen by including an additional scalar field σ which amounts to the replacement $V_0 \to V_0(\sigma)$ (see [168] for details). In that case, the field σ [the potential of which would be described by $V_0(\sigma)$] could acquire a mass through spontaneous breaking of scale invariance. However, this is incompatible with the runaway of ϕ, driving the system towards $\phi = -\infty$ [where all masses vanish due to (1.12)].

As a result of these considerations, there is no local 4D adjustment mechanism that could avoid the naturalness problem. Note that the reasoning is unchanged if, instead of a Minkowski vacuum, we demand a de Sitter vacuum with curvature scale H_0. In that case, the potential (1.12) is endowed with an additional (constant) term $6M_{\mathrm{Pl}}^2 H_0^2$ which cannot improve the situation.

There are several loopholes that one might hope to exploit in order to circumvent the theorem:

1. *The extra dimension loophole*: The outcome of Weinberg's theorem is closely related to the fact that the CC corresponds to a source with (local) Poincaré invariance, which hence makes it compatible with a de Sitter geometry. As mentioned before, in a braneworld context, the CC plays the role of a localized source that breaks the higher-dimensional Poincaré invariance explicitly. Thus, in general, we do not expect Weinberg's theorem to apply in the presence of a higher-dimensional bulk theory. This loophole is exploited in this thesis. Let us stress, though, that this way of avoiding the theorem is only ensured for infinite (or sufficiently large) volume extra dimensions, but (as we exemplify in this thesis) may fail in the presence of finite volume extra dimensions. The reason was discussed in [71, 61, 66]: In the low energy description of the compact models there is a zero mode graviton coupling with strength $1/M_{\mathrm{Pl}}$; in other words, a local theory of 4D GR (supplemented with a finite number of massive KK modes) is recovered and makes Weinberg's argument applicable again (cf. Sec. 1.5.). On the other hand, if the extra space volume is

infinite, there is no normalizable zero mode, rather the graviton is a collective state. This implies that there is no limit for which the theory is solely described in terms of a (massless) 4D graviton.

2. *The nonlocality loophole*: The 4D theory might be nonlocal which is certainly incompatible with the assumptions of Weinberg's theorem. This is in fact closely related to the extra-dimensional loophole. If the extra space volume is infinite, the corresponding 4D theory turns out to be nonlocal (as a consequence of integrating out an infinite number of arbitrarily light KK modes [66]). Thus, this is just another (but equivalent) way of stating the previous extra dimension loophole. Of course, this loophole is also interesting in its own right and has been used in different ways [12, 70, 105].

3. *The non-constant ϕ loophole*: For the theorem to apply, the additional degrees of freedom—represented by ϕ in our language—are required to settle to a static value, i.e. $\phi_0 = \text{const}$. This assumption can be relaxed without necessarily preventing the existence of a Minkowski vacuum. This is the loophole exploited for example in the Fab Four theory [40]. In the case of Fierz-Pauli massive gravity, which admits a Minkowski vacuum in the presence of a non-vanishing (sufficiently small) CC, the same loophole applies. To be precise, the helicity-zero field, used to make diffeomorphism invariance manifest via the Stückelberg trick, is known to develop an explicit time dependence in the presence of a CC source [159, 70].

1.3 The extra-dimensional paradigm

The idea that nature features more than three spatial dimensions has attracted the interest of physicists since a long time and gave rise to a plethora of different models. In this thesis, we are interested in a specific class of 6D braneworld models.[17] Before going into any details, let us discuss a specific 6D prototype model to illustrate the virtue of higher-dimensional setups with respect to the CC problem. Further motivations are invoked afterwards.

1.3.1 Our universe as a string

We consider the simple theory of a three-brane with tension λ embedded in a 6D bulk of infinite size. Correspondingly, the 6D Einstein-Hilbert action is supplemented with a (constant) tension term,

$$\mathcal{S} = \mathcal{S}^{(6)}_{\text{EH}}[\boldsymbol{g}_6] - \lambda \int \mathrm{d}^4x \, \sqrt{-g} \,, \tag{1.13}$$

[17] For a concise pedagogical introduction see for example [152], and for a review on braneworld models [122].

where $\boldsymbol{g}_6$ and $\boldsymbol{g}$ are the bulk and the 4D brane induced metric, respectively. This theory admits the vacuum solution

$$\mathrm{d}s_6^2 = \eta_{\mu\nu}\,\mathrm{d}x^\mu \mathrm{d}x^\nu + \mathrm{d}r^2 + \left(1 - \frac{\delta}{2\pi}\right)^2 r^2 \mathrm{d}\phi^2\,, \tag{1.14}$$

where δ is an integration constant, corresponding to a deficit angle in the bulk. From an extra space perspective, the solution can be understood as a two-dimensional Euclidean space with a wedge of opening angle δ removed [according to the last two terms in (1.14)]. In an embedding picture, the extra space corresponds to a cone with the brane sitting at its tip.[18]

This simple geometry is of particular significance with regard to the CC problem. Physically, this can be understood as follows: The conical defect is caused by the brane tension; specifically, by matching the vacuum solution to the brane, we find

$$\delta = \lambda/M_6^4\,, \tag{1.15}$$

where M_6 denotes the higher-dimensional gravity scale. Thus, the gravitational effect of the tension consists in curving the extra space into a cone, whereas—contrary to 4D GR—the brane geometry remains perfectly flat [according to the first term in (1.14)]. Moreover, the solution exists for every value of λ provided $\lambda \leq 2\pi M_6^4$.[19] This is remarkable, because it means that a brane observer (like us) is blind to the gravitational effect of the tension or 4D CC, equivalently. Hence, this solution corresponds to a nonlinear realization of the degravitation mechanism. From a 4D perspective, (1.13) gives rise to a landscape of different brane vacua, labeled by λ. The observation that extra dimensions might help with the CC problem was made long ago [154, 66] and also generalized to higher dimensions (cf. for example [71, 41]).

As we will demonstrate in this thesis, this solution is also an attractor in the sense that if we start with initial conditions corresponding to a deficit angle different from (1.15), it will be approached dynamically. The corresponding change is mediated by cylindrically symmetric waves, so-called Einstein-Rosen waves, that are emitted by the brane and propagate into the bulk.[20] In other words, there is an adjustment mechanism that—in an extra-dimensional picture—relies on gravitational waves as the dynamical ingredient. These waves are an extrinsic curvature effect and are hence not detectable on the brane.

It thus seems we have successfully isolated the mechanism we were looking for. This readily raises the question how Weinberg's theorem is avoided in this case. The answer was already given in Sec. 1.2.2: The mechanism makes use of the extra dimension loophole because the CC now plays the role of a localized source that breaks the translational invariance of the classical vacuum. Hence, Weinberg's theorem is not applicable (this is

[18] Note that this solution is the higher-dimensional analog of the cosmic sting solution in 4D [166, 88, 96].

[19] The setup hence qualifies as *sub-critical*. The *super-critical* case for which $\lambda > 2\pi M_6^4$ will also be investigated in this thesis.

[20] They were first introduced in [78] and later reviewed for example in [163].

different for finite volume extra dimensions, where Weinberg enters via the backdoor after integrating out the bulk fields, as we will discuss later).

Albeit we have found a promising mechanism, it is clear that this is not the final answer. To be specific, (1.13) is a theory of 6D gravity and as such it predicts a 6D gravitational potential in the Newtonian limit. In particular, if we calculate the potential between two point masses, localized on the brane and separated by the distance r, it will scale as $1/r^3$, in clear contradiction to what we observe, say on solar system scales. To put it differently, every model using the 6D mechanism, as outlined above, needs to come up with some way of restoring the 4D scaling of the gravitational laws. In fact, there are at least two known ways to realize a 4D regime in that case. Accordingly, we distinguish two different classes of models:

1. Models with *infinite* volume extra dimensions [63, 61, 71, 65, 66] . Here, a 4D Einstein-Hilbert term is included on the brane. As it turns out, this term dominates the gravitational dynamics for short distances (or large energies), thereby restoring the 4D regime. On the other hand, for large distances the 6D gravity term kicks in, thus leading to a higher-dimensional behavior. Correspondingly, these models are IR modifications of gravity. An extensive introduction will be offered in Sec. 1.4.

2. Models with *finite* volume extra dimensions [33, 34, 35]. Here, the 4D regime is recovered at large distances (or small energies equivalently). These models hence constitute a UV modification of GR. The physical picture is simple: For small enough energies, the extra space dimension can no longer be resolved and the theory enters a 4D regime. We will introduce this class of models in Sec. 1.5.

There is another obstacle we have to circumvent when we want to make use of the deficit angle solution. So far the mechanism is incompatible with having a non-vanishing on-brane curvature, rather the CC is completely diverted into extrinsic bulk curvature. We will see that this is also the case for other types of matter, like dust and radiation. Therefore, we have to find a way to account for the observed curvature in our universe. There are in principle two possibilities (each of which will become relevant for one setup): First, we can choose an initial value for Hubble $H_i \gtrsim H_0$ and check whether the subsequent evolution (during which Hubble decreases as the attractor value $H_a = 0$ is approached) can be made compatible with observations (by choosing the model parameters appropriately). Second, we can deform the attractor solution itself to yield a value $0 < H_a \lesssim H_0$. Of course, this is not a sufficient condition, and it still has to be shown that with $H_i \gtrsim H_a$ the Hubble evolution follows a phenomenologically viable trajectory.

As the central result of this thesis, we come to a conclusion about the phenomenological potential of both setups. Moreover, we check whether the degravitation property of the original deficit angle solution is maintained despite these additional manipulations.

1.3.2 Motivations beyond lambda

We invoked the CC problem as the main motivation for introducing additional dimensions. However, there are further physical reasons why braneworld constructions are interesting candidates for describing our universe. Let us mention two of them:

1. Due to the advances in observational cosmology during the last decades, (1.1) was put to the test at the largest accessible scales in nature. In that context, the ΛCDM model, which relies on GR to describe the expansion history of our universe, has proven extremely successful: Only six independent parameters allow to fit the observations consistently (for recent parameter values see [3]). In that context, we might ask a simple question:

   > *Are there consistent competitor theories to GR that are both predictive and phenomenologically viable?*

   If such a theory exists, it would constitute a veritable touchstone for the superiority of GR. However, finding theories that consistently modify GR is known to be a notoriously difficult task (for recent reviews on the topic see [102, 103]). In fact, there is a plethora of possible (technical) obstacles one has to deal with; just to name a few historical examples: ghost instabilities, breakdown of perturbative unitarity on solar size distances, quantum stability. And this still leaves aside the question whether a particular model is phenomenologically viable. After all, modifying GR normally implies the occurrence of new degrees of freedom, which, quite generically, lead to additional observable forces.

   With regard to these consistency issues, extra-dimensional models stand out because they are typically based on higher-dimensional GR which is a healthy theory with a clear physical (and geometrical) interpretation. Thus, braneworld models are a promising playground to devise consistent competitor theories to GR.

2. Another motivation comes from string theory, which generically predicts more than four spacetime dimensions (26 for bosonic and 10 for superstring theory). Thus, there has to be a mechanism which leads to the emergence of our apparent four spacetime dimensions. One possibility is provided by topological defect solutions, so-called D-branes (for a review see [145]). They are defined by the property that the endpoints of open strings can live on them, and hence they provide a fundamental explanation for the localization of matter on the brane. Accordingly, our universe might be a D-brane of three spatial dimensions. Gravity, which is represented by the vibrational modes of closed strings, is not confined and hence propagates freely in the bulk, in agreement with our classical braneworld construction (1.13).

1.4 Towards BIG – infinite volume extra dimensions

The central part of this thesis is devoted to the BIG model in 6D. It was first introduced in a 5D version, known as the DGP model [63]. While the 5D model is interesting as

a consistent competitor theory to GR—and as such gives rise to a modified Friedman cosmology [51]—it was soon realized that it cannot solve the CC problem (though it serves as a dark energy model [52]).[21] Yet, there is no obvious obstacle in generalizing the model to higher dimensions, which was first done in [61]. There, the prospects with respect to the CC problem were much better, which is owed to the deficit angle solution (1.14) in 6D and comparable solutions in higher dimensions [71, 61, 66]. However, the further development of these models was hampered for the following reasons:

1. An instability of a particular Minkowski vacuum (the one with $\lambda = 0$) was encountered [58, 94], hence raising concerns about the consistency of the model.

2. In comparison to the 5D model, it is much harder to find cosmological solutions. The reason is that in six (and more) dimensions a three-brane with FLRW symmetries acts as an antenna that emits and absorbs bulk gravitational waves; in 6D they are given by the direct generalization of Einstein-Rosen waves in 4D [78]. This in turn renders the dynamical system on the brane highly sensitive to the initial conditions in the bulk. By contrast, in the 5D case FLRW symmetries imply a static bulk geometry due to a generalization of Birkhoff's theorem applying to planar symmetry [162].

While we will discuss the stability issue extensively in Chap. 2, we turn to cosmology in Chap. 3. In fact, we will see that both difficulties can be circumvented.

In the next section, we derive the BIG model as the low energy version of a simple braneworld model. This approach serves two purposes: First, it nicely exemplifies the virtue of the EFT paradigm. Second, it provides a physical understanding of the origin of the BIG model and in turn admits a clear-cut assessment on the stability issue.

1.4.1 A first example of an effective field theory

To gain a more profound understanding of the physics of the BIG model, it is instructive to start with the simple setup of 6D GR and to add a minimally coupled scalar field ϕ of mass M localized on an infinitely thin three-brane (with positive tension λ),[22]

$$\mathcal{S} = \mathcal{S}^{(6)}_{\mathrm{EH}}[\boldsymbol{g}_6] + \mathcal{S}_{\lambda_0}[\boldsymbol{g}] + \mathcal{S}_{\mathrm{UV}}[\boldsymbol{g}, \phi, M] + \mathcal{S}_{\mathrm{m}}[\boldsymbol{g}, \Psi] \,, \tag{1.16}$$

where the first two terms equal the toy model action (1.13) [and are defined in (C1) and (C3)]. Ψ collectively denotes additional, localized degrees of freedom with masses below M. For example, these fields could represent the SM that is also assumed to be confined

[21] One cosmological branch features "self-acceleration", i.e., it admits a 4D de Sitter vacuum on the brane in the absence of any source. However, this solution is neither able to shield a non-zero brane tension, nor is it stable. In fact, it is believed to suffer from perturbative ghost instabilities [121, 130, 110, 42, 91, 87]. We provide a short review on the DGP cosmology in Sec. 3.1.

[22] The restriction to a 6D bulk is made for notational convenience only. All considerations of this section can directly be generalized to higher-dimensional configurations.

on the brane. For completeness, the UV sector of the action reads explicitly,

$$\mathcal{S}_{\text{UV}}[\boldsymbol{g}, \phi, M] = -\frac{1}{2} \int \mathrm{d}^4x \, \sqrt{-g} \left(\nabla_\mu \phi \nabla^\mu \phi + M^2 \right) . \tag{1.17}$$

Let us first motivate the existence of the heavy scalar field ϕ by providing an explicit example of a possible microscopic origin. The idea is to endow the brane with a microscopic width R; after all, some transverse spread of the brane is expected to be present in every physical system. Specifically, we describe the brane as a ring in extra space (with circumference $2\pi R$). Then, size fluctuations of the compact ring/brane dimension can be described in terms of a scalar field φ, to which we refer as the radion.[23] Provided the brane is sufficiently stabilized, the radion acquires a mass $m_\varphi \propto 1/R$.[24] Such a heavy degree of freedom has to exist in any sensible UV theory that resolves the brane microscopically. All dynamical effects related to the brane size are then represented by φ. For our subsequent considerations it is convenient to forget about the microscopic origin of φ, and thus to again use the (over-)idealization of an infinitely thin brane (which for example can be modeled by a 2D delta function) where we identify $\phi \equiv \varphi$ (and $M \equiv m_\varphi$ correspondingly). In other words, ϕ carries the system's memory about the physical presence of brane size fluctuations.

Let us first comment on the stability of (1.16). By using the deficit angle solution (1.14) as the classical background, it can be shown that the Hamiltonian corresponding to S_{UV} is bounded from below. In fact, this follows trivially from the fact that the on-brane geometry is Minkowski. Thus, the ϕ sector of the theory is stable.[25]

It is now crucial to note that this setup gives rise to localized ϕ loops on the brane that couple to the bulk graviton $\boldsymbol{h}_6 := \boldsymbol{g}_6 - {}^{(0)}\boldsymbol{g}_6$ (or, to be more precise, to the pullback of the bulk graviton on the brane, denoted by $\boldsymbol{h}$). Here, we expanded around the deficit angle background ${}^{(0)}\boldsymbol{g}_6$ [defined before in (1.14)], which corresponds to a 4D Minkowski space on the brane. The corresponding contributions to the quantum effective action admit an identification of an induced gravity and tension term. Specifically, at one loop and two graviton order,

$-\,\mathrm{i}\ \times$ 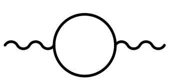

$$= M_{\text{ind}}^2 \, \frac{1}{8} h^{\mu\nu} \Diamond_{\mu\nu}^{\gamma\delta} h_{\gamma\delta} \ - \lambda_{\text{ind}} \frac{1}{4} \left[h_{\mu\nu} h^{\mu\nu} - \frac{1}{2} \left(h^\gamma{}_\gamma \right)^2 \right] + \ \ldots \tag{1.18}$$

---

[23] This particular regularization is of course an arbitrary choice, we could as well have smeared the brane fields over a disc of radius R (instead of confining them on a codimension-one object). The point is that we expect low energy physics, taking place on length scales far above R, to be insensitive to that choice. In the bulk of this thesis, we will provide explicit evidence for the correctness of that claim. Moreover, similar (but solitonic) constructions can be found in [62], there the "breathing mode" of the soliton plays the role of the radion.

[24] The exact relation (including a detailed derivation) is given in Sec. 2.4.3.

[25] Note that this result would not change if additional gravitational fluctuations are included, which simply follows from the stability of the deficit angle vacuum for sub-critical values of λ.

where the first and second term are the 4D Einstein-Hilbert and the tension term, respectively, both at second order in field fluctuations $\boldsymbol{h}$ around a 4D Minkowski background.[26] The ellipsis stands for higher-dimensional operators, e.g. the perturbative expansion of $\mathcal{R}_{\mu\nu}\mathcal{R}^{\mu\nu}$. These terms are suppressed by higher powers of $1/M_{\rm ind}$ and should be included anyhow if GR is treated as an EFT.[27] On the other hand, loop diagrams with more graviton legs attached yield terms of higher order in $\boldsymbol{h}$. As a consequence of diffeomorphism invariance, they have to match the corresponding terms in a weak field expansion of $\sqrt{-g}\,\mathcal{R}$ and $\sqrt{-g}$. After applying minimal subtraction, both the induced 4D Planck Mass $M_{\rm ind}$ and tension $\lambda_{\rm ind}$ are set by the scale M (up to factors of order one).[28] Thus, the two constants are not independent, but rather derived quantities.

Let us now assume that we are only interested in low energy questions far below the scale M. In such a regime, the dynamics of the field ϕ can be neglected, which in turn suggests to work in a version of (1.16) that no longer includes the scalar field ϕ; in other words, we integrate out ϕ. Technically, this amounts to include all quantum induced terms (including (1.4.1) and higher orders) in the classical action. The effective theory without ϕ then reads

$$\mathcal{S} = \mathcal{S}^{(6)}_{\rm EH}[\boldsymbol{g}_6] + \mathcal{S}_{\rm ind}[\boldsymbol{g}] + \mathcal{S}_{\rm m}[\boldsymbol{g}, \Psi] \,, \tag{1.19}$$

where the new term $\mathcal{S}_{\rm ind}$ comprises the resummed loop contributions (plus the UV value of the tension, λ_0),

$$\mathcal{S}_{\rm ind}[\boldsymbol{g}] = \int \mathrm{d}^4x\,\sqrt{-g}\,\left[\frac{M_{\rm ind}^2}{2}\,\mathcal{R} - (\lambda_0 + \lambda_{\rm ind}) + \ldots\right] , \tag{1.20}$$

here the ellipsis represents higher curvature combinations that are suppressed by additional powers of $M_{\rm ind}$.

Let us reconsider these findings from a general perspective based on the EFT paradigm. The latter simply states that high and low energy physics can be decoupled from each other. In other words, if we want to describe a system at energies below a scale Λ, we do not need to dynamically resolve particles with masses greater than Λ. Instead, we use a theory that only describes the dynamics of particles with masses lighter than Λ. Accordingly, there is a simple guideline to devise a valid low energy EFT that qualifies as technically natural:

1. Include all operators into the low energy action that are compatible with the symmetries and field content of the setup under consideration.

2. Demand the coefficients to be technically natural, i.e. stable under quantum corrections (their value then depends on the dynamical particle spectrum of the EFT). Otherwise, the theory would rely on a fine tuning, which, according to our previ-

[26] The operator $\Diamond^{(4)}$ denotes the 4D Einstein operator as defined in 4D inertial coordinates (2.48).

[27] For a seminal work on GR as an EFT see [56, 55], and for a more pedagogical introduction to EFT's [57, 23, 26] (also in a general context).

[28] For an explicit calculation see [37]. The result for $\lambda_{\rm ind}$ matches the final expression in (1.7).

ous discussion in the case of the CC, would be a logical but rather not a physical possibility.

3. Use theoretical consistency as a further means to constrain the theory (without spoiling the naturalness requirement).

Our results nicely exemplify (and justify) this framework. The original action (1.16) can be understood as an EFT theory with cutoff $\Lambda_{UV} > M$ (and of course $\lesssim M_6$). Then, (1.19) plays the role of the low energy EFT with cutoff $\Lambda_{IR} \lesssim M$. Now, let us check whether all three requirements are compatible with our findings:

The first one is fulfilled since on the brane all operators that respect 4D diffeomorphism invariance have been included. For our UV prototype, however, their physical significance becomes obvious: They are the low energy fingerprint of the presence of ϕ in nature. As for the second point, all quantum corrections within the low energy EFT (stemming from the fields Ψ) give contributions to $M_{\rm ind}$ and $\lambda_{\rm ind}$ that are set by masses smaller than M, and hence are relatively suppressed. Our approach also admits a statement about the last point. In fact, we already argued that the classical Hamiltonian corresponding to (1.16) is positive definite, so there should be no doubt—at least from the UV perspective—about the stability of the IR theory (1.19).

As a result, we have seen that (1.19) is an explicit example of a low energy EFT that arises when a localized scalar particle of mass M is integrated out. However, this is just the most primitive example of a possible UV theory. The virtue of this approach lies in its universality: When we work in the low energy regime, we do not have to specify the UV sector. Specifically, this means that we do not have to know which particles contribute to $M_{\rm ind}$ (or $\lambda_{\rm ind}$). As a result, we can generalize (1.20) according to

$$M_{\rm ind} \to M_{\rm Pl} \qquad \text{and} \qquad \lambda_0 + \lambda_{\rm ind} \to \lambda \tag{1.21}$$

where we are agnostic about the UV composition of the new parameters. We even treat them independently (keeping in mind that not every UV sector needs to contribute equally to $M_{\rm Pl}$ and λ). The identification of one of the parameters with the Planck mass is demanded by phenomenology and will be motivated in Sec. 1.4.3.[29]

The action (1.19) subject to the replacement (1.21) describes the BIG model in its final form, where the 4D curvature term (proportional to $M_{\rm Pl}$) is normally referred to as the brane induced gravity (BIG) term [see also Def. (1.19)]. In that context, it is important to stress that (1.16) merely serves as a prototype for a UV model; for example, there exist explicit constructions how the BIG model might be embedded in superstring theory [10].

1.4.2 Ghost or no ghost

The EFT discussion of the last section clearly shows that the induced terms should be included in any natural braneworld setup for two reasons: First, they represent unknown

[29]For the present discussion it suffices to treat $M_{\rm Pl}$ as an arbitrary model parameter.

UV physics (if existent), and second, they are induced anyhow by quantum loops of massive particles localized on the brane. Having said this, we arrive at a surprising puzzle. According to claims in the literature, the 6D BIG model (as well as its higher-dimensional generalizations) with *vanishing* brane tension exhibits a ghost instability in a weak coupling regime on a Minkowski background [58, 94]. In light of our general EFT reasoning, this is very unexpected because we can always understand the BIG model as the low energy version of some parent theory that contains massive localized particles. And indeed, we know that those theories exist. Here, we just stated the most primitive example of a scalar localized on a delta brane in (1.16), but there are more advanced constructions, as for example described in [62], where particles are localized within topological defects, e.g. the Nielsen-Olesen vortex in two codimensions [136]. This leads to the immediate question:

> *How is it possible that the EFT description of gravity induced on higher-dimensional surfaces is plagued by a ghost instability even though there exist stable UV theories of localized massive particles?*

To get a first idea of the resolution, note that the crucial limitation of the derivation of the ghost was to set the brane tension to zero (mainly for simplicity). However, from our UV prototype discussion it is clear that this is a problematic choice. In fact, we have seen that a tension is inevitably induced by loops on the brane and hence should be included in a natural setup. On the other hand, a vanishing tension corresponds to a tuning of model parameters. In particular, for (1.16) it can be shown by an explicit one loop calculation that the induced tension and gravity term are related by[30]

$$\frac{M^2 M_{\rm ind}^2}{\lambda_{\rm ind}} = \frac{1}{3}\,, \tag{1.22}$$

where M is the mass of the scalar that has been integrated out in the low energy EFT. Thus, for this particular UV model, it is not possible to set $\lambda_{\rm ind}$ to zero while keeping $M_{\rm ind}$ finite (without imposing some sort of unwanted tuning). This observation suggests that the occurrence of the ghost might be a relict of setting the brane tension to zero.[31] To answer that question rigorously, we have to study the setup with non-vanishing brane tension, which is done in Chap. 2. Here, we limit ourselves to a condensed version of the full story.

The classical vacuum of (1.19) is again given by the deficit angle solution (1.14) (the induced gravity term does not have any impact because it vanishes for a flat on-brane geometry). In order to probe the quantum stability of that background, the corresponding fluctuation theory is studied, which in turn allows us to find an expression for the vacuum-to-vacuum amplitude $\langle 0|0\rangle_T$. To be precise, we ask for the probability that the vacuum

[30] This result is independent of the renormalization scheme because the divergent terms cancel in this ratio.

[31] In an earlier work (to which the author contributed), the absence of the ghost was claimed even for a tensionless brane [19]. However, in the bulk of this thesis, we show that this is not the case. By correcting and generalizing the old analysis, we arrive at the new result presented here.

persists in the presence of a non-vanishing external source $\boldsymbol{T}$. Perturbative unitarity then requires the amplitude to be ≤ 1. Whenever the theory contains a ghost, this condition is violated, and hence, we loose a sensible probabilistic interpretation. As a result of these considerations, we obtain a lower bound on λ:

$$\boxed{\lambda > \frac{2}{3} M_{\rm Pl}^2 m_\varphi^2} \tag{1.23}$$

Here, m_φ is the mass of the radion φ which describes fluctuations of the microscopic brane size (with mass $m_\varphi^2 \propto 1/R^2$).[32]

Let us first check whether our particular UV model (1.16) is compatible with the above bound. To that end, remember that we identified $M \equiv m_\varphi$. In other words, the radion gives the only contribution to the induced terms in (1.20)—at least in this simple model. By using (1.22) (as well as $M_{\rm ind} \equiv M_{\rm Pl}$ and $\lambda_{\rm ind} \equiv \lambda$), it is then straightforward to show that the above bound is fulfilled.[33]

As a result of these considerations, we are able to resolve the initial puzzle: For a sufficiently large tension the theory is stable and hence not in conflict with the existence of a healthy UV construction. We therefore conjecture [and have explicitly proven for the particular example (1.16)] that any healthy parent theory to (1.19) admits an IR value of the tension that fulfills the above bound. Moreover, we expect these result also to apply to braneworld models with more than six dimensions. The stability of BIG for branes with sufficiently large tension opens a new window of opportunity for studying consistent modifications of GR and their potential with respect to the CC problem.

1.4.3 Observational aspects

In this section, we want to briefly comment on the phenomenology of the 6D BIG model, in particular on how the model parameters are constrained by observations. In that context, the crucial quantity is the crossover scale r_c. In this thesis, we define it as the length scale at which the 4D Newtonian potential of a point mass M_0, localized on the brane, changes from a 4D to a 6D regime; to be specific,

$$V(r) \sim -M_0 \begin{cases} \dfrac{1}{M_{\rm Pl}^2 r} & (\text{for } r \ll r_c) \\ \dfrac{1}{M_6^4 r^3} & (\text{for } r \gg r_c) \end{cases} . \tag{1.24}$$

[32] Again, since we are mainly interested in cosmological length scales, we do not need to resolve the substructure of the brane. Correspondingly, the radion field has been integrated out in the low energy EFT. The occurrence of the scale R (or m_φ equivalently) can then be understood as the low energy fingerprint of the existence of φ in nature.

[33] If we also take into account a UV value $\lambda_0 > 0$ [as occurring in (1.19)], the bound is fulfilled even better. On the other hand, a choice $\lambda_0 < 0$ would be problematic already in the UV theory [124].

In technical terms, the crossover determines the scale below which the brane induced term in (1.19) dominates relative to the 6D Einstein-Hilbert term. This observation motivates to identify the induced gravity scale with $M_{\rm Pl}$ [see (1.21)]; only that way gravity couples with the observed strength on solar system scales (and below).

In anticipation of or results, we will derive an upper bound on the crossover in 6D (thereby confirming the result of [104]), $r_c \lesssim M_{\rm Pl}^2/(RM_6^4)$, which is valid in a near-critical regime when the deficit angle is close to (but still below) 2π. In a conservative approach, we would identify the crossover with the Hubble length today $1/H_0$. As R describes the microscopic size of the brane, we set $R \sim 1/M_6$. Plugging in numbers then yields an upper bound on the bulk scale, specifically $M_6 \lesssim 10\,\text{MeV}$.[34] Note that the bound could be raised by assuming a crossover scale that is smaller than the present Hubble length; in fact, this is a possibility which so far has not been excluded. To be specific, r_c might be constrained by the Lunar Laser Ranging Experiment that measures the distance between the earth and the moon (cf. [139] for a review).[35] However, as we will see in Sec. 3, the sub-critical cosmology (for which the upper bound on r_c is applicable) is incompatible with having a stable 4D regime irrespective of the numerical value of r_c. Thus, deriving an explicit observational bound on r_c is a somewhat obsolete task.

For the purpose of this work, it is therefore sufficient to keep in mind that the bulk Planck mass is below the TeV scale (while it still might be close to it). This potentially low scale, however, raises concerns about a strong coupling of the bulk gravity sector, which might for example strongly affect collider experiments. This issue—which is also present in the 5D DGP model—was addressed in [72], where, in the case of the 5D model, it was shown that the SM on the brane is successfully shielded from a strongly coupled bulk gravity sector due to the induced gravity term (which completely dominates the gravitational dynamics at high energies). In fact, the lower bound on the bulk gravity scale was found to be as low as the meV scale—based on accelerator experiments, astroparticle physics and gravitational measurements. This reasoning was then also applied to the 6D model in [62]. After all, as we are mostly addressing cosmological questions, taking place at extremely low energies, our analysis is not sensitive to that issue.

1.5 Towards SLED – large extra dimensions

In contrast to the last section, we now turn to models with a compact (but large) extra space. These models have first been discussed in [13, 9, 14, 148, 149, 15] as potential solutions to the electroweak hierarchy problem. As before in models with infinitely large extra dimensions, the essential idea is to hide the extra space from an observer by confining all SM matter fields—and hence the observer itself—on a three-brane of microscopic width set by the inverse bulk scale $R \sim 1/M_D$. As usual in braneworld models, gravity plays a

[34] Note that M_6 can be hierarchically smaller away from the near-critical regime. In fact, in the tensionless 6D model, discussed in [62], the bulk scale is $M_6 \sim$ meV.

[35] For example, in the case of the 5D DGP model this leads to the lower bound $r_{c,1} \gtrsim H_0^{-1}/100$ [69, 5]. It is conceivable that a similar bound applies here, too.

special role because it is allowed to propagate freely in the bulk.

In the first part of this section, we will review the physics of these compact models. In particular, we will see that they represent a UV modification of GR (in contrast to the BIG model which is an IR modification), admitting hence a local 4D EFT at low energies. This in turn elucidates the model's prospects with respect to the electroweak hierarchy problem, raising also hope about its potential to address the CC problem.

In the second part, we discuss a simple prototype model based on 6D GR, a standard Maxwell compactification and two pure tension branes that curve the extra space into a rugby ball shape. Although the model fails in addressing the CC problem, it guides us towards more sophisticated supersymmetric constructions. In addition, we introduce the diagnostic means needed to infer the potential of a particular proposal with respect to the naturalness issue. In other words, the discussion here is a blueprint for our investigation of the SLED proposal in Chap. 6.

1.5.1 A second example of an effective field theory

In this section, we briefly summarize the physics of models with compact extra dimensions. Yet again, this can be done by employing the EFT framework. We introduce the length scale L_B, representing the characteristic size of the extra dimensions. Due to the compactness of the extra space, the bulk fields (including the metric $\boldsymbol{g}$) can be decomposed into a discrete set of Fourier modes, which from a 4D perspective play the role of an infinite tower of massive fields, so-called Kaluza Klein (KK) modes.[36] To be precise, the familiar 4D metric, subject to (1.1), arises as the zero mode (corresponding to a vanishing extra space momentum) of the 4D components of the bulk metric $\boldsymbol{g}$. Furthermore, the higher momentum modes in the expansion of $\boldsymbol{g}$ give rise to additional massive spin-two fields, viz. the KK-modes. The typical mass scale is set by the inverse size of the extra dimensions, i.e. $m_{\rm KK} \sim 1/L_B$. It is straightforward to show that the coupling of the zero mode to the SM is controlled by an effective Planck mass,

$$M_{\rm Pl}^2 \sim M_D^{D-2}\, V\,, \tag{1.25}$$

where $V \sim L_B^n$ is the volume of the compact space. Thus, also in the compact framework, $M_{\rm Pl}$ should be thought of as a derived quantity, albeit the physical mechanism is different: While in the BIG context $M_{\rm Pl}$ arises due to loops of localized particles, here it is a consequence of integrating out the extra space. On the other hand, the extra space components of $\boldsymbol{g}$ are the moduli that describe the size and shape of the extra space. In a realistic setup where the extra space is stabilized they are all massive.[37]

[36] Originally, Kaluza and Klein considered 5D gravity compactified on $\mathcal{M}_4 \times \mathcal{S}_1$ [106, 108].

[37] As a simple illustration consider the ring regularization of the brane, as used before in Sec. 1.4. There, the additional brane dimension itself is a simple example of a compact space of scale R. Then, a radion field, constituting a particular extra space component of the brane induced metric, describes fluctuations of the ring/brane size. Stabilizing it endows the radion with a mass of order $\sim 1/R$, in agreement with the present discussion.

We now turn to the crossover physics of compact dimensions. They can be best understood by considering a point mass M_0 on the brane, giving rise to a 4D Newtonian potential

$$V(r) \sim -\frac{M_0}{M_D^{D-2}} \begin{cases} \dfrac{1}{r^{D-3}} & (\text{for } r \ll L_B) \\ \dfrac{1}{Vr} & (\text{for } r \gg L_B) \end{cases} . \tag{1.26}$$

Both limiting cases, can be inferred from a simple geometrical picture:

For short distances far below the bulk scale, we encounter a higher-dimensional scaling. The reason is that at those scales, the field lines are insensitive to the compactness of the bulk space; in fact, they spread as they would in the non-compact six-dimensional case, and hence, due to Gauss's theorem, give rise to the above scaling. This is also compatible with the KK-language because, on short scales, we have to take into account the whole tower of KK-modes, which in turn necessitates to work in the higher-dimensional representation of the theory.

On the other hand, for large distances, the gravitational flux is strongly affected by the compactness of the extra space. Now, with the flux lines being effectively confined inside the compact space, the potential is only SO(3) symmetric [instead of SO$(3+n)$], implying a 4D scaling law, where $M_{\rm Pl}$ can be identified according to (1.25). A reasoning in terms of KK-modes leads to the same outcome: For distances $r \gg L_B$ the massive KK-modes can be integrated out, thus yielding the theory of 4D GR with an effective gravity scale (1.25). This is possible because there is a mass gap between the graviton zero mode and the first KK-mode of typical size $\sim 1/L_B$.

Now, the phenomenologically interesting question is how (1.26) is corrected in an intermediate regime. To answer that question, we start in the 4D regime and then move to smaller and smaller distances. Accordingly, the KK-modes have to be integrated in successively. As the they couple with gravitational strength, their (Yukawa type) contribution to the gravitational potential becomes

$$-\mathcal{O}(1)\frac{M_0}{M_{\rm Pl}^2}\frac{\mathrm{e}^{-r/L_B}}{r} , \tag{1.27}$$

and hence gets relevant for distances $r \lesssim L_B$, i.e. close to the size of the extra dimension. Effectively, these contributions make the gravitational force weaker. From an extra space perspective, this can be understood as a consequence of the spread of gravitational field lines into the bulk, which dilutes the gravitational field.

The model has different desirable properties:

- It admits a fundamental Planck scale M_D of the order of the TeV scale, thereby (almost completely) avoiding the quantum instability of the Higgs mass.
- Here, the large value of $M_{\rm Pl}$ is a consequence of the large extra space volume, and thus, the hierarchy problem changes its guise dramatically: Instead of explaining

why $M_{\rm Pl}$ is so large (compared to the electroweak scale), we have to come up with a reason why V is so large (compared to M_D). While this does not avoid the problem, it paves the way towards a new class of solutions.

- The six-dimensional model is most predictive and hence of particular interest: Here, due to (1.25), an extra-dimensional volume that is set by the length scale $100\,\mu$m leads to a bulk scale of order 10 TeV. In other words, if deviations from the Newtonian inverse square law are measured not far below the hundred micron scale (which has not yet been ruled out observationally), we expect quantum gravity effects at the 10 TeV scale, which might lead to detectable signatures in present collider experiments.[38] On the other hand, for higher-dimensional realizations this class of models is less predictive. To be specific, in 7D, a bulk gravity scale of the same size as before (or above) requires nanometer (or smaller) sized extra dimensions which is far beyond today's observational reach. For the rest of this thesis, we hence focus on the six-dimensional case.

The most stringent phenomenological input exists for the extra space volume (instead of M_D). We hence proceed by discussing the present (upper) limit on V ($\sim L_B^2$). In fact, such a bound is obtained in lab experiments (successors of the Cavendish experiment) by searching deviations from the Newtonian inverse square law, as parametrized in (1.27).[39] To be specific, the characteristic bulk scale L_B should be below a hundred microns, corresponding to a KK mass scale (or compactification scale) of at least 10 meV. This implies that the bulk scale is not allowed to be significantly below ~ 10 TeV. The bound is conveniently stated in a dimensionless way,

$$V M_6^2 \lesssim 10^{28}\,. \tag{1.28}$$

Note that even though the compactification scale is rather small (compared to the electroweak energy scale), from the perspective of a brane observer, the presence of the extra dimensions is only mediated gravitationally, and hence very weakly. That is the reason why high energy processes of SM particles on the brane are only very mildly affected by the presence of the extra dimensions.

Let us finally discuss what prospects models with compact extra dimensions offer with respect to the CC problem. Due to the compactness of the extra space, we encounter a potential pitfall: We have seen that at low energies the bulk fields (or KK-modes equivalently) can be integrated out yielding a local theory of 4D gravity. However, within this 4D EFT Weinberg's theorem seems to be applicable again, making a fine-tuning necessary. Yet, this is only true if the corresponding EFT cutoff lies significantly above the observed energy density $M_{\rm Pl}^2 H_0^2$. Otherwise, there is no CC problem to start with because all (dynamically resolved) particle masses are below the EFT cutoff and hence give a quantum contribution

[38] Recent measurements, which typically look for an energy loss into the extra dimensions [84, 85], provide a lower bound on M_D of about 3 TeV [81] (the precise value depends on the model under consideration).
[39] For recent experimental bounds see [107] and for a general review [103] (and references therein).

to the CC below the observed value. And indeed, by comparing the (smallest possible) compactification scale, 10 meV, and the observed energy density $M_{\rm Pl}^2 H_0^2 \sim (\text{meV})^4$, we find that both scales are in the same ballpark. In other words, whatever mechanism might be responsible for diminishing the gravitational impact of the CC, it has to be based on nontrivial bulk physics (and hence might circumvent Weinberg's argument). The prospects of compact 6D models mainly rely on this observation.

However, so far this is merely a hope based on several necessary requirements; in particular, by integrating in KK-modes we can raise the cutoff scale of the 4D theory. In that case, we again lack a clear understanding of how Weinberg can be avoided.[40] Thus, to make the above arguments more concrete (and to provide a motivation for supersymmetric models), we are going to discuss a simple prototype model in the next section.

1.5.2 A prototype study

To set the stage for the discussion of compact braneworld models, we consider the simplest realization, comprising two branes, a Maxwell sector to stabilize the compact space and 6D GR with Planck scale M_6 as the gravitational theory active in the bulk. The corresponding action reads,[41]

$$\mathcal{S} = \int \mathrm{d}^6X\sqrt{-g_6}\left\{\frac{M_6^4}{2}\left[\mathcal{R}_6 - 2\lambda_6\right] - \frac{1}{4}F_{MN}F^{MN}\right\} - \sum_b \int \mathrm{d}^4x_b\sqrt{-g_b}\,\lambda\ , \tag{1.29}$$

where λ_6 is a bulk CC and the index $b \in \{+,-\}$ runs over both branes situated at the north $(+)$ and south $(-)$ pole of the compact space. For simplicity both tensions have the same value λ.[42]

Here, we limit ourselves to a brief discussion of the main properties of the model (1.29) while further details can be found in Chap. 6. A 4D maximally symmetric solution, corresponding to a rugby ball shaped extra space, is given by [27]

$$\mathrm{d}s^2 = -\mathrm{d}t^2 + \mathrm{e}^{2H_0 t}\,\mathrm{d}\boldsymbol{x}^2 + \mathrm{d}r^2 + \left(1 - \frac{\delta}{2\pi}\right)^2 \sin^2\left(\frac{r}{L}\right) L^2\mathrm{d}\phi^2\ , \tag{1.30}$$

where the deficit angle is determined by the brane tensions, $\delta = \lambda/M_6^4$. This matches the relation inferred for our prototype model (1.13) with infinite volume extra dimensions. In fact, we recover the solution (1.14) in the limits $r \to 0$ and $r \to L$, which demonstrates that both solutions have the same conical geometry close to the brane. With regard to the Maxwell solution, it suffices to state that it corresponds to a topologically nontrivial

[40] This is the crucial difference between models with finite and infinite extra dimensions. For the latter, the mass gap vanishes, implying the existence of a continuous spectrum of KK-modes, which in turn renders the 4D theory nonlocal [66].

[41] This model has been discussed for instance in [43, 112, 38, 127, 47].

[42] This condition will be relaxed in the bulk of this thesis, though, without changing the main conclusions. Here, we merely use it to simplify the presentation.

solution with winding number n.[43]

The integration constant L is related to the extra space volume V via

$$V = 4\pi L^2(1-\bar{\lambda}) \qquad \text{with} \qquad \bar{\lambda} := \frac{\lambda}{2\pi M_6^4} \,. \tag{1.31}$$

There are two phenomenological constraints the model has to comply with: the bound on V in (1.28) and the observed curvature scale H_0 in (1.2). The system admits a solution which relates both quantities, specifically we find[44]

$$12H_0^2V = 2\pi P + \mathcal{O}\left(P^2\right) \quad \text{with} \quad P := \left(1-\bar{\lambda}\right)^{-1}\left[\frac{\lambda_6}{M_6^4}\left(\frac{n}{e}\right)^2 - 2\left(1-\bar{\lambda}\right)^2\right] \,, \tag{1.32}$$

where P only depends on model parameters.[45] As the Hubble length $1/H_0$ is hierarchically larger than the typical size of the extra dimensions, the parameter combination P has to be extremely tiny (which justifies the expansion above). At this point, we encounter a major deficiency of (1.29). To be precise, by using the bounds (1.2), (1.28) and Def. (1.25), we derive an observational constraint on the left side of (1.32),

$$12H_0^2V \lesssim 10^{-66} \,. \tag{1.33}$$

If we now consider variations $\delta\lambda$ of the brane tension (or 4D CC equivalently), they have to be extremely small in order not to be in conflict with (1.33), explicitly,

$$\frac{\delta\lambda}{M_6^4} \lesssim 10^{-66} \,. \tag{1.34}$$

This means that the tension (measured in units of the fundamental bulk scale $M_6 \sim 10\,\text{TeV}$) has to be tuned with a precision of 66 decimal places. This is exactly what we consider not to be technically natural. On the other hand, if we refrain from introducing hierarchies into (1.29) by hand, all dimensionful parameters are set generically by the bulk gravity scale M_6, leading to $P \sim 1$, which is vastly incompatible with the observational constraints. To make contact to the literature, we consider the special case of a vanishing on-brane curvature, i.e. $H_0 = 0$. Then, Eq. (1.32) implies the parameter constraint $P \equiv 0$, which convincingly reproduces the result in [82, 128, 137].

Even if we are willing to accept the tuning (1.34), we encounter a second drawback. The extra space volume is related to the bulk CC via

$$VM_6^2 = \left(1-\bar{\lambda}\right)\frac{2\pi M_6^2}{\lambda_6} + \mathcal{O}\left(P\right) \,. \tag{1.35}$$

[43] A winding number $n > 0$ implies a nontrivial bulk profile of the Maxwell solution. It cannot be transferred into a trivial profile without violating the continuity of F along the compact space. In other words, n is a conserved quantity.

[44] There is also a second branch that only worsens the situation and is thus omitted in our discussion.

[45] The constant e is the U(1) gauge coupling related to the Maxwell sector in (1.29).

Yet again, this implies a tuning of model parameters: In order to saturate the phenomenological bound (1.28) (which is the physically interesting scenario), we have to tune λ_6 close to zero with a precision of (at least) 14 decimal places. To arrive at that statement, we used $P \approx 0$ to simplify the right side of (1.35).

With respect to the CC problem, we are basically back at square one. The situation is even worse because the phenomenological bounds imply two independent and unacceptable tunings of model parameters. However, this was only the first trial and we should further press on with these model. In particular, there is an important lesson to be learned: The second problem is solely caused by the presence of a bulk CC. In fact, this observation suggests to include supersymmetry in the bulk to make a small (or vanishing) value of λ_6 a technically natural choice.

Historically, this reasoning gave rise to the SLED model [156, 6, 24, 25]. In its simplest form it is obtained from (1.29) by including a dilaton field ϕ which renders the bulk theory scale invariant (SI). As a bulk CC is incompatible with SI, this implies that λ_6 can be set to zero consistently. This theory will be the starting point of our considerations in Chap. 6. In particular, we will critically assess claims in the literature stating that the model with a localized Maxwell term on the brane (which breaks SI explicitly) solves the CC problem [33, 34, 35]. To that end, we will employ a similar approach to the one used here for the non-supersymmetric model (1.29). Specifically, we will derive a relation between the 4D curvature and the extra space volume, similar to the one in (1.32), which in turn allows us to confront the model with phenomenological bounds.

In anticipation of our results, it will be possible to make the volume hierarchically large without tuning the model parameters. Thus, the problem related to Eq. (1.35) is indeed avoided. However, this comes always at the price of a 4D curvature that is way too large.

1.6 Summary of results

In this section our main scientific results are summarized. At the same time, we provide a structural guide for this thesis.

Chapter 2

We investigate the linear stability of the BIG setup in 6D for a conical background geometry, originating from a brane with sub-critical tension, i.e. $\lambda < 2\pi M_6^4$. The vacuum persistence amplitude is used as a diagnostic tool to probe for ghost instabilities. After regularizing the brane as a ring of microscopic size, we find that the parameter space is divided into two regions: If the brane tension is sufficiently large, the model is free of any ghost instabilities and hence represents a fully consistent modification of GR. In particular, for a choice of induced brane parameters that is compatible with the requirements of a natural EFT, the theory is stable. On the other hand, if the tension is tuned to be unnaturally small, a ghost occurs in the dynamical spectrum and thus leads to an (unacceptable) instability of the background spacetime. In accordance with a former result in

the literature [104], a small near-critical stripe of the stable parameter regime is singled out as being phenomenologically interesting.

For the special case of a vanishing brane tension, we are able to reconcile old contradicting statements in the literature. Specifically, by uncovering the errors made in [19] (to which the author contributed), we confirm that the ghost is present in accordance with [58, 94]. By performing a full-fledged Hamiltonian analysis, this result is generalized to arbitrary codimensions. There, the ghost manifests itself as a negative, brane localized contribution to the energy density. This analysis, as it does not rely on a specific regularization, admits a nontrivial (and successful) test of the universality of our previously used regularization scheme.

Chapter 3

Motivated by the observation that the 6D BIG vacuum is stable if the brane tension is large enough, we study the cosmology of the model. To that end, we solve the nonlinear system of bulk equations and brane matching conditions numerically. We find that a brane with FLRW symmetries acts as an antenna that absorbs and emits cylindrically symmetric gravitational waves, a generalization of Einstein-Rosen waves in 4D. We find three different types of solutions:

1. Unstable sub-critical cosmologies for which the Hubble parameter grows unbounded and the effective energy density that sources the 6D Einstein equations becomes negative. Moreover, it is no longer possible to stabilize the transverse size of the brane in terms of physical matter. The ghost mode of the linear analysis is identified as the cause of this pathological and highly unphysical behavior.

2. Stable sub-critical cosmologies that feature a dynamical degravitation mechanism. Despite the presence of a non-vanishing brane tension, Hubble settles to zero within a few Hubble times. From an extra space perspective, this process is accompanied by the emission of Einstein-Rosen waves into the bulk. Unfortunately, these cosmologies are incompatible with having a 4D regime and therefore have to be dismissed on phenomenological grounds.

3. Super-critical solutions for which the 4D energy density on the brane exceeds the fundamental gravity scale in the bulk. In that case, the bulk spacetime closes in a second axis, representing a further sub-critical brane. We find a special (sub-)class of fully analytic scaling solutions in the 4D maximally symmetric case. They are stable under FLRW fluctuations and predict a non-vanishing (constant) value of the Hubble parameter. However, to be compatible with observations, the brane tension has to be tuned with an unacceptably high precision.

Although we find solutions that realize degravitation and other ones that might be phenomenologically viable, both features never occur simultaneously. Nevertheless, our findings pave the way towards higher-dimensional BIG models, for which the prospects are better. In particular, the methods developed for the 6D case can also be applied to higher dimensions.

Chapter 4

We take the super-critical scaling solutions, discussed in the BIG context, as the starting point of a new class of compact 6D models. There, a super-critical brane tension, i.e. $\lambda > 2\pi M_6^4$, curves the bulk spacetime into a cigar, hosting two branes at its respective ends: a super-critical one, which sets the transverse size of the extra space, and a second sub-critical one, which is microscopically small. The latter is then identified as a candidate of our universe. The important finding is that both branes expand at a different (constant) rate set by both brane tensions. In other words, these solutions exemplify how a 4D de Sitter geometry can be realized in a braneworld context. This makes them also interesting from a phenomenological point of view. We find two branches of solutions, for one of them we are able to numerically prove its stability under FLRW fluctuations. In the next step, we ask whether these solutions help with the CC problem and find a negative answer: For both branches the tensions have to be tuned to an unacceptable degree in order to realize a phenomenologically small curvature on one of the branes. This failure is attributed to the compactness of the extra space, which ultimately makes Weinberg's theorem applicable again. We conclude by sketching possible directions of future research.

Chapter 5

The 5D DGP model is supplemented with an additional compact brane dimension, which makes it a 6D hybrid as it now consists of an infinite as well as a finite extra dimension. In a embedding picture the bulk spacetime corresponds to a cylinder around which a codimension-one brane is wrapped. The model is interesting for two reasons: First, it is the simplest model for which a brane with FLRW symmetries emits bulk gravitational waves. Second, the model admits degravitating solutions and hence is interesting with respect to the CC problem. We derive a (closed) set of modified and local Friedmann equations on the brane which in turn enables us to study the cosmological expansion history. We find two types of cosmologies:

1. If the compact dimension is stabilized, we reproduce the normal branch of the DGP cosmology for early times. However, at late times the stabilization in terms of physical matter breaks down, thus implying a new modified regime, physically characterized by the existence of outgoing gravitational waves. This solution is particularly interesting because the strength of the modification can be arbitrarily adjusted (by dialing the model parameters) as required to be compatible with observations.

2. If the compact brane dimension is allowed to freely expand (and contract), a new type of degravitating solution is found. Physically, the mechanism relies on diverting the gravitational effect of the brane tension in an expansion of the compact dimension (instead of the three infinite, spatial brane dimensions). This solution has a wide attractor regime, however, by performing a supernova fit, we find that it fits observational data only poorly. On a conceptual level, though, it nicely exemplifies the virtue of models with infinite dimensions as potential solutions to the CC problem.

Chapter 6

According to claims in the literature [33, 34], the CC problem can be solved in a particular 6D braneworld construction—usually referred to as SLED model—that relies on a sub-millimeter sized extra space, stabilized by a Maxwell flux that winds around its compact dimensions. A 6D dilaton field is employed to make the bulk theory scale invariant. The mechanism then relies on two ingredients: First, the tension curves the bulk into the shape of a rugby ball, and second, a fine-tuning which normally enters via the flux quantization condition is avoided by introducing an additional brane localized flux term, which breaks scale invariance explicitly. That way, Weinberg's theorem is supposedly circumvented. We carefully assess that claim and find that the mechanism does not work the way it was designed. This is done in two steps:

1. We show that a vanishing 4D curvature (in other words degravitation) is only guaranteed by a brane localized flux that preserves scale invariance. However, this makes Weinberg's theorem applicable again and thus reinstates the constraint character of the flux quantization condition. The mismatch with the old results is traced back to an erroneous dilaton boundary condition.

2. We ask whether a non-vanishing but phenomenologically small 4D curvature can be realized for generic values of the model parameters. This constitutes the ultimate check of the model's capacity to solve the CC problem. To dispose of divergent radial derivatives at the brane position, we regularize the brane as a ring of fixed circumference. Then, we discuss two sources of scale invariance breaking, which effectively contribute to the 4D curvature and should both be included in a physical setup: An explicit breaking caused by a coupling of the dilaton to the brane tension as well as additional contributions related to the finite microscopic width of the brane. Unfortunately, we arrive at a negative result. Provided that the tension and the microscopic size of the brane take generic values set by the fundamental bulk Planck scale, we encounter a severe phenomenological problem: Either the 4D curvature or the size of the extra dimensions is unacceptably large. Subsequently, we confirm the assumptions used to derive that result by solving the whole system numerically. Moreover, we quantify the amount of tuning needed to fulfill the phenomenological bounds. And indeed, we find that the tuning for each individual bound can be avoided by adapting the brane-dilaton coupling, but never for both of them simultaneously. In addition, the phenomenological problem becomes even worse in that case.

We conclude that these findings provide the biggest challenge to the SLED proposal.

Chapter 2

BIG: Consistency of 6D braneworlds

Note: Most of the results presented in this chapter were published together with Felix Berkhahn and Stefan Hofmann [19], and more recently together with Ludwig Eglseer and Robert Schneider [75]. Sec. 2.3 and Sec. 2.4.3 are verbatim reproductions of corresponding sections in [75].

We start with an extensive discussion of the linear consistency of the BIG model. The scope of our findings goes beyond the BIG setup and addresses the consistency of braneworlds in general. The reason is that the localized part of the BIG action generically arises as the low energy description of any (covariant) braneworld theory (cf. introductory discussion in Sec. 1.4). With regard to the dimensionality, we first consider the general D-dimensional case and specialize later to 6D. The corresponding action reads,

$$\mathcal{S} = \mathcal{S}^{(D)}_{\rm EH}[\boldsymbol{g}_D] + \mathcal{S}_{\rm EH}[\boldsymbol{g}] + \mathcal{S}_\lambda[\boldsymbol{g}] + \mathcal{S}_{\rm m}[\boldsymbol{g}] \,, \tag{2.1}$$

where the first term is the bulk Einstein-Hilbert term and the second one its brane localized counterpart, both defined in (C1). The third term, specified in (C3), represents an effective description of the localized energy density λ, normally referred to as the brane tension. Physically, it can be understood as the binding energy which holds the brane together.[1] The last term denotes additional matter fields that are localized on the brane. According to the braneworld paradigm, it contains all non-gravitational matter our apparent universe consists of. The corresponding model parameters are the bulk gravity scale M_6, the brane induced scale $M_{\rm Pl}$ and the brane tension λ. A priori, all three of them can be chosen independently (cf. Sec. 1.4).

First, it is straightforward to show that the model admits the deficit angle solution. The reason is that the induced gravity term simply vanishes if evaluated for (1.14) due to the flat 4D part of the metric. In other words, there is a continuum of Minkowski vacua on the brane, corresponding to different (sub-critical) values of λ ($< 2\pi M_6^4$). To this solution the model owes all its potential with regard to the CC problem. As explained extensively in the introduction, it constitutes a nonlinear realization of the degravitation idea (cf. [66, 65, 70, 50]) because the gravitational impact of the 4D CC (which otherwise

[1] This becomes more transparent if the brane is resolved microscopically, for example, as a Nielsen-Olesen vortex [136]. Then the brane tension is associated with the gradient and potential energy of a (topologically nontrivial) field vacuum configuration.

gives rise to the CC problem) is diverted into extrinsic bulk curvature, invisible to a brane observer [154, 41, 12].

There is an old controversy in the literature about the stability of these vacua. To be specific, for $\lambda = 0$ the authors in [58, 94] revealed the existence of a ghost mode in the dynamical spectrum of the theory. On the other hand, in [19] (to which the author also contributed) the absence of a ghost was claimed—again exclusively for $\lambda = 0$. Moreover, the analysis in [104], valid for general λ, provided evidence for a stable (near-critical) regime while in another parameter region a strongly coupled scalar was identified (instead of a ghost), thus signaling the breakdown of the linear expansion. The main purpose of this first chapter is to reconcile the old results and to arrive at a final verdict about the linear stability of (1.14) as a vacuum of the BIG model. On a technical level, this is achieved by deriving the fluctuation theory on that background, which in turn admits a statement about its (classical and quantum) stability. As this is a rather complicated analysis, we will follow a three step approach:

1. In Sec. 2.2, we will start by studying a scalar toy model in one and two codimensions, which serves as a warm-up exercise. That way, we elucidate (and review) the crossover physics, which make the model interesting from a phenomenological point of view. Moreover, this study provides us with the techniques needed to infer the consistency of the full gravitational model. Specifically, we calculate the vacuum persistence amplitude $\langle 0|0\rangle_J$ in the presence of an external source J. This object is then used as a diagnostic tool to detect the presence of a ghost mode. To be precise, if it evaluates to > 1, this is incompatible with having a unitary time evolution, hence signaling the presence of a ghost mode.

2. In the subsequent Sec. 2.3, we turn to the full gravitational model and first probe the stability of the trivial geometry with $\lambda = 0$ (or vanishing deficit angle equivalently). This is done in two ways: First, by using the vacuum persistence amplitude in a manifestly covariant language, and second, by deriving the Hamiltonian on the constraint surface. Both analysis are valid for general dimensionality D and yield an unambiguous answer: The ghost result of [58, 94] is correct. We are also able to reconcile this outcome with the contradicting statement in [19]; accordingly, the errors made therein are pined down explicitly.

3. The last step is made in Sec. 2.4 where we generalize the covariant analysis to arbitrary (but sub-critical) values of λ. By deriving yet again the vacuum persistence amplitude, we arrive at our final result:[2]

   The model is stable—and hence ghost free—if and only if the tension is large enough.

[2] In [64] it was shown in the DGP case that a strong coupling of the helicity-0 mode can be avoided in the presence of a domain wall with non-vanishing tension. As from the bulk perspective a domain wall corresponds to a codimension-two object, it is plausible that the ghost avoidance in our case has the same physical origin (though a detailed analysis is still missing).

Before we plunge into the details, we still have to deal with a technical complication that generically shows up in higher-codimensional scenarios: The bulk fields diverge at the position of an infinitely thin brane. Of course, this divergence is just a relict of the over-idealization of having a vanishing thickness, and hence no physical threat. We deal with this by promoting the codimension-two brane to a codimension-one object. Form an extra space perspective, we replace the point-like brane by a ring of circumference $2\pi R$. We discuss the physics behind this choice extensively in Sec. 2.1. In particular, we put a lot of emphasis on the question of how the compact brane dimensions can be stabilized consistently. We provide a final discussion in Sec. 2.5. There, we first demonstrate that our findings are compatible with an EFT picture, and second, we assess the phenomenological significance of our results.

2.1 Our universe as a hollow sphere

Braneworld models are all based on the assumption that our SM matter fields are localized on a space-like hypersurface that is embedded in a higher-dimensional bulk spacetime. From a fundamental perspective, this requires the existence of an appropriate localization mechanism. A simple and yet effective way of achieving this can be realized in the context of topological defect models. Let us focus on a codimension-one and -two example.

In models with a spontaneously broken discrete symmetry domain wall solutions, also called *kinks*, may arise. These topologically nontrivial field configurations separate two space regions (domains), each corresponding to a specific vacuum which is—due to the discrete nature of the symmetry—not continuously connected to the other. They can be constructed in any number of spatial dimensions. Accordingly, the transition region between the two domains corresponds to a codimension-one brane. Bearing in mind this underlying model, it is clear that the brane cannot have zero width because this would imply a diverging gradient energy. On the other hand, if the transition region is broadened, the potential energy grows. Thus, seeking the minimum of the combined energies, leads to a characteristic defect width $R \neq 0$. Within this microscopic picture, the brane tension emerges as the non-vanishing gradient and potential energy within the transition region. So far the brane is a rather boring object, however, by introducing interactions to other fields, it is possible to localize fields within the defect [153], which are ultimately intended to represent our SM particles.

Similarly, a codimension-two brane can be realized within a model that allows for a spontaneously broken U(1)-symmetry. As a prototype model, we consider the Abelian Higgs model which admits a topologically nontrivial solution that in three spatial dimensions is known as a Nielsen-Olesen vortex [136]. Yet again, it comes equipped with a nonzero transverse thickness and admits a localization of particles within the defect.

As discussed in [62], the idea of having a smooth solitonic brane, can be generalized to any codimension. Having this fundamental picture in mind, it is clear that the thin brane model (2.1) is only valid as some sort of effective description valid at low energies. In other words, as long as we want to describe physics at a length scale $\ell_0 \gg R$, we do not need

to resolve the microscopic structure of the brane, in particular, there are cases where the brane can even be described as an infinitely thin object.[3]

However, on a technical level, a thin brane description gives rise to certain difficulties: In higher codimension, the gravitational field generically diverges at the position of an infinitely thin brane. From a physical perspective, these singularities have the same origin as those arising in electrostatics: While a (homogeneously) charged plate does not produce a divergent electrostatic potential, this is no longer true for a charged string, for which the potential diverges logarithmically at the source position. The divergence becomes more severe when the number of codimensions is increased. Since in the case of braneworld models we want to describe physics inside and very close to the brane, we have to find a way of regularizing the theory. In other words, we have to omit the over-idealization of having a thin brane. Different methods have been used throughout the literature to achieve this:

1. The simplest possibility consists in introducing a momentum cutoff Λ when calculating for example the brane-to-brane propagator in the linear theory on some background. While this is a very convenient method, it has the disadvantage of being limited to the linear theory.

2. Another possibility consists in including higher order operators in the action that are suppressed by a scale M_*. From an EFT viewpoint these operators are present anyhow and can thus be naturally included by identifying $M_* \sim M_D$. It can be shown that they effectively cut off the momentum integration at the bulk gravity scale M_*. Moreover, this tells us that we cannot resolve the brane at length scales below $1/M_*$ within a consistent EFT.[4] Again, it is hard to implement this method on a nonlinear level.

3. Further methods are usually based on introducing a transverse brane width R; there are different known implementations: The authors in [62, 94] used a blurring function with limited (transverse) support to smear out the brane fields, in [129] (without BIG terms) a generic (but regular) radial profile of the localized matter fields was demanded, and in [142, 104, 32] the codimension-two brane was replaced by a ring in extra space, thus giving rise to a codimension-one brane with one additional compact dimension of microscopic size R. Moreover, it would be even possible to go back to the more fundamental solitonic description discussed above and dynamically resolve the fields that created the brane in the first place.[5]

The crucial point is that as long as we are interested in low energy questions taking place at length scales $\ell_0 \gg \{1/\Lambda\,, 1/M_*\,, R\}$, respectively, we should be insensitive to the details of the regularization scheme. In particular, when giving a thickness to the brane, it should not matter in which precise way this is done. Throughout this work we will check

[3]The DGP model (in 5D) is normally treated in the thin brane approximation.
[4]This observation gave rise to the UV softness idea of [66].
[5]An explicit construction for a compact model was discussed in [28].

that this is indeed the case. Note that, although our results will not depend on how we regularize the brane, there will be a certain dependence on the regularization scale itself. That can be understood as the low energy manifestation of the—so far unexplored—UV sector (cf. the EFT discussion in Sec.1.4).

2.1.1 Regularized action

In this thesis, we mostly employ the third regularization strategy. To be precise, we replace the brane by a $(n-1)$-sphere, denoted by $\mathcal{S}_{n-1}$, with proper surface area A_n. In codimension-two this corresponds to a ring with circumference $2\pi R$. Thus, the brane is a d-dimensional manifold consisting of $(3+1)$ infinite and $(n-1)$ compact dimensions. This regularization has certain technical advantages: We can use the covariant formalism of [100, 101] to describe the matching between the interior and exterior vacuum region. The on-brane geometry is then fully characterized by the induced metric on the n-sphere which is the pullback of the bulk metric. A successive dimensional reduction à la Kaluza and Klein of the compact sphere dimensions then allows us to recover a four-dimensional gravity regime [106, 108, 152]. Technically, this regularization amounts to a formal replacement in (2.1),

$$\mathcal{S}_{\rm EH}[\boldsymbol{g}] + \mathcal{S}_{\lambda}[\boldsymbol{g}] + \mathcal{S}_{\rm m}[\boldsymbol{g}] \;\longrightarrow \int\limits_{\mathcal{M}_4\times\mathcal{S}_{n-1}} \mathrm{d}^d\tilde{x}\,\sqrt{-\tilde{g}}\left[\frac{\tilde{M}^{d-2}}{2}\tilde{\mathcal{R}} - \tilde{\lambda} + \tilde{\mathcal{L}}_{\rm m} + \mathcal{L}_{\rm stab}\right] , \tag{2.2}$$

where the following d-dimensional objects on the codimension-one brane were introduced: the induced gravity scale $\tilde{M}$, the tension $\tilde{\lambda}$, the induced metric $\tilde{\boldsymbol{g}}$ and its corresponding Ricci scalar $\tilde{\mathcal{R}}$. The induced coordinates are denoted by $\tilde{x}^\alpha$. The previously introduced brane tension λ and induced Planck mass $M_{\rm Pl}$ can be identified according to

$$\lambda = A_n\,\tilde{\lambda} \qquad\qquad \text{and} \qquad\qquad M_{\rm Pl}^2 = A_n\,\tilde{M}^{d-2}\,. \tag{2.3}$$

The regularization length scale R is related to A_n via

$$A_n \equiv S_{n-1}R^{n-1}\,, \tag{2.4}$$

where S_{n-1} denotes the surface area of a unit n-sphere. To convince ourselves that these definitions are sensible, we evaluate them for a Minkowski geometry in the six-dimensional model ($d=5$), and indeed, we find the usual expression for the relation between the 4D and 5D gravity scale, $M_{\rm Pl}^2 = 2\pi R\,\tilde{M}^3$ [cf. Eq. (1.25)], and between the 4D and 5D tension, $\lambda = 2\pi R\,\tilde{\lambda}$.

In general, the surface area of the sphere, A_n, will depend on time (and the brane coordinates) because the volume factor $\sqrt{-\tilde{g}}$ is time-dependent. However, in order to have a consistent regularization, we require in the majority of cases the proper surface area to be strictly constant. This can be achieved by assuming the existence of some underlying stabilization mechanism in the microscopic theory [represented by $\mathcal{L}_{\rm stab}$ in (2.2)]. In our

low energy description, this can be effectively achieved by dialing the pressure in angular direction. Of course, we always have to check a posteriori that this pressure can be realized through physical matter, meaning that the corresponding equation of state parameter has to be ≥ -1. Stabilizing the surface area in such a way corresponds to the assumption that the microscopic theory is stable, too. However, such a requirement is not too far-fetched because we know that there *are* stable configurations like the vortex solutions discussed above.

In the course of our 6D analysis in Sec. 2.4.3, we even go one step further and resolve the stabilization mechanism by wrapping a scalar field around the compact ring/brane dimension. This construction goes back to Scherk and Schwarz (cf. [157]) and introduces the radion of mass $m_\varphi \propto 1/R$ as the size modulus of the ring dimension. According to our introductory discussion in Sec. 1.4, this field can be integrated out if we are interested in the low energy dynamics of the system. In fact, we will see that this is equivalent to ignoring fluctuations of the brane size from the outset (by setting the ring circumference—or the surface area A in higher dimensions—to a constant value). Thus, we provide explicit prove of the validity of our effective pressure stabilization.

To summarize, we describe the brane as a hollow $(n-1)$-sphere of constant proper surface area A. This can always be achieved by imposing a certain angular pressure corresponding to a time-dependent equation of state parameter. This effective low energy description is valid for length scales

$$\ell_0 \gg R\,, \tag{2.5}$$

in particular, we expect it to be insensitive to the details of the regularization in this regime. For (late time) cosmological applications, where $\ell_0 \sim 1/H_0$, this consistency requirement corresponds to a hierarchy of at least 30 orders of magnitude (when R satisfies the experimental bound) and hence is well satisfied. On the other hand, if we were interested in describing sub-millimeter physics, we would need to specify a certain UV model.

2.1.2 Modified Einstein equations

The aim of this section is to provide an explicit expression for the modified Einstein equations when the hollow sphere regularization is applied. They constitute the starting point for all further discussions of the BIG model in this thesis.

The bulk is assumed to be free of any sources except for the brane.[6] This implies a $\mathrm{SO}(n)$-symmetry in the extra space and motivates the use of (generalized) spherical coordinates $X^A = (t, x^i, r, \phi_1, \ldots, \phi_{n-1})$ with the standard index ranges. The brane position in extra space is then denoted by $r_0(t, x^i)$, which in general is a function of time and the spatial coordinates x^i. The dynamical description of the full system comes in two parts. First, since the bulk is free of any sources, the D-dimensional Einstein tensor has to satisfy the

[6] For simplicity, we set the bulk CC to zero. This is certainly not a natural choice but simplifies the calculations a lot. Of course, if we find a promising solution with respect to the CC problem, we would need to drop that assumption ultimately.

vacuum field equations away from the brane ($r \neq r_0$),

$$G^{(D)}_{AB} = 0\,. \tag{2.6}$$

Second, these equations have to be supplemented by appropriate boundary conditions and matching equations. At the axis ($r = 0$) the metric has to be regular,

$$\lim_{r\to 0} \partial_r g_{AB} = 0\,, \tag{2.7}$$

as well as elementary flat which translates to[7]

$$\lim_{r\to 0} \frac{1}{r^{n-1}} \int_{\mathcal{S}_{n-1}} \mathrm{d}\Omega \sqrt{g_\Omega} = S_{n-1}\,, \tag{2.8}$$

where $\boldsymbol{g}_\Omega$ denotes the angular part of the metric; due to the rotational symmetry in extra space, it factorizes from the rest of the metric. The physical reason for the last requirement is that there is no matter sitting at the (regularized) axis, which prevents the spacetime from being singular at that point. Furthermore, we have to demand appropriate fall-off conditions at radial infinity. Finally, we match the interior to the exterior geometry by taking into account the presence of induced matter fields $\tilde{\boldsymbol{T}}$. This can be done in a manifestly covariant way by using Israel's junction conditions [100, 101], describing the jump of the extrinsic curvature across the brane,

$$M_D^{D-2}\Big(\delta^\alpha{}_\beta\,[\tilde{K}^\gamma{}_\gamma]_{\mathrm{disc}} - [\tilde{K}^\alpha{}_\beta]_{\mathrm{disc}}\Big) = \tilde{T}^\alpha{}_\beta - \tilde{M}^{d-2}\tilde{G}^\alpha{}_\beta\,, \tag{2.9}$$

where the discontinuity bracket is defined as

$$[f]_{\mathrm{disc}} := \lim_{\epsilon\to 0} [f(r_0+\epsilon) - f(r_0-\epsilon)]\,, \tag{2.10}$$

and the induced extrinsic curvature tensor $\tilde{K}^\alpha{}_\beta$ is the pullback of the bulk extrinsic curvature,

$$K^A{}_B = \nabla_B n^A\,, \tag{2.11}$$

on the brane. Here, n^A denotes the outward-pointing normal vector on the brane. Eq. (2.9) generically relates the radial profile of the bulk metric to the localized matter fields. In the case of BIG, it also mediates the effect of the localized gravity term, which now contributes to $\tilde{\boldsymbol{T}}$. This equation is also crucial in inferring the modification of 4D Einstein gravity. In fact, if we set the left side of (2.9) to zero, the remaining equation equals the field equation of d-dimensional gravity with $(n-1)$ compact dimensions. We expect this theory in a low energy effective description to reduce to 4D GR (provided of course the size of the sphere is sufficiently stabilized). While this will be shown explicitly in all our 6D calculations, we expect this to happen also for higher codimensions.

[7] In the codimension-two case this corresponds to the absence of a conical singularity, and (2.8) translates to the obvious flat space requirement that the circumference at the coordinate position r equals $2\pi r$.

2.2 Spin-zero prototype

In order to investigate the linear model (2.1), we first focus on a scalar prototype model that is defined on a Minkowski background. As we will see, this model is general enough to capture the dynamics of all gravitational degrees of freedom separately. To be precise, the graviton field $\boldsymbol{h}_D$ ($:= \boldsymbol{g}_D - \boldsymbol{\eta}_D$) can be decomposed in such a way that the equations for all dynamical fields (including helicity-two, -one and -zero modes) completely decouple and can all be independently derived from a scalar action of a particular simple and universal form. Thus, by studying the scalar model, we are able to concentrate on the essential physics without being distracted by technicalities related to the tensor structure of the full model. In Section 2.3 and 2.4.1 we will provide the full-fledged tensor calculation.

In the Minkowski case the brane sits at constant coordinate position $r_0 = R$ and its coordinates can be identified trivially with the bulk coordinates: $\tilde{x}^\alpha = X^\alpha$. The action can be decomposed into a bulk and localized brane part

$$\mathcal{S} = \mathcal{S}_{\text{Bulk}} + \mathcal{S}_{\text{Brane}} \,. \tag{2.12}$$

The first term,

$$\mathcal{S}_{\text{Bulk}} = -\frac{M_D^{2+n}}{2} \int \mathrm{d}^D X \;\; (\partial_A \Phi)^2 \;, \tag{2.13}$$

mimics the linearized Einstein-Hilbert term in D infinite spacetime dimensions, where the bulk Planck scale is denoted by M_D. The second term plays the role of the induced gravity term on a (regularized) codimension-one brane:

$$\mathcal{S}_{\text{Brane}} = \int \mathrm{d}^d \tilde{x} \;\; \left[\frac{\tilde{M}^{d-2}}{2} f \;\; (\partial_\alpha \Phi)^2 + J\Phi \right]_0 \;. \tag{2.14}$$

where the subscript "0" denotes evaluation at the brane. We also consider a coupling to the localized source J. f is a dimensionless coefficient; a priori, we do not make any assumptions about its sign. Later in the 6D case, we will derive f from the full theory and show that it has a definite sign for all modes except of one peculiar scalar. In that case, f is promoted to a function of the model parameters M_6, M_{Pl}, and R as well as the defect angle δ, and its sign determines the stability of the model.

Again, the dynamical system is given in two parts: First, the vacuum equation in the bulk,

$$\Box_D \Phi = 0, \tag{2.15}$$

where $\Box_D$ is the D-dimensional d'Alembert operator in flat space. Second, these equations have to be equipped with the correct boundary and matching conditions. The analog of

Israel's matching equations can be readily derived,

$$[\Phi']_{\text{disc}} - f\, L_n\, \Box_4\, \Phi|_0 = -\frac{1}{M_D^{2+n}}\, J\,, \tag{2.16}$$

with the characteristic length scale

$$L_n := \frac{\tilde{M}^{1+n}}{M_D^{2+n}}\,. \tag{2.17}$$

Here and henceforth the prime denotes ∂_r. We also made use of the SO(n)-symmetry by setting to zero all angular derivatives. Regularity at the axis requires additionally $\lim_{r\to 0} \Phi' = 0$ (for $n \geq 2$).

2.2.1 Brane-to-brane propagation

In the following, we derive an expression for the (tree-level) propagation of Φ-quanta between to brane-localized vertices. Classically, it can be used to derive the potential between two Φ-sources on the brane, whereas quantum mechanically, we will use it to calculate the vacuum-to-vacuum amplitude in the presence of an external source. In the GR case, it simply encodes the gravitational potential of a brane-localized source.

It will be convenient to work in 4D Fourier space. To this end, we define

$$\hat{\Phi}(p, r) := \int \mathrm{d}^4x\; \mathrm{e}^{-\mathrm{i}\, p\cdot x} \Phi(x, r) \qquad (p \cdot x := p_\mu x^\mu)\,. \tag{2.18}$$

Note that Φ does not depend on the angular coordinates due to the SO(n)-symmetry. For later convenience we introduce the frequency ω according to $p^2 =: \boldsymbol{p}^2 - \omega^2$. With this definition the bulk equation becomes

$$\left(-p^2 + \Delta_n\right) \hat{\Phi} = 0 \qquad (p^2 := p_\mu p^\mu)\,, \tag{2.19}$$

where Δ_n denotes the n-dimensional Laplace operator in flat space.

In the following we will solve the system (2.19) and (2.16) for the special case of one and two codimensions. While those two cases are quite distinct due to different topologies, the models with $n \geq 2$ are all very similar. As a consequence, we limit ourselves to extensively discussing these two cases. It is then straightforward to generalize our results to higher codimensions.

2.2.1.1 Codimension-one

The (linearized) codimension-one scenario has been discussed extensively in the literature [63, 73, 70]. In our case it will serve as a warm up exercise, which introduces different techniques that will become important for $n \geq 2$.

In one codimension the topology is different since we do not have an axis. Instead, there

is a $\mathbb{Z}_2$-symmetry across the brane and we can directly identify $\tilde{M} = M_{\rm Pl}$. To distinguish this case from the higher-codimensional scenarios, the extra space coordinate is termed y and has the range $(-\infty, \infty)$. The brane is located at $y = 0$ (=: y_0).

The two linearly independent vacuum solutions of (2.19) are $\propto \mathrm{e}^{\pm\sqrt{p^2}y}$. In order to create a discontinuity in the first y-derivative at the brane position, the two solutions have to be clued together at $y = 0$, thereby yielding

$$\hat{\Phi}(p, y) = \hat{\Phi}|_0(p)\, \mathrm{e}^{\mp\sqrt{p^2}\,|y|} \,. \tag{2.20}$$

We will refer to both solutions as the normal branch (NO) (upper sign) and the self-accelerating branch (SA) (lower sign). It can be shown that the two branches found here in the linear analysis, correspond to the two (equally termed) branches occurring in the cosmological setup (which is briefly reviewed in Sec. 3.1).[8]

A priori, this solution is only defined for $p^2 > 0$ but can be analytically continued by choosing the branch cut in the usual way along the negative real axis. The result for $\hat{\Phi}(p, y)$ then depends on the prescription under consideration. Although we will mostly employ the Feynman prescription (as it is required for calculating quantum amplitudes), it is instructive to show that the two solutions correspond to purely outgoing and incoming waves if the retarded prescription is used. To be precise, let us consider a mode with fixed momentum $\boldsymbol{p}^2 < \omega^2$ (which holds for all massive KK-modes); by employing the retarded prescription we get

$$\mathrm{e}^{-\mathrm{i}\,\omega t}\hat{\Phi}(p, y) \propto \exp\left\{-\mathrm{i}\ \mathrm{sign}(\omega)\left(|\omega| t \mp \sqrt{\omega^2 - \boldsymbol{p}^2}\,|y|\right)\right\} \,. \tag{2.21}$$

And indeed, we find that the NO branch corresponds to outgoing and the SA branch to incoming waves.[9] Already at this stage it is clear that the SA branch has a somewhat problematic status since its solution does either not fall off at radial infinity or corresponds to incoming waves. The last observation is of course not compatible with having a source-free bulk. And indeed, there a various investigations in the literature which show that the corresponding nonlinear cosmology (which is continuously connected to the SA solution found here in the weak field limit) exhibits a ghost instability (cf. Sec. 3.1 for more details and references). Moreover, in Chap. 5, we study a model that is continuously connected to the DGP model and leads to exactly the same conclusion, namely that the SA branch corresponds to outgoing waves. In that case, the statement is made on a nonlinear level and the DGP limit can be taken explicitly. In the remainder of this chapter we will therefore restrict ourselves to the NO branch and prove its stability.

Note that in one codimension, we can set $f = -1$ because there will be no DOF with a different sign in the full GR setup (as opposed to two codimensions). After plugging (2.20)

[8] In principle, this can be shown by solving the linearized BIG setup (including the full tensorial structure) for FLRW matter on the brane. We omit the corresponding calculation as it does not lead to new insights.

[9] Here, the qualifications "outgoing" and "incoming" are meant relative to the brane at $y = 0$.

in the matching equation (2.16), we find

$$M_5^3 Z_1(p)\hat{\Phi}|_0 = -\hat{J}\,, \tag{2.22}$$

where $Z_1(p)$ is the inverse brane-to-brane propagator in one codimension,

$$Z_1(p) := -L_1\, p^2 \mp 2\sqrt{p^2}\,. \tag{2.23}$$

It describes the propagation of Φ-quanta between two brane-localized vertices. The general propagator can then be read off from (2.20) by substituting $\hat{\Phi}|_0$.

The interpretation of $r_{c,1} := L_1/2$ as a crossover scale can be directly inferred from the propagator $1/Z_1$ that is being convoluted with a constant point source $J \propto \delta_3(\boldsymbol{x})$. The time-independence of the source then implies $\omega = 0$ and the crossover momentum $\boldsymbol{p}_{c,1} = 1/r_{c,1}$ can be readily derived by comparing both terms in (2.23). Once they are of the same order, the induced graviton dynamics is as important as the bulk dynamics, thereby signaling a transition between a 4D and 5D scaling behavior of the gravitational potential on the brane, in accordance with the literature [63].

Finally, let us note that due to phenomenological considerations the crossover scale should be at least of the order of todays Hubble length, $L_1 \gtrsim 1/H_0$, which in turn implies $M_5 \lesssim 10\,\mathrm{MeV}$.

2.2.1.2 Codimension-two

In higher codimensions the topology changes significantly as there is a symmetry axis reflecting the SO(n)-symmetry in the bulk. For $n = 2$ the solution that is regular at the axis, continuous at $r = R$ and falls of at radial infinity[10] is given by

$$\hat{\Phi}(p,r) = \begin{cases} \dfrac{I_0(r\sqrt{p^2})}{I_0(R\sqrt{p^2})}\,\hat{\Phi}|_0 & (r < R) \\[2ex] \dfrac{K_0(r\sqrt{p^2})}{K_0(R\sqrt{p^2})}\,\hat{\Phi}|_0 & (r > R)\,, \end{cases} \tag{2.24}$$

where I_n and K_n denote the modified Bessel functions of the first and second kind, respectively. As before, we can explicitly check that this solution corresponds to outgoing waves for $p^2 < 0$, provided we use a standard analytic continuation of the square root. Inserting the bulk solution in (2.16) yields

$$\frac{M_6^4}{R} Z_2(p)\hat{\Phi}|_0 = -\hat{J}, \tag{2.25}$$

[10] In the whole codimension-two discussion we limit ourselves to radially bounded solutions.

with $Z_2(p)$ the inverse brane-to-brane propagator in two codimensions,

$$Z_2(p) := f\,\frac{L_2}{R}z^2 - \,z\left(\frac{I_1(z)}{I_0(z)}+\frac{K_1(z)}{K_0(z)}\right)\,, \tag{2.26}$$

where the dimensionless variable

$$z :=\, R\sqrt{p^2} = R\sqrt{\boldsymbol{p}^2-\omega^2}$$

was introduced.

As before, the codimension-two crossover scale r_c can be derived by equating both terms on the right side of (2.26) for a constant point source, i.e. for $\omega = 0$. The requirement (2.5) implies that only low momentum modes with $|\boldsymbol{p}|\,R \ll 1$ can be described consistently. This allows a small argument expansion of the Bessel functions and in turn yields a characteristic momentum scale $\boldsymbol{p}_c$. We thus arrive at the final expression for the crossover distance valid on a tensionless ($\lambda = 0$) codimension-two brane,[11]

$$r_c^2|_{\lambda=0} \sim 3L_2\,R\log\left(L_2/R\right) \sim \frac{3M_{\rm Pl}^2}{2\pi M_6^4}\,, \tag{2.27}$$

where in the last term we have neglected the logarithm and introduced $M_{\rm Pl}$ according to (2.3) (as it is the phenomenologically relevant scale).[12] From this we see that—typically for two codimensions—there is only a logarithmic divergence with R. This crossover has been derived before in [62], and later also in [104] by using a shock wave analysis. We will see in Sec. 2.4.1 (in accordance with [104]) that this result gets significantly altered on the deficit angle background, i.e. for $\lambda \neq 0$. In fact, there the crossover can be parametrically larger by a factor L_2/R. As a consequence, an extensive phenomenological discussion of the model requires to take into account the λ dependence of r_c (which can significantly reduce the hierarchy between the bulk and the EW scale.)

2.2.2 Vacuum persistence

In this section, we want to investigate the quantum stability of the prototype model. To be concrete, we investigate whether the vacuum state in the presence of an external source J is stable. To that end, we calculate the vacuum-to-vacuum probability

$$\left|\langle 0|0\rangle_J\right|^2 = \exp\left[-\,\mathrm{Im}(\mathcal{A})\right]\,, \tag{2.28}$$

with the corresponding source-to-source amplitude defined as

$$\mathcal{A} := \int \mathrm{d}^d\tilde{x}\; J\,\Phi|_0\,. \tag{2.29}$$

[11] For notational convenience the crossover in the codimension-two case will be denoted by r_c (instead of $r_{c,2}$).

[12] The additional factor 3 is introduced for later convenience.

The expression $\exp(\mathrm{i}\,\mathcal{A}/2)$ is also known as the vacuum persistence amplitude (cf. [126] for a pedagogical introduction). A unitary time evolution requires the probability to be ≤ 1. In particular, a ghost mode would lead to a probability greater than one (or a negative imaginary part of the amplitude equivalently), which is of course not compatible with a consistent quantum description. Therefore, we can employ (2.28) as a tool to detect ghosts.

As an aside note that, in principle, it is possible by using an unconventional iϵ-prescription to flip the sign of the imaginary part; this was for example suggested in [61]. However, this does not help with the problem: As a ghost also implies an unbounded Hamiltonian already at the classical level, it necessarily leads to an instability that cannot be avoided. This will be explicitly demonstrated in Sec. 2.3 in the case of the tensionless codimension-two model.

We will start with the codimension-one model and show that the NO branch is healthy. In the codimension-two case, we will see that the quantum stability hinges on the sign of f.

2.2.2.1 Codimension-one

The amplitude (2.29) can be expressed as

$$\mathcal{A} = -\frac{1}{M_5^3}\int \frac{\mathrm{d}^4p}{(2\pi)^4}\,\left|\hat{J}(p)\right|^2\,\frac{1}{Z_1(p)}\,. \tag{2.30}$$

There is a useful result in the literature [70] according to which the brane-to-brane propagator can be represented as a continuous superposition of massive KK-states,

$$Z_1^{-1}(p) = -\frac{4}{\pi}\int_0^\infty \mathrm{d}m\,\frac{1}{4+(m\,L_1)^2}\,\frac{1}{-\omega^2+m^2+\boldsymbol{p}^2}\,. \tag{2.31}$$

When we plug this expression in (2.30), we can commute the m and the ω-integration, where the latter becomes of the standard type and simply describes the exchange of a massive Φ mode. We use the Feynman prescription, $\mathrm{Im}(\omega^2) = +\epsilon$, to perform the ω-integration and finally get

$$\mathrm{Im}(\mathcal{A}) = \frac{4}{M_5^3\,\pi}\int_0^\infty \mathrm{d}m\,\int \frac{\mathrm{d}^3\boldsymbol{p}}{(2\pi)^3}\,\frac{1}{4+(m\,L_1)^2}\,\frac{|\hat{J}(p)|^2}{2\,\omega}\bigg|_{\omega=\sqrt{\boldsymbol{p}^2+m^2}}\,. \tag{2.32}$$

The positive definiteness of this expression, due to (2.28), proves that the NB branch of the codimension-one model is ghost-free.[13]

[13] We leave a corresponding discussion of the SA branch for future work, though, we expect a ghostly sign (in accordance with statements in the literature about the corresponding nonlinear cosmology).

2.2.2.2 Codimension-two

The codimension-two case is much more involved. Substituting (2.25) in (2.29) yields

$$\mathcal{A} = -\frac{2\pi R^2}{M_6^4} \int \frac{\mathrm{d}^4 p}{(2\pi)^4} \left|\hat{J}(p)\right|^2 \frac{1}{Z_2(p)}\,, \tag{2.33}$$

where again the Feynman prescription applies. Let us first look for potential isolated poles, viz. solutions z_* of

$$f\,\frac{L_2}{R}\,z_* = \frac{I_1(z_*)}{I_0(z_*)} + \frac{K_1(z_*)}{K_0(z_*)}\,. \tag{2.34}$$

To that end, we plot the right side of the equation in Fig. 2.3 (it corresponds to the solid line with $\delta = 0$). It follows that a solution exists if and only if $f > 0$. The associated pole corresponds to a mass $m_* = z_*/R > 0$, which yields the dispersion relation

$$\omega = \pm\sqrt{\boldsymbol{p}^2 - m_*^2} =: \pm\omega_*\,. \tag{2.35}$$

The negative sign under the square root shows that this mode is a tachyon, hence leading to exponentially growing modes with momentum $|\boldsymbol{p}| < m_*$, which subsequently destabilize the theory. In the complex ω-plane it manifests itself through poles on the imaginary axis. For larger momenta these poles disappear and reemerge on the real axis, cf. Fig. 2.1a. This corresponds to the physical statement that the corresponding particle can be excited only for $|\boldsymbol{p}| \geq m_*$. Beside the isolated poles at $\pm\omega_*$, the square root in the argument of the Bessel functions introduces a branch cut[14] along the real axis, starting at $\pm|\boldsymbol{p}|$, cf. Fig. 2.1a. As for one codimension, this branch cut can be interpreted as a continuous superposition of massive KK-modes.

Next, we calculate the contributions of the branch cut and the isolated pole (for $f > 0$) to the imaginary part of $\mathcal{A}$, separately. To this end, it is convenient to decompose the integration contour $\mathcal{C}$ into two parts: One that is not closed and wraps around the branch cut, $\mathcal{C}_2$, as well as another closed one that contains one of the isolated poles (if it exists), $\mathcal{C}_1$. Both of them are depicted in Fig. 2.1b for the case of a closure in the upper half plane. Alternatively, we could have closed the contour in the lower half plane, which yields the same result. The important point is that the half circle contribution vanishes if sent to infinity. The sum of both integrations is therefore identical to the Feynman-contour integration in Fig. 2.1a.

Note that we do not expect the branch cut contribution $\mathcal{C}_2$ to be pathological since it originates from the bulk gravity term and would survive in the pure GR limit $\tilde{M} \to 0$. Nevertheless, we explicitly confirm this for an ω-independent source. To be specific, the integrand of the $\mathrm{d}^3\boldsymbol{p}$-integration in (2.33) is then given by (up to an irrelevant positive

[14] We verified that there is no additional branch cut, which follows from the analytic properties of the Bessel functions.

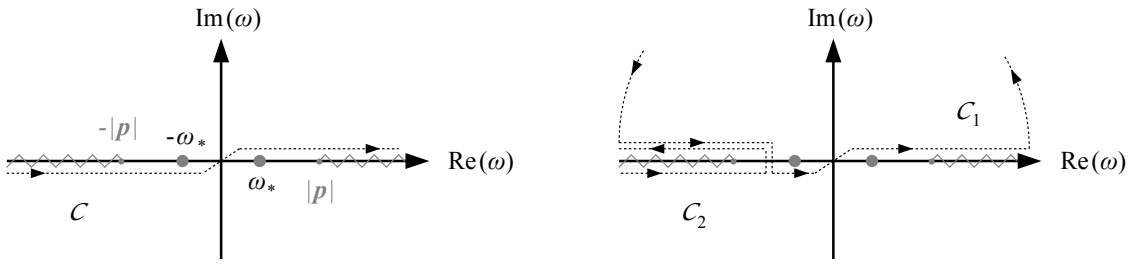

(a) Feynman contour (dotted line) for the ω-integration in (2.33).

(b) The Feynman contour can be decomposed into two parts: a closed path $\mathcal{C}_1$ around one of the poles and a branch cut contribution $\mathcal{C}_2$. The half circle vanishes.

Figure 2.1: Complex ω-plane [75]: The branch cuts along the real axis can be interpreted as a continuum of healthy, massive KK-modes. In the case $f > 0$ and for $|\boldsymbol{p}| > m_*$ a tachyonic ghost can be excited, which manifests itself by the two poles at $\pm\omega_*$ (gray dots).

factor)

$$-\operatorname{Im}\left[R\int_{\mathcal{C}_2} \mathrm{d}\omega\, Z_2^{-1}(\omega,\boldsymbol{p})\right]. \tag{2.36}$$

Since we could not infer the sign analytically, we performed a numerical integration along the branch cut contour $\mathcal{C}_2$, which showed that irrespective of the sign and absolute value of f the contribution to $\operatorname{Im}\mathcal{A}$ is always positive. Later, in the full GR case, we perform the analog integration and provide a corresponding plot with our numerical results [cf. Fig. 2.5].

Now let us turn to contour $\mathcal{C}_1$: For $f < 0$ it is zero because there are no poles enclosed, implying a healthy, ghost-free theory. As discussed before, for $f > 0$ there is an additional isolated pole and the $\mathcal{C}_1$-integration yields a non-vanishing contribution. Its overall sign is determined by three factors: the residue of the pole, the sign in (2.33) and another one related to the orientation of the contour denoted by $\operatorname{sign}(\mathcal{C}_1)$; to be precise, the imaginary part of $\mathcal{A}$ receives a contribution (again up to an irrelevant positive factor)

$$-\operatorname{sign}(\mathcal{C}_1)\,\operatorname{Res}\left(\frac{1}{Z_2(p)},\,\omega=\pm\,\omega_*\right) = -\frac{1}{\omega_* R^2}\left[2f\,\frac{L_2}{R}+\left(\frac{I_1}{I_0}\right)^2-\left(\frac{K_1}{K_0}\right)^2\right]^{-1} \tag{2.37}$$

$$= -f\,\frac{L_2}{\omega_* R^3}\left[2+z_\star\left(\frac{I_1}{I_0}-\frac{K_1}{K_0}\right)\right]^{-1}, \tag{2.38}$$

where $\operatorname{sign}(\mathcal{C}_1)$ is positive if we close the contour in the upper half plane and negative if we close it in the lower half plane. Moreover, we used (2.34) to derive the second line in which f is factored out. The important point is that the expression in square brackets is positive irrespective of z_* (this follows from a a simple numerical check). Since f has to be positive

for the pole to exist, the contribution to the imaginary part of $\mathcal{A}$ is always negative.

To summarize, while the theory is healthy for negative f, there are two contributions to the imaginary part in the opposite case—one from the branch cut that is always positive and another one from the pole which is negative and hence pathological. In general, we can not hope for a cancellation between the two contributions because they are both related to different sectors in the ω-plane. With other words, it is always possible to construct a source that only excites the ghost but not the KK-continuum represented by the branch cut.

2.3 Tensionless vacuum

In the last section, we have seen under which conditions the scalar prototype theory in 6D is healthy. Let us know extend these considerations to the full GR setup where we start by considering a flat bulk *and* brane background (corresponding to a brane with $\lambda = 0$). For the moment, we will keep $D > 5$ arbitrary, only later for the nontrivial background (with $\lambda > 0$) we specialize to $D = 6$. Moreover, in this section we will mostly use a thin brane description, i.e., we work in the limit $R \to 0$. Technically this is achieved by using n-dimensional delta functions. However, at one point we solve the equations (for the 6D model) explicitly, which requires to use a regularization. We achieve this by replacing the two-dimensional delta functions with one-dimensional ones, describing a ring instead of a point in extra space. We will check the validity of this ad hoc approach a posteriori by comparing the physical degrees of freedom and their matching equations to the results derived later in Sec. 2.4.1 for a regularized brane in the limit $\lambda \to 0$. We will find perfect agreement if the proper circumference of the brane/ring is stabilized. This provides an important and nontrivial check of the consistency of our method.

On a technical level, we decompose the bulk and the brane metric into a Minkowski and a fluctuation part; explicitly, $\boldsymbol{g}_D = \boldsymbol{\eta}_D + \boldsymbol{h}_D$ and $\boldsymbol{g} = \boldsymbol{\eta} + \boldsymbol{h}$. In more physical terms, this is equivalent to saying that we perform a stability analysis of a tensionless brane. In Sec. 2.4 we will generalize our results to a non-vanishing brane tension. Since we are considering a flat bulk *and* brane background, it is most convenient to work in Cartesian coordinates $X^A \equiv (x^\mu, y^a)$ for which the brane sits at $y^a = 0$ (the brane coordinates are hence trivially identified through $x^\mu = X^\mu$). This further implies that the induced fluctuations are given as a sub-matrix of the bulk metric fluctuations, i.e. $h_{\alpha\beta} = h_{D\alpha\beta}$.[15] In that case, the fluctuation theory is invariant under transformations

$$\delta h_{AB} = \partial_{(A}\xi_{B)}\,, \tag{2.39}$$

where ξ^A are D functions of the spacetime coordinates. As usual, this can be understood as a manifestation of the general coordinate invariance of the nonlinear theory. Since the brane sits at $y^a = 0$, we have to impose the restriction $\xi^a|_0 = 0$ in order not to spoil that choice.

[15]Here and henceforth, we will drop the subscript D for convenience, i.e. $\boldsymbol{h}_D \equiv \boldsymbol{h}$.

To assess the stability of the model in arbitrary codimensions, we employ two different diagnostic tools: First, we perform a manifestly 4D Lorentz covariant analysis similar to the one in [19]; here, the results derived for the scalar prototype model can be used. Second, we reformulate the theory by deriving the Hamiltonian on the constraint surface. This expression offers an independent way of inferring the stability of the background geometry.

2.3.1 Covariant analysis

The covariant analysis is convenient because the corresponding equations have a compact form. Moreover, it allows us to make contact to the analysis in [19] (which claimed the absence of a ghost). On the downside, we have to deal with technical difficulties related to ambiguities of the inverse d'Alembert operator. We will provide an exhaustive discussion of this issue, which in turn admits a solid counting of degrees of freedom, as well as a first assessment on the stability issue.

2.3.1.1 Gauge invariant variables

We decompose the graviton field in a 4D Lorentz covariant way,

$$h_{\mu\nu} =: \mathcal{D}_{\mu\nu} + \partial_{(\mu}\mathcal{V}_{\nu)} + \partial_\mu\partial_\nu\,\mathcal{B} + \eta_{\mu\nu}\,\mathcal{S}\,, \tag{2.40a}$$

$$h_{ab} =: d_{ab} + \partial_{(a}v_{b)} + \partial_a\partial_b b + \delta_{ab}s\,,\,, \tag{2.40b}$$

$$h_{\mu b} =: \mathcal{E}_{\mu b} + \partial_\mu\mathcal{F}_b + \partial_b\mathcal{G}_\mu + \partial_\mu\partial_b\mathcal{H}\,. \tag{2.40c}$$

Here, $\boldsymbol{\mathcal{D}}$ is a transverse and traceless 4D tensor, $\boldsymbol{\mathcal{V}}$, $\boldsymbol{\mathcal{E}}$, $\boldsymbol{\mathcal{G}}$ are transverse 4D vectors and $\mathcal{B}$, $\mathcal{S}$, $\boldsymbol{\mathcal{F}}$, $\mathcal{H}$ as well as all functions appearing in (2.40b) are 4D scalars. Furthermore, $\boldsymbol{v}$, $\boldsymbol{\mathcal{F}}$ and $\boldsymbol{\mathcal{E}}$ transform as vectors and $\boldsymbol{d}$ as a tensor under the SO(n) group, the vectors are again transverse and the tensor is transverse and traceless.

Even though this decomposition makes the 4D Lorentz covariance of the dynamical equations manifest, it has the general disadvantage that the components are not determined uniquely. More precisely, this ambiguity can be parametrized in terms of a set of homogeneous functions $\chi^{(i)}$, where here and henceforth "homogeneous" refers to solutions of the 4D homogeneous wave equation, i.e. $\Box_4\chi^{(i)} = 0$. It can be easily checked that the decomposition (2.40) is then invariant under the transformations

$$\delta\mathcal{S} = \chi^{(1)}\,, \tag{2.41a}$$

$$\delta\mathcal{B} = \chi^{(2)} - \frac{4}{\Box_4}\chi^{(1)}\,, \tag{2.41b}$$

$$\delta\mathcal{V}_\mu = \chi^{(3)}_\mu + \frac{3}{\Box_4}\partial_\mu\chi^{(1)}\,, \tag{2.41c}$$

$$\delta\mathcal{D}_{\mu\nu} = \left[4\,\partial_\mu\partial_\nu\frac{1}{\Box_4} - 3\,\partial_{(\mu}\frac{1}{\Box_4}\partial_{\nu)} - \eta_{\mu\nu}\right]\chi^{(1)} - \partial_\mu\partial_\nu\chi^{(2)} - \partial_{(\mu}\chi^{(3)}_{\nu)}\,, \tag{2.41d}$$

as well as

$$\delta\mathcal{H} = \chi^{(4)}\,, \qquad \delta\mathcal{F}_a = \chi_a^{(5)}\,, \tag{2.42a}$$

$$\delta\mathcal{G}_\mu = -\partial_\mu\chi^{(4)}\,, \qquad \delta\mathcal{E}_{\mu b} = -\partial_\mu\chi_b^{(5)}\,, \tag{2.42b}$$

where $\boldsymbol{\chi}^{(3)}$ and $\boldsymbol{\chi}^{(5)}$ are subject to the two conditions[16]

$$\partial^\mu\chi_\mu^{(3)} = -3\partial^\mu\frac{1}{\Box_4}\partial_\mu\chi^{(1)}\,, \qquad \partial^a\chi_a^{(5)} = 0\,. \tag{2.43}$$

Besides the split ambiguity, there is the usual gauge freedom (2.39). Instead of fixing a particular gauge, we will again use a complete set of gauge invariant variables, viz. $\mathcal{S}, s, \boldsymbol{\mathcal{D}}, \boldsymbol{\mathcal{E}}$ and $\boldsymbol{d}$, as well as

$$\mathcal{O} := \mathcal{B} + b - 2\mathcal{H}\,, \tag{2.44a}$$

$$\mathcal{W}_\mu := \mathcal{G}_\mu - \mathcal{V}_\mu\,, \tag{2.44b}$$

$$\mathcal{Y}_a := \mathcal{F}_a - v_a\,. \tag{2.44c}$$

Although these are invariant under gauge transformations, they are not invariant under the homogeneous transformations (2.41) and (2.42), but transform as

$$\delta\mathcal{O} = -\frac{4}{\Box_4}\chi^{(1)} + \chi^{(2)} - 2\chi^{(4)}\,, \tag{2.45a}$$

$$\delta\mathcal{W}_\mu = -\frac{3}{\Box_4}\partial_\mu\chi^{(1)} - \chi_\mu^{(3)} - \partial_\mu\chi^{(4)}\,, \tag{2.45b}$$

$$\delta\mathcal{Y}_a = \chi_a^{(5)}\,. \tag{2.45c}$$

Now, it is crucial to realize that one certain combination of the functions $\chi^{(2)}, \boldsymbol{\chi}^{(3)}$ and $\chi^{(4)}$ does not affect the gauge invariant quantities. Explicitly, one can check that they only enter via the combinations[17]

$$\tilde{\chi}^{(2)} := \chi^{(2)} - 2\chi^{(4)}\,, \qquad \tilde{\chi}_\mu^{(3)} := \chi_\mu^{(3)} + \partial_\mu\chi^{(4)}\,, \tag{2.46}$$

(or any linear combination thereof) in the relevant Eqs. (2.41d), (2.45a) and (2.45b).

In summary, the gauge invariant variables $\{\mathcal{S}, s, \mathcal{O}, \boldsymbol{\mathcal{W}}, \boldsymbol{\mathcal{Y}}, \boldsymbol{\mathcal{D}}, \boldsymbol{\mathcal{E}}, \boldsymbol{d}\}$ are only unique up to the $(4+n)$ independent homogeneous functions $\{\chi^{(1)}, \tilde{\chi}^{(2)}, \tilde{\boldsymbol{\chi}}^{(3)}, \boldsymbol{\chi}^{(5)}\}$. This will be crucial for correctly inferring the number of dynamical degrees of freedom (DOF), because each of the χ's can be used to eliminate one would-be dynamical component.

[16] Here and henceforth, $(1/\Box_4)\psi$ is a shorthand notation for the convolution of ψ with the retarded Green's function of the 4D d'Alembert operator $\Box_4$.

[17] Note that $\tilde{\chi}_\mu^{(3)}$ is subject to the same relation (2.43) as $\chi_\mu^{(3)}$, and thus also only has three independent components.

2.3.1.2 Bulk and brane dynamics

The full dynamical system, consisting of the vacuum Einstein equations in the bulk (2.6) and the matching equations at the brane (2.9) (in the limit $r_0 \to 0$), can be written in a compact form by using n-dimensional delta functions, which will be denoted by the shorthand $\delta_n(y)$,[18]

$$M_D^{D-2} \Diamond_{MN}^{(D)\,AB} h_{AB} = \delta^{\mu}{}_{M} \delta^{\nu}{}_{N}\, \delta_n(y) \left(U_{\mu\nu} - M_{\rm Pl}^2 \Diamond_{\mu\nu}^{\rho\sigma} h_{\rho\sigma} \right) . \tag{2.47}$$

where $\Diamond_{MN}^{(D)\,AB}$ is the first order Einstein operator in D dimensions

$$\Diamond_{MN}^{(D)\,AB} = \delta^{A}{}_{M} \delta^{B}{}_{N}\, \Box_D + \eta^{AB} \partial_M \partial_N - 2\, \delta^{B}{}_{(N}\, \partial^A \partial_{M)} + \eta_{MN} \left(\partial^A \partial^B - \eta^{AB}\, \Box_D \right) , \tag{2.48}$$

and $\boldsymbol{U}$ is the 4D localized source.[19]

To derive the equations of motion for our variables, we start by investigating the (μb) components of (2.47). Taking their double divergence $\partial_\mu \partial_b$ leads to

$$\Box_4 \Delta_n \left(3\, \mathcal{S} + (n-1) s \right) = 0 . \tag{2.49}$$

Demanding fall-off conditions at spatial infinity allows us to simply drop the extra-space Laplace operator Δ_n. The general solution then becomes $3\,\mathcal{S} + (n-1)s = \kappa^{(s)}$ with $\kappa^{(s)}$ an arbitrary homogeneous function. Instead of choosing initial conditions to fix $\kappa^{(s)}$, we make use of the split ambiguity (2.41a) parametrized by $\chi^{(1)}$ to remove it from the equation. s is therefore constrained by the relation (valid only for $n \geq 2$)

$$s = -\frac{3}{n-1} \mathcal{S} , \tag{2.50}$$

and hence no independent DOF.

By acting with a single divergence ∂_μ or ∂_b on the (μb) components of (2.47) and using (2.50), we obtain

$$\Box_4 \Delta_n \mathcal{W}_\mu = 0 , \qquad\qquad \Box_4 \Delta_n \mathcal{Y}_a = 0 , \tag{2.51}$$

respectively. As before, Δ_n can be dropped, and the freedom to choose initial conditions gets "eaten" by $\tilde{\boldsymbol{\chi}}^{(3)}$ and $\boldsymbol{\chi}^{(5)}$, yielding

$$\mathcal{W}_\mu = \mathcal{Y}_a = 0 . \tag{2.52}$$

These relations can be used to simplify the (μb) sector of (2.47), leading to the wave

[18] In general, this is only possible for a metric that is in Gaussian normal form, meaning that on the level of fluctuations the gauge $h_{rA} = 0$ has to be imposed. Instead, we will work with gauge invariant variables which are valid for *all* gauge choices (including the Gaussian normal gauge).

[19] There is a factor of -2 relative to the definition in (C2), explicitly $\boldsymbol{U} \equiv -2\ {}^{(1)}\boldsymbol{T}$, where ${}^{(1)}\boldsymbol{T}$ is the first order fluctuation of the 4D brane induced EMT.

equation

$$\Box_D \mathcal{E}_{\mu b} = 0\,. \tag{2.53}$$

Thus, the fields $\boldsymbol{\mathcal{E}}$ constitute $3(n-1)$ DOF that are not sourced by brane-localized matter fields.

There is only one freedom left in choosing the decomposition, namely the function $\tilde{\chi}^{(2)}$. We will use it in the same way as before to derive a constraint equation for $\mathcal{O}$. After taking the trace of the (ab) components of (2.47) and using (2.50), we find

$$\Box_4 \mathcal{O} = -\frac{n-2}{n-1}\mathcal{S}\,. \tag{2.54}$$

A priori, this is a dynamical equation for $\mathcal{O}$ sourced by $\mathcal{S}$. However, according to (2.45a) the decomposition is invariant under the shift $\delta\mathcal{O} = \tilde{\chi}^{(2)}$. Again, this implies that $\mathcal{O}$ is not a true DOF as we can impose arbitrary initial conditions without affecting the solution for $\boldsymbol{h}$. For instance, we can choose $\tilde{\chi}^{(2)}$ such that $\mathcal{O}$ becomes

$$\mathcal{O} = -\frac{n-2}{n-1}\frac{1}{\Box_4}\mathcal{S}\,. \tag{2.55}$$

Once we plug this solution back into the (ab) components of (2.47), we find a wave equation for the transverse and traceless $\mathrm{SO}(n)$ tensor modes,

$$\Box_D d_{ab} = 0\,, \tag{2.56}$$

which therefore constitute further $[(n+1)(n-1)/2]$ DOF that are not coupled to on-brane matter.

Finally, let us consider the $(\mu\nu)$ components of (2.47). Taking its trace and making use of all solutions we derived before yields an equation for the scalar $\mathcal{S}$,

$$M_D^{D-2}\,\Box_D \mathcal{S} = \frac{1}{3}\frac{n-1}{n+2}\left(U^{\mu}{}_{\mu} + 6M_{\mathrm{Pl}}^2\,\Box_4 \mathcal{S}\right)\delta_n(y)\,. \tag{2.57}$$

Since we already made use of all shift ambiguities, $\mathcal{S}$ is a real dynamical mode. We will show that this mode constitutes a tachyonic ghost.

Before doing so, let us derive the remaining sourced DOF. In order to derive the dynamical equation for the 4D tensor $\boldsymbol{\mathcal{D}}$, we need to solve for $\mathcal{S}$ more explicitly. To be precise, $\mathcal{S}$ fulfills the equation

$$M_D^{D-2}\left(\frac{\Delta_n}{\Box_4}+1\right)\mathcal{S} = \frac{1}{3}\frac{n-1}{n+2}\left(\frac{1}{\Box_4}U^{\mu}{}_{\mu} + 6M_{\mathrm{Pl}}^2\,\mathcal{S}\right)\delta_n(y) + \kappa^{(\mathcal{S})}\,, \tag{2.58}$$

where we introduced the homogeneous function $\kappa^{(\mathcal{S})}$, which keeps track of the freedom to choose initial conditions for $\mathcal{S}$. Recall that there is no split ambiguity left which could be used to set $\kappa^{(\mathcal{S})}$ to zero. This subtlety was missed in [19]. To be precise, there $\kappa^S = 0$

was imposed implicitly, corresponding hence to a specific choice of initial conditions. This enables us to derive an equation for the tensor $\mathcal{D}_{\mu\nu}$,

$$M_D^{D-2}\,\Box_D\mathcal{D}_{\mu\nu} = \left(U_{\mu\nu}^{(\mathcal{D})} - M_{\rm Pl}^2\,\Box_4\mathcal{D}_{\mu\nu}\right)\delta_n(y) + \partial_\mu\partial_\nu\kappa^{(\mathcal{S})}\,, \tag{2.59}$$

with the transverse and traceless tensor $\boldsymbol{U}^{(\mathcal{D})}$ defined as

$$U_{\mu\nu}^{(\mathcal{D})} := U_{\mu\nu} + \frac{\partial_\mu\partial_\nu}{3}\frac{1}{\Box_4}U^\rho{}_\rho - \frac{1}{3}\eta_{\mu\nu}U^\rho{}_\rho\,. \tag{2.60}$$

This equation is not completely decoupled, since it depends on the initial conditions for $\mathcal{S}$ through $\kappa^{(\mathcal{S})}$. As $\boldsymbol{\mathcal{D}}$ is also subject to the five constraint equations $\mathcal{D}^\mu{}_\mu = 0$ and $\partial^\mu\mathcal{D}_{\mu\nu} = 0$, it describes five healthy DOF.

In summary, the theory contains 6 sourced $\{\mathcal{S}, \boldsymbol{\mathcal{D}}\}$ and $[(3+n/2)(n-1)-1]$ non-sourced $\{\boldsymbol{\mathcal{E}}, \boldsymbol{d}\}$ DOF, which makes a total of $D(D-3)/2$, corresponding to the number of DOF in D-dimensional GR.

Now let us turn to the question whether the six sourced DOF, described by (2.57) and (2.59), are stable. To that end, let us map both equations to the scalar prototype system given by (2.15) and (2.16). We first have to regularize the system as before by replacing the brane with a $(n-1)$-sphere at coordinate position $r_0 = R$,

$$\delta_2(y) \to \frac{\delta(r-R)}{A_n}\,. \tag{2.61}$$

The vacuum equation [corresponding to (2.15)] is readily obtained by evaluating both equations for $r \neq R$. Moreover, integrating the equations over the interval $[R-\epsilon, R+\epsilon]$ yields the matching equations

$$\left[\mathcal{D}'_{\mu\nu}\right]_{\rm disc} + L_n\,\Box_4\mathcal{D}_{\mu\nu}|_0 = \tilde{U}_{\mu\nu}^{(\mathcal{D})}/M_D^{D-2}\,, \tag{2.62a}$$

$$3\frac{n+2}{n-1}\left[\mathcal{S}'\right]_{\rm disc} - 6\,L_n\,\Box_4\mathcal{S}|_0 = \tilde{U}^\mu{}_\mu/M_D^{D-2}\,, \tag{2.62b}$$

where we defined $L_n := M_{\rm Pl}^2/(M_D^{2+n}S_{n-1}R^{n-1})$ and $\tilde{U}_{\mu\nu} := U_{\mu\nu}/A_n$. By comparing (2.16) with (2.62), it is possible to map the tensor sector and the scalar sector to two different prototype models with different values of f. Accordingly, the tensor sector is described by a model with $f \to f^{(\mathcal{D})} := -1$, and the scalar sector requires the identification $f \to f^{(\mathcal{S})} := 2\,(n-1)/(n+2)$. Let us now discuss there respective contributions to the vacuum persistence amplitude.

2.3.1.3 Vacuum persistence

With our scalar prototype analysis in Sec. 2.2, we prepared the ground for an easy stability analysis of the Minkowski background. The GR analog of the source-to-source amplitude

$\mathcal{A}$, introduced in (2.28), is given by

$$\mathcal{A} := -\frac{A_n}{2} \int \mathrm{d}^4x\, \tilde{U}_{\mu\nu} h^{\mu\nu}|_0 \tag{2.63}$$

$$= -\frac{A_n}{2} \int \mathrm{d}^4x\, \left[\tilde{U}^{(\mathcal{D})}_{\mu\nu} \mathcal{D}^{\mu\nu} + \tilde{U}^{\mu}{}_{\mu} \mathcal{S}\right]\Big|_0 , \tag{2.64}$$

where $h^{\mu\nu}|_0$ is the Feynman-prescribed solution in the presence of an external source $\tilde{\boldsymbol{U}}$. It is possible by choosing an appropriate source to exclusively excite one of the two sectors, i.e. either the tensor or the scalar DOF. The amplitude can be decomposed accordingly into two separate contributions, $\mathcal{A} \equiv \mathcal{A}^{(\mathcal{D})} + \mathcal{A}^{(\mathcal{S})}$. Instead of determining the imaginary part of $\mathcal{A}^{(\mathcal{D})}$ or $\mathcal{A}^{(\mathcal{S})}$, we can use the fact that both amplitudes coincide (up to an irrelevant positive constant related to different source definitions) with the respective amplitudes calculated in the prototype model. We will discuss the three cases $n = 1$, $n = 2$ and $n \geq 3$ separately:

The above analysis does not apply for $n = 1$ entirely. Instead, the mode $\mathcal{S}$ is found to be non-dynamical (this can be derived from (2.49) once the split ambiguity (2.41a) is taken into account). The equation for $\boldsymbol{\mathcal{D}}$ however is valid. We are thus left with five sourced DOF carried by $\boldsymbol{\mathcal{D}}$, in accordance with the literature (see for example [70]). As $f^{(\mathcal{D})} = -1$, the codimension-one discussion in Sec. 2.2.2 implies that these DOF are stable or equivalently $\mathrm{Im}[\mathcal{A}^{(\mathcal{D})}] > 0$.

In the special case of $n = 2$, the detailed analysis of Sec. 2.2.2 applies. Again, the five DOF associated with $\boldsymbol{\mathcal{D}}$ are stable and correspond to a consistent vacuum state. On the other hand, for the mode $\mathcal{S}$ [or s due to (2.50)], we find $f^{(\mathcal{S})} > 0$, which implies $\mathrm{Im}[\mathcal{A}^{(\mathcal{S})}] < 0$, hence proving its tachyonic ghost character.

For higher codimensions with $n \geq 3$ we did not perform an explicit calculation of the vacuum-to-vacuum amplitude, however, we expect the same results to apply there. In any case, it is instructive to note, that the sign of $f^{(\mathcal{S})}$ is positive, irrespective of n. In the next section, we will show that this implies a negative contribution to the energy density at the brane position, which we consider strong evidence that the Minkowski theory, i.e. the theory with vanishing brane tension, is unstable for *any* higher codimension.

This result confirms what was found previously in the literature (cf. [58, 94]) but is in contradiction to a recent statement in [19], where the theory on a Minkowski background was claimed to be stable by means of a very similar Lorentz covariant analysis. As we have argued, the discrepancy was caused by (effectively) setting $\kappa^{(\mathcal{S})} = 0$ in (2.58), which then leaves no more freedom to chose initial conditions for $\mathcal{S}$. This in turn led to the erroneous conclusion that $\mathcal{S}$ (and hence the ghost) was not associated with a state in the Hilbert space.

2.3.2 Classical Hamiltonian

In six dimensions, we have rigorously proven that a tensionless brane with nonzero BIG scale is plagued by a scalar ghost mode. For dimensions $D > 6$, the same scalar shows

up, again with different signs of the bulk and brane kinetic terms, hence signaling the presence of a ghost. Yet, we did not calculate the vacuum persistence amplitude in those cases explicitly. In this section, we gather (further) evidence that the ghost persists in any higher dimension ($n \geq 2$). In so doing, we also provide a complementary picture to the previous analysis (mostly in six dimensions). To be precise, we show that the ghost mode leads to a *negative* contribution to the energy density at the brane position. As a diagnostic tool, we use the Hamiltonian on the constraint surface, which we derive for the sourceless theory, i.e. $\boldsymbol{U} = 0$.

2.3.2.1 Gauge invariant variables

As before, we will study small metric perturbations on a bulk (and brane) Minkowski background, $\boldsymbol{g}_6 = \boldsymbol{\eta}_6 + \boldsymbol{h}$. Instead of the 4D Lorentz covariant decomposition, we employ a $(3+1+n)$-split, which is more adapted to the needs of a Hamiltonian analysis. Specifically, it is based on linearized ADM variables, c.f. [17]. We introduce accordingly

$$
\begin{aligned}
h_{00} &=: -N && \text{(2.65a)}\\
h_{0i} &=: N_i + \partial_i L\,, && \text{(2.65b)}\\
h_{0a} &=: n_a + \partial_a l\,, && \text{(2.65c)}\\
h_{ij} &=: D_{ij} + \partial_{(i}V_{j)} + \partial_i\partial_j B + \delta_{ij} S\,, && \text{(2.65d)}\\
h_{ab} &=: d_{ab} + \partial_{(a}v_{b)} + \partial_a\partial_b b + \delta_{ab} s\,, && \text{(2.65e)}\\
h_{ia} &=: E_{ib} + \partial_i F_a + \partial_a G_i + \partial_i\partial_a H\,, && \text{(2.65f)}
\end{aligned}
$$

where we distinguish transverse and traceless tensors, transverse vectors and scalars either with respect to the SO(n) or the SO(3) group. For example, $\boldsymbol{D}$ is a 3D tensor but a scalar under the SO(n) group. This decomposition has the clear advantage that it does not introduce any "split-ambiguities" as the one used before. The reason is that—unlike the d'Alembert operator—the Laplace operator in three or n spatial dimensions has an empty kernel on the space of bounded functions. In other words, the decomposition is invertible.

Instead of fixing a particular gauge, we will again work with gauge invariant variables, i.e. combinations of the fields invariant under (2.39). To that end, we introduce the definitions

$$
\begin{aligned}
D_{ij}\,, &\qquad s\,, && \text{(2.66a)}\\
d_{ab}\,, &\qquad E_{ib}\,, && \text{(2.66b)}\\
J &:= 3S + (n-1)s\,, \qquad O := B + b - 2H\,, && \text{(2.66c)}\\
P &:= \dot{B} - \dot{b} - 2(L - l)\,, \qquad Q := \ddot{B} - N - 2\dot{L}\,, && \text{(2.66d)}\\
C_i &:= N_i - \dot{G}_i\,, \qquad W_i := 2G_i - V_i\,, && \text{(2.66e)}\\
w_a &:= 2F_a - v_a\,, \qquad c_a := n_a - \dot{F}_a\,. && \text{(2.66f)}
\end{aligned}
$$

A crucial benefit of the constraint analysis is that it corresponds to a simple reformulation of the theory and does not require to find any explicit solution. As a consequence, we do not have to regularize the setup (to avoid singularities), instead we work with an infinitely thin defect described by n-dimensional delta functions (like for the most part of the 4D covariant analysis).

2.3.2.2 Reduced Lagrangian

Due to gauge invariance, it is possible to fully express the Lagrangian $\mathcal{L}$ in terms of gauge invariant variables. The calculation is straightforward but little enlightening; thus, we do not display the rather lengthy resulting expression. Varying it with respect to the Lagrange multipliers P and Q yields the constraint

$$2\dot{J} + \Delta_3 \left(\dot{O} + P\right) = 0\,, \tag{2.67}$$

which allows to eliminate P, as well as

$$M_D^{D-2}\Big[(2\Delta_3 + 3\Delta_n)J + (2+n)\Delta_3 s + 3\Delta_3\Delta_n O\Big] + M_{\rm Pl}^2\,\delta_n(y) 2\Delta_3\Big[J - (n-1)s\Big] = 0\,, \tag{2.68}$$

constraining O. A third scalar constraint for Q arises in this language by differentiating (2.67) with respect to time and using another dynamical equation (which follows from varying the action with respect to O) to eliminate $\ddot{O}$; we find[20]

$$3\Delta_3 Q - 2\Delta_3 J + 3\ddot{J} - (n-1)\Delta_3 s = 0\,. \tag{2.69}$$

A similar calculation reveals two vector constraints, determining $\boldsymbol{W}$ and $\boldsymbol{w}$; for the sake of completeness,

$$\Delta_3 W_i + 2\dot{C}_i = 0\,, \tag{2.70}$$

$$\Delta_n w_a + 2\dot{c}_a = 0\,. \tag{2.71}$$

We now use the constraints to eliminate the $(4+n)$ non-dynamical variables O, P, Q, $\boldsymbol{W}$ and $\boldsymbol{w}$ (as well as their time derivatives) in the Lagrangian, which consequently is expressed solely in terms of dynamical degrees of freedom. The resulting Lagrangian is diagonal, and by decomposing it into its tensor, vector, and scalar contributions, $\mathcal{L} = \mathcal{L}_{\rm T} + \mathcal{L}_{\rm V} + \mathcal{L}_{\rm S}$, we get:

- Tensor:

$$4\,\mathcal{L}_{\rm T} = M_D^{D-2}\Big[-(\partial_A D_{ij})^2 - (\partial_A d_{ab})^2\Big] + M_{\rm Pl}^2\Big[-(\partial_\mu D_{ij})^2\Big]\delta_n(y) \tag{2.72}$$

[20] In the terminology of the Dirac constraint formalism, this would correspond to a tertiary constraint (while (2.67) and (2.68) are secondary constraints) [54].

The 3D tensor describes two DOF which also have kinetic support on the brane. They correspond to the helicity-two modes in 4D GR and are thus crucial in realizing a 4D regime. The extra space tensor carries $(n+1)(n-2)/2$ DOF which all decouple from the brane. In particular, they would not couple to a localized source on the brane.

- Vector:

$$2\,\mathcal{L}_{\rm V} = M_D^{D-2}\Big[-(\partial_A C_i)^2 - (\partial_A c_a)^2 - (\partial_A E_{ia})^2\Big] + M_{\rm Pl}^2\Big[-(\partial_\mu C_i)^2\Big]\delta_n(y) \tag{2.73}$$

There are two vector DOF, described by $\boldsymbol{C}$, which have a standard DGP type action and hence a localized kinetic term. The remaining $3(n-1)$ vector DOF are decoupled from the brane.

- Scalar:

$$6\,\mathcal{L}_{\rm S} = M_D^{D-2}\Big[-(\partial_A J)^2 - \frac{(n-1)(n+2)}{2}(\partial_A s)^2\Big] + M_{\rm Pl}^2\Big[-(\partial_\mu J)^2 + (n-1)^2(\partial_\mu s)^2\Big]\delta_n(y) \tag{2.74}$$

We find two DOF in the scalar sector. They are decoupled from each other, and, as expected, s has a wrong sign kinetic term on the brane. Also note that for $n = 1$ the scalar s simply disappears, confirming that the codimension-one model is indeed ghost-free on a Minkowski background.

In summary, for $n > 1$ there are always six degrees of freedom that can be excited by an on-brane source. Five of them ($\boldsymbol{D}$, $\boldsymbol{X}$ and J) have a standard DGP-type action, whereas the scalar s comes with a wrong sign kinetic term on the brane—irrespective of the number of codimensions. Therefore, tuning the tension to zero seems to cause the same ghost pathology in any higher dimension. In addition, there are further $[n(n+5)/2-4]$ DOF that only propagate in the bulk and are invisible to a brane observer. In total, we have $D(D-3)/2$ DOF corresponding exactly to the number of propagating degrees of freedom in D-dimensional Einstein gravity. This result agrees with what we have found in the Lorentz covariant analysis in Sec. 2.3.1. To be precise, the five healthy DOF can be identified according to $\boldsymbol{\mathcal{D}} \to \{\boldsymbol{D}, \boldsymbol{C}, J\}$, where in both cases the ghost is described by s (or $\mathcal{S}$ equivalently). Let us stress that our calculation is also valid for one codimension; in that special case s completely drops out of the equations, thus leaving a theory of five healthy degrees of freedom as expected.

2.3.2.3 Reduced Hamiltonian

A ghost mode necessarily leads to a classical instability, which manifests itself in a Hamiltonian that is *not* bounded from below. In the remainder of this section, we will show that excitations of the ghost mode indeed lower the local energy density at the brane, thereby

revealing a pathology[21]. Since all tensor and vector modes have a DGP type action like the scalar J, it suffices to investigate the scalar sector only. The only difficulty in deriving the Hamiltonian consists in a proper treatment of the localized terms. This can be consistently done by decomposing the conjugate momentum fields

$$\tilde{\Pi}_J := \delta\mathcal{L}/\delta\dot{J} \qquad \text{and} \qquad \tilde{\Pi}_s := \delta\mathcal{L}/\delta\dot{s} \tag{2.75}$$

into a regular and an irregular part according to

$$3\,\tilde{\Pi}_J = \Big[M_D^{D-2} + M_{\rm Pl}^2\,\delta_n(y)\Big]\Pi_J\,, \tag{2.76a}$$

$$6\,\tilde{\Pi}_s = \Big[(n-1)(n+2)\,M_D^{D-2} - 2(n-1)^2\,M_{\rm Pl}^2\,\delta_n(y)\Big]\Pi_s\,, \tag{2.76b}$$

where we defined

$$\Pi_J := \dot{J} \qquad \text{and} \qquad \Pi_s := \dot{s}\,. \tag{2.77}$$

This decomposition is well defined because $\dot{J}$ and $\dot{s}$ are regular functions at the brane (only r-derivatives would introduce discontinuities). The scalar Hamiltonian density for both fields,

$$\mathcal{H}_J := \tilde{\Pi}_J\dot{J} - \mathcal{L}_J \qquad \text{and} \qquad \mathcal{H}_s := \tilde{\Pi}_s\dot{s} - \mathcal{L}_s\,, \tag{2.78}$$

can then be readily derived. For the healthy scalar we get a contribution

$$6\,\mathcal{H}_J = M_D^{D-2}\Big[(\Pi_J)^2 + (\partial_i J)^2 + (\partial_a J)^2\Big] + M_{\rm Pl}^2\Big[(\Pi_J)^2 + (\partial_i J)^2\Big]\delta_n(y)\,, \tag{2.79}$$

which indeed shows that J contributes positively to the energy of the system. The tensor- and vector contributions take the same (manifestly positive) form, with J replaced by D_{ij} and X_i, respectively. Hence, they also constitute healthy (brane-coupled) fields. However, the expression for the scalar s becomes

$$\begin{aligned} 12\,\mathcal{H}_s = (n-1)(n+2)\,M_D^{D-2}\Big[(\Pi_s)^2 + (\partial_i s)^2 + (\partial_a s)^2\Big] \\ - 2(n-1)^2\,M_{\rm Pl}^2\Big[(\Pi_s)^2 + (\partial_i s)^2\Big]\delta_n(y)\,, \end{aligned} \tag{2.80}$$

thus displaying a *negative* energy contribution at the brane position. In accordance with the result of the last section, it is present for an arbitrarily small coefficient $M_{\rm Pl}$ and only vanishes if the induced term is set to zero exactly. In the latter case our result simply reflects the stability of higher-dimensional Einstein gravity.

As an aside, note that we also derived the Hamiltonian from the full Lagrangian and

[21] Note that we did not calculate the vacuum persistence amplitude for $n > 2$, but we also expect a violation of unitarity in that case.

applied the Dirac constraint formalism in order to obtain the Hamiltonian on the constraint surface. After appropriate redefinitions of the conjugate fields, it is possible to check that both Hamiltonians are identical. For the sake of simplicity, here we only presented the more compact (but equivalent) derivation starting with the reduced Lagrangian.

This diagnostic tool was also used in an earlier work [19]. However, there it led to the erroneous claim that the theory in 6D without a brane-tension is ghost-free.[22] The purpose here was to present a corrected analysis which also extends to higher dimensions.

2.4 Pure tension vacuum

At first sight, the results of the last section seem discouraging and raise the question whether gravity induced on higher-codimensional surfaces is generically unstable. However, from the perspective of an EFT, such an outcome is little satisfying (see the discussion in Sec. 1.4). And indeed, as mentioned before, the assumption of having a vanishing brane tension corresponds to a fine-tuning and hence does not represent a natural EFT. In this part, we therefore extend the previous stability analysis to the case of a sub-critical pure tension brane in six dimensions.

We start by discussing the background geometry. In a second step, we derive the corresponding perturbation theory and again apply the vacuum-to-vacuum amplitude as a tool to infer the classical and quantum stability of the model. Finally, we discuss whether our results are compatible with a natural EFT, and will answer that question in the affirmative. Subsequently, the phenomenology of the model is studied and further conclusions about its viability are drawn. As opposed to the Minkowski analysis, we will work in polar coordinates (r, ϕ), to be precise $x^A = (x^\mu, r, \phi)$ with the standard ranges $r \in [0, \infty)$, $\phi \in [0, 2\pi)$.

2.4.1 Conical background

It is widely known that a pure tension brane in six dimensions corresponds to a flat bulk geometry with a wedge removed. In more physical terms, this means that the proper circumference an observer would measure at some distance away from the brane is reduced by a factor $(1 - \delta/2\pi)$, with δ the deficit angle. Correspondingly, in an embedding picture, this geometry corresponds to a cone, where the conical singularity is produced by the brane (see also Sec. 1.3). Moreover, in four dimensions, it is the well-known geometry of an infinitely thin (local) cosmic string [166, 88, 96].

As already discussed in Sec. 2.1, we have to regularize the setup to avoid the conical singularity at the brane position and thus to get well-defined expressions for the extrinsic curvature evaluated at the brane. As before, we do this by replacing the brane with a codimension-one object, i.e. a ring of circumference $2\pi R$ in the 6D model. By assuming a regular and flat interior geometry, the correct embedding picture corresponds to a capped

[22] The reason for that failure is discussed in the appendix of [75].

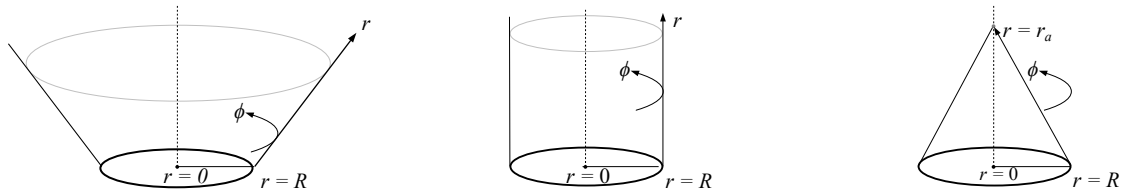

(a) $\delta < \delta_{\text{crit}}$ (b) $\delta = \delta_{\text{crit}}$ (c) $\delta > \delta_{\text{crit}}$

Figure 2.2: Embedding diagrams of the regularized static geometry in the case of a pure tension brane. The circle at $r = R$ describes the brane. As the tension approaches the critical value, the deficit angle approaches 2π, and the bulk geometry becomes cylindrical (b). For super-critical tensions a naked singularity develops in the bulk at a finite distance away from the brane.

cone. The (regularized) defect line element is then given by the following expression:

$$\begin{aligned} \mathrm{d}s^2 &= {}^{(0)}g_{6AB}\,\mathrm{d}x^A\mathrm{d}x^B \\ &:= \eta_{\mu\nu}\,\mathrm{d}x^\mu\mathrm{d}x^\nu + \mathrm{d}r^2 + g(r)^2\mathrm{d}\phi^2 \end{aligned} \tag{2.81a}$$

$$g(r) := \begin{cases} r & (r < R) \\ R + \left(1 - \dfrac{\delta}{2\pi}\right)(r - R) & (r > R) \end{cases} \tag{2.81b}$$

It is straightforward to check that the metric ${}^{(0)}\boldsymbol{g}_6$ fulfills Einstein's equations (as specified in Sec. 2.1.2) for a localized pure tension source,

$$\tilde{T}^\alpha{}_\beta = -\frac{\lambda}{2\pi R}\delta^\alpha{}_\mu\delta^\mu{}_\beta\,, \tag{2.82}$$

if we identify $\delta = \lambda/M_6^4$.[23] As a first consistency check note that (2.81) coincides with (1.14) in the limit $R \to 0$. At this point, let us also stress that the angular pressure $\tilde{T}^\phi{}_\phi$ has to vanish for the static solution to exist.

For $\delta < 2\pi$ this solution has two interesting properties: First, the intrinsic brane geometry is flat, and second, the bulk geometry exhibits a deficit angle as a global curvature effect.[24] This constitutes the *sub-critical* vacuum we will study in this section. However, we see from (2.81) that there exists a *critical* value of the tension $\lambda_{\text{c}} := 2\pi M_6^4$ corresponding to a deficit angle of 2π. In that case, the geometry becomes cylindrical meaning that one of the extra space dimensions has become compact (of constant size $2\pi R$). If the tension is raised above that critical value, i.e. becomes *super-critical*, the exterior of the ring closes

[23] Here, the factor $2\pi R$ is chosen such that λ corresponds to a 4D brane tension.

[24] Later in Sec. 3.2.5, we will see that it falls into a class of solution derived long ago by Levi-Civita [114] to describe the geometry of a cylinder in 4D.

in a second (conical) singularity away from the brane at the coordinate position

$$r_a = \frac{\delta}{\delta - 2\pi} R \,. \tag{2.83}$$

It qualifies as a naked singularity because there is no horizon shielding it from some outside region. Physically, it can be understood as the presence of a second sub-critical brane with tension $\lambda_a = 4\pi M_6^4 - \lambda$. We will provide a complete discussion of this vacuum in Sec. 3.5. The corresponding embedding diagrams are depicted in Fig. 2.2. The super-critical case will be discussed extensively in Chapter 3.5.

In summary, there is a static solution describing a sub-critical and super-critical brane. In this section we infer the stability of the sub-critical solution—best described as a capped cone in extra space—by performing a linear stability analysis.

2.4.2 Perturbation theory

The stability analysis of Sec. 2.3 used a manifestly 4D Lorentz covariant decomposition of the graviton field. As we discussed in detail there, due to the occurrence of the inverse d'Alembert operator in the projectors, this split is not unambiguous but introduces another gauge freedom restricted to homogeneous functions. In the Hamiltonian analysis this difficulty was avoided by using ADM like variables as well as a three and n-dimensional decomposition thereof. As the corresponding projectors only involve the inverse Laplace operators, they are invertible on the space of bounded functions. In this part we will thus specialize the decomposition of the ADM variables, defined in (2.65), to $n = 2$.

2.4.2.1 Gauge invariant variables

Let us define fluctuations around the background solution (2.81),[25]

$$g_{6AB} = {}^{(0)}g_{6AB} + h_{AB} \,. \tag{2.84}$$

In this analysis we make explicit use of the SO(2)-symmetry. This allows us to set $h_{\phi\mu} = h_{\phi r} = 0$. Like in the Minkowski analysis, we require the brane to sit at a constant coordinate position $r = R$ which neither depends on time nor the spatial brane coordinates x^i. Note that this is no physical restriction as a (x^i-dependent) movement of the brane can always be accommodated by non-vanishing $h_{r\mu}$ components. We then have

$$h_{AB} = \begin{pmatrix} h_{\mu\nu} & h_{\mu r} & 0 \\ h_{r\nu} & h_{rr} & 0 \\ 0 & 0 & h_{\phi\phi} \end{pmatrix} =: \begin{pmatrix} -N & h_{0j} & l' & 0 \\ h_{i0} & h_{ij} & h_{ir} & 0 \\ l' & h_{rj} & h_{rr} & 0 \\ 0 & 0 & 0 & h_{\phi\phi} \end{pmatrix} . \tag{2.85}$$

The 3D components h_{ij} , h_{0i} are decomposed according to (2.65d) and (2.65b), respectively.

[25] Indices are raised with the background metric ${}^{(0)}\boldsymbol{g}_6$.

The h_{ir} components are decomposed as

$$h_{ir} =: G_i' + \partial_i H' \,, \tag{2.86}$$

corresponding to (2.65f) in polar coordinates. The covariantized version of Def. (2.40b) reads[26]

$$h_{ab} =: \nabla_a \nabla_b b + \gamma_{ab} s \,, \tag{2.87}$$

where ∇_a is the covariant derivative constructed with $g^{(0)}_{6ab}$. Then, $h_{\phi\phi}$ and h_{rr} can be related to s and b via

$$h^r{}_r = b'' + s \,, \qquad\qquad h^\phi{}_\phi = \frac{g'}{g} b' + s \,. \tag{2.88}$$

In order to make the presentation more compact, we will focus on the scalar sector as it covers all interesting physics. The results for the vector and tensor sector will not be derived in detail and just stated for the sake of completeness. We will again work with gauge invariant variables $\{s, J, O, P, Q\}$ as defined in (2.87), (2.66c) and (2.66d), respectively. It is straightforward to check that they are invariant under

$$\delta h_{AB} = \nabla_{(A} \xi_{B)} \,, \tag{2.89}$$

where ξ^A is subject to the restrictions

$$\xi_r|_0 = 0 \,, \qquad\qquad \xi_\phi = 0 \,, \qquad\qquad \partial_\phi \xi_\mu = \partial_\phi \xi_r = 0 \,. \tag{2.90}$$

While the first relation takes into account that the brane resides at a specific constant coordinate position, the latter two are just a consequence of the rotational symmetry in the bulk. From this we can derive a further gauge invariant (localized) field,

$$\varphi := h^\phi{}_\phi|_0 \,. \tag{2.91}$$

It describes fluctuations of the circumference of the brane and is thus referred to as the radion. As already discussed in Sec. 2.1, we set this field to zero by assuming the existence of some underlying stabilization mechanism. The fact that φ is gauge invariant ensures that this is indeed a physical requirement—as opposed to a mere coordinate statement. We will provide a justification for this approach by discussing an explicit microscopic construction in Sec. 2.4.3. Here, we rather try to keep the calculation as general as possible by not referring to a specific UV model.

[26] In two codimensions there is neither a transverse and traceless tensor $\boldsymbol{d}$ nor a transverse vector $\boldsymbol{v}$ (due to the ϕ-symmetry).

2.4.2.2 Bulk dynamics

Away from the brane ($r \neq R$) the vacuum bulk equations (2.6) have to be applied; at linear order in h_{AB} they read

$$\Box_6 h_{AB} + \nabla_A \nabla_B h^C{}_C - 2\nabla_C \nabla_{(A} h^C{}_{B)} + \gamma_{AB} \left(\nabla^C \nabla^D h_{CD} - \Box_6 h^C{}_C \right) = 0 \,. \tag{2.92}$$

The covariant 6D box operator is

$$\Box_6 = \Box_4 + \partial_r^2 + \frac{g'}{g}\partial_r = \begin{cases} \Box_4 + \partial_r^2 + \dfrac{1}{r}\partial_r & (r < r_0) \\ \Box_4 + \partial_r^2 + \dfrac{1}{r + \beta r_0}\partial_r & (r > r_0) \,, \end{cases} \tag{2.93}$$

where $\Box_4 = \partial_\mu \partial^\mu$ is the 4D d'Alembert operator and

$$\beta := \frac{\delta}{2\pi - \delta} \,. \tag{2.94}$$

Let us now extract the scalar parts from (2.92) in the same way as we did for the graviton decomposition. The (00) component,

$$(2\Delta_3 + 3\Delta_2)\, J + 4\Delta_3 s + 3\Delta_2 \Delta_3 O = 0 \,, \tag{2.95}$$

is a constraint on O. Unsurprisingly, it coincides with (2.68) (for $n = 2$ and evaluated away from the brane) in the Hamiltonian analysis. The $(0r)$ component once integrated w.r.t. r becomes

$$2\dot{J} + \Delta_3 \left(\dot{O} + P \right) = 0 \,, \tag{2.96}$$

thereby reproducing (2.67) and fixing P. The difference of the (rr) and $(\phi\phi)$ equation is

$$J - s - Q + \Delta_3 O + \dot{P} = 0 \,, \tag{2.97}$$

hence determining Q in terms of the other variables[27]. Therefore, the three fields O, P and Q are not dynamical and thus fully determined once the solutions for J and s are obtained. The latter two are the real dynamical degrees of freedom; we find accordingly

$$\Box_6 J = 0 \qquad \text{and} \qquad \Box_6 s = 0 \,, \tag{2.98}$$

which can be both inferred from the scalar projections of the (ij) component by using the constraint relations. There are two further scalar equations, viz. $(0i)^{(C)}$ and $(ir)^{(H)}$, which are redundant due to the Bianchi identities.

In accordance with the previous analysis on a Minkowski background, there are two dynamical scalars. For the sake of completeness, note that the tensor sector contains two DOF carried by D_{ij} and the vector sector another two associated with C_i as defined in

[27] Eq. (2.69) turns out to be a certain combination of the three constraint equations above.

(2.66e). There is thus a total of six dynamical DOF, which is the proper number for six-dimensional GR with azimuthal symmetry[28].

2.4.2.3 Matching equations

Having established the vacuum equations, we still have to impose matching conditions at the brane. This can be done in a covariant way by using Israel's junction conditions (2.9), which relate the localized energy momentum $\tilde{\boldsymbol{T}}$ to the extrinsic curvature $\tilde{\boldsymbol{K}}$ at the brane. To obtain its first oder approximation on a pure tension background, we introduce matter fluctuations according to[29]

$$\tilde{T}^{\alpha}{}_{\beta} = {}^{(0)}\tilde{T}^{\alpha}{}_{\beta} + {}^{(1)}\tilde{T}^{\alpha}{}_{\beta} \tag{2.99a}$$

$$=: -\frac{\lambda}{2\pi R}\delta^{\alpha}{}_{\mu}\delta^{\mu}{}_{\beta} - \frac{1}{2}\tilde{U}^{\alpha}{}_{\beta}\,, \tag{2.99b}$$

where $\tilde{\boldsymbol{U}}$ is assumed to be ϕ-independent. Like for the graviton field in (2.65d), we also decompose the first order energy momentum tensor into 3D scalars, vectors and tensors,

$$\tilde{U}_{0i} = \tilde{U}^{(N)}_i + \partial_i \tilde{U}^{(L)}\,, \tag{2.100a}$$

$$\tilde{U}_{ij} = \tilde{U}^{(D)}_{ij} + \partial_{(i}\tilde{U}^{(V)}_{j)} + \partial_i\partial_j\tilde{U}^{(B)} + \delta_{ij}\tilde{U}^{(S)}\,. \tag{2.100b}$$

While $\tilde{\boldsymbol{U}}^{(D)}$ is completely unconstrained, energy conservation implies for the other components of the decomposition

$$-\dot{\tilde{U}}_{00} + \Delta_3\tilde{U}^{(L)} = 0\,, \tag{2.101a}$$

$$-\dot{\tilde{U}}^{(L)} + \Delta_3\tilde{U}^{(B)} + \tilde{U}^{(S)} = 0\,, \tag{2.101b}$$

$$-2\dot{\tilde{U}}^{(N)}_i + \Delta_3\tilde{U}^{(V)}_i = 0\,. \tag{2.101c}$$

Moreover, as mentioned before, the $\tilde{U}_{\phi\phi}$ component will be fixed by the requirement of having a constant proper circumference also on the level of fluctuations. The first order expression for the extrinsic curvature tensor is found to be

$${}^{(1)}\tilde{K}^{\mu}{}_{\nu} = \frac{1}{2}\left(\partial_r h^{\mu}{}_{\nu} - \partial^{\mu}h_{\nu r} - \partial_{\nu}h^{\mu}{}_{r}\right)\big|_0\,, \tag{2.102a}$$

$${}^{(1)}\tilde{K}^{\phi}{}_{\phi} = -\frac{1}{2}\left(\frac{g'}{g}h^{r}{}_{r}\right)\bigg|_0\,, \tag{2.102b}$$

where the radion contribution was already set to zero.

[28] Since we did not implement that symmetry in the Minkowski analysis, we found more than six DOF there. However, all additional DOF are not sourced by an on-brane source and therefore irrelevant.

[29] The 5D matter tensor $\tilde{\boldsymbol{U}}$ introduced here is related to its 4D counterpart introduced in Sec. 2.3.1 via $\boldsymbol{U} = 2\pi R\tilde{\boldsymbol{U}}$.

The scalar matching equations can then be derived by projecting the linearized Israel junction conditions. By taking a appropriate linear combination of the 4D trace, the scalar $(ij)^{(S)}$ and the $(\phi\phi)$ component, we find the two junction conditions for J and s; explicitly,

$$[J']_{\rm disc} + L_2\,\Box_4 J|_0 = \frac{1}{M_6^4}\left(-\tilde{U}^{\mu}{}_{\mu} + 3\tilde{U}^{(S)}\right)\,, \tag{2.103a}$$

$$4[s']_{\rm disc} + L_2\,\Box_4 s|_0 = \frac{1}{M_6^4}\left(-\tilde{U}^{\mu}{}_{\mu} + 3\tilde{U}^{\phi}{}_{\phi}\right)\,. \tag{2.103b}$$

To derive the final form of the localized kinetic terms, we use the bulk vacuum equations in the limit $r \to R$, which imply for the induced Einstein tensor, which we denote by $\tilde{\boldsymbol{G}}$:

$$\tilde{G}^{\alpha}{}_{\alpha} = 2\,\tilde{G}^{\phi}{}_{\phi} = -\Box_4 s|_0\,. \tag{2.104}$$

Subsequently, we consider the $(\phi\phi)$ component,

$$-\left[(h^{\alpha}{}_{\alpha})'\right]_{\rm disc} + L_2\,\Box_4 s|_0 = \frac{1}{M_6^4}\,\tilde{U}^{\phi}{}_{\phi}\,. \tag{2.105}$$

To further simplify it, we use the discontinuity in the r-derivative of (2.97), yielding[30]

$$\left[(h^{\alpha}{}_{\alpha})'\right]_{\rm disc} = -\Box_4[b']_{\rm disc}\,, \tag{2.106}$$

and a further relation which follows from the second equation in (2.88) after using the continuity of $h^{\phi}{}_{\phi}$

$$[b'] = -\left[\frac{g}{g'}\right]_{\rm disc} s|_0 = -\frac{R\,\delta}{2\pi-\delta}\,s|_0\,. \tag{2.107}$$

Then, the final form of the $(\phi\phi)$ junction condition is

$$\tilde{U}^{\phi}{}_{\phi} = M_6^4\,(L_2 - \beta R)\,\Box_4 s|_0\,. \tag{2.108}$$

This equation determines the momentum in angular direction, $\tilde{U}^{\phi}{}_{\phi}$, which is needed to stabilize the circumference or to set $\varphi = 0$, equivalently.[31] Substituting $\tilde{U}^{\phi}{}_{\phi}$ in (2.103b) yields the final junction condition for s

$$4[s'] - 2f^{(s)}L_2\Box_4 s|_0 = -\tilde{U}^{\mu}{}_{\mu}/M_6^4\,, \tag{2.109}$$

where the following dimensionless constants have been introduced

$$f^{(s)} := 1 - \frac{3R}{2L_2}\,\beta\,. \tag{2.110}$$

[30]Note that $[H']_{\rm disc} = [l']_{\rm disc} = 0$ due to the continuity of the metric.
[31]In the non-stabilized case it would constitute a dynamical equation for φ (cf. the appendix in [75]).

Let us first check that the last equation has a proper Minkowski limit by setting $\beta = 0$ and comparing it to (2.62b) for $n = 2$ and $s = -3\mathcal{S}$. And indeed, both equations coincide. This nicely demonstrates that the thin brane setup is physically equivalent to the regularized setup (in the limit $R \to 0$), provided the ring circumference is stabilized.

In summary, we derived a closed system for the two dynamical scalars J and s consisting of the vacuum equations (2.98) and the matching equations (2.103a) and (2.109), respectively. As a new and interesting feature, we find that the function $f^{(s)}$, appearing in the junction condition for s, has no longer a definite sign. Instead, it defines a hypersurface in the parameter space characterized by $f^{(s)} = 0$ separating two regions corresponding to different signs of $f^{(s)}$. We will discuss the physics of both regions below. For the sake of completeness note that the tensor and vector equations take the same form as (2.98) and (2.103a) with J formally replaced by either $\boldsymbol{D}$ or $\boldsymbol{C}$.

2.4.2.4 Vacuum persistence

Expressed through the gauge invariant variables J and s, the source-to-source amplitude (2.63) becomes

$$\mathcal{A} = \frac{2\pi R}{6} \int \mathrm{d}^4x \, \left[2 \left(\tilde{U}^{\mu}{}_{\mu} - 3\tilde{U}^{(S)} \right) J + \tilde{U}^{\mu}{}_{\mu} s \right] \Big|_0 , \tag{2.111}$$

which contains separate contributions from J and s; accordingly we identify two amplitudes $\mathcal{A}^{(J)}$ and $\mathcal{A}^{(s)}$. The Minkowski analysis in Sec. 2.3 has revealed s as the only unstable mode. Therefore, we will mostly focus on $\mathcal{A}^{(s)}$ to infer the stability of the deficit background. In fact, it is possible by specializing on a source with $\tilde{U}^{\mu}{}_{\mu} - 3\tilde{U}^{(S)} = 0$ to exclusively excite this particular scalar mode. Having derived the amplitude for our prime suspect s, it is straightforward to deduce that J is healthy in the whole parameter regime. The amplitude in question is

$$\mathcal{A}^{(s)} = \frac{2\pi R}{6} \int \mathrm{d}^4x \, \tilde{U}^{\mu}{}_{\mu} s|_0 \, . \tag{2.112}$$

As before, in order to infer its imaginary part, we can borrow most of the work from the prototype discussion in Sec. 2.2 by identifying $f \to f^{(s)}/2$. However, there is a small complication due to the nontrivial background geometry which causes a tension dependence of the 6D wave operator, cf. (2.93). This leads to a couple of changes in the derivation, which will be briefly presented below; however, the central conclusion, namely that the sign of $f^{(s)}$ determines the stability of the model, remains unaltered.

The solution for the exterior region (2.24) is modified due to the defect geometry,

$$\hat{s}(p, r) = \frac{K_0(\tilde{r}\sqrt{p^2})}{K_0(\tilde{r}_0\sqrt{p^2})} \, \hat{s}|_0 \quad (r > R) \, , \tag{2.113}$$

where $\tilde{r} := r + \beta R$ [and $\tilde{r}_0 = (1 + \beta) R$]. This leads to a modified inverse propagator $Z_2^{(s)}(p)$

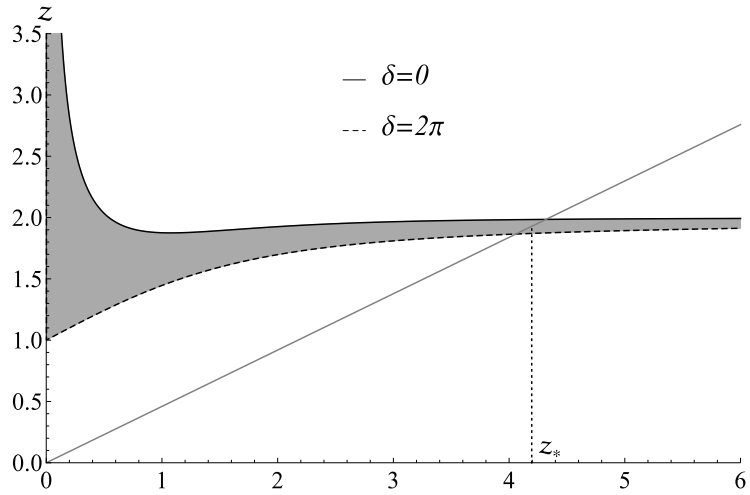

Figure 2.3: Right-hand side (all curves inside the shaded region) and left-hand side (gray line) of Eq. (2.115). The intersection determines the ghost mass $m_* \equiv z_*/r_0$. While for a positive slope of the left-hand side there is always a solution, it vanishes for a negative slope.

[cf. Eq. (2.26)], which now becomes

$$Z_2^{(s)}(p) = f^{(s)}\,\frac{L_2}{2R}\,z^2 - \,z\left(\frac{I_1(z)}{I_0(z)} + \frac{K_1((1+\beta)z)}{K_0((1+\beta)z)}\right)\,. \tag{2.114}$$

This in turn implies a slightly different mass $m_* = z_*/R > 0$ for the tachyon pole, which is given as a solution of

$$f^{(s)}\,\frac{L_2}{2R}\,z_* = \frac{I_1(z_*)}{I_0(z_*)} + \frac{K_1((1+\beta)z_*)}{K_0((1+\beta)z_*)}\,. \tag{2.115}$$

The right side of this equation is depicted in Fig. 2.3. We find that for $f^{(s)} > 0$ there is a pole—irrespective of the value of δ—corresponding to the intersection at the point z_*. Therefore, the qualitative statement is unaltered on a deficit angle background, only the precise value of the mass differs.

To check whether this tachyon again corresponds to a ghost, we have to determine the sign of its residue. The expression (2.37) can be readily generalized to

$$\begin{aligned} -\,\mathrm{sign}\,(\mathcal{C}_1)\,\mathrm{Res}\left(\frac{1}{Z_2^{(s)}(p)},\,\omega = \pm\,\omega_*\right) \\ = -\frac{1}{\omega_* R^2}\left[f^{(s)}\,\frac{L_2}{R} + \beta + \left(\frac{I_1}{I_0}\right)^2 - (1+\beta)\left(\frac{K_1}{K_0}\right)^2\right]^{-1}\,, \end{aligned} \tag{2.116}$$

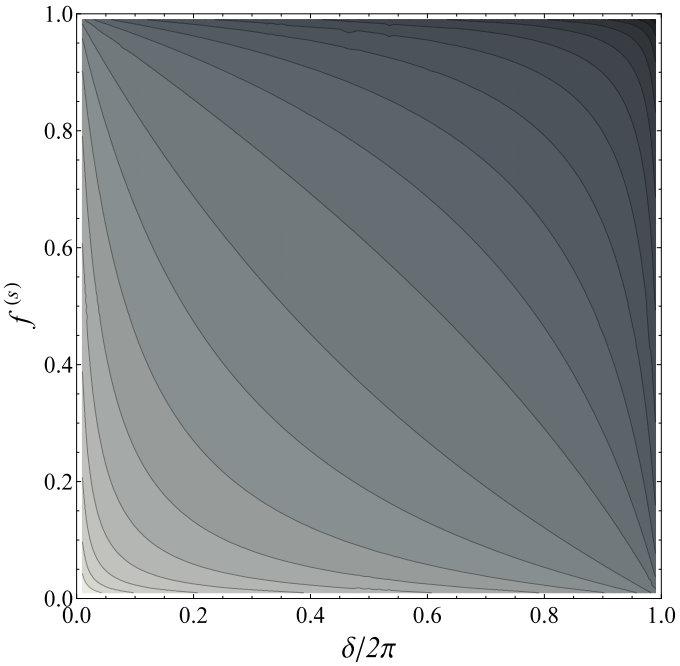

Figure 2.4: Contour plot of the square bracket expression in (2.116). It is positive in the whole relevant parameter space, i.e. when the pole at ω_* exists. The values range from ∞ (in the lower left corner / bright) to 0 in the (upper right corner / dark).

where $\text{sign}\,(\mathcal{C}_1)$ depends on the orientation of the closed contour encircling the pole (cf. Fig. 2.1a) and ω_* is defined in (2.35). The Bessel I and K functions are evaluated at z_* and $(1+\beta)z_*$, respectively. As opposed to the Minkowski background, it is not possible to further simplify the expression in square brackets. However, we can show numerically that it has a ghostly sign for all parameter values; to be precise, we plot its value as a function of the model parameters $\delta/2\pi = \beta/(1+\beta)$ and $f^{(s)}$. The relevant parameter regime is

(i) $\delta \in [0, 2\pi)$ (since we are considering sub-critical branes) and

(ii) $f^{(s)} \in (0, 1]$ (since the pole only exists for $f^{(s)} > 0$ and $f^{(s)} \leq 1$ by definition).

The result is shown in Fig. 2.4 and nicely illustrates that the expression in square brackets is positive in the whole relevant parameter regime, hence implying that (2.116) is strictly negative. Since this sign already reflects the sign of the corresponding contribution to the imaginary part of $\mathcal{A}^{(s)}$, we conclude that the tachyon is always a ghost.

On the other hand, for $f^{(s)} < 0$ the pole contribution totally vanishes and only the branch cut contribution is left. As before, we checked by numerically solving the corresponding integral in the case of an ω-independent source that it always has a positive imaginary part in the whole parameter regime (even for $f^{(s)} > 0$). Our results are depicted in Fig. 2.5. We consider a more exhaustive analysis (by analytical means) of this contribution to be

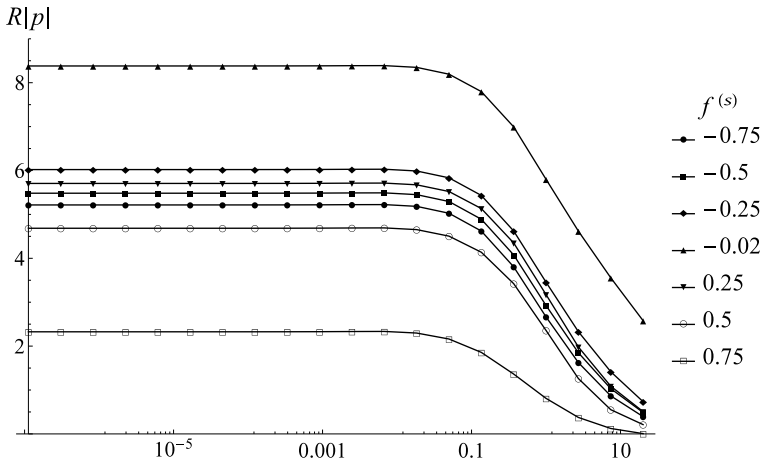

Figure 2.5: Numerical evaluation of $-\operatorname{Im}\left[R\int_{\mathcal{C}_2}\mathrm{d}\omega\, Z_2^{-1}(\omega,\boldsymbol{p})\right]$ for different values of $f^{(s)}$. We find that the branch cut always yields a positive contribution. The deficit angel is chosen to be $\delta=\pi$; though, we checked that others choices lead to the same qualitative outcome. We only consider cases for which $R\boldsymbol{p}\lesssim 1$ to be insensitive to the details of the regularization.

unnecessary; after all, we do not expect the KK-sector (represented by the branch cut) to cause any pathologies as it is present even without the induced gravity term.

The crucial findings of this section are summarized in Fig. 2.6. To conclude, the deficit angle background is unstable for model parameters characterized by $f^{(s)}>0$, and stable otherwise. The statement can be rephrased as a stability bound on $\bar{\lambda}$:

$$\boxed{\bar{\lambda}>\frac{2L_2}{2L_2+3R}} \tag{2.117}$$

This constitutes the central result of this chapter. A subsequent discussion of related prospects is provided in Sec. 2.5.

2.4.3 Dynamical stabilization

In the previous discussion, we set size fluctuations of the compact brane dimensions to zero, corresponding to the choice $\varphi=0$. The physical motivation should be clear: Our approach assumes the existence of an underlying stabilization mechanism. Since we are interested in low energy questions, we expect them to be insensitive to this sector (which is operative on much shorter distances, cf. Sec. 2.1). Correspondingly, we turned of the dynamics related to the brane modulus φ. On a technical level, this was achieved by dialing the angular pressure component according to (2.108).

The aim of this section is to make the above reasoning more concrete and thus to provide an explicit example of a microscopic mechanism that stabilizes the brane. To that end, we follow the approach described in [157] (and in the context of BIG also in [104]).

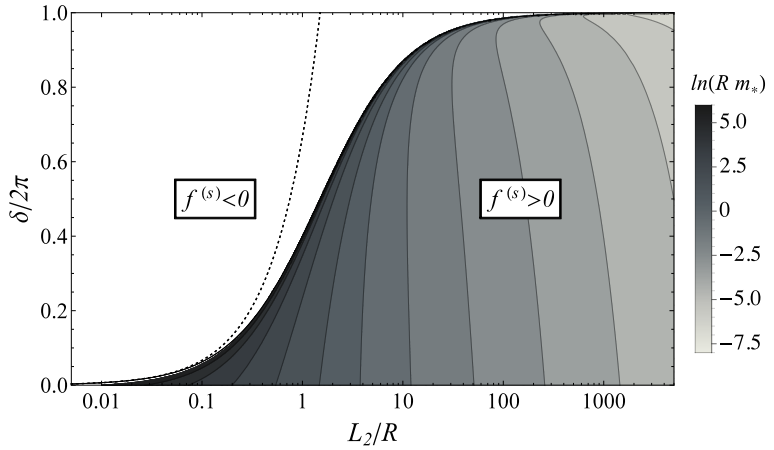

Figure 2.6: Parameter plot depicting the stable ($f^{(s)} < 0$) and unstable ($f^{(s)} > 0$) regions in parameter space. The contours in the unstable regime correspond to the ghost mass m_* (measured in units of $1/R$), which increases towards the separatrix $f^{(s)} = 0$. The dotted line is a stronger stability bound: the parameter space to its left exhibits natural configurations, i.e. those without fine-tuning.

We start by putting a massless scalar field Σ on the brane; to be specific, we choose

$$\mathcal{S}_{\text{stab}} = -\int \mathrm{d}^5\tilde{x}\,\sqrt{-\tilde{g}}\,\frac{1}{2}\nabla^\alpha\Sigma\nabla_\alpha\Sigma \tag{2.118}$$

in the localized action (2.2), and then consider a background solution for which the scalar field winds around the ring,

$$\Sigma = q\phi\,, \tag{2.119}$$

where q is a constant. Together with (2.2), this leads to the following background energy momentum tensor (EMT),

$$\tilde{T}^\mu{}_\nu = -\left(\tilde{\lambda} + \frac{q^2}{4}g^{\phi\phi}\right)\delta^\mu_\nu\,, \tag{2.120a}$$

$$\tilde{T}^\phi{}_\phi = -\tilde{\lambda} + \frac{q^2}{4}g^{\phi\phi}\,, \tag{2.120b}$$

where $g^{\phi\phi} = 1/R^2$ at the background level. As discussed in Sec. 2.4.1, the static pure tension solution only exists for $\tilde{T}^\phi{}_\phi = 0$, which can now be achieved by choosing q such that

$$\frac{q^2}{4R^2} = \tilde{\lambda}\,. \tag{2.121}$$

From (2.120a) we see that this doubles the contribution of $\tilde{\lambda}$ to the 4D EMT. After ab-

sorbing this factor by a trivial renormalization[32], $\tilde{\lambda}_{(\text{ren})} \equiv 2\tilde{\lambda}_{(\text{bare})}$, and identifying the 4D brane tension as usually via

$$\lambda \equiv 2\pi R \tilde{\lambda}_{(\text{ren})} \,, \tag{2.122}$$

we arrive at the background EMT (2.82). Thus, winding Σ around the ring in this way indeed leads to the static deficit angle solution presented in Sec. 2.4.1. But a successful stabilization should also suppress the fluctuations of the brane circumference, as measured by the radion field $\varphi \equiv h_{\phi\phi}$. Let us now show that this can also be achieved in this particular example.

First, note that the fluctuations of Σ can be consistently set to zero, since this field is not sourced. Next, perturbing the background metric in (2.120) leads to the following first order contribution to the EMT,

$$\tilde{U}^{\phi}{}_{\phi} = \frac{M_6^4}{R} \frac{\delta}{2\pi} \varphi \,, \tag{2.123}$$

where we eliminated $\tilde{\lambda}$ in favor of the deficit angel δ. At this point, we see the difference to the previous analysis: Now $\tilde{U}^{\phi}{}_{\phi}$ is fully determined by φ [instead of being implicitly fixed by the requirement of $\varphi = 0$ via (2.108)].[33] To put it differently, the radion describes the dynamics of the compact brane dimension and as such leads to a pressure component in angular direction. Whether this leads to a sufficient stabilization, can now be answered.

In order to obtain a dynamical equation for φ, we have to redo the analysis of Sec. 2.4.2.2 and Sec. 2.4.2.3 with φ ($\neq 0$) restored. This calculation is straightforward and hence we only state the final equation

$$\left(\Box_4 - m_\varphi^2\right) \varphi - \left(1 - \frac{L_2}{\beta R}\right) \Box_4 s|_0 = 0 \,, \qquad\qquad m_\varphi^2 := \frac{1 - \delta/2\pi}{R^2} \,. \tag{2.124}$$

The physical picture is compelling: The stabilization endows φ with a mass. Since $m_\varphi \propto 1/R$, the radion gets heavier as the regularization size R decreases, and so it costs more energy to excite this DOF. In the low energy regime we are aiming at, i.e. at energies well below $1/R$, the kinetic term of φ is negligible, [34] and we obtain

$$\varphi \approx \left(\frac{L_2}{\beta R} - 1\right) \frac{\Box_4}{m_\varphi^2} s|_0 \,. \tag{2.125}$$

[32] In the main text, we work with the renormalized quantity $\tilde{\lambda}_{(\text{ren})}$.

[33] In principle, we might also include additional unresolved contributions to $\tilde{U}^{\phi}{}_{\phi}$, from which we restrain for the sake of simplicity.

[34] This is not true in the near-critical regime, where the factor $1 - \delta/2\pi$ suppresses the radion mass. However, we are here only discussing one particular stabilization mechanism. There might as well be other examples, where the brane width is also stabilized in the near-critical regime, in which case the analysis in the main text applies there as well. Furthermore, we showed in [75] that our qualitative results persist if the brane is not stabilized.

Plugging this back into (2.123) yields an approximate expression for the angular pressure,

$$\tilde{U}^{\phi}{}_{\phi} \approx \left(M_5^3 - \beta M_6^4 R\right) \Box_4 s|_0 \,. \tag{2.126}$$

This exactly equals (2.108), and in addition, we also reproduce the scalar equations (2.103) from the last section. While there, they were derived by assuming some underlying stabilization mechanism, and then inferring the required $\tilde{U}^{\phi}{}_{\phi}$ from the field equations, we have now seen an explicit example that gives the radion a large mass, and consistently yields the same $\tilde{U}^{\phi}{}_{\phi}$ and field equations after the radion has been integrated out in a low energy regime. The stability bound (2.117) can now be rewritten in terms of the radion mass, thus yielding the initially advertised relation (1.23).

2.5 Discussion

We conclude this chapter with a discussion of our previous results. In the first part, we assess the question whether our results are compatible with a natural EFT. In the second part, we provide a phenomenological discussion. The central question is whether there are stable regions in parameter space that allow for a 4D regime at small distances as required by observations. Both questions will be answered in the affirmative. This in turn paves the way towards the study of consistent cosmologies within the 6D BIG model.

2.5.1 Effective field theory perspective

Braneworld models are based on the idea that particles are localized on a spatial hypersurface, which then constitutes our universe. Quite generically, the corresponding fields, due to their coupling to the bulk gravity sector, induce 4D curvature terms on the brane. Following this reasoning, the induced part of (2.1) cannot be avoided in any braneworld setup unless we assume the existence of some fine-tuning of model parameters. While being a logical possibility, this would be very unsatisfactory and unexpected from a conceptual point of view. The crucial question, therefore, is whether a technically natural, i.e. radiatively stable, choice of model parameters allows to avoid the ghost instability.

A first answer was given in the introduction, where it was shown in Sec.1.4 that in a simple theory that only consist of a (stabilized) ring with (massive) size modulus φ the resulting low energy theory (which is obtained by integrating out φ) is stable. In other words, there the radion was used as a prototype for a localized, massive particle. That way, we could explicitly demonstrate that the stability bound (2.117) is always fulfilled provided no tuning on model parameters is imposed. However, the ring model is just a convenient example. In fact, we could devise various other UV models, which all lead to the BIG model in the low energy regime. Thus, it is crucial to have a general criterion that allows us to single out consistent, i.e. ghost-free realizations. As we will see, naturalness turns out to be the right one. Let us therefore clarify on a quantitative level what the qualification "natural" means. To that end, we parametrize the coefficients of all possible

induced operators via

$$\lambda = c_1^4 M_*^4 \,, \qquad M_{\rm Pl} = c_2 M_* \,, \qquad R^{-1} = c_3 M_* \,, \tag{2.127}$$

where c_1, c_2 and c_3 are dimensionless constants and M_* is an arbitrary mass scale. Since the transverse width R is also set by microscopic physics, it has to be included into the discussion. Then, the central statement is that the above model parameters are natural if c_1, c_2 and c_3 are all of order one. It is clear that their exact values cannot be calculated without a fundamental UV description, and thus they have to be inferred from observations.

The following discussion only applies to codimension-two.[35] When we plug (2.127) into (2.110), we obtain

$$f^{(s)} = 1 - \frac{3c_1^4}{2(c_2c_3)^2} \frac{1}{1-\delta/(2\pi)} \,, \tag{2.128}$$

where the last factor can take any value in the range[36] $[0, 1)$. When we replace the last factor in (2.128) by its least upper bound 1 and require $f^{(s)} < 0$, a sufficient condition for stability is found to be $(c_2c_3)^2/c_1^4 < 3/2$. It is depicted as the dashed line in Fig. 2.6. It is now crucial to notice that this can always be achieved by choosing parameters of order one, i.e. without any fine-tuning. However, once we introduce a large hierarchy between scales—for example by decreasing the parameter c_1 while keeping c_2 fixed—the bound gets quickly violated. This is exactly the reason why the zero tension vacuum was unstable. To summarize our results: A consistent theory of gravity induced on a brane requires the inclusion of a sufficiently large brane tension. As we have shown, this requirement is met by any natural EFT.

As a final remark, note that we made the unnatural choice of setting the bulk CC $\lambda^{(D)} = 0$ to zero. Albeit, this is not in line with the above promoted EFT picture, our results show that it does not affect the stability of the model. Nevertheless, it would be desirable to generalize our analysis to non-zero values.

2.5.2 Phenomenology

We have seen that the model features a stable and natural parameter regime. A question which is rather decoupled concerns its phenomenological viability. To further investigate it, we first have to derive a crossover scale r_c, characterizing the point where the model changes from a 4D to a 6D regime. Like in the discussion for the scalar toy model in Sec. 2.2, the crossover can be directly inferred from the brane-to-brane propagator of the healthy mode[37] $J|_0$ that is being convoluted with a constant point source $T_{00} \propto \delta^3(\boldsymbol{x})$.

The correct expression for the propagator can be obtained from (2.114) via the replacement $f^{(s)} \to -2$ [to see this compare (2.103a) to (2.109)]. As before, the time-independence of the source implies $\omega = 0$ and a crossover momentum $\boldsymbol{p}_c$ can be derived by comparing

[35] However, we expect the qualitative results to be true in any higher codimension $n \geq 2$.

[36] Larger values would correspond to the super-critical case which is not covered by the current analysis.

[37] Instead, we could also calculate the Newtonian potential for a point source which would contain a contribution from s, too. However, this would not change any of the conclusions.

both terms in (2.114). To deduce a bound on $\boldsymbol{p}_c$, we consider again Fig. 2.3 which depicts the second term of (2.114) (divided by $z = R|\boldsymbol{p}|$) as a function of z. Now $\boldsymbol{p}_c$ can be derived by looking for intersections with the linear function $(L_2/R)\, z$. The crossover momentum has to be much smaller than the inverse regularization scale, $R|\boldsymbol{p}_c| \ll 1$; otherwise, the derivation would be sensitive to the unknown UV sector of the theory and, more importantly, we would loose a four-dimensional regime (instead $|\boldsymbol{p}_c|$ would be a crossover between a 5D and a 6D regime) which is certainly incompatible with observations. By a short inspection of Fig. 2.3, we see that this condition implies $L_2 \gg R$ irrespective of the value of β. A lower bound on the momentum crossover is then readily found to be (neglecting factors of order one)

$$|\boldsymbol{p}_c| \gtrsim \frac{1}{L_2} \qquad \text{for } L_2 \gg R\,, \tag{2.129}$$

which leads in position space to an upper bound for the crossover scale $r_c \lesssim L_2$. It is (almost) saturated in the near-critical regime and matches the scale derived in [104]. This result generalizes the crossover $r_c|_{\lambda=0}$ obtained in the scalar prototype model for a tensionless brane, c.f. Eq. (2.27), to physically relevant setups with $\lambda \neq 0$. Also note that r_c can be hierarchically larger (by a factor L_2/R) compared to the tensionless case, which makes the deficit angle setup particularly interesting. To be precise, if we identify $L_2 = 1/H_0$, we find $M_6 \sim 10\,\text{MeV}$, which is the same bulk scale as in the 5D DGP model. On the other hand, if the crossover lies far below its upper bound, M_6 is much smaller, which at some point certainly leads to phenomenological problems (cf. the discussion in Sec. 1.4.3). That way, the conical setup clearly improves the general prospects of the model (as compared to the tensionless case, which is unstable anyway).

Let us comment on further implications of the above discussion. The requirement of having a 4D regime (instead of a 5D regime), i.e. $R|\boldsymbol{p}_c| \ll 1$, implies that only the right half of Fig. 2.6 is phenomenologically interesting. While in the sub-critical regime this is incompatible with having a stable theory, for near-critical values of the tension, i.e. $1 - \delta/(2\pi) \ll 1$, there is still a small stable stripe (also observed in [104]) between the stability line described by $f^{(s)}$ and the criticality line $\delta = 2\pi$.

To summarize, the near-critical parameter regime is the remaining window of opportunity for the sub-critical model. In the following chapter, we will push our investigation further and study fully nonlinear cosmological solutions. The upper bound on the crossover scale derived here, will be an important ingredient to further assess the model's phenomenological status.

Finally, let us comment on the range of applicability of the linear analysis presented here. Around static and spherically symmetric sources the codimension-one model is known to possess a Vainshtein-like radius below which the linear approximation breaks down. It is parametrically large compared to the Schwarzschild radius, and plays a crucial role in restoring a 4D regime on solar system scales (by removing a vDVZ like discontinuity in the graviton propagator) [53, 93, 146, 155, 121].[38] It is thus natural to ask whether a similar

[38] Originally, these concepts were developed in the case of Fierz-Pauli [80] massive gravity [165, 172, 164].

strong coupling effect could exist in two codimensions.[39] However, inferring the regime of applicability of the linear approximation would require to derive higher order corrections to the propagator in (2.114), which is beyond the scope of the present work. Instead, we always assume to be in a weak coupling regime (which can be understood as a requirement on the source terms). Whether this issue becomes relevant though depends on the success of the cosmological analysis (which does not rely on a weak coupling assumption) we perform in Sec. 3.

[39]Indeed, there are general arguments strongly suggesting that this should happen [60].

Chapter 3

BIG: Extra space as a cone

> *Note: The first part of this chapter (sub-critical universe) is based on a publication together with Stefan Hofmann, Justin Khoury and Robert Schneider [135]; verbatim reproductions have been used within Sec. 3.2 and 3.4. The second part (super-critical universe) applies the ideas of another publication together with Robert Schneider [132] to the BIG setup (but is unpublished so far).*

The linear analysis of the last chapter revealed a window of opportunity for studying consistent modified cosmologies within the BIG model. To be specific, in six dimensions a near-critical parameter window was identified, featuring different interesting characteristics:

- The pure tensions vacuum has promising properties with regard to the CC problem: Instead of producing 4D curvature on the brane, λ curves the bulk into a cone. In the near-critical regime the cone is very close to a cylinder.
- On a linear level, the model is stable and ghost-free provided the tension is large enough. This observation makes the near-critical regime—for which the stability bound (2.117) can always be fulfilled—particularly interesting.
- The stable near-critical regime admits a large crossover scale, viz. $r_c \sim M_{\rm Pl}^2/(RM_6^4)$, which is compatible with a 4D regime up to astrophysical scales without the need of choosing M_6 hierarchically small (compared to the EW scale). This makes the regime phenomenologically attractive and potentially interesting with respect to the electroweak hierarchy problem.

So far it is not clear whether these favorable properties persist on a nonlinear level. Moreover, the previous analysis was performed in the case of a pure tensions source. Whether other types of matter lead to a different behavior still needs to be checked. Correspondingly, the main question of this chapter can be summarized as follows:

> *Is it possible to generalize the static deficit angle geometry* (2.81) *to a cosmological solution that admits a phenomenologically viable expansion history on the brane?*

In other words, we look for a modified Friedmann equation stemming from (2.1) and describing the nonlinear evolution of the Hubble parameter H on the brane. A similar program was successfully pursued before in the case of the 5D DGP model in [51]. A short review on the DGP cosmology, provided in Sec. 3.1, therefore allows us to sharpen our intuition about 4D FLRW solutions in the braneworld context. However, we will soon see that there is a major difference between the 5D model and its higher-dimensional counterparts: In the latter case the brane acts as an antenna that absorbs and emits gravitational waves. For FLRW symmetries on the brane they correspond to cylindrically symmetric bulk waves—a direct generalization of Einstein-Rosen (ER) waves in 4D [78]. This leads to a dramatic change because now the brane curvature evolution strongly depends on the wave content in the bulk.

These findings demand for a new strategy to solve the full dynamical problem. This is achieved in Sec. 3.2, where we derive the nonlinear system of bulk and brane matching equations by using a convenient, axially symmetric metric ansatz. Yet again, we employ the ring regularization, first discussed in Sec. 2.1, to dispose of divergent field contributions. This approach in turn admits an exhaustive discussion of the geometrical properties of axial symmetric systems, which, in a great part, is inspired by pioneering work done by Thorne in [163, 11]. The main technical obstacle consists in solving the full set of partial differential equations (PDE) describing the bulk-brane system. This is achieved numerically, as described in Sec. 3.3, and can be rightly considered the main technical challenge that had to be overcome in this thesis. The subsequent discussion of the results comes in two parts:

In Sec. 3.4, we discuss the sub-critical setup, characterized by $\lambda < 2\pi M_6^4$. As in the linear analysis, the parameter space is again divided into two regions: an unstable one, which is caused by the ghost discussed before, and a stable one, for which the ghost is absent. The second class of solutions is indeed interesting with respect to the CC problem: The system approaches the deficit angle solution (2.81) within a few Hubble times, thereby effectively shielding the brane tension from a brane observer. The main task then consists in inferring the phenomenological potential of these degravitating solutions. By borrowing the expression for the crossover scale r_c from the precedent linear analysis, we are able to give a final answer: Stability and phenomenological viability are mutually incompatible within the sub-critical parameter regime.

The remaining hope thus relies on the super-critical parameter window, characterized by $\lambda > 2\pi M_6^4$, which is discussed in Sec. 3.5. We restrict the brane to be 4D maximally symmetric. That way, we are able to derive fully analytic solutions of the system, which has not been achieved before. The geometrical picture is simple: For super-critical tensions the extra space becomes compact and cigar-shaped while the three spatial brane directions are expanding at a constant rate H. The corresponding modified Friedmann equations relating H and λ are derived analytically. A subsequent numerical analysis shows that the cosmological background is indeed stable under fluctuations with (more general) FLRW symmetries and in addition features interesting attractor properties; in particular, the super-critical system might very well be compatible with observations (a complete investigation still remains to be done). However, as we will see, these solutions cannot solve the

CC problem as they still rely on a tuning of model parameters.

We conclude in Sec. 3.6 with a discussion of the full parameter space of the 6D model (sub- and super-critical). We then assess possible future directions. In particular, based on our new insights in 6D, we present promising prospects for models in seven or more dimensions.

3.1 Prelude: DGP cosmology

In this section, we review the codimension-one cosmology, first derived in [21, 51]. For simplicity, we restrict ourself to the case of a vanishing bulk CC. Moreover, we assume FLRW symmetries on the brane. In other words, we look for a solution of the bulk-brane system, defined by (2.6) and (2.9) for $D = 5$, where the brane induced EMT is given by $\tilde{\mathbf{T}} \equiv \mathbf{T} = \mathrm{diag}(-\rho, p, p, p)$. Having a source-free bulk then implies a planar symmetry; to be precise, the solution has to be invariant under $y \to -y$. In that case, there is a version of Birkhoff's theorem [162] stating that the bulk curvature has to be static. As a consequence, the only possible solution in the bulk is either Minkowski or some nontrivial static geometry reflecting the symmetries of the system: For vanishing spatial curvature on the brane this is the static plane solution first derived in 4D by Levi-Civita [113] (see [8] for a more recent discussion) and for positive spatial curvature it is the Schwarzschild geometry with the curvature scale given by the Schwarzschild mass parameter [91]. As we will see, this fact greatly simplifies the analysis because we expect the on-brane curvature to be described by a closed and local system of ordinary differential equations. The reason is that the dependence on the bulk geometry only enters through a bulk integration constant (that can be fitted to observations). On the other hand, for higher-codimensional setups, we will find that the symmetries allow for the existence of bulk waves. This implies that the evolution on the brane is strongly affected by their presence and we do no longer expect to get a closed on-brane system. And indeed, the modified Friedmann equation (which assumes spatial flatness) reads [51],

$$H^2 - \frac{\rho}{3M_{\mathrm{Pl}}^2} = \mp r_{c,1}^{-1}\sqrt{H^2 - \frac{\mathcal{C}}{a^4}}\,. \tag{3.1}$$

Here, $r_{c,1} = M_{\mathrm{Pl}}^2/(2M_5^3)$ is the crossover, as previously derived in Sec. 2.2, and $\mathcal{C}$ is an integration constant related to the (constant) bulk curvature. The important point is that this together with the standard energy conservation constitutes a closed system for the 4D scale factor a.

In order to gain some intuition about the meaning of $\mathcal{C}$, let us consider a pure tension brane $\rho = -p = \lambda = \text{const}$. In that case, we can set $H^2 = 0$, implying a vanishing on-brane curvature, and find $\mathcal{C} = -\lambda^2/(36\,M_5^6)$ as a purely static solution of (3.1) (where we made the choice $a = 1$). Since the intrinsic curvature on the brane is vanishing, it is clear that $\mathcal{C}$ has to correspond to a constant (extrinsic) curvature in the bulk. This is the

higher-dimensional generalization of the before-mentioned Levi-Civita solution.[1] We hence see that (3.1) indeed depends on the bulk curvature only via a constant parameter.

Let us briefly discuss the physics of (3.1) in the case of vanishing Levi-Civita curvature, $\mathcal{C} = 0$. If the crossover is large compared to the Hubble length, meaning that $Hr_{c,1} \gg 1$, we can neglect the right side of this equation thus reproducing standard 4D cosmology. This observation motivates to identify the crossover with the Hubble length today: $r_{c,1} \sim 1/H_0$. As a result, for early times ($r_{c,1}H \gg 1$) 4D Friedmann evolution is reproduced and for late times ($r_{c,1}H \ll 1$) the modification, described by the right side of Eq. (3.1), kicks in. Depending on the branch, it may lead to two different effects:

First, if we take the negative (upper) sign, the gravitational effect of ρ is weakened, meaning that H is smaller than it would be when following the 4D standard evolution. The physical picture is again the same as in the linear case: Once the Hubble length exceeds the crossover scale, the gravitational field becomes sensitive to the presence of the extra dimension and thus gets diminished. Due to the high degree of symmetries in the bulk, this turns out to be an ultra-local curvature effect. In other words, there is a localized amount of extrinsic curvature at the brane position, given by the right side of (3.1). This branch is usually referred to as the normal (NO) branch.

Second, there is the self-accelerating (SA) branch corresponding to the positive (lower) sign. It behaves quite differently because the modification term acts as an additive source. In particular, this leads to a non-vanishing solution of the Hubble parameter even in the case of a vanishing source, to be specific, $H = 1/r_{c,1}$ for $\rho = 0$. This peculiar behavior goes under the name of "self-acceleration" and made this branch quite famous because it provides an explanation of dark energy[2]. However, there are many claims in the literature stating that the SA branch is perturbatively unstable [121, 130, 110, 87, 141, 42, 91].

The phenomenology of both branches was discussed extensively in the literature [117, 120, 119, 118]. While both of them might be viable if a 4D CC is included, the SA branch with vanishing tensions has been ruled out lately. In particular, there is no phenomenological indication for unique DGP modifications. Correspondingly, the crossover scale has to be larger than the Hubble scale, viz. $H_0 r_{c,1} > 3$ [116] (for further phenomenological tests see [49] and references therein).

3.2 The geometry of a string

The goal of this section is to provide a complete discussion of the codimension-two geometry ($D = 6$) in the general dynamical case. In other words, we want to generalize the static, cosmic string solution (2.81) to a time-dependent configuration with FLRW symmetries on the brane. Correspondingly, the assumed symmetries are homogeneity, isotropy and (for simplicity) spatial flatness along the three spatial brane dimensions, as well as axial

[1] For a non-vanishing spatial curvature the constant plays the role of a Schwarzschild mass parameter in accordance with the changed topology of the setup [91].

[2] Of course, this branch cannot help with the CC problem, because it relies on tuning the brane tension to zero.

symmetry in the bulk. This motivates the following fluid ansatz of the localized 5D energy-momentum tensor

$$\tilde{\mathbf{T}} = \frac{1}{2\pi R}\,\mathrm{diag}(-\rho, p, p, p, p_\phi)\ , \tag{3.2}$$

where the overall factor is chosen such that $\mathbf{T} = 2\pi R\,\tilde{\mathbf{T}}$ defines a 4D energy-momentum tensor. The occurrence of the angular pressure p_ϕ is related to the compact ring dimension. As in the linear case, it will be implicitly determined by demanding a fixed circumference.

Like in the linear analysis, we first introduce polar coordinates (r, ϕ), to be precise $x^A = (x^\mu, r, \phi)$ with the standard ranges $r \in [0, \infty)$, $\phi \in [0, 2\pi)$.

We will first discuss the bulk vacuum equations in Sec. 3.2.1 and then introduce the brane in Sec. 3.2.2. Both sectors are related by Israel's matching equations discussed in Sec. 3.2.3. Several nontrivial checks are performed by taking the static limit in Sec. 3.2.5. To show the universality of our approach, we introduce an alternative regularization in Sec. 3.2.7.

3.2.1 The bulk

The symmetries of the system suggest the use of cylindrical coordinates. A particularly convenient metric ansatz in the case of "whole-cylinder symmetry" is discussed in [163] or Chap. 22 of [158]. The 4D ansatz therein can be easily generalized to 6D, where the axis has three intrinsic spatial dimensions,

$$\mathrm{d}s_6^2 = \mathrm{e}^{2(\eta-3\alpha)}\left(-\mathrm{d}t^2 + \mathrm{d}r^2\right) + \mathrm{e}^{2\alpha}\,\mathrm{d}\boldsymbol{x}^2 + \mathrm{e}^{-6\alpha}\,W^2\mathrm{d}\phi^2\,. \tag{3.3}$$

Here, η, α and W are functions of (t, r). The corresponding bulk vacuum equations are

$$\partial_r^2 W - \partial_t^2 W = 0, \tag{3.4a}$$

$$\partial_r^2\alpha - \partial_t^2\alpha + \frac{\partial_r W}{W}\partial_r\alpha - \frac{\partial_t W}{W}\partial_t\alpha = 0, \tag{3.4b}$$

$$6\left[(\partial_r\alpha)^2 - (\partial_t\alpha)^2\right] + \partial_r^2\eta - \partial_t^2\eta = 0, \tag{3.4c}$$

$$6\left[(\partial_r\alpha)^2 + (\partial_t\alpha)^2\right] - \frac{\partial_r W}{W}\partial_r\eta - \frac{\partial_t W}{W}\partial_t\eta + \frac{\partial_t^2 W}{W} = 0, \tag{3.4d}$$

$$12(\partial_r\alpha)(\partial_t\alpha) - \frac{\partial_r W}{W}\partial_t\eta - \frac{\partial_t W}{W}\partial_r\eta + \frac{\partial_t\partial_r W}{W} = 0\,. \tag{3.4e}$$

The first three equations are dynamical equations for W, α and η, and the last two constitute additional constraint equations.

The ansatz (3.3) does not completely fix the (t, r)-coordinates since it is still invariant

Character	**Orientation of $\boldsymbol{\nabla} W$**	W'_+	W'_-
D^+	space-like outward	> 0	< 0
D^-	space-like inward	< 0	> 0
$D^\uparrow$	time-like future	> 0	> 0
$D^\downarrow$	time-like past	< 0	< 0
$D^{+\uparrow}$	light-like outward-future	> 0	$= 0$
$D^{+\downarrow}$	light-like outward-past	$= 0$	< 0
$D^{-\uparrow}$	light-like inward-future	$= 0$	> 0
$D^{-\downarrow}$	light-like inward-past	< 0	$= 0$
$D^\times$	zero	$= 0$	$= 0$

Table 3.1: Space time classification by means of $\boldsymbol{\nabla} W$, i.e. the gradient of W. In the flat space limit the spacetime is D^+.

under a residual transformation

$$(t, r) \mapsto (\check{t}, \check{r}) \,, \tag{3.5a}$$

$$\eta \mapsto \check{\eta} = \eta - \frac{1}{2} \ln \left[(\partial_r \check{r})^2 - (\partial_t \check{r})^2 \right] \,, \tag{3.5b}$$

subject to the condition

$$\begin{pmatrix} \partial_t \check{r} \\ \partial_r \check{r} \end{pmatrix} = \pm \begin{pmatrix} \partial_r \check{t} \\ \partial_t \check{t} \end{pmatrix} \,. \tag{3.6}$$

This in turn implies an integrability condition for $\check{r}$,

$$\partial_r^2 \check{r} = \partial_t^2 \check{r} \,. \tag{3.7}$$

Before fixing the remaining gauge freedom, let us classify the different geometries described by (3.3). Following the discussion in the appendix of [11], this can be achieved by focusing on the function $W(t, r)$, which measures (up to a factor of 2π) the circumference of the extra space at a fixed radial position. Away from the brane, $W(t, r)$ fulfills the 1D wave equation (3.4a), which can be readily solved in terms of two arbitrary functions $W_-(x)$ and $W_+(x)$; explicitly,

$$W(t, r) = W_+(t + r) + W_-(t - r) \,. \tag{3.8}$$

With these two functions we can write the gradient of $W(t, r)$ explicitly as

$$\boldsymbol{\nabla} W = (W'_+ + W'_-, W'_+ - W'_-, 0, 0, 0, 0) \,. \tag{3.9}$$

It then admits a convenient classification of the geometry, specified in Table 3.1. Note that the standard intuition for an axial symmetric system solely applies to D^+. In that case, the circumference of space grows with increasing radial coordinate. On the contrary,

in the case of a D^- spacetime, the circumference grows with decreasing radial coordinate. These two cases can be best exemplified with the help of the (regularized) static deficit angle geometries visualized in Fig. 2.2. The interior geometry is demanded to be flat and thus categorized as D^+. On the other hand, the exterior geometry corresponds to D^+ for a sub-critical tension, to $D^\times$ for a critical tension and to D^- for a super-critical tension brane.

In the general time-dependent case, we discuss here, the picture becomes more involved. As before, we will assume that the interior is D^+ and hence continuously connected to flat space. Then, the exterior classification is determined by the matter content of the brane and the curvature in the interior. We first turn to the interior space time as it has a definite classification. There, we fix the residual gauge freedom by introducing a new radial coordinate

$$\check{r} = W(t, r) \,. \tag{3.10}$$

where (3.7) is obviously fulfilled due to (3.4a). The new time coordinate $\check{t}$ is then determined implicitly via (3.6) and the transformed line element reads

$$\mathrm{d}s^2_{(\mathrm{int})} = \mathrm{e}^{2(\check{\eta}-3\check{\alpha})}\left(-\mathrm{d}\check{t}^2 + \mathrm{d}\check{r}^2\right) + \mathrm{e}^{2\check{\alpha}}\mathrm{d}\boldsymbol{x}^2 + \mathrm{e}^{-6\check{\alpha}}\check{r}^2\mathrm{d}\phi^2 \,, \tag{3.11}$$

where $\check{\eta}$ and $\check{\alpha}$ are functions of $(\check{t}, \check{r})$.[3] By contrast, the exterior metric is still described by the previous line element (3.3). Note that by formally replacing $3\check{\alpha} \to \check{\alpha}$ in the first and last term and $\boldsymbol{x} \to z$, we recover the ansatz that was used by Einstein and Rosen to derive the existence of cylindrically symmetric waves in GR [78] (see also, *e.g.*, [123]). The additional factor 3 in the generalized case simply counts the dimensionality of the symmetry axis. In the remainder of the paper we will refer to (3.3) as the *ER coordinates*.

In summary, we introduced different coordinates, $(t, r, \boldsymbol{x}, \phi)$ and $(\check{t}, \check{r}, \boldsymbol{x}, \phi)$, in the exterior and interior of the brane, respectively. How the residual gauge freedom is fixed in the exterior region depends on its classification. We will infer it from the (00) component of the matching equation (2.9), as explained later in Sec. 3.2.3.

3.2.2 The brane

In this section, we set up the description of the brane geometry. Like in the linear analysis, we use a ring regularization to endow the brane with a microscopic thickness (cf. Sec. 2.1 for an extensive physical discussion). To that end, we introduce two functions, $r_0(t)$ and $\check{r}_0(\check{t})$ describing the position of the brane in the exterior and interior region, respectively. Continuity of the line element (3.3) and (3.11) across the brane implies

$$\alpha_0 = \check{\alpha}_0, \,, \qquad\qquad W_0 = \check{r}_0 \,, \qquad\qquad \frac{1}{\gamma}\mathrm{d}t = \frac{1}{\check{\gamma}}\mathrm{d}\check{t} \,, \tag{3.12}$$

[3] Here and henceforth interior quantities (including coordinates and metric functions) are distinguished from its exterior counterpart X by writing $\check{X}$.

where we defined

$$\gamma := \frac{\mathrm{e}^{-\eta_0}}{\sqrt{1-\dot{r}_0^2}} \qquad \text{and} \qquad \check{\gamma} := \frac{\mathrm{e}^{-\check{\eta}_0}}{\sqrt{1-\dot{\check{r}}_0^2}} \,. \tag{3.13}$$

We used $\dot{r}_0 := \mathrm{d}r_0/\mathrm{d}t$ (and $\dot{\check{r}}_0 := \mathrm{d}\check{r}_0/\mathrm{d}\check{t}$) as shorthand; here and henceforth, dots refer to $\mathrm{d}/\mathrm{d}t$ (and $\mathrm{d}/\mathrm{d}\check{t}$).

The induced cosmological metric on the brane is

$$\mathrm{d}s_5^2 = -\mathrm{d}\tau^2 + \mathrm{e}^{2\alpha_0}\,\mathrm{d}\boldsymbol{x}^2 + R^2\mathrm{d}\phi^2 \,, \tag{3.14}$$

where the subscript "0" denotes evaluation at the brane position, e.g. $\alpha_0(t) = \alpha(t, r_0(t))$. The scale factor is recognized as $a(\tau) = \mathrm{e}^{\alpha_0}$, with the Hubble parameter $H = \mathrm{d}\alpha_0/\mathrm{d}\tau$. The proper time τ on the brane is related to the "bulk time" via

$$\mathrm{d}\tau = \frac{\mathrm{e}^{-3\alpha_0}}{\gamma}\mathrm{d}t = \frac{\mathrm{e}^{-3\check{\alpha}_0}}{\check{\gamma}}\mathrm{d}\check{t} \,. \tag{3.15}$$

In accordance with the discussion in Sec. 2.1 and in order to recover 4D gravity in the appropriate regime, we assume that the proper circumference (divided by 2π) is stabilized,

$$R \equiv W_0\mathrm{e}^{-3\alpha_0} = \check{r}_0\mathrm{e}^{-3\check{\alpha}_0} = \text{const.} \tag{3.16}$$

The physical justification is obvious: A realistic defect requires some underlying bulk forces to keep its core stable. Technically, this is imposed by introducing a suitable azimuthal pressure component p_ϕ. We must of course check a posteriori whether the pressure thus inferred satisfies physically reasonable energy conditions, such as the *null energy condition* (NEC). As an immediate consequence of the stabilization condition, the 4D Planck mass,

$$M_{\mathrm{Pl}}^2 = 2\pi R M_5^3 \,, \tag{3.17}$$

is constant. Fixing R also implies that the energy density and pressure satisfy the standard 4D conservation equation

$$\boxed{\frac{\mathrm{d}\rho}{\mathrm{d}\tau} + 3H\,(\rho + p) = 0} \,. \tag{3.18}$$

Now, we have introduced all objects needed to characterize the brane geometry. They will be related to the bulk sector in the next section.

3.2.3 Junction conditions

Let us now further evaluate the Israel matching equation (2.9). The extrinsic curvature at the exterior and interior boundary of the codimension-one brane are calculated using the

properly normalized (outward-pointing) normal vectors

$$n^A = \gamma \mathrm{e}^{3\alpha_0} \left(\dot{r}_0, 1, 0, 0, 0, 0\right) , \tag{3.19}$$

$$\check{n}^A = \check{\gamma} \mathrm{e}^{3\check{\alpha}_0} \left(\dot{\check{r}}_0, 1, 0, 0, 0, 0\right) , \tag{3.20}$$

respectively. With these definitions the (00) junction condition reads

$$\check{\gamma} - \gamma \left(\dot{r}_0 \partial_t W + \partial_r W\right)|_0 = \frac{\rho_{\text{eff}}}{2\pi M_6^4} , \tag{3.21}$$

where an effective energy density incorporating the effect of the induced gravity terms was introduced,

$$\rho_{\text{eff}} := \rho - 3M_{\text{Pl}}^2 H^2 . \tag{3.22}$$

As usual the dimensionless combination is denoted by $\bar{\rho}_{\text{eff}} := \rho_{\text{eff}}/(2\pi M_6^4)$. Moreover, differentiating $W = \check{r}_0$ with respect to τ and using the third relation in (3.12) yields

$$\check{\gamma}\, \dot{\check{r}}_0 - \gamma \left(\partial_t W + \dot{r}_0 \partial_r W\right)|_0 = 0 . \tag{3.23}$$

Eqs. (3.21) and (3.23) can be used to infer the geometry classification of the exterior spacetime. This will in turn motivate a fixing of the residual gauge freedom in the exterior space. To be specific, by using the solution (3.8), we obtain expressions for $W'_+\big|_0$ and $W'_-\big|_0$,

$$W'_+\big|_0 = \frac{1}{2\,\gamma\,(1+\dot{r}_0)} \left[\check{\gamma} \left(1 + \dot{\check{r}}_0\right) - \frac{\rho_{\text{eff}}}{\lambda_{\text{c}}}\right] , \tag{3.24a}$$

$$W'_-\big|_0 = \frac{1}{2\,\gamma\,(1-\dot{r}_0)} \left[\frac{\rho_{\text{eff}}}{\lambda_{\text{c}}} - \check{\gamma} \left(1 - \dot{\check{r}}_0\right)\right] . \tag{3.24b}$$

According to Tab. 3.1, we distinguish three different cases:

1. In the *sub-critical* regime $\boldsymbol{\nabla} W|_0$ is space-like and outward pointing (D^+). The system (3.24) then implies

$$\rho_{\text{eff}} < \rho^{\downarrow}_{\text{crit}} \qquad \text{with} \qquad \rho^{\downarrow}_{\text{crit}} := 2\pi M_6^4 \left(\check{\gamma} - 3|H|R\right) . \tag{3.25}$$

   We will refer to it as the (generalized) lower criticality bound. As a consistency check, let us insert the static deficit angle solution (2.81) (corresponding to $\rho_{\text{eff}} = \lambda$, $\gamma^* = 1$ and $H = 1$). As expected, we recover the static criticality bound $\rho^{\downarrow}_{\text{crit}} = \lambda_{\text{c}}$ ($\equiv 2\pi M_6^4$) introduced previously in Sec. 2.4.1.

2. In the *critical* regime $\boldsymbol{\nabla} W|_0$ is time-like ($D^\uparrow$ or $D^\downarrow$). This happens for

$$\rho^{\downarrow}_{\text{crit}} < \rho_{\text{eff}} < \rho^{\uparrow}_{\text{crit}} \qquad \text{with} \qquad \rho^{\uparrow}_{\text{crit}} := 2\pi M_6^4 \left(\check{\gamma} + 3|H|R\right) , \tag{3.26}$$

where we introduced the upper criticality bound $\rho^{\uparrow}_{\text{crit}}$. The orientation depends on the sign of H: it is $D^{\uparrow}$ for $H > 0$ and $D^{\downarrow}$ for $H < 0$. Note that this interval vanishes in the static case. In fact, there is only a critical point in parameter space corresponding to a (constant) energy density $2\pi M_6^4$. There is a clear physical reason: The kinetic energy described by the Hubble expansion contributes to the conical deficit and thus leads to an earlier transition to the critical phase.

3. In the *super-critical* regime $\boldsymbol{\nabla} W|_0$ is space-like and inward pointing (D^{-}). This implies the peculiar effect that the circumference of the exterior space decreases with increasing distance to the brane. Fig. 2.4.1 illustrates this behavior for a static geometry. In that case, $W(r,t)$ eventually becomes zero, thus signaling the existence of a second (or exterior) axis, which in general hosts a conical singularity. The condition on the energy density becomes

$$\rho^{\uparrow}_{\text{crit}} < \rho_{\text{eff}} \,. \tag{3.27}$$

Accordingly, in the sub-critical (1.) and super-critical (3.) case, $W(t,r)$ can be promoted to a new radial coordinate $\hat{r}$ in the exterior region by identifying[4]

$$\hat{r} = W(t,r). \tag{3.28}$$

A new time coordinate $\hat{t}$ can then be inferred via (3.6). Thus, the line element is also of ER form (3.3) with $\vee$ replaced by $\wedge$. In the first case, $\hat{r}$ behaves like an ordinary radial coordinate, i.e. it increases if we move further away from the brane, and has the range $[\hat{r}_0, \infty)$. However, in the second case, due to the fact that $\boldsymbol{\nabla} W$ is inward-pointing, the new radial coordinate decreases if we move further outwards, thus implying the unusual range $[0, \hat{r}_0]$. We have to keep this "reversed" behavior in mind when we use the ER ansatz. In particular, the super-critical geometry introduces an exterior axis at $\hat{r} = 0$. In general, this second axis hosts a conical singularity corresponding to a further brane with tension

$$\lambda_a \equiv 2\pi M_6^4 \left(1 - \mathrm{e}^{-\eta_a}\right) , \tag{3.29}$$

where η_a is shorthand for evaluation at the second axis at $r = 0$.[5]

In summary, the ER coordinates can be used to describe the interior *and* exterior spacetime. The corresponding extra space extends to infinity ($\hat{r} \to \infty$) for a sub-critical brane while it is compact and closes in a second axis (at $\hat{r} = 0$) for a super-critical brane.

3.2.4 Summary of bulk-brane geometry

Finally, let us give a summary of the geometry for both the sub- and super-critical regime. As explained before, we can work in the ER form of the metric (3.11) inside and outside of the brane. However, this is not possible by using a single coordinate patch, instead we

[4]This definition assumes that $\boldsymbol{\nabla} W(t,r)$ cannot change its character when we move further outwards. We will see in Sec. 4.1 that this is indeed the case.

[5]Here and henceforth evaluation at the second brane is denoted by the subscript a.

have to distinguish between interior, $(\check{t}, \check{r}, \boldsymbol{x}, \phi)$, and exterior, $(t, r, \boldsymbol{x}, \phi)$, coordinates.[6] In these coordinates the bulk vacuum equations (3.4) in the exterior simplify to

$$\partial_t^2 \alpha = \partial_r^2 \alpha + \frac{1}{r} \partial_r \alpha \,, \tag{3.30a}$$

$$\partial_r \eta = 6r \left[(\partial_r \alpha)^2 + (\partial_t \alpha)^2 \right] , \tag{3.30b}$$

$$\partial_t \eta = 12r \, \partial_r \alpha \, \partial_t \alpha \,. \tag{3.30c}$$

The corresponding equations in the interior can be obtained from the formal replacement $(\alpha, \eta, t, r) \to (\check{\alpha}, \check{\eta}, \check{t}, \check{r})$. Furthermore, $\check{\alpha}$ and $\check{\eta}$ are subject to the boundary conditions (2.7) and (2.8), viz.

$$\lim_{\check{r} \to 0} \partial_{\check{r}} \check{\alpha} = 0 \qquad \text{and} \qquad \lim_{\check{r} \to 0} \check{\eta} = 0 \,, \tag{3.31}$$

which ensures regularity and flatness at the interior axis. In the exterior, on the other hand, we demand either

$$\lim_{r \to \infty} \partial_r \alpha = 0 \qquad \text{or} \qquad \lim_{r \to 0} \partial_r \alpha = 0 \tag{3.32}$$

for a sub- and super-critical brane, respectively. In the first case, this guarantees an asymptotically flat space time, and in the second case, it prevents a singularity of the exterior axis [except for a conical one related to a non-vanishing of η_a according to (3.29)].

Since α obeys a linear[7] 2D wave equation, the ER coordinates are especially convenient for both analytical and numerical studies. Moreover, this also explains why the system admits cylindrical waves in the bulk, so called ER waves. In fact, this is the main benefit of these coordinates as they permit to describe the bulk wave content in terms of simple (and well-studied) 2D linear wave solutions. Note also that η is not a dynamical variable but completely fixed in terms of α once appropriate boundary conditions have been imposed.

The corresponding matching equations are derived as before. The outwards pointing normal vectors (3.19) now read

$$n^A = \sigma \, \gamma \mathrm{e}^{3\alpha_0} \, (\dot{r}_0, 1, 0, 0, 0, 0) \,, \tag{3.33}$$

$$\check{n}^A = + \check{\gamma} \mathrm{e}^{3\check{\alpha}_0} \left(\dot{\check{r}}_0, 1, 0, 0, 0, 0 \right) , \tag{3.34}$$

where $\sigma = +1$ in the sub-critical and $\sigma = -1$ in the super-critical case. The relative sign is explained by the fact that in the super-critical case the radial coordinate r decreases as one moves further away from the brane. With these normal vectors the extrinsic curvature

[6] For notational convenience, we drop $\wedge$ on the exterior coordinates and metric functions.

[7] Despite the linearity of this equation, the complete brane-bulk system is still highly nonlinear due to the junction conditions.

components in the exterior can be readily derived

$$\tilde{K}^0{}_0 = \frac{\sigma\gamma}{R}\frac{r_0\ddot{r}_0}{1-\dot{r}_0^2} + n^A\partial_A\left(\eta_0 - 3\,\alpha_0\right)\,, \tag{3.35a}$$

$$\tilde{K}^i{}_j = n^A\partial_A\alpha_0\,\delta^i{}_j\,, \tag{3.35b}$$

$$\tilde{K}^\phi{}_\phi = \frac{\sigma\gamma}{R} - 3\,n^A\partial_A\alpha_0\,. \tag{3.35c}$$

The interior counterparts $\check{\tilde{K}}^\alpha{}_\beta$ are of the same form with $\sigma = +1$. To further evaluate the above expressions, we infer from the stabilization condition (3.16)

$$\dot{r}_0 = \frac{HR}{\gamma} \qquad \text{and} \qquad \dot{\check{r}}_0 = \frac{HR}{\check{\gamma}}\,, \tag{3.36}$$

which in turn enables us to rewrite (3.13) as

$$\gamma = \sqrt{\mathrm{e}^{-2\eta_0} + 9H^2R^2} \qquad \text{and} \qquad \check{\gamma} = \sqrt{\mathrm{e}^{-2\check{\eta}_0} + 9H^2R^2}\,. \tag{3.37}$$

Then, a straightforward calculation yields

$$\frac{r_0\ddot{r}_0}{1-\dot{r}_0^2} = \frac{3R^2}{\gamma^2}\Big(\frac{\mathrm{d}H}{\mathrm{d}\tau} + H\frac{\mathrm{d}\eta_0}{\mathrm{d}\tau}\Big). \tag{3.38}$$

Using the above relations as well as the the localized EMT (3.2), we derive the final form of the (00) component of the matching equation (2.9), which constitutes a modified Friedmann equation,

$$\boxed{H^2 = \frac{\rho}{3M_{\mathrm{Pl}}^2} + \frac{1}{\ell_2^2}\left(\sigma\gamma - \check{\gamma}\right)}, \tag{3.39}$$

where we introduced the length scale

$$\ell_2^2 := 3R\,L_2\,. \tag{3.40}$$

It can be identified with the approximate crossover scale in a small tension regime, first introduced in (2.27), i.e. $\ell_2^2 \equiv r_c^2|_{\lambda=0}$. This interpretation applies in the nonlinear case iff $(\sigma\gamma - \check{\gamma}) \sim 1$: While for $H\ell_2 \gg 1$ the last term in (3.39) becomes negligible and the equation reduces to the standard 4D Friedmann equation, the situation is opposite for $H\ell_2 \ll 1$ where the dynamics is dominated by the modification term and we expect a transition to a 6D regime. On the other hand, in the general case where $(\sigma\gamma - \check{\gamma})$ deviates from one, the physical crossover scale gets modified. In the later phenomenological discussion, we will therefore use the upper bound $L_2 \gg \ell_2$ on the crossover scale (derived in the linear analysis in Sec. 2.5.2) to arrive at a reliable assessment on the phenomenological status of the model.

The crucial difference to the 5D case, described by Eq. (3.1), is that there the modified Friedmann equation [together with the energy conservation (3.2)] constitutes a closed system—solely expressed in terms of the on-brane quantities H and ρ (and p). The situation is different here, since γ and $\check{\gamma}$ depend on the bulk metric function η and $\check{\eta}$; these two functions mediate the effect of bulk ER waves propagating in the exterior and interior, respectively. It is this explicit dependence on the bulk geometry which necessitate to solve the full bulk-brane system. We will do this in Sec. 3.3 by employing a full-fledged numerical analysis. To that end, it is useful to first identify the whole dynamical system: It is given by the bulk equations (3.30) in the interior and exterior, the modified Friedmann equation (3.39), playing the role of a matching condition that relates γ to $\check{\gamma}$, and finally the energy conservation equation (3.18). How the system can be solved systematically will be discussed extensively when we implement the numerics in Sec 3.3.

A redundant yet very useful equation is given by the (i,j) component of the junction conditions and can be expressed as

$$\frac{\mathrm{d}H}{\mathrm{d}\tau} = -\frac{3}{2F(\tau)}\left[\frac{p}{3M_{\mathrm{Pl}}^2} + H^2 - \frac{1}{\ell_2^2}\Big(\sigma\gamma\, g(\xi,\chi) - \check{\gamma}\, g(\check{\xi},\check{\chi})\Big)\right], \tag{3.41}$$

where

$$\boxed{F(\tau) := 1 + \frac{9R^2}{2\ell_2^2}\left(\frac{1}{\check{\gamma}} - \frac{\sigma}{\gamma}\right)}. \tag{3.42}$$

and

$$g(\xi,\chi) := 1 + 2\,(9\chi - 1)\Big[3\chi + \xi\,(3\xi - 2)\,(9\chi - 1)\Big], \tag{3.43a}$$

$$\xi := r\partial_r\alpha|_0\,, \qquad \check{\xi} := \check{r}\partial_{\check{r}}\check{\alpha}|_0\,, \qquad \chi := \frac{H^2R^2}{\gamma^2}\,, \qquad \check{\chi} := \frac{H^2R^2}{\check{\gamma}^2}\,. \tag{3.43b}$$

This modified second Friedmann equation will prove itself very useful for the numerical implementation. Moreover, a short inspection of (3.41) shows that $F(\tau) = 0$ corresponds to a singular time evolution. In fact, we will see that the sign of F determines whether or not the system is stable. This already suggests that F is related to the function $f^{(s)}$ derived in the linear analysis on a deficit background [cf. Eq. (2.110)]. And indeed, in the next section, we will show that the function found here is the nonlinear completion (including the effect of $H \neq 0$) of the function $f^{(s)}$.

Finally, let us derive the $(\phi\phi)$ matching equation. As already explained, it can be used to infer the value of p_ϕ needed to stabilize the compact dimension; explicitly,

$$\frac{p_\phi}{3M_{\mathrm{Pl}}^2} = -\frac{\mathrm{d}H}{\mathrm{d}\tau}\left[1 + \frac{3R^2}{\ell_2^2}\left(\frac{1}{\check{\gamma}} - \frac{\sigma}{\gamma}\right)\right] - 2H^2 + \frac{6}{\ell_2^2}\Big[\sigma\gamma\, h(\xi,\chi) - \check{\gamma}\, h(\check{\xi},\check{\chi})\Big], \tag{3.44}$$

where we introduced

$$h(\xi,\chi) := \chi + \left[3\chi - \xi\,(9\chi - 1)\right]^2. \tag{3.45}$$

3.2.5 Static solutions

To gain further trust in the validity of the above derived system, let us check whether we can re-derive the static solution from Sec 2.4 for a pure tension brane. As a byproduct, we will encounter a broader class of static geometries corresponding to other types of localized matter.

For a purely static solution $\dot{r}_0 = \dot{\check{r}}_0 = 0$ and all metric functions solely depend on the coordinate r or $\check{r}$. The solution for the exterior field equations (3.30) then reads

$$\alpha = c \log \frac{r}{R} + \alpha_0 \quad \text{and} \quad \eta = 6\, c^2 \log \frac{r}{R} + \eta_0 \,. \tag{3.46}$$

By a local rescaling of the (t, r) coordinates at the brane position we can set $\alpha_0 = 0$ without loss of generality. In the interior, regularity at the axis and continuity at the brane implies $\check{\alpha} = 0$ as well as $\check{\eta} = 0$. The two integration constants c and η_0 are determined by the junction conditions (3.39) and (3.41):

$$\eta_0 = -\log \left| 1 - \frac{\rho}{2\pi M_6^4} \right| , \tag{3.47a}$$

$$c = \frac{1}{3} \left(1 \mp \sigma \sqrt{\frac{4\pi M_6^4 + (1+3w)\rho}{2\,(2\pi M_6^4 - \rho)}} \right) , \tag{3.47b}$$

where $w = p/\rho$ is the equation of state parameter. The third junction condition (3.44) then becomes

$$p_\phi = 6c^2 \left(2\pi M_6^4 - \rho \right) . \tag{3.48}$$

For both sub- and super-critical branes there are two branches corresponding to the two signs in (3.47b). However, when we demand a consistent underlying stabilization mechanism, one branch has to be excluded. More specifically, in one case the angular equation of state parameter $w_\phi := p_\phi/\rho$ drops below -1, thus showing that the brane circumference cannot be stabilized in terms of physical matter. That branch is normally referred to as the "Melvin" or "Kasner" branch [111, 45]. It is straightforward to check that this can be avoided by choosing the respective other branch: This corresponds to keeping the upper sign in (3.47b) in the sub-critical ($\sigma = 1$) and the lower sign in the super-critical ($\sigma = -1$) case. The same kind of quality management will be applied later in the full dynamical analysis.

The line element for the exterior reads

$$\mathrm{d}s^2_{(\mathrm{ext})} = \mathrm{e}^{2\eta_0} \left(\frac{r}{R} \right)^{12c^2 - 6c} \left(-\mathrm{d}t^2 + \mathrm{d}r^2 \right) + \left(\frac{r}{R} \right)^{2c} \mathrm{d}\boldsymbol{x}^2 + \left(\frac{r}{R} \right)^{-6c} r^2 \mathrm{d}\phi^2 \,. \tag{3.49}$$

Since the brane induced terms vanish identically for static configurations, this solution is the 6D version of the exterior metric of a static cylinder first derived by Levi-Civita [114]. It generalizes the (regularized) cosmic string solution (2.81) to other types of matter, characterized by an equation of state parameter w. To make contact with the deficit angle

solution in Sec. 2.4, we specialize to the case of a pure tension brane; specifically,

$$\rho = -p \equiv \lambda \quad \Rightarrow \quad c = 0 = p_\phi \,. \tag{3.50}$$

The coordinate rescaling $(\bar{t}, \bar{r}) = (\mathrm{e}^{\eta_0} t, \mathrm{e}^{\eta_0}(r - R) + R)$ then yields the famous wedge geometry in Gaussian normal coordinates, characterized by the deficit angle $\delta \equiv \lambda / M_6^4$ (cf. Eq. (2.81) and Fig. 2.2). Therefore, we have seen that the full dynamical system described before, correctly captures the (well-known) static physics in the sub- as well as super-critical case.

3.2.6 Interlude: Radiating strings

While in one codimension the symmetries do not allow for propagating waves in the bulk, the situation is different for two (and higher) codimensions. In that case, the brane acts as an antenna that emits and absorbs cylindrical gravitational waves. This fact complicates the analysis because it implies that the curvature on the brane depends on the wave content in the bulk. To be more precise, if we prepare an α-wave packet at initial time far away from the brane that propagates inwards, it will reach the brane eventually and influence its time evolution through the α_0 dependence of the induced metric (3.14). Consequently, it is not possible to derive a *closed* on-brane evolution equation for the Hubble parameter $H = \mathrm{d}\alpha_0/\mathrm{d}\tau$ as it was possible in the codimension-one case without imposing further restrictions.

One possible way out would be to demand a flat bulk geometry. After all, this is a consistent choice in the DGP case. However, a short inspection of the vacuum equations in the bulk shows that this implies $H = 0$, which is of course not acceptable from a phenomenological point of view. To demonstrate this, let us try to set the (x^2, x^1, x^2, x^1) and (x^1, ϕ, x^1, ϕ) components of the Riemann tensor to zero, which is a necessary condition for flatness. This in turn demands (in the exterior)

$$(\partial_t \alpha)^2 - (\partial_r \alpha)^2 = 0 \qquad \text{and} \qquad r\, \partial_r \alpha = 0 \,. \tag{3.51}$$

The only solution to these equations is indeed the trivial configuration $\alpha = \text{const}$. Therefore, a dynamical codimension-two brane inevitably curves the extra-dimensional spacetime, and since the on brane geometry will be time-dependent, the same has to hold for the bulk geometry. As a result, gravitational waves are unavoidable in the cosmological setup.

Alternatively, one could try to implement an "outgoing wave condition" at the outer boundary of the brane to exclude incoming bulk waves. This would be physically justified, since the bulk is assumed to be source-free. However, such a condition is non-local in time. For the symmetries under consideration it can be expressed explicitly as

$$\partial_r \alpha(t, r)\Big|_0 = -\int \frac{\mathrm{d}\omega}{2\pi} \int \mathrm{d}t' \, \frac{H_1^{(1)}(\omega r)}{H_0^{(1)}(\omega r)} \omega e^{-i\omega(t-t')} \alpha(t', r_0(t)) \,, \tag{3.52}$$

where $H_n^{(1)}$ denote the Hankel functions of the first kind. A similar condition has to hold in the interior where we require regularity at the axis

$$\partial_{\check{r}}\check{\alpha}(\check{t},\check{r})\Big|_0 = -\int \frac{\mathrm{d}\omega}{2\pi}\int \mathrm{d}\check{t}'\,\frac{J_1(\omega\check{r})}{J_0(\omega\check{r})}\omega e^{-i\omega(\check{t}-\check{t}')}\check{\alpha}(\check{t}',\check{r}_0(\check{t}))\,, \tag{3.53}$$

where J_n denote the Bessel functions of the first kind.[8] The time dependence of $r_0(t)$ and $\check{r}_0(\check{t})$ further complicate the situation because in order to evaluate the integrals, the history of α and $\check{\alpha}$ has to be known for different values of r and $\check{r}$, respectively. Obviously, implementing these two nonlocal conditions is not any easier than solving the full system of bulk and brane equations from the outset. In general, this can be achieved only numerically. We will present a corresponding numerical scheme in Sec. 3.3.

3.2.7 Alternative regularization

In Sec 2.1, we argued that our results should be insensitive to the details of our regularization provided $HR \ll 1$. In order to explicitly check that assumption, we introduce a slightly modified regularization to which we will refer as the *static regularization*; by contrast, the original regularization will be called *dynamical regularization*. In general terms, the idea is to avoid any dependence on the gravitational dynamics in the interior. There is a clear physical motivation: Even though the regularization of the brane as a ring, used so far, allows us to solve Einstein's equations consistently in the whole space, it is obvious that the predictions for the interior geometry strongly depend on that specific regularization scheme. In particular, we have to specify initial conditions for α also in the interior vacuum region and it is a priori not clear which profile is best suited to describe a natural brane setup. It is therefore crucial to verify that our final results, in particular the evolution of the scale factor on the brane, do not depend on the details of the interior gravitational dynamics (and initial conditions).

In more technical terms, the alternative regularization amounts to setting the extrinsic curvature in the interior to a constant value given by a static ring,

$$\check{\check{K}}^{\phi}{}_{\phi} = \frac{1}{R}\,, \qquad \check{\check{K}}^{0}{}_{0} = \check{\check{K}}^{i}{}_{j} = 0\,. \tag{3.54}$$

Of course, it has to be checked that these ad-hoc assumptions are consistent with the remaining dynamical system. This can be (successfully) verified by explicitly evaluating all constraints that are not used to solve the system. Moreover, it seems conceivable that the solutions thus obtained are freed from any (unwanted) dependence on the initial conditions for α in the interior vacuum region. This expectation will be confirmed by our numerical study.

It is straightforward to adapt the derivation of the matching equations (3.39), (3.41) and (3.44) to the case of the static regularization. For simplicity, we limit the discussion to the

[8] For a more detailed derivation and discussion see [86], as well as [97] in the context of GR.

sub-critical system, i.e., we set $\sigma = 1$. We find for the first and second modified Friedmann equation

$$H^2 = \frac{\rho}{3M_{\rm Pl}^2} + \frac{1}{\ell_2^2}\,(\gamma - 1)\ , \tag{3.55}$$

as well as,

$$\frac{\mathrm{d}H}{\mathrm{d}\tau} = -\frac{3}{2\bar{F}(\tau)}\left[\frac{p}{3M_{\rm Pl}^2} + H^2 - \frac{1}{\ell_2^2}\Big(\gamma\, g(\xi,\chi) - 1\Big)\right]\ , \tag{3.56}$$

where a slightly modified form of F [previously defined in (3.42)] is defined,

$$\bar{F}(\tau) := 1 - \frac{9R^2}{2\ell_2^2}\frac{1}{\gamma}\,. \tag{3.57}$$

As before, $\bar{F} = 0$ defines a boundary in parameter space delineating stable from unstable regions. The pressure that is needed to stabilize the compact dimension can be inferred from

$$\frac{p_\phi}{3M_{\rm Pl}^2} = -\frac{\mathrm{d}H}{\mathrm{d}\tau}\left(1 - \frac{3R^2}{\ell_2^2\gamma}\right) - 2H^2 + \frac{6\gamma}{\ell_2^2}\left\{\chi + \Big[3\chi - \xi(9\chi - 1)\Big]^2\right\}\ .$$

The definitions for ξ , χ and $g(\xi,\chi)$ are unaltered, see (3.43b) and (3.43a), respectively. Moreover, the bulk vacuum equation in the exterior are still described by (3.30).

The expressions for the lower and upper criticality bound, $\rho_{\rm crit}^{\downarrow}$ in (3.25) and $\rho_{\rm crit}^{\uparrow}$ in (3.26), are also changed in the static regularization. The correct expressions can be obtained from the formal replacement $\check{\gamma} \to 1$. Solving the above set of equations (in addition to the ones in the dynamical regularization) allows us to quantify the regularization dependence of our results and thus to extract the physical essence. That way, the significance of our results will be propelled to a higher rank.

3.3 Numerical implementation

We now turn to the numerical implementation of the full brane-bulk system consisting of (3.30), (3.18) and (3.39) (and their counterparts in the static regularization). The solutions are obtained by specifying initial data for α as well as $\check{\alpha}$ and numerically integrating the system forward in time. The corresponding details are provided in Sec. 3.3.1.

Since the dynamical bulk equation in (3.30) is just the standard, linear 2D wave equation on flat space, a stable integration scheme for the PDE part of the problem can be easily found. Once the solution for α and $\check{\alpha}$ is obtained, η and $\check{\eta}$ can be determined by numerically integrating the corresponding constraint equations in (3.30). While solving the linear wave equation is straightforward in the bulk, the nontrivial part is the matching of the interior and exterior solution at the brane. From the perspective of each of the two vacuum regions the brane corresponds to a moving boundary. The corresponding boundary values are

specified by the junction conditions which mediate the effect of the localized matter sector. We discuss the details of the numerical algorithm in Sec. 3.3.2.

3.3.1 Initial data

The numerical integration starts at some initial time $t = t_i$, $\check{t} = \check{t}_i$ and $\tau = \tau_i$. Let us denote all functions evaluated at this time with a subscript i. Through a global rescaling of coordinates, we can always set α and $\check{\alpha}$ to zero on the brane initially, i.e.

$$(\alpha_0)_i = (\check{\alpha}_0)_i = 0\,. \tag{3.58}$$

Consequently, the initial brane position is

$$(r_0)_i = (\check{r}_0)_i = R\,. \tag{3.59}$$

In the bulk, we must specify the initial radial profiles $\alpha_i(r)$ and $\check{\alpha}_i(\check{r})$, as well as $(\partial_t\alpha)_i$ and $(\partial_{\check{t}}\check{\alpha})_i$. To be definite, we choose the static profile given by (3.46), viz.

$$\alpha_i(r) = c\ln\left(\frac{r}{R}\right) \qquad \text{and} \qquad \check{\alpha}_i(\check{r}) = 0\,, \tag{3.60}$$

where the constant c is given by (3.47b) with $\rho \to \rho_i$. In particular, for a cosmological constant ($w = -1$), we get $c = 0$, and hence $\alpha_i(r) = 0$. Note that by choosing the static profile we are not putting any potential energy into the bulk gravitational field initially.

At the brane position, the exterior velocity profile is related to the initial Hubble parameter H_i via

$$\begin{aligned}(\partial_t\alpha_0)_i &= \left.\frac{\mathrm{d}\alpha_0}{\mathrm{d}t}\right|_i - \left.\frac{\mathrm{d}r_0}{\mathrm{d}t}\right|_i (\partial_r\alpha_0)_i \\ &= \left.\frac{\mathrm{d}\alpha_0}{\mathrm{d}t}\right|_i \left[1 - 3\,(\partial_r\alpha_0)_i\right] \\ &= \frac{H_i}{\gamma_i}\left[1 - 3c\right]\,,\end{aligned} \tag{3.61}$$

where for the interior profile we find

$$(\partial_{\check{t}}\check{\alpha}_0)_i = \left.\frac{\mathrm{d}\check{\alpha}_0}{\mathrm{d}\check{t}}\right|_i = \frac{H_i}{\check{\gamma}_i}\,. \tag{3.62}$$

In order to extend this to the bulk, we write

$$(\partial_t\alpha)_i = \frac{H_i}{\gamma_i}(1-3c)P(r) \qquad \text{and} \qquad (\partial_{\check{t}}\check{\alpha})_i = \frac{H_i}{\check{\gamma}_i}\check{P}(\check{r})\,, \tag{3.63}$$

where $P(r)$ and $\check{P}(\check{r})$ are two profile functions satisfying the boundary condition $P(R) = \check{P}(R) = 1$. At this point, we have to distinguish between the two regimes:

1. In the sub-critical case, the exterior space is infinite and potentially occupied with gravitational waves. To minimize the amount of kinetic energy put into the gravitational field initially (which might impact the brane cosmology considerably) we will choose a profile function $P(r)$ which is sharply localized around the brane. For definiteness, we will focus on a Gaussian profile of width W,

$$P(r) = \exp\left[-\frac{(r-R)^2}{W^2}\right] . \tag{3.64}$$

2. In the super-critical case, the exterior space is compact and hosts a second brane with tension λ_a. According to (3.29), this translates to a boundary condition on η, which, due to the constraint (3.30b), can be implemented by choosing the profile $(\partial_t\alpha)_i$ [and hence $P(r)$] appropriately.[9] Specifically, we focus on a cosmological constant source (implying $c = 0$) and make the quadratic ansatz

$$P(r) \to P_d(r) := 1 + d\left(\frac{r^2}{R^2} - 1\right) . \tag{3.65}$$

   First note that this profile fulfills the boundary condition (3.32). By plugging it into the constraint (3.30b), we obtain an expression for $(\partial_r\eta)_i$, which can be integrated and thus fixes d in terms of η_a (or λ_a equivalently),

$$d = \frac{3}{2} - \sqrt{\frac{\gamma_i^2}{H_i^2R^2}\left[(\eta_0)_i - \eta_a\right] - \frac{3}{4}} . \tag{3.66}$$

For definiteness, we will choose a flat profile in the interior,

$$\check{P}(\check{r}) \equiv 1 . \tag{3.67}$$

This choice is motivated by the observation that for R small enough the regularity condition at the axis (3.31) implies $\partial_{\check{r}}\check{\alpha} \approx 0$. With this choice, we expect the on-brane evolution to rapidly become insensitive to the initial conditions.

In order to complete the discussion of of initial data, let us derive the value of the remaining variables $(\eta_0)_i$ and $(\check{\eta}_0)_i$. They are obtained from the regularity condition together

[9] Note that the condition (3.29) holds for all times as $\partial_t\eta_a = 0$ due to the boundary condition on α (3.32) and the constraint (3.30c).

with (3.39) and the constraint equations for[10] $\eta, \check{\eta}$ in (3.30). Specifically,

$$\begin{aligned}(\check{\eta}_0)_i &= 6\int_0^R \mathrm{d}\check{r}\,\check{r}\left[(\partial_{\check{r}}\check{\alpha}_i)^2 + (\partial_{\check{t}}\check{\alpha}_i)^2\right] \\ &= \frac{6H_i^2}{\gamma_i^2}\int_0^R \mathrm{d}\check{r}\,\check{r}\check{P}^2 \\ &= \frac{3H_i^2R^2}{\mathrm{e}^{-2(\check{\eta}_0)_i} + 9H_i^2R^2}\,,\end{aligned} \tag{3.68}$$

an implicit equation for $(\check{\eta}_0)_i$ which can be solved numerically.[11] It is also interesting that $(\check{\eta}_0)_i$ is a direct measure of the gravitational energy stored inside the ring initially [which is suggested by its positive definiteness due to (3.68)]. In fact, it is (up to a constant factor) nothing but the so called *C-energy* first introduced by Thorne [163] and now generalized to 6 dimensions. We will come back to this point in Sec. 3.4.1.4 when discussing the dependence on the interior initial data. 5 The exterior $(\eta_0)_i$ is finally obtained from (3.39), which can be rewritten as

$$\frac{\rho_i}{2\pi M_6^4} = 3\,\ell_2^2 H_i^2 + \check{\gamma}_i - \sigma\sqrt{\mathrm{e}^{-2(\eta_0)_i} + 9H_i^2R^2}\,. \tag{3.69}$$

The specification of initial conditions can readily adopted to the static regularization. Since in that case the junction conditions do no longer depend on any of the interior metric functions $\check{\alpha}$, $\check{\eta}$, we only use the above definition for α_i and $(\partial_t\alpha)_i$ (which are unaltered). Moreover, $(\eta_0)_i$ is again determined by (3.69) with the identification $\check{\gamma}_i \to 1$.

3.3.2 Numerical algorithm

Here, the numerical solver used to integrate the initial conditions forward in time is presented. We will focus on the sub-critical setup that fully resolves the interior of the ring; the other cases, i.e. the super-critical setup and the static regularization, are in fact very similar and hence omitted in the following discussion. Each iteration of the numerical integration is divided into several steps:[12]

1. We start in one of the two vacuum regions and evolve the solution by a finite time step Δt in the exterior (or $\Delta\check{t}$ in the interior). To that end, we use a discretization that is equal in time and space,[13]

$$\Delta t = \Delta r =: \epsilon \qquad \text{and} \qquad \Delta\check{t} = \Delta\check{r} =: \check{\epsilon}\,. \tag{3.70}$$

[10] The full radial profile of $\check{\eta}, \eta$ can be calculated from (3.30b), but is actually not needed for the evolution of α. Only $\check{\eta}_0, \eta_0$ enter through the junction conditions, and those can be calculated at later times from their initial values using (3.30b), (3.30c) only locally at the brane position.

[11] Note that for any value of H_iR there exists a unique real solution for $(\check{\eta}_0)_i$ to this equation.

[12] We used two independent implementations, one in Python and one in Objective-C.

[13] Note that the Courant condition $\Delta t/\Delta r \leq 1$ is satisfied, which implies a stable numerical scheme [147].

The wave equation (3.30a) is then discretized by identifying

$$\partial_r^2 \alpha(t,r) \to \frac{\alpha_{j+1}^n - 2\alpha_j^n + \alpha_{j-1}^n}{\epsilon^2}\,, \tag{3.71a}$$

$$\partial_r \alpha(t,r) \to \frac{\alpha_{j+1}^n - \alpha_{j-1}^n}{2\epsilon}\,, \tag{3.71b}$$

$$\partial_t^2 \alpha(t,r) \to \frac{\alpha_j^{n+1} - 2\alpha_j^n + \alpha_j^{n-1}}{\epsilon^2}\,, \tag{3.71c}$$

where $\alpha_j^n := \alpha(t_n, r_j)$.[14] This in turn admits an expression for α_j^{n+1} in terms of the past values α_j^n and α_j^{n-1}; specifically

$$\alpha_j^{n+1} = -\alpha_j^{n-1} + \alpha_{j+1}^n + \alpha_{j-1}^n + \left(\alpha_{j-1}^n - \alpha_{j+1}^n\right) \frac{\epsilon}{2r_j}\,, \tag{3.72}$$

and likewise for $\check{\alpha}_{\check{j}}^{\check{n}+1}$. This step is only applicable inside the domain of integration but not at its boundaries situated at $\check{r} = 0$ (axis), $\check{r} = \check{r}_0$ (interior brane position), $r = r_0$ (exterior brane position) and $r = r_{\max}$ (artificial outer boundary). We proceed with step 2.a if we integrate the interior, and otherwise with 2.b.

2.a At the axis, corresponding to $\check{j} = 0$, we implement the regularity condition (3.31) which in a discretized version reads $\tilde{\alpha}_0^{\check{n}+1} = \tilde{\alpha}_1^{\check{n}+1}$.

2.b In order to avoid any problems related to the finiteness of the integration domain, we choose $r_{\max}$ large enough so that no wave that is reflected at the outer boundary can affect the evolution on the brane; specifically $r_{\max} \geq N\epsilon/2 + r_0$, where N denotes the total number of time steps. After all, we want to describe the physics of infinitely large extra dimensions. With this choice, we can choose an arbitrary boundary condition at $r_{\max}$ without affecting the solution on the brane (we are actually interested in). A convenient choice could be $\alpha(t_{n+1}, r_{\max}) = 0$.

3. In this step we calculate the new value of α at the brane: $\check{\alpha}_0(\check{t}_{\check{n}+1})$ or $\alpha_0(t_{n+1})$. This can be done by using the dynamical junction condition (3.41). Assume that for instance we want to calculate $\alpha_0(t_{n+1})$. Due to (3.41), this requires the values of the interior quantities $\check{\eta}_0$ and $\partial_{\check{r}}\check{\alpha}|_0$. However, there occurs a complication at this point: Since we use different time coordinates in the interior and exterior, Δt and $\Delta\check{t}$ correspond to different physical (or proper) time steps. A quantitative relation follows from (3.15),

$$\frac{\Delta t}{\gamma} = \frac{\Delta\tilde{t}}{\tilde{\gamma}}\,, \tag{3.73}$$

where in general $\check{\gamma} \neq \gamma$. In other words, the grid points in the exterior and interior do not correspond to the same physical time τ on the brane. Therefore, we establish

[14] The indices n and j (as well as $\check{n}$ and $\check{j}$) label grid points of different times and radial position, respectively.

a dictionary $t(\check{t}_{\check{n}})$ [and $\check{t}(t_n)$] translating the interior to the exterior time [and vice versa]. Let us now assume that the interior integration is slightly "ahead in time", i.e. $\check{t}_{\check{n}-1} < \check{t}(t_n) \leq \check{t}_{\check{n}}$. We then estimate $\check{\eta}_0(\check{t}(t_n))$ by linearly interpolating between $\check{\eta}_0(\check{t}_{\check{n}-1})$ and $\check{\eta}_0(\check{t}_{\check{n}})$ (and likewise for $\partial_{\check{r}}\check{\alpha}|_0$), which in turn yields $\alpha_0(t_{n+1})$.

4. The new value of η_0 (or $\check{\eta}_0$) is obtained from (3.30b) and (3.30c) evaluated in the limit $r \to r_0$ (or $\check{r} \to \check{r}_0$); to be precise, we use the discretized version of

$$\begin{aligned} \frac{\mathrm{d}\eta_0}{\mathrm{d}t} &= \partial_t\eta_0 + \dot{r}_0\,\partial_r\eta_0 \\ &= 6r_0\left[2\left(\partial_t\alpha_0\right)\left(\partial_r\alpha_0\right) + \dot{r}_0\left(\partial_t\alpha_0\right)^2 + \dot{r}_0\left(\partial_r\alpha_0\right)^2\right] . \end{aligned} \tag{3.74}$$

5. It seems that we have now determined all discretized values of α at time t_{n+1}. However, this is in general not true for the grid points next to the brane. The reason is that the brane coordinate position[15] $r_0(t)$ is time-dependent. Therefore, if one chooses a fixed spatial grid size in the bulk (as we do), r_0 in general lies in between those grid points. Yet again, this problem is resolved by using a linear interpolation. Assuming for instance the boundary crossed one grid point at r_J between t_n and t_{n+1} such that $r_0(t_{n+1}) < r_J$, then the value of α_J^{n+1} is obtained by linear interpolating between $\alpha_0(t_{n+1})$ and α_{J+1}^{n+1}.

6. The discretized values of $\check{\eta}$ are obtained by integrating the constraint equation (3.30b) subject to the boundary condition (3.31) (at the axis), and similar for η in the exterior.

7. In the last step, we have to decide which vacuum region we evolve next. Assuming we have determined all values at time t_{n+1} in the exterior and at time $\check{t}_{\check{n}}$ in the interior, we now have to check which integration is further ahead in proper time. If for instance $\check{t}(t_{n+1}) > \check{t}_{\check{n}}$, the exterior has proceeded further in proper time τ and we need to evolve the interior next (by starting over with step 1).

Before concluding the discussion of the numerical algorithm, let us comment on the numerical error control. The error can be quantified in a convenient way by using the constraint equation (3.39), which is only imposed at initial time and thus should be fulfilled at all later times automatically. We therefore define its violation via

$$\delta C := \frac{H^2}{H_i^2} - \frac{\rho}{3M_{\mathrm{Pl}}^2 H_i^2} - \frac{(\gamma - \check{\gamma})}{H_i^2 \ell_2^2} . \tag{3.75}$$

As a consistency check we confirmed that $\delta C \to 0$ as the grid spacing $\epsilon \to 0$. Moreover, we also used the usual error estimate $\delta H := H(2\epsilon) - H(\epsilon)$ and found it to be of the same order as δC.[16] In particular, for the Hubble plots presented in this thesis the error bars

[15] Note that the coordinate position $r_0(t)$ is in general time dependent even though we fixed the proper circumference $2\pi R$.

[16] The corresponding error plots can be found in the appendix of [135].

would not exceed the line thickness. Thus, we do not depict the errors explicitly; however, we ensured that they are completely under control.

3.4 Sub-critical universe

This section has its focus on the cosmology in the sub-critical scenario. In accordance with the discussion of the initial conditions, we consider a conical geometry that is strongly perturbed by the presence of ER waves. That way, we start with a non-vanishing Hubble parameter H_i and track its dynamical evolution. Two specific questions are at the core of this section:

1. *Does the deficit angle geometry has attractor properties?* This is crucial with respect to the CC problem because only then the system is able to dynamically adapt to a change in the tension (or the CC equivalently).

2. *Are there stable sub-critical solutions that lead to a phenomenologically viable cosmology?* It is clear that the deficit angle solution with $H = 0$ is not compatible with observations. However, our hope is that the Hubble evolution gives rise to a viable 4D regime while it approaches zero.

A final answer will be given to both questions—unfortunately for the second one not in the affirmative. We will start with a presentation of our numerical results in Sec. 3.4.1. An extensive discussion of the phenomenological implications follows thereafter in Sec. 3.4.3.

3.4.1 Numerical results

The system was solved along the lines of Sec. 3.3. The sub-critical equations are obtained by setting $\sigma = 1$. We find two qualitatively different classes of solutions, depending on the initial conditions. The first class, called *degravitating* solutions, features a geometry which at late times approaches the static deficit angle profile, in particular, $H \to 0$ on the brane. The second class, called *super-accelerating* solutions, features a run-away behavior for the Hubble parameter on the brane. The source for this apparent instability is a ρ_{eff} which violates the NEC.

After describing a fiducial degravitating and super-accelerating solution, we will assess the consistency of our regularization. The regions of parameter space spanned by each class are discussed thereafter in Sec. 3.4.1.4.

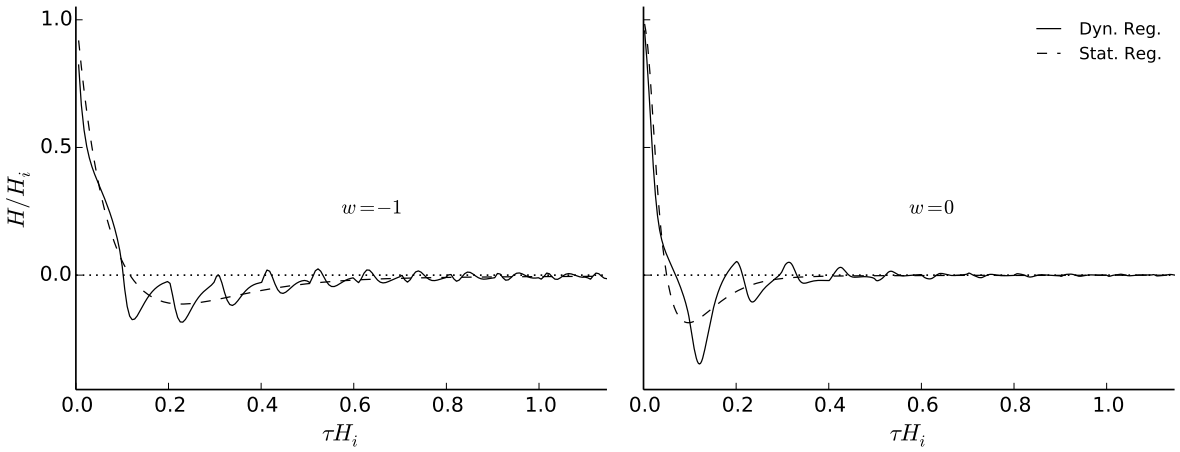

Figure 3.1: Example of dynamical degravitation for a pure tension and a pure dust brane. The Hubble parameter settles to zero within a few Hubble times. In the static regularization the curve smoothly traces the mean of the one in the dynamical regularization.

3.4.1.1 Degravitating solution

As a first example, let us consider the regime with small value of ℓ_2. Specifically, we choose parameters[17]

$$H_i\ell_2 = \frac{1}{20}\,, \qquad H_iR = \frac{1}{20}\,, \qquad \bar{\rho}_i = \frac{1}{2}\,. \tag{3.76}$$

For this choice, the energy density lies in the sub-critical regime. Meanwhile, the characteristic scale ℓ_2 is smaller than the initial Hubble radius $1/H_i$, hence suggesting a large modification to standard 4D gravity. This expectation follows from the Friedmann equation (3.39) where the modification term $(\gamma - \check{\gamma})$ is controlled by ℓ_2. Note, however, that in general ℓ_2 is not the physical crossover, which in a near-critical regime can be larger by a factor of ℓ_2/R, as was shown in the Chap. 2. The reason is that the combination $(\gamma - \check{\gamma})$ does not need to be of order one; in fact, it could be much smaller. We will incorporate this effect in our phenomenological discussion in Sec. 3.4.3.

We will mainly focus on a 4D cosmological constant source but will also refer to a dust source for comparison. One of the crucial results of our numerics is depicted in Fig. 3.1. We see that H initially decreases to negative values, turns around and approaches zero at late times. While we exemplify this behavior in the case of a pure tension ($w = -1$) and a pure dust ($w = 0$) brane, we checked that it persists for other types of physical matter. In particular, this confirms that the deficit angle geometry, discussed in Sec. 2.4.1, as well as the broader class of static solutions derived in Sec. 3.2.5, has a finite basin of attraction.

[17]For completeness, the width of the initial Gaussian profile (3.64) is set to $W = R/50$, and the step size for integration is $\check{\epsilon} = 2 \times 10^{-3}R$ and $\epsilon = 10^{-3}R$ in the interior and exterior, respectively.

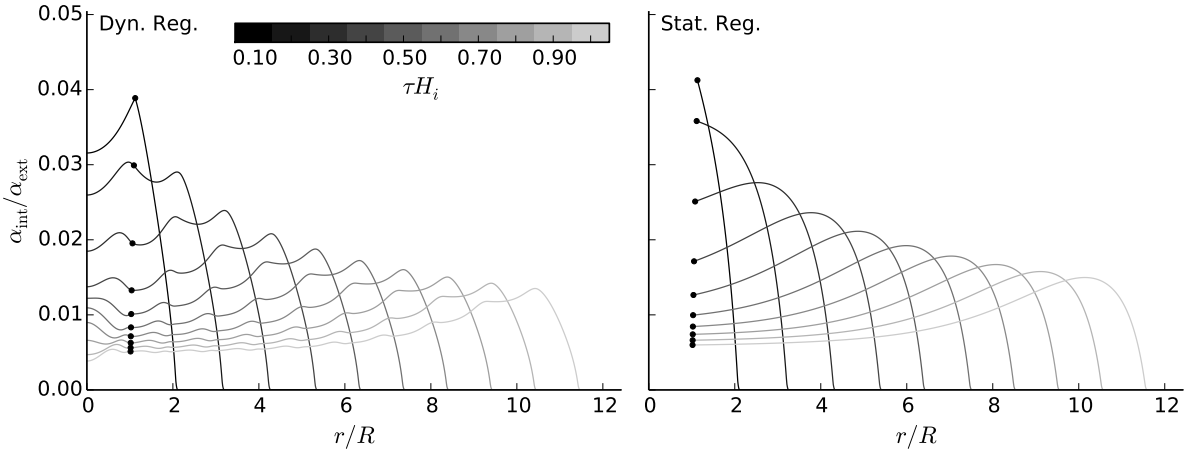

Figure 3.2: The radial profile of α at different values of τ for both regularizations and a pure tension brane. The dots indicate the brane position, left of which the plotted function is the interior $\check{\alpha}(\check{r})$. The wave travels outwards and settles to zero eventually.

This is one of the central results of this thesis: it is an example of dynamical *degravitation* and demonstrates how the brane tension can be absorbed into extrinsic curvature (while the intrinsic brane geometry tends to flat Minkowski space).

The evolution of the bulk geometry, characterized by α and $\check{\alpha}$, is shown in Fig. 3.2. The initial configuration, as discussed in Sec. 3.3.1, leads during the first few time steps to a rather narrow Gaussian profile. As time evolves, we see that α describes a two-dimensional gravitational wave that moves outwards, gets more and more diluted and asymptotically settles to a constant.

It is evident from this plot that dynamically resolving the interior indeed allows for gravitational waves moving back and forth between the axis $\check{r} = 0$ and the brane, where they are partially transmitted to the exterior. Those additional wave perturbations are recognizable as the wiggly structure on top of the smooth wave profile in the left plot of Fig. 3.2. In the Hubble plot they produce small oscillations (with frequency $\sim 1/R$). As mentioned before, those structures can be understood as a dynamical relict of our particular regularization scheme and thus do not represent a generic prediction of a codimension-two braneworld setup. To prove this, we also present the numerical results for the static regularization. There, we find that the wiggly structure has completely disappeared. In particular, the dashed line in the Hubble diagram perfectly follows the mean of the previous oscillatory behavior. The same observation can be made for the radial α profiles. This nicely confirms that the static regularization is indeed an efficient way to get rid of the dependency on the interior geometry in such a way that the long-time evolution (on time scales $\sim 1/H_i$) is not affected. Furthermore, it shows that the predicted Hubble evolution on the time scales of interest $\Delta t \sim 1/H_i \gg R$ is completely insensitive to what is going on inside the brane, and is in that sense regularization independent.

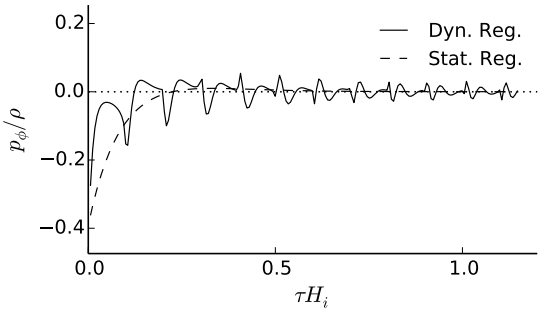

(a) Equation of state of p_ϕ that is needed to keep the brane circumference fixed. It never falls below -1 corresponding to unphysical matter.

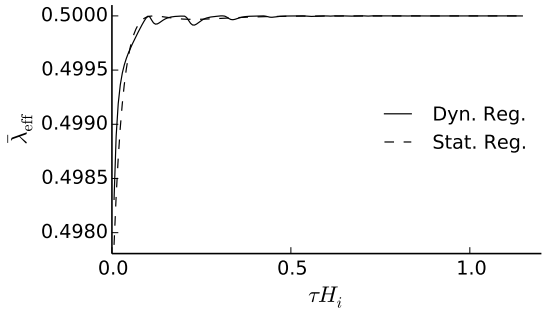

(b) The effective brane tension $\bar{\lambda}_{\text{eff}}$ as "seen" by 6D GR. It approaches a positive value consistent with the static solution.

Figure 3.3: Physicality checks in the degravitating case for $w = -1$.

It remains to check the physicality of the azimuthal pressure component p_ϕ required for stabilization. The equation of state corresponding to this pressure component is shown in Fig. 3.3a. The equation of state satisfies the NEC ($w_\phi \geq -1$), and is therefore physically reasonable. At late times, $p_\phi \to 0$, which is consistent with the static solution of a pure tension brane (cf. Eq. (3.49) for $w = -1$). Figure 3.3b shows the effective brane tension $\bar{\lambda}_{\text{eff}}$ ($\equiv \bar{\rho}_{\text{eff}}$) that sources the 6D bulk gravity theory. This quantity remains positive at all times, which indicates a healthy source from the bulk perspective. At late times, $H \to 0$, and $\bar{\lambda}_{\text{eff}} \to 1/2$, which is consistent with a static solution with brane energy density given by (3.76).

We have repeated the analysis with a dust ($w = 0$) (cf. the right plot in Fig. 3.1) and radiation ($w = 1/3$) component on the brane and found similar behavior. The system approaches the corresponding static solution, defined in (3.49), at late times. The azimuthal pressure p_ϕ and effective density ρ_{eff} are healthy at all times. We also checked that this remarkable agreement between the two regularizations is not altered in that case.

3.4.1.2 Super-accelerating solution

Consider once again a 4D cosmological constant source ($w = -1$), with the same parameters as before except for a somewhat larger value of ℓ_2,[18]

$$H_i \ell_2 = \frac{1}{2}\,. \tag{3.77}$$

In this case, we find completely different behavior. The Hubble parameter on the brane, shown in Fig. 3.4, grows monotonically in time, which indicates an effective violation of the NEC. This growth propagates into the bulk, as can be seen from Fig. 3.5: the wave

[18]For completeness, the width of the initial Gaussian profile (3.64) is set to $W = R/50$, and the step size for integration is $\check{\epsilon} = 10^{-3}R$ and $\epsilon = 2 \times 10^{-3}R/5$ in the interior and exterior, respectively.

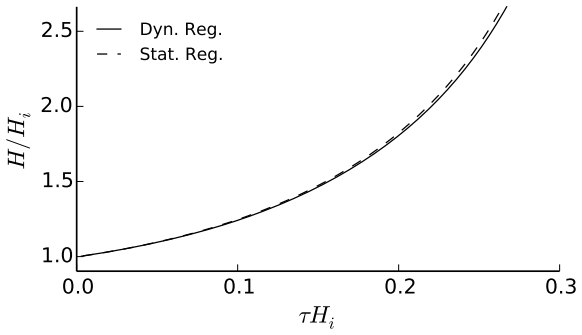

Figure 3.4: Example of a super-accelerating pure tension solution ($w = -1$). The Hubble parameter grows in time unbounded in both regularizations, thereby signaling a classical instability.

function $\alpha(\tau, r)$ grows in time at any r.

This pathological behavior is reflected in the azimuthal pressure p_ϕ, whose equation of state (Fig. 3.6a) becomes less than -1 and tends to $-\infty$. Such an equation of state violates the NEC and is rather unphysical. This suggests that no consistent stabilization mechanism exists for a super-accelerating solution. One might wonder whether this apparent instability is solely due to this strange azimuthal component required to fix the brane circumference. However, this is not the case. In fact, in the appendix of [135] it is shown that fixing $p_\phi = 0$ by hand, and therefore allowing the circumference to evolve in time, still results in super-acceleration.

The evolution of H is qualitatively the same as in the static regularization (dashed line).[19] Contrary to the degravitating solution, there are no visible small oscillations because the dynamics is completely dominated by the overall super-acceleration. Moreover, we checked that the curves approach each other as the regularization size R is decreased. Note that the value $R = 0.05 H_i^{-1}$ is still vastly larger than a phenomenologically realistic value, e.g. $R = 10^{-39} H_i^{-1}$ for $1/R \sim M_6 \sim 10\,\mathrm{MeV}$ and $H_i \sim H_0 \sim 10^{-33}\mathrm{eV}$.[20]

The instability can be clearly seen by looking at the effective tension $\bar{\lambda}_{\text{eff}}$ that sources 6D gravity. As shown in Fig. 3.6b, it starts out positive but eventually turns around and reaches negative values. This behavior bears resemblance to the DGP model, where the self-accelerating branch leads to a negative effective energy density [91] and, as discussed before in Sec. 3.1, is widely believed to contain a ghost in its spectrum. The instability is even more severe in our case, since $\bar{\lambda}_{\text{eff}}$ decreases monotonically at late times, whereas it is bounded from below in the DGP case.

In the following discussion, we are able to trace the instability back to the ghost mode found in the linear analysis. As a result, the super-accelerating solutions have to be dis-

[19] The faster growth in the static regularization is due to the fact that in this case the parameter choice (3.77) is closer to the stability bound defined by $F(\tau) = 0$.

[20] This choice for M_6 leads to a phenomenologically acceptable crossover in the near-critical regime for which $r_c \sim L_2$ (cf. the discussion in Sec. 3.4.3).

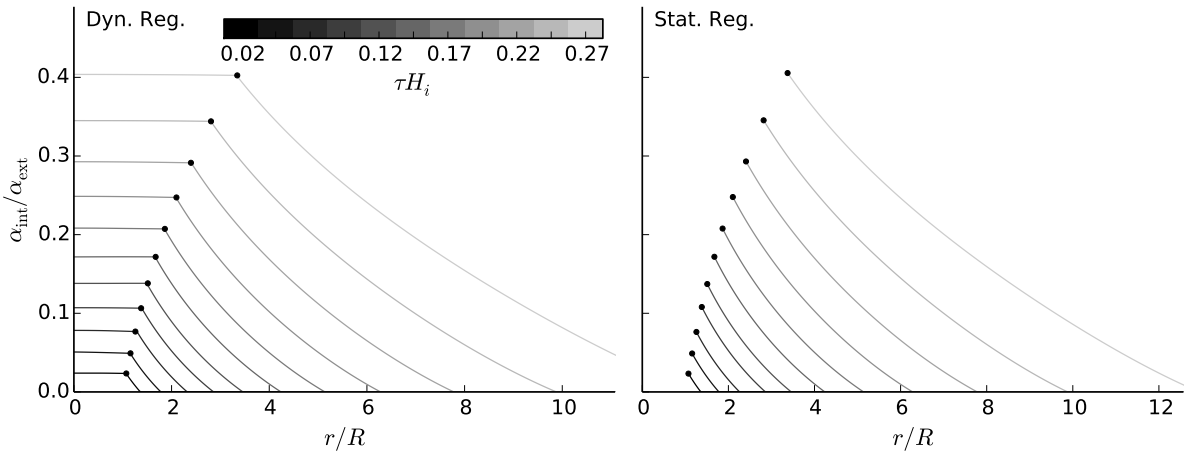

Figure 3.5: The radial profile of α at different values of τ for both regularization. The dots indicate the brane position, left of which the plotted function is the interior $\check{\alpha}(\check{r})$. At fixed radius α grows in time.

missed on consistency grounds.

3.4.1.3 Volume stabilization

For consistency reasons, we should address the question whether the extra space volume in the interior, i.e. inside the ring/brane, is approximately constant and, in particular, vanishes for $R \to 0$. In an unfavorable scenario a bubble of space could form in the interior which would be unrelated to the circumference. This would be at odds with the physical brane setting we have in mind and could be a possible source for the instability. A priori, the stability of the interior volume is not obvious because we only fixed the circumference R by hand but not the volume itself. The interior (extra space) volume is given by (3.11),

$$V_{\rm int}(\tau) = 2\pi \int_0^{\check{r}_0(\tau)} \mathrm{d}\check{r}\; \check{r}\, \mathrm{e}^{\check{\eta}-6\check{\alpha}} \;, \tag{3.78}$$

which can be integrated numerically, and is depicted in the pure tension case ($w = -1$) by the solid lines in Fig. 3.7.

In the degravitating case, we find that the interior volume oscillates with a frequency of order R^{-1}. The oscillations are again due to small wave excitations in the interior and are thus an artifact of the initial conditions. The closer we approach the attractor solution, the more they are washed out, and $V_{\rm int}$ approaches the flat space value πR^2, which lies slightly below the initial volume $V_{\rm int}(0)$ (dotted line). The dashed curves describe the evolution of a certain initial 3D volume $V_{\rm b}(\tau) \propto \mathrm{e}^{3\alpha_0}$ intrinsic to the brane. Evidently, the interior volume can be regarded as approximately constant as compared to the brane volume, in both the degravitating and super-accelerating case. We consequently conclude that by fixing the circumference, the interior (extra-) space is sufficiently stabilized in the

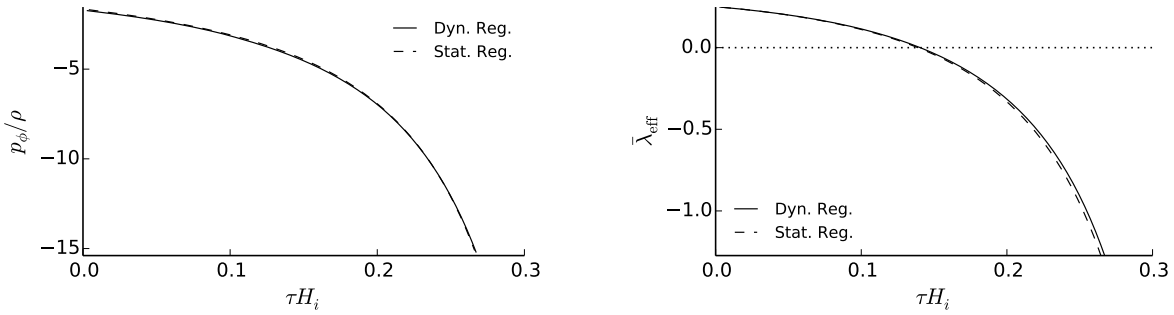

(a) Equation of state of p_ϕ that is needed to keep the brane circumference fixed. It is negative and falls rapidly below -1.

(b) The effective tension, as "seen" by 6D GR, becomes negative. This is interpreted as the source of the physical instability.

Figure 3.6: Physical consistency checks in the degravitating case for $w = -1$.

dynamical regularization. Furthermore, this volume vanishes for $R \to 0$ as demanded by a consistent regularization.

Regarding the super-accelerating solution note that the volume inside the ring does not collapse, which could have been a potential source of energy driving the super-acceleration in the brane directions. Instead, the energy for this expansion is provided by the brane induced gravity terms which allow the effective tension (or energy density equivalently) to become negative. The same conclusion can also be drawn from the fact that we find the same Hubble evolution for the static regularization, where the system is not influenced by an interior geometry.

In summary, the interior space is sufficiently stabilized in all cases. In particular, it has to be discarded as a potential source for the instability.

3.4.1.4 Parameter space

As the above examples show emphatically, our 6D model yields qualitatively very different solutions, depending on the choice of parameters. To study this more systematically, we now perform a scan over $\rho_i \equiv \lambda$ and ℓ_2, keeping $H_i R = 0.05$ fixed. This will allow us to understand the border delineating degravitating and super-accelerating solutions.

The results are shown in Fig. 3.8, where each dot corresponds to one set of parameters for which we ran the numerics. Region (1) corresponds to degravitating solutions. As in the example of Sec. 3.4.1.1, the brane Hubble parameter H tends to zero at late times, and the effective energy density $\bar{\lambda}_{\rm eff}$ is always positive. Region (2) indicates super-accelerating solutions. As in Sec. 3.4.1.2, H grows unbounded, while $\bar{\lambda}_{\rm eff}$ eventually becomes negative, indicating a classical instability. Finally, region (3) corresponds to parameter choices for which the criticality bound (3.25) is violated. It corresponds to the critical regime defined in (3.26) and hence vanishes in the phenomenologically relevant limit $H_i R \to 0$.[21]

[21] Above the critical still lies a super-critical regime, which will be discussed in Sec. 3.5.

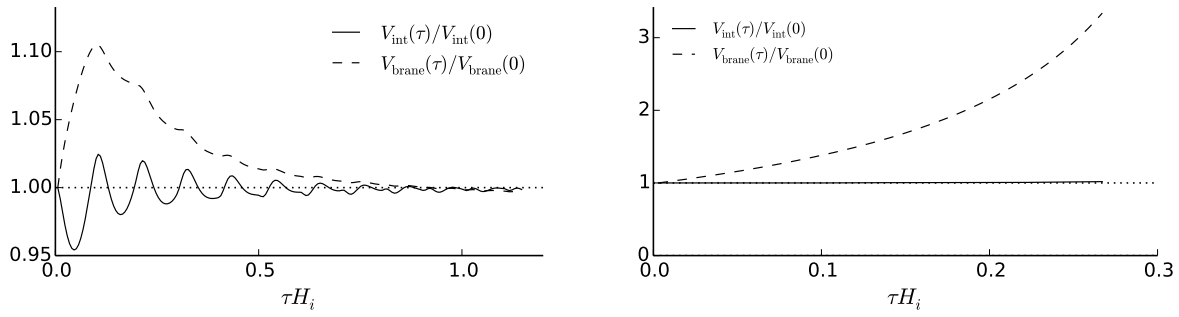

(a) The degravitating solution.

(b) The super-accelerating solution.

Figure 3.7: The 2D volume of the interior space [as defined in(3.78)] is approximately constant as compared to the 3D brane volume $V_{\rm brane}(\tau) \propto \mathrm{e}^{3\alpha_0}$, confirming a successful stabilization.

It turns out that the border between the stable and unstable regions matches perfectly the location in parameter space where F, as defined in (2.110), vanishes. This is drawn as a solid line in Fig. 3.8a and 3.8b. In the degravitating regime, F is negative, and in the super-accelerating regime it is positive. Since F appears in the denominator on the right-hand side of the $\mathrm{d}H/\mathrm{d}\tau$ equation (3.41), the evolution of H becomes ill-defined when F vanishes. The system hits a (physical) singularity, where the numerics of course break down. To better understand the boundary between the stable and unstable regions, Fig. 3.8b zooms in on the boxed region of Fig. 3.8a. For parameters sufficiently close to the $f = 0$ line, $F(\tau)$ dynamically approaches zero after a short time, and thus the system hits a singularity. The basin of attraction for the singularity corresponds to region (4), in which case one starts in the "healthy" region, and region (5), in which case one starts in the "unstable" region. This is shown in more detail in Fig. 3.9 for the static regularization.

The attractor region of the singularity, which is hardly visible in Fig. 3.8b, can be broadened by injecting more energy into the bulk initially. This can be achieved by widening the initial Gaussian velocity profile. As a result, the two regions are dynamically separated; it is therefore not possible to evolve from one region to the other.

We checked that these results are largely unchanged if one uses dust ($w = 0$) or radiation ($w = 1/3$) on the brane. Furthermore, we repeated the entire analysis for a different value of the circumference, namely $R = 0.025 H_i^{-1}$, and found similar agreement. In particular, the border between the stable and unstable regimes again coincides with the $F = 0$ line in parameter space.

The results for the static regularization are depicted in Fig. 3.8c and 3.8d. Again, the function $\bar{F}$ divides the parameter regime into stable and unstable regions. However, the precise shape of the boundary is altered, in fact the green region is enlarged compared to the full dynamical regularization. We will discuss the origin of this difference in Sec. 3.4.3.

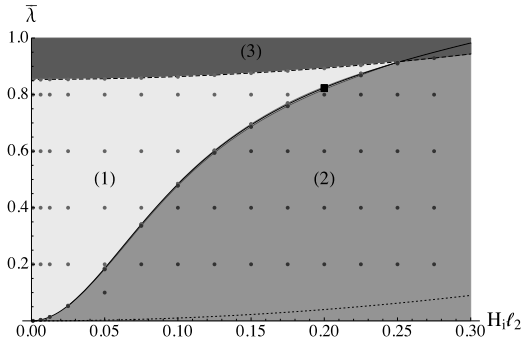

(a) Dynamical regularization: $F = 0$ defines the boundary between stable and unstable regions.

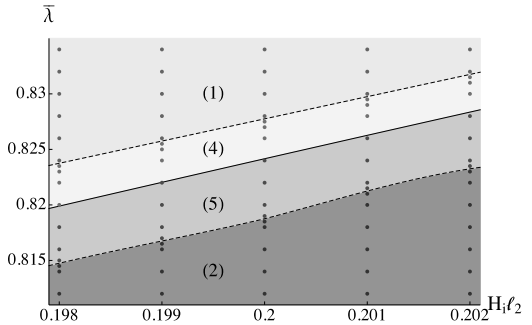

(b) Zoom into the small rectangle depicted in Fig. (a). The dashed lines were inferred from the numerical results.

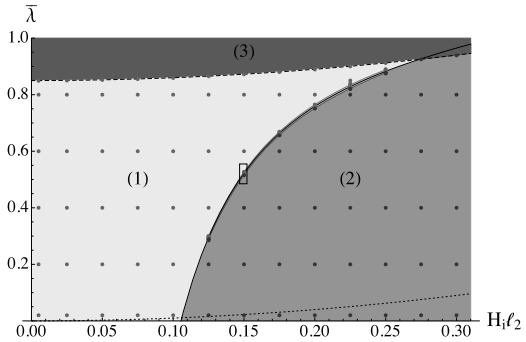

(c) Static regularization: $\bar{F} = 0$ defines the boundary between stable and unstable regions.

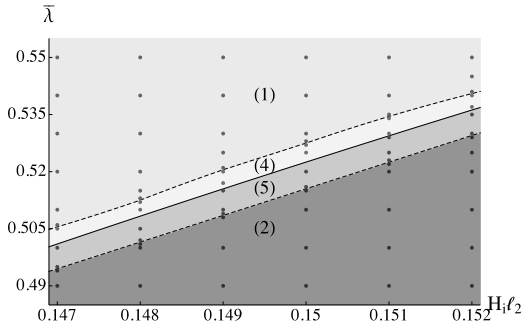

(d) Zoom into the small rectangle depicted in Fig. (c).

Figure 3.8: Behavior of solutions for different parameter choices $H_i\ell_2$ and $\bar{\lambda} \equiv \lambda/2\pi M_6^4$ with $H_iR = 0.05$ fixed. Region (1) corresponds to stable and region (2) to unstable solutions. Region (4) and (5) represent solutions which hit the singularity at $F = 0$ (or $\bar{F} = 0$) in finite time.

3.4.2 Embedding picture

To obtain a better geometrical understanding of how degravitation is realized dynamically, it is instructive to visualize the extra-dimensional geometry in an embedding picture. To that end, we introduce a new coordinate Y via

$$\mathrm{d}Y^2 = \mathrm{d}A^2 - \mathrm{d}C^2 \tag{3.79}$$

where $\mathrm{d}A := \mathrm{e}^{3\alpha-\eta}\mathrm{d}r$ measures the proper distance from the brane and $\mathrm{d}C := \mathrm{d}(\mathrm{e}^{-3\alpha}r)$ the (2π reduced) proper circumference of the extra space. In particular, for $\alpha = 0$ and $\eta = \text{const}$, we find $\mathrm{d}Y = \pm\,(\mathrm{e}^{-2\eta} - 1)\,\mathrm{d}r$, which describes a cone in the (C, Y, ϕ)-space.

With these definitions, we can create embedding pictures of the extra space for every

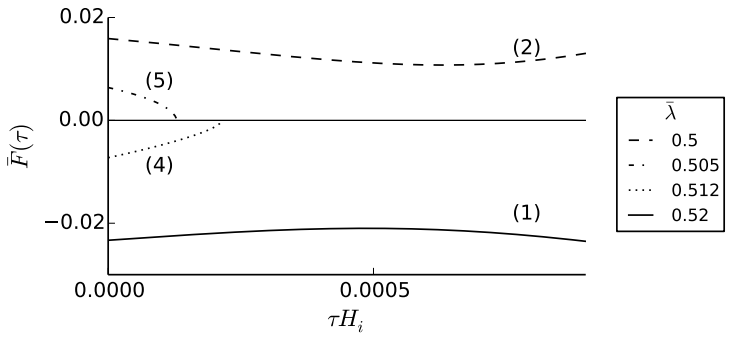

Figure 3.9: The evolution of $\bar{F}(\tau)$ for $H_i r_c = 0.148$ and different values of $\bar{\lambda}$. The labels of the curves match those of Fig. 3.8. Line (4) and (5) hit the singularity at $\bar{F} = 0$ in finite time, while (1) and (2) avoid the singularity (which was checked by going to later times).

moment in time.[22] The corresponding diagrams are depicted in Fig. 3.10. We see that the initial geometry is described by a perfect cone but gets perturbed due to the nontrivial (Gauss shaped) initial velocity profile [see Eq. (3.63)] in the bulk.[23] This perturbation moves outwards (to infinity) and the geometry settles back to a static cone characterized by a smaller deficit angle. The physical reason is that the ER waves transport energy away from the brane, which in turn reduces the conical singularity.

This picture also provides further intuition about what would happen if the tension changed its value (which could occur during a phase transition on the brane): The geometry would react by adopting a new deficit angle. Of course, this could not happen instantaneously, but would be mediated by ER waves in a causal way.[24]

3.4.3 Phenomenology

The main achievement of the numerical analysis consists in clarifying the significance of the function $F(\tau)$ (or $\bar{F}(\tau)$ in the static regularization) as defining a stability line in parameter space: For sub-critical energy densities, the model is stable iff the function $F(\tau) < 0$.

As a first important consistency check, let us compare our results with the linear analysis in Chap. 2. At first sight, it is clear that the two parameter plots, Fig. 2.6 and Fig. 3.8, are very similar: In both cases there is a stable window corresponding to somewhat smaller values of ℓ_2. To be precise, while in the linear case the parameter combination L_2/R $[= \ell_2^2/(3R^2)]$ was used to scan the parameter space, the nonlinear analysis employs $H_i\ell_2$ in order to include the dependence on the initial conditions. To work out the agreement more

[22] Although the embedding diagrams are time slicing dependent, they allow to get an understanding of the physical curvature evolution.

[23] Here we work in the static regularization corresponding to an interior spacetime that is literally empty.

[24] Practically, this could be simulated by including an Abelian Higgs sector into the theory and tracking the spontaneous symmetry breaking.

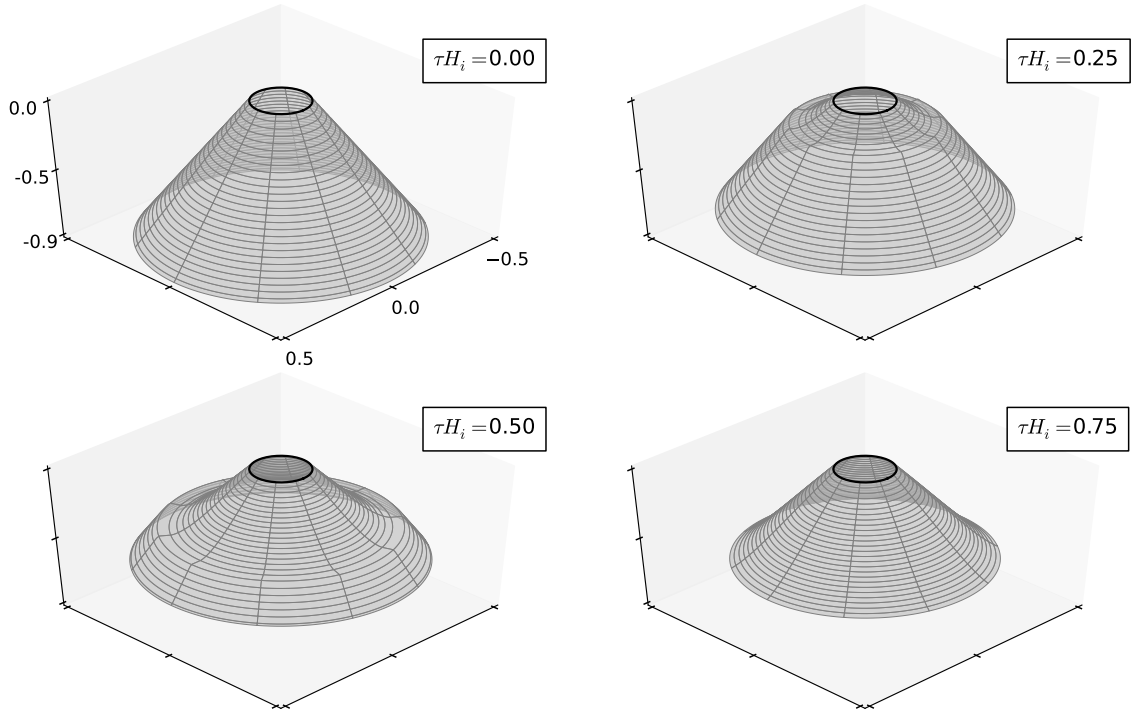

Figure 3.10: Embedding picture of the perturbed "cosmic string" geometry. The brane corresponds to the black ring and the parameters are chosen as in (3.76), except for $H_i R = 0.1$, which leads to a more accentuated initial perturbation. The perturbation moves outwards and the geometry settles back to a wider (static) cone.

explicitly, we attempt to derive $f^{(s)}$ [cf. Def. (2.110)] from the nonlinear expression F. Since $f^{(s)}$ was defined for a static pure tension background, we evaluate F in the corresponding limit, i.e., we set $\check{\gamma} = 1$ and identify $\gamma \to \left[1 - \bar{\lambda}\right]$ according to (3.47a), which in turn implies

$$F \to 1 - \frac{3R}{2L_2}\beta \equiv f^{(s)} \,. \tag{3.80}$$

This convincingly demonstrates the compatibility of the linear and nonlinear analysis[25] and shows that F is indeed a generalized version[26] of $f^{(s)}$ valid for a generic FLRW brane background with non-vanishing H. In particular, we are now able to pin down the physical source of the instability: the scalar mode s introduced in the linear analysis. Consequently,

[25] We did not use the static regularization in the linear analysis but we expect the same agreement in that case.

[26] Alternatively, for a pure tension source, F can be understood as a particular nonlinear completion of f because it includes the effect of higher order perturbations described by H, η_0 and $\check{\eta}_0$. These time-dependent functions parametrize deviations from the static deficit angle background.

the agreement between both analysis further strengthens our assessment on the status of the super-accelerating solutions as being pathological.

The main benefit that can be drawn from F is the possibility to infer the stability of solutions with non-vanishing Hubble parameter. In other words, while the deficit angle background was of conceptual interest to study the stability of a degravitating background, the symmetry-reduced analysis of this section allows to investigate *realistic* cosmological scenarios. In particular, we can address the question whether the near-critical regime, which was revealing itself in the linear analysis, is compatible with observations, i.e. persists for $H \neq 0$.

As the interpretation of F is sufficiently settled now, the further analysis focuses on the parameter dependence of the stability line. Given the analytic expressions in (3.42) [and (3.57)] this analysis can be done without using any numerical input and therefore provides us with exact analytic results. This in turn is crucial when we want to arrive at a final statement about the phenomenological viability of (2.1). To that end, let us rewrite $F(\tau)$ as a stability bound on $\bar{\rho} := \rho/(2\pi M_6^4)$. After eliminating γ by using the constraint (3.39), the condition $F < 0$ (and $\bar{F} < 0$) can be cast into the form:

$$\bar{\rho} > \begin{cases} \ell_2^2 H^2 + \dfrac{2\,\ell_2^2 \check{\gamma}^2}{9R^2 + 2\,\ell_2^2 \check{\gamma}} & \text{(dynamical regularization)} \\ \ell_2^2 H^2 + 1 - \dfrac{9}{2}\dfrac{R^2}{\ell_2^2} & \text{(static regularization)} \end{cases} \tag{3.81a}$$

This constitutes a stability bound for the localized energy density: If it is fulfilled, it implies that ρ_{eff} is always positive. On the other hand, if violated, the sign of ρ_{eff} is not determined (in Fig. 3.8 it is negative below and positive above the dotted line). In that case, H shows an unstable behavior as in Fig. 3.4; as a result, ρ_{eff} becomes negative at some (later) time. For the sake of completeness, let us also cite the criticality bound (3.25) in both regularizations:

$$\bar{\rho} < \begin{cases} \ell_2^2 H^2 + \check{\gamma} - 3|H|R & \text{(dynamical regularization)} \\ \ell_2^2 H^2 + 1 - 3|H|R & \text{(static regularization)} \end{cases} \tag{3.82a}$$

One disturbing fact with the two bounds in the dynamical regularization is their dependence on the interior bulk geometry, through the appearance of $\check{\gamma}$. Since $\check{\gamma}$ can only take values in the interval

$$3\,|H|\,R < \check{\gamma} < \sqrt{1 + 9H^2R^2}\,, \tag{3.83}$$

it is convenient to introduce the parameter

$$q := \frac{\check{\gamma} - 3\,|H|\,R}{\sqrt{1 + 9H^2R^2} - 3\,|H|\,R} \in (0, 1)\,. \tag{3.84}$$

The maximum value $q = 1$ corresponds to $\check{\eta}_0 = 0$, which by inspection of Eq. (3.68) is equivalent to $\partial_{\check{r}}\check{\alpha} = \partial_{\check{t}}\check{\alpha} = 0$, or in other words, to zero gravitational energy inside

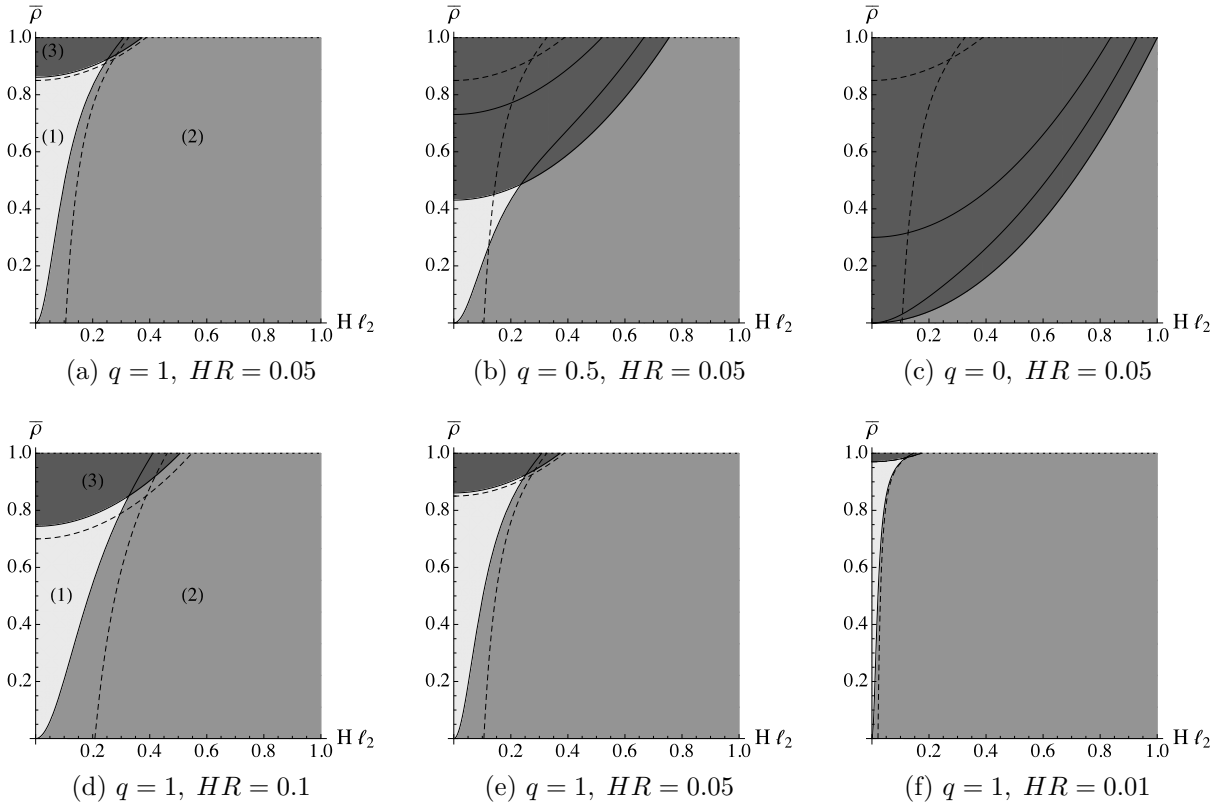

(a) $q = 1,\ HR = 0.05$ (b) $q = 0.5,\ HR = 0.05$ (c) $q = 0,\ HR = 0.05$

(d) $q = 1,\ HR = 0.1$ (e) $q = 1,\ HR = 0.05$ (f) $q = 1,\ HR = 0.01$

Figure 3.11: Contour plots for different values of q and HR. The dashed lines are obtained for the static regularization. First row: a smaller value of q corresponds to a higher energy insertion through initial conditions. Second row: decreasing HR (as required by phenomenology) leads to a smaller stable regime.

the brane/ring. Initially, for $H_i \neq 0$, this can never be achieved exactly, because of the constraint (3.61). However, by making the profile function $\check{P}$ sharply localized, it could be approached asymptotically. On the other hand, the minimum value $q = 0$ would correspond to $\check{\eta}_0 = \infty$, i.e. an infinite amount of gravitational energy in the interior. This is clearly not what we want, so we are mainly interested in values of q close to 1. In particular, for the flat initial conditions that we used for our numerics and $H_i R = 0.05$ (which was chosen in Fig. 3.8) one finds $q = 0.9915$.

The first row of Fig. 3.11 shows how the contour plots depend on the parameter q: As q decreases, region (1) becomes smaller and is replaced by region (3). This is due to the fact that as $q \to 0$, we are putting more and more energy into the gravitational field and so the configuration becomes super-critical for smaller values of ρ. As just mentioned, this is not the situation we are interested in. Therefore, in the second row of Fig. 3.11, comparing the contours for different values of HR, q was set equal to 1. There are two things that can be learned from a closer inspection of the contour plots:

1. The stable and unstable regions in both regularizations agree in the limit $R \to 0$.

2. The stable region gets diminished when HR is decreased.

While the first point further strengthens our trust in the regularization procedure, the second one raises strong concerns about the phenomenological viability of the model because $HR \ll 1$ in any realistic setup. To summarize, we were able to single out a sub-critical window in parameter space that is both stable and theoretically consistent.

It is now of particular importance to answer whether phenomenologically viable points can lie inside this region. To make this more precise, let us reformulate the two bounds on ρ. By using the expression (3.82) and (3.81), we find that sub-critical and stable solutions only exist if

$$2\,(H\ell_2)^2 < 3\,|H|\,R\,. \tag{3.85}$$

This bound is applicable in the case of both regularizations (which is another demonstration of the universality of our result). In order to have a standard 4D cosmological evolution on the brane, we need $Hr_c \gg 1$, where r_c is the crossover scale. The problem is that the crossover r_c, in general, is a function that can depend on the model parameters in a complicated way. However, we learned from the linear analysis in Chap. 2 that there is an upper bound, viz. $r_c < L_2 \equiv \ell_2^2/(3R)$. Using this to substitute ℓ_2 in (3.85) leads to

$$\boxed{Hr_c < 1\,.} \tag{3.86}$$

This is one of the main results of the sub-critical analysis. It shows that the requirement of having a stable and sub-critical solution is incompatible with a 4D evolution of the Hubble parameter. However, this would be imperative to reproduce the success of 4D GR for early times. We thus arrive at our final conclusion about the sub-critical model:

> *The sub-critical model admits no solutions that are both stable and phenomenologically viable.*

3.4.4 Digression: DGP parameter space

Before concluding the sub-critical discussion, let us draw some parallels to the codimension-one case. There, the modified Friedmann equation is given by (3.1). At initial time, this can be rewritten as

$$\frac{\rho_i}{6M_5^3 H_i} = H_i r_{c,1} \mp 1 \tag{3.87}$$

As discussed in Sec. 3.1, the minus sign corresponds to the "normal" branch and the plus sign to the "self-accelerated" branch. The ratio $\rho_i/(6M_5^3 H_i)$, which is the 5D analogue of $\bar{\rho}$, is fixed (up to the choice of branch) for a given crossover scale $r_{c,1}$. Therefore, the DGP parameter space is only one-dimensional. This difference is due to the fact that in 6D we have the additional freedom to choose the initial deficit angle. The resulting DGP "contour" plot, shown in Fig. 3.12, is remarkably similar to the 6D setup. The solid line corresponds to the normal branch of DGP; this branch is stable, and the effective energy density ρ_{eff} is always positive. The dashed line is the self-accelerated branch. On

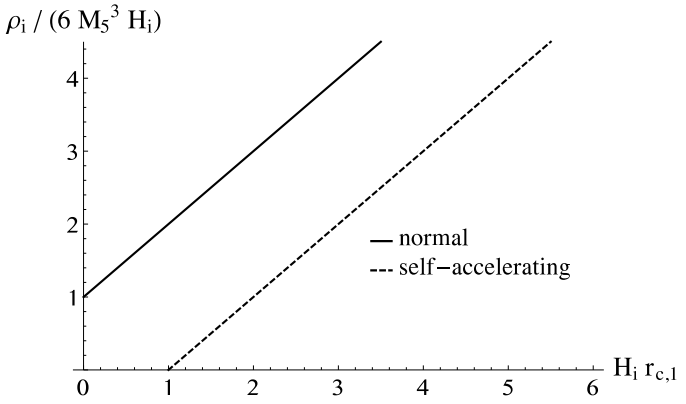

Figure 3.12: The "contour" plot for the DGP model consists of two disjoint lines. The solid line is the normal branch, which is stable. The dashed line is the self-accelerated branch, which is unstable.

this branch, H is always larger than $1/r_{c,1}$, and ρ_{eff} negative. Our results generalize this peculiarity of the DGP model to codimension-two. The main differences are:

1. The stable/unstable solutions lie on disconnected branches in the 5D DGP model, whereas they are separated by a physical singularity in the 6D model. This is related to the fact that, due to the deficit angle, there is more freedom in 6D to choose initial conditions on the brane.

2. There is no criticality bound on ρ in the DGP case, hence no gray region. This difference is caused by the different topology in the codimension-two case.

3.4.5 Effective field theory bounds

Before concluding the sub-critical analysis, the validity of the EFT description is investigated. We will find that, depending on the value of R, there are further bounds on the model parameters stemming from the requirement of having a valid EFT.

Since the fundamental cutoff scale in the bulk is given by M_6, the breakdown of the EFT occurs once the bulk curvature terms are of the same order. We can use the extrinsic curvature as a diagnostic tool by comparing it to the M_6 scale. To be precise, we focus on the combination $\tilde{\mathcal{K}} \equiv [\tilde{K}^{\alpha}{}_{\alpha}] - [\tilde{K}^{0}{}_{0}]$ which occurs in the (00) component of the junction conditions (2.9). Accordingly, the dimensionless combination of $\mathcal{K}$ and M_6 can be evaluated to

$$\frac{\tilde{\mathcal{K}}}{M_6} = \frac{1}{RM_6}\left[(\ell_2 H)^2 - \bar{\rho}\right] . \tag{3.88}$$

When this expression becomes of order unity, we expect the EFT to break down. At this point higher order operators, which are normally suppressed by M_6, would modify the right hand side of (2.9), thus invalidating our previous analysis. Obviously, this strongly depends on the scale R. Fig. 3.13 visualizes the regime of validity for different values of

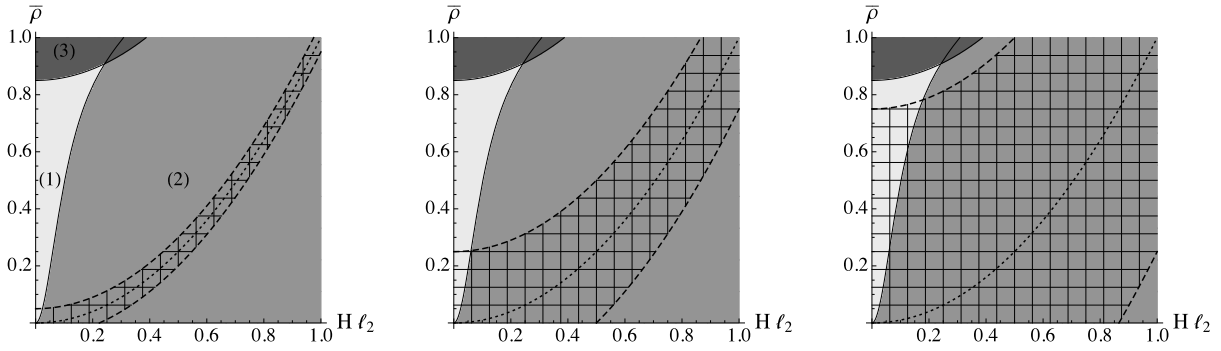

(a) $RM_6 = 0.05$ (b) $RM_6 = 0.25$ (c) $RM_6 = 0.75$

Figure 3.13: Contour plots for different values of RM_6 with $HR = 0.05$ fixed. The grid lines (framed by the dashed lines) indicate the parameter regime with a valid EFT. The dotted line in the center corresponds to $\mathcal{K} = 0$, the dashed lines to $\mathcal{K} = \pm M_6$.

RM_6. Outside the structured area (framed by the dashed lines) the EFT breaks down since $\mathcal{K} > M_6$. The dotted line corresponds to a vanishing extrinsic curvature and hence to a standard 4D evolution due to (3.88).

As a result, for small radii, $R \ll M_6^{-1}$, only small deviations from standard GR can be studied within a valid EFT. In particular, we could never enter the super-critical regime. We will therefore assume $R \gtrsim M_6^{-1}$ [which is also in accordance with having a natural EFT as explained in Sec. 2.5.1]. Let us note that the conclusions of the previous sub-critical analysis are unaffected by this because the phenomenologically relevant equations only depend on HR (instead of $M_6 R$). The requirement $RM_6 \gtrsim 1$ is rather an additional theoretical input that further constrains the model's parameter space. To be precise, assuming the crossover saturates its upper bound L_2 [which is valid in the near critical regime, cf. (2.129)], we get

$$R \gtrsim \left(r_c M_{\rm Pl}^{-2}\right)^{1/3} \quad \left[\sim 0.1\,\text{MeV}^{-1} \text{ for } r_c = 1/H_0\right] . \tag{3.89}$$

The estimate in squared bracket is valid if the crossover is identified with todays Hubble length $1/H_0$. However, note that this discussion is somewhat obsolete because our cosmological analysis already showed that the sub-critical system does in principle not admit a stable 4D regime. On the other hand, $R \gtrsim M_6^{-1}$ might be a relevant restriction for the super-critical model, which will be considered next in Sec. (3.5).

3.5 Super-critical universe

Let us now turn to the super-critical regime. As already mentioned in Sec. 3.2.3, where the junction conditions were derived, we expect the emergence of a second axis at which

the exterior spacetime closes. In general, this axis has a conical singularity, which can be interpreted as the presence of a second brane with tension λ_a. Therefore, in this case, the system is characterized by one additional parameter.

In the sub-critical case, our discussion had its focus on the deficit angle geometry (2.81) [or on generalized versions for other types of matter, cf. Eq. (3.49)]. This solution is of particular interest as it describes the 4D maximally symmetric case (corresponding to the symmetries of a 4D CC) and effectively hides a tension from a 4D observer. By studying its attractor properties, we could make statements about both the model's potential with respect to the CC problem and its cosmological predictions. Here, the situation is slightly more involved. There exists a static solution with $H = 0$ and $\delta > 2\pi$ [cf. Eq. (2.81)], which, however, comes at the price of introducing a tuning relation on both brane tensions. We explicitly find[27]

$$\bar{\lambda} + \bar{\lambda}_a = 2\,. \tag{3.90}$$

As a consequence, this solution cannot help with the CC problem. This unfortunate relation has to be understood a consequence of over-constraining the system by requiring $H = 0$. In this work, we attempt to circumvent the problem by considering the generic case with $H \neq 0$. In other words, we look for new, 4D maximally symmetric solutions that describe an inflating brane. There are two specific possibilities how this might help with the original problem:

1. If these new solutions are continuously connected to the old one with $H = 0$, we expect the parameter constraint to be relaxed by the occurrence of a modification term $M(H)$, which obeys $M(H) \to 0$ in the limit $H \to 0$. This means that (3.90) is no longer a constraint equation but simply fixes the integration constant H in terms of model parameters. Then, it "only" remains to be seen whether this new relation has the potential to avoid a tuning of λ for a phenomenologically relevant choice of the Hubble parameter.

2. Alternatively, there might exist a completely new branch of solutions [hence not continuously connected to the static one that leads to (3.90)]. It is not clear what we should expect from that solution, but it might offer a new perspective on the super-critical scenario.

In the following, we are able to realize this program on a fully analytical level. First, we derive a new class of super-critical scaling solutions with $H \neq 0$, which—at least to our knowledge—have never been associated with a super-critical brane before. Second, the solution space divides into two relevant branches, each of which corresponds to one of the above proposed scenarios. This in turn enables us to discuss the potential of the super-critical model with respect to the CC problem.

[27] This relation persists in the (super-critical) BIG model because the induced terms vanish for $H = 0$.

3.5.1 Bulk-brane solutions

The aim of this section is to find a solution with $H \neq 0$ of the brane-bulk system defined by (3.30), (3.18) and (3.39) for a pure tension brane. Given the complexity of the system, this seems to be quite a difficult task. On the other hand, compared to the FLRW solutions in the sub-critical case, we will see that the degree of complexity is reduced by limiting ourselves to maximally symmetric sources on the brane, viz. a tension with $\rho \equiv \lambda =$ const. It is clear that a relaxation to FLRW symmetries would significantly complicate the analysis.

We derive a solution under the assumption of a constant brane coordinate velocity in both the interior and exterior region, viz.

$$\dot{\check{r}}_0(\check{t}) \equiv \check{v} \qquad \text{and} \qquad \dot{r}_0(t) \equiv v\,. \tag{3.91}$$

This assumption is strongly tied to the symmetry of a pure tension brane in an empty bulk. From the perspective of a brane observer, the source is maximally symmetric, and so is the brane geometry, i.e. $H =$ const. In other words, the three brane dimensions expand at a constant rate. Therefore, it is natural to assume the same to be true for the "rate" at which the brane moves through the bulk. That way, we will be able to derive an analytic solution of the 6D Einstein equations, which is properly matched to the brane. Moreover, by employing our numerics, we will demonstrate that this is indeed a stable solution—at least under 3D isotropic fluctuations—with a finite basin of attraction.

Using (3.91) to eliminate $\dot{\check{r}}_0$ and $\dot{r}_0$ in (3.36) yields

$$\check{\gamma} = \frac{3HR}{\check{v}}\,, \qquad\qquad \gamma = \frac{3HR}{v}\,. \tag{3.92}$$

Deriving an expression for v (and $\tilde{v}$) requires to solve the vacuum Einstein equations in the bulk. By using (3.16), the condition of having a constant brane velocity translates to a boundary condition on $\check{\alpha}$ and α,

$$\check{\alpha}_0 = \ln\left(\frac{\check{v}\check{t}}{R}\right) \qquad \text{and} \qquad \alpha_0 = \ln\left(\frac{vt}{R}\right)\,, \tag{3.93}$$

where we assumed for simplicity[28] that $(\check{r}_0)_i = (r_0)_i = 0$ at initial time $\check{t}_i = t_i = 0$. In other words, the desired bulk solution has to reduce to (3.93) at the brane. The crucial idea is now to look for scaling solutions that depend on r or $\check{r}$ only through the combination[29]

$$x := r/t \qquad \text{and} \qquad \check{x} := \check{r}/\check{t}\,. \tag{3.94}$$

With this new variable, the brane position corresponds to the constant value $x_0 = v$ (and

[28] This can always be achieved by a constant time rescaling $\check{t} \to \check{t} + \text{const}$.

[29] The scaling property implies that the shape of the solution is always the same, it gets simply "re-scaled" over time, comparable to a zoom-effect.

$\check{x}_0 = \check{v}$).

As already stated in [74], there is a unique scaling solution that fulfills the linear wave equation (3.30a), is regular at the axis and satisfies the above boundary condition at all times,

$$\alpha(t,r) = \frac{1}{3}\ln\left[\frac{t}{\Omega}\left(1+\sqrt{1-x^2}\right)\right], \tag{3.95}$$

with

$$\Omega := \frac{R}{v}\left(1+\sqrt{1-v^2}\right). \tag{3.96}$$

To find an expression for η, we can integrate the vacuum constraint equation (3.30b), yielding

$$\eta(t,r) = \frac{4}{3}\ln\left(\frac{1+\sqrt{1-x^2}}{2\sqrt{1-x^2}}\right) + \eta_a\,. \tag{3.97}$$

The complete scaling solution for the exterior region then reads

$$\begin{aligned}\mathrm{d}s^2_{(\mathrm{ext})} = \left[\frac{1+\sqrt{1-x^2}}{16\sqrt{1-x^2}}\right]^{2/3} &\frac{\mathrm{e}^{2\eta_a}\,\Omega^2}{t^2(1-x^2)}\left(-\mathrm{d}t^2+\mathrm{d}r^2\right)\\ &+\left[\frac{t}{\Omega}\left(1+\sqrt{1-x^2}\right)\right]^{2/3}\mathrm{d}\boldsymbol{x}^2+\left(\frac{\Omega\,x}{1+\sqrt{1-x^2}}\right)^2\mathrm{d}\phi^2\,,\end{aligned} \tag{3.98}$$

which is an exact vacuum solution of Einstein's equations (3.30). The corresponding interior line element $\mathrm{d}s^2_{(\mathrm{int})}$ as well as $\check{\alpha}$, $\check{\Omega}$ and $\check{\eta}$ are obtained by formally replacing $(t,x,v,\eta_a) \to (\check{t},\check{x},\check{v},0)$, where the regularity condition (3.31) was used. As for the coordinate ranges, $\check{r}$ and r run in the intervals $[0,\check{v}\check{t}]$ and $[0,vt]$, respectively, where $\check{t}$ and t are both positive real numbers. As mentioned before, in the exterior region, moving outwards (or away from the brane) corresponds to a decreasing value of r.

We can now evaluate (3.97) at the shell, use (3.29), (3.37) and (3.92) to finally obtain

$$\boxed{\frac{3HR}{\check{v}} = \mathrm{h}(\check{v})} \qquad \text{and} \qquad \boxed{\frac{3HR}{v} = \left(1-\bar{\lambda}_a\right)\mathrm{h}(v)}, \tag{3.99}$$

where

$$\mathrm{h}(v) := \left(1-v^2\right)^{\frac{1}{6}}\left(\frac{2}{1+\sqrt{1-v^2}}\right)^{\frac{4}{3}}. \tag{3.100}$$

Moreover, with (3.92) the (00) junction condition (3.39) reads

$$\boxed{\bar{\lambda} - \ell_2^2 H^2 = 3HR\left(\frac{1}{\check{v}} + \frac{1}{v}\right)}\,, \tag{3.101}$$

where $\sigma = -1$ was used due to the D^- character of the exterior space (cf. Sec. 3.2.1).[30] From the last equation we see that the whole dependence on the bulk geometry is mediated by the constant velocities v and $\check{v}$. The three boxed equations constitute a closed system of algebraic equations, which, for example, allow to determine $H\ell_2$, $\check{v}$ and v as a function of HR, $\bar{\lambda}$ and $\bar{\lambda}_a$.[31]

For later convenience, we also provide an expression for the angular pressure that is needed to stabilize the compact brane dimension. To that end, we further evaluate ξ and χ, defined in (3.43b), by using (3.92) and the scaling solution (3.95),

$$\xi = \frac{1}{3}\frac{v^2}{v^2 - 1 - \sqrt{1-v^2}} \qquad \text{and} \qquad \chi = \frac{v^2}{9}\,, \tag{3.102}$$

where as usual $\check{\xi}$ and $\check{\chi}$ are obtained by formally replacing $v \to \check{v}$. Moreover, 4D maximal symmetry implies $\mathrm{d}H/\mathrm{d}\tau = 0$. With these relations the angular pressure (3.44) can be simplified to

$$\bar{p}_\phi = -2H^2\ell_2^2 - 4HR\left(\frac{1-\sqrt{1-v^2}}{v} + \frac{1-\sqrt{1-\check{v}^2}}{\check{v}}\right)\,. \tag{3.103}$$

A first important observation is that $p_\phi \leq 0$, where the bound is saturated for $HR = 0$, i.e. the fully static solution, in accordance with (3.48) (for $c = 0$). This raises the question whether such a pressure can be realized in terms of physical matter. We will answer that question in the affirmative in Sec. 3.5.4.

Before explicitly solving the algebraic system (3.99) and (3.101), let us pause for a moment to discuss some properties of the scaling solution. First, it describes a compact extra-dimensional space. To be specific, we see from the last term in (3.98) that the circumference of the extra space shrinks monotonically when we move away from the brane, until it eventually vanishes at the exterior axis (at $r = x = 0$). Second, $\eta(t,r)|_{r=0} \equiv \eta_a$, which, in general, is non-vanishing. Physically, this term corresponds to a conical singularity and has to be interpreted as the presence of a second brane with tension (3.29), situated at the exterior axis . Further details on the geometry will be discussed in Chap. 4, where the line element (3.98) will be expressed in terms of co-moving coordinates.

[30] For convenience, we introduced again the dimensionless tension parameters $\bar{\lambda} := \lambda/(2\pi M_6^4)$ and $\bar{\lambda}_a := \lambda_a/(2\pi M_6^4)$.

[31] There is a degeneracy because a rescaling of H can always be compensated by a simultaneous rescaling of R and ℓ_2 without changing $\check{v}$ and v.

3.5.2 On-brane curvature

In the part to follow, we investigate different solutions of this system, where we put special focus on deriving the 4D curvature on the brane. To keep the discussion generic, it is useful to absorb the induced gravity term in a re-definition of $\bar{\lambda}$,

$$\bar{\lambda}_{\text{eff}} = \bar{\lambda} - \ell_2^2 H^2 \,, \tag{3.104}$$

and to keep in mind its H dependence (this definition is in accordance with (3.22) for $w = -1$).

A straightforward analysis of the first equation in (3.99) shows that it admits a real solution if (and only if) $HR \leq 2^{4/3}/(\sqrt{3}\,5^{5/6}) \sim 0.38$. As we are interested in the regime $HR \ll 1$, this is no relevant limitation. In general, there are two branches,[32]

$$\check{v}_I = 1 - \mathcal{O}\left[(HR)^6\right] \qquad \text{(branch I)}\,, \tag{3.105a}$$

$$\check{v}_{II} = 3HR\left(1 + \mathcal{O}\left[(HR)^2\right]\right) \qquad \text{(branch II)}\,, \tag{3.105b}$$

where one is close to the speed of light and another one suppressed by HR.[33] Their correctness can be checked by expanding $\mathrm{h}(\check{v})$ in (3.99) according to

$$\mathrm{h}(v) = \begin{cases} 1 + \mathcal{O}(v^2) & (\text{for } v \ll 1) \\ 2\sqrt{2}\,(1-v)^{1/6} + \mathcal{O}\left[(1-v)^{2/3}\right] & (\text{for } (1-v) \ll 1) \end{cases} . \tag{3.106}$$

In the next step, we use (3.101) to rewrite the second equation in (3.99) as

$$\frac{\bar{\lambda}_{\text{eff}} - b_{\text{I/II}}}{1 - \bar{\lambda}_a} = h(v)\Big|_{v = 3HR/(\bar{\lambda}_{\text{eff}} - b_{\text{I/II}})}\,, \tag{3.107}$$

where $b_{\text{I/II}} := 3HR/\check{v}_{\text{I/II}}$ ($\equiv \check{\gamma}_{\text{I/II}}$). This equation relates $\bar{\lambda}_a$ to $(\bar{\lambda}_{\text{eff}} - b_{\text{I/II}})$ and is plotted in Fig. 3.14 for different values of HR. The important observation is that in the limit $HR \to 0$ the function approaches a piecewise linear curve (dashed). While for the first segment $\bar{\lambda}_{\text{eff}}$ is independent of λ_a, there is a linear dependence for the second segment. The two segments correspond to two different scaling solutions. Hence, there is an additional splitting of the solution space into two further branches, which makes a total of four branches (given the previously defined branches I and II). The corresponding parameter relations can be read

[32] Here the minus sign indicates that $\check{v}_I$ is strictly smaller than one as long as $HR > 0$.
[33] By plotting the function $\check{v}\,\mathrm{h}(\check{v})$, it becomes obvious that these two are the only solutions.

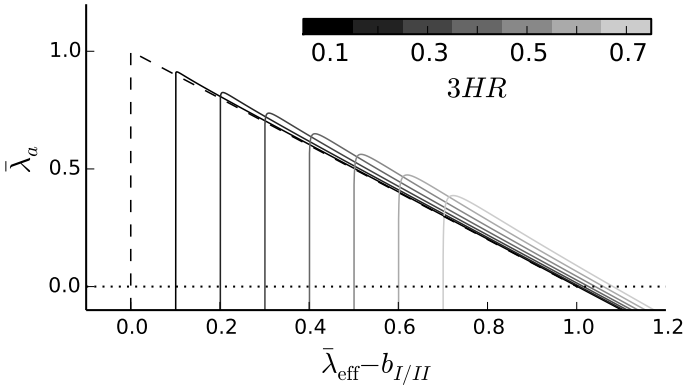

Figure 3.14: $\bar{\lambda}_a$ as a function of $(\bar{\lambda}_{\text{eff}} - b_{\text{I/II}})$. For $HR \to 0$ a piecewise linear curve (dashed) is approached. Each triple $(HR, \bar{\lambda}_{\text{eff}}, \bar{\lambda}_a)$ corresponds to a specific scaling solution.

off from the plot,[34]

$$\bar{\lambda}_{\text{eff}} + \bar{\lambda}_a - b_{\text{I/II}} - 1 = \mathcal{O}\left[(HR)^2\right] \qquad (\text{branch } \text{A}_{\text{I/II}}) \,, \tag{3.108a}$$

$$\bar{\lambda}_{\text{eff}} - b_{\text{I/II}} - 3HR = \mathcal{O}\left[(HR)^7\right] \qquad (\text{branch } \text{B}_{\text{I/II}}) \,. \tag{3.108b}$$

Alternatively, this can be verified by using the expansion (3.106) to rewrite (3.107) in both regimes. From the plot it is also obvious that there exists a maximal possible tension at the second axis; a short calculation yields $\bar{\lambda}_a \lesssim (1 - 2.62HR)$ (which is still compatible with having $\bar{\lambda}_a = 0$ for all admissible values of HR).

In order to obtain a better physical understanding of the branches I and II, it is instructive to derive their respective (interior) extra space volume as defined in (3.78). After substituting $\check{x} = \check{r}/\check{t}$ and expanding the integrand for small values of x, we find

$$\begin{aligned} V_{\text{int}} :&= 2\pi\, t^2 \int_0^{\check{v}} \mathrm{d}\check{x}\, \check{x}\, \mathrm{e}^{-6\check{\alpha}+\check{\eta}} \\ &\to \pi R^2 \quad (\text{for} \quad \check{v} \to 0) \,. \end{aligned} \tag{3.109}$$

This shows that for $\check{v} \ll 1$ the interior volume is arbitrarily close to its Minkowski value (whereas it approaches a different value for $v \to 1$). By a short inspection of (3.105), we see that this limit can indeed be realized for branch II by taking $HR \to 0$. For branch I, on the contrary, $v \to 1$, hence V_{int} does not approach its flat space value. This is opposed to the spirit of considering a regularized thin brane. Therefore, we will limit our discussion to branch II.

[34] Note that branch $\text{B}_{\text{I/II}}$ without BIG term coincides (up to numerical factors of order one) with the super-critical solution found in [64] by studying a (thick) domain wall localized on a codimension-one brane.

Moreover, by numerically integrating (3.109) for different values of t (and $\check{v}$), we find that V_{int} is time independent (and finite for $\check{v} < 1$), which demonstrates the stability (and consistency) of our regularization scheme.[35] In other words, there is no singular behavior of the interior volume, which might question our physical conclusions about the brane curvature. We will provide a more extensive discussion of the volume in Sec. 4.2.

Let us now derive an expression for H solely in terms of model parameters; after all, this is exactly what we are looking for. By making the dependence of $\bar{\lambda}_{\text{eff}}$ on H explicit again and substituting b_{II}, the two equations in (3.108) read

$$H^2 = \frac{\lambda + \lambda_a - 4\pi M_6^4}{3M_{\text{Pl}}^2} + \mathcal{O}(HR) \qquad (\text{branch } \text{A}_{\text{II}}) \,, \tag{3.110a}$$

$$H^2 = \frac{\lambda - 2\pi M_6^4}{3M_{\text{Pl}}^2} + \mathcal{O}(HR) \qquad (\text{branch } \text{B}_{\text{II}}) \,, \tag{3.110b}$$

where we used the definition (3.40) for ℓ_2. These two parameter relations are the central result of the super-critical analysis. We make the following observations:

- The $\mathcal{O}(HR)$ contributions result from the ring regularization. In our low energy EFT they can be safely neglected. Moreover, we expect their precise value to be regularization dependent.

- The standard 4D Friedmann equation can be restored through a simple tension shift, viz. $\lambda \to \lambda + 2\pi M_6^4$ and $\lambda \to \lambda + 4\pi M_6^4 - \lambda_a$, respectively. Thus, both solutions sill have the potential of being phenomenologically viable.

- From a 4D point of view the CC gets reduced by a constant amount ($4\pi M_6^4 - \lambda_a$ for A_{II} or $2\pi M_6^4$ for B_{II}). This corresponds to a (trivial) form of degravitation. It is clear that this will not avoid the naturalness problem because the shifted value of the CC still needs to be tuned with the same precision as before.

- Branch A_{II} consistently reproduces the static solution (1.14) in the limit $H \to 0$. In that case, according to (3.110), a parameter constraint on both tensions, $\bar{\lambda} + \bar{\lambda}_a = 2$, follows. In reverse, a violation implies a non-vanishing H determined by (3.110a).

- For branch B_{II}, the Hubble expansion has no knowledge about the sub-critical tension at the exterior axis λ_a. The physical reason is that, from the exterior perspective, the brane moves almost with the speed of light ($v \approx 1$). A change in the value of λ_a could therefore hardly be communicated to the brane by means of ER waves.

[35] This does not come as a surprise because we will show in Sec. 4.2 that the time dependence of $\check{\alpha}$ is a mere coordinate artifact.

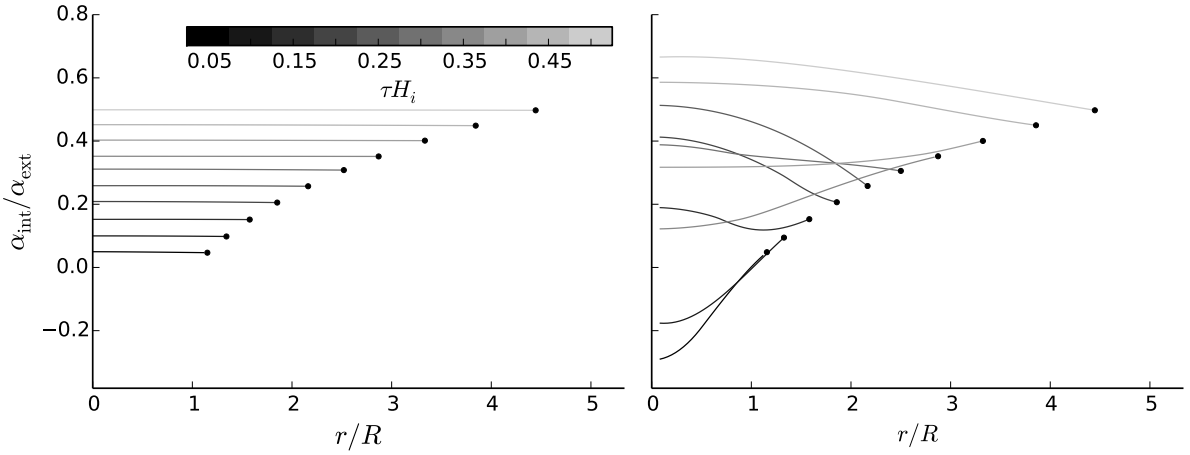

Figure 3.15: Radial profile of $\check{\alpha}$ ($\equiv \alpha_{\rm int}$; left) and α ($\equiv \alpha_{\rm ext}$; right) at different times, parameters defined in (3.111). The interior profiles are close to the (almost flat) scaling prediction. The exterior profiles are dominated by ER waves, washed out successively. The dots indicate the position of the brane.

3.5.3 Numerical results

The aim of this section is to provide numerical evidence that the scaling solutions (3.110) are attractors, i.e. solutions which are approached for different values of H_i. To that end, we make use of our numerical implementation presented in Sec. 3.3. The main difference to the sub-critical case is the occurrence of a a second brane (at $r = 0$) with constant tension λ_a. On a technical level, the value of λ_a can be adapted by deforming the initial profile for $\partial_t\alpha$. As discussed in Sec. 3.3.1, this is most easily achieved by making a quadratic ansatz for the profile function $P_d(r)$. In our numerics, we will use d as a dial to achieve the desired value of λ_a according to (3.66).[36]

While we were very careful about the regularization dependence of our results in the sub-critical case, we now limit the presentation of the numerical results to those obtained in the dynamical regularization, keeping in mind that other regularizations yield the same result up to $\mathcal{O}(HR)$ corrections. In accordance to the sub-critical case, we choose a flat initial profile for $\partial_{\check{t}}\check{\alpha}$ [cf. Sec. 3.3.1]. Like in the analytic discussion, we only consider a (super-critical) tension. The discussion of other types of matter is left for future work. As an example, let us consider parameters,[37]

$$H_i\ell_2 = 1\,, \qquad H_iR = \frac{1}{20}\,, \qquad \bar{\lambda} = \frac{5}{2}\,, \qquad \bar{\lambda}_a = \frac{1}{4}\,, \tag{3.111}$$

[36]The numerical implementation requires also adaption: The main difference is that the exterior domain of integration is now bounded by the second axis. Thus, the appropriate boundary conditions on α, specified in (3.32) have to be imposed there.

[37]For completeness, the step size for integration is $\check{\epsilon} = R/100$ and $\epsilon = R/150$ in the interior and exterior, respectively.

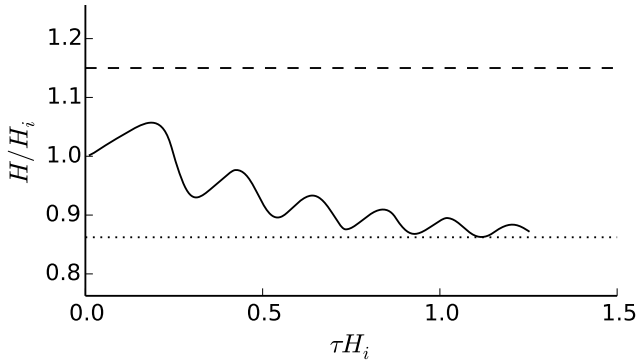

Figure 3.16: The Hubble parameter approaches the A_{II} value (dotted line), instead of the B_{II} value (dashed line). The oscillations correspond to ER waves propagating between the two branes. Parameters as defined in (3.111).

which corresponds to a super-critical (regularized) brane at $r = r_0$ and a second, sub-critical one at $r = 0$. The characteristic scale ℓ_2 is of the size of the initial Hubble parameter.[38]

So far we did not use our knowledge about the scaling solutions. Accordingly, the quadratic initial profile in the exterior is completely different to the logarithmic r-dependence of (3.95) and in that sense an arbitrary choice. The resulting evolution of $\check{\alpha}$ and α is depicted in Fig. 3.15. While the interior profiles are almost flat (and thus very close to the scaling prediction), the exterior ones are dominated by the presence of ER waves propagating between the brane and the second axis (at $r = 0$). This has to be understood as a result of the somewhat extreme initial velocity profile in the exterior. However, as the figure shows emphatically, the wave amplitude gets smaller in time and α hence settles to a somewhat flatter configuration. In fact, we will show that it approaches the scaling solution described by (3.98).

With this—at least initially—strongly perturbed exterior α-profile, we can test the attractor properties of both scaling solutions. To be specific, we solve the algebraic system consisting of (3.99) and (3.101) for the above parameter choice and, depending on the branch, obtain

$$H/H_i \approx 0.86\,, \qquad v \approx 0.17\,, \qquad \check{v} \approx 0.13 \qquad (\text{branch } A_{II})\,, \tag{3.112a}$$

$$H/H_i \approx 1.15\,, \qquad v \approx 1\,, \qquad \check{v} \approx 0.17 \qquad (\text{branch } B_{II})\,. \tag{3.112b}$$

Both values for H are depicted in Fig. 3.16 as the dotted and the dashed line, respectively. Therefore, we see that the scaling solution A_{II} is approached and hence stable under FLRW fluctuations. On the other hand, the B_{II} branch was not approached. While we confirmed this behavior for different parameter choices, we lack a final statement about the B_{II} branch. In particular, choosing a different initial profile closer to the scaling prediction might still reveal a finite attractor region for B_{II}. Let us stress though that the purpose of

[38]Note that this choice leads to an instability in the sub-critical case (cf. Sec. 3.4.1.2).

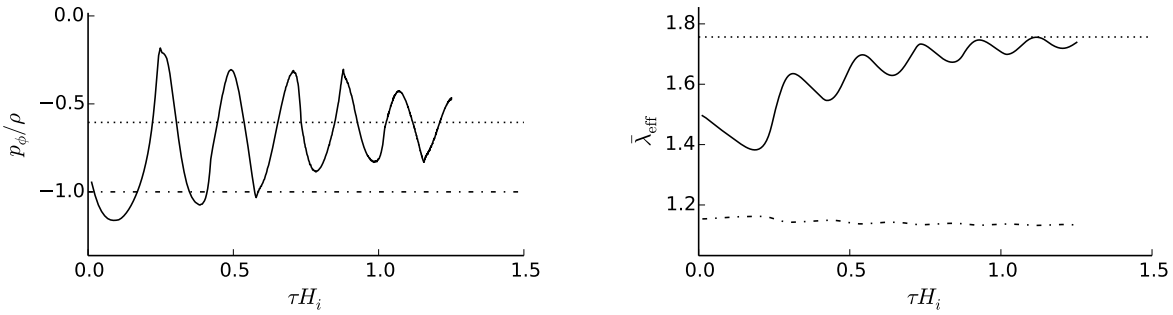

(a) The equation of state of p_ϕ needed to keep the brane circumference fixed approaches a value above -1.

(b) The effective energy density is always above the super-critical bound (dashed-dotted line).

Figure 3.17: Physical consistency checks for parameters (3.111). The dotted lines depict the value inferred from the scaling branch $\mathrm{A_{II}}$.

this numerical analysis was to show that at least one of the two scaling branches is stable in a certain parameter regime and thus physically interesting. A complete investigation of the whole parameter space for different initial profiles and parameters is left for future work. Accordingly, we focus our discussion on the (numerically verified) branch $\mathrm{A_{II}}$ with parameters (3.111).

Finally, we perform two consistency checks. First, we investigate whether the brane/ring can be stabilized by means of physical matter. The answer is given in Fig. 3.17a, where it is shown that the equation of state for p_ϕ is always above -1. Moreover, the dotted line is obtained from (3.103) by inserting the scaling values (3.112). Within the probed time interval, our numerical solution is fully compatible with this analytic prediction. Second, we depict the effective energy density $\bar{\lambda}_{\rm eff}$ as it is "seen" by 6D GR. The important (and nontrivial) observation is its positivity, otherwise the NEC would be violated indicating the emergence of (unwanted) ghost degrees of freedom. Moreover, it always satisfies the bound (3.27) (plotted as the dashed-dotted line), which is required to be in a super-critical regime.[39] To conclude, we showed for a generic choice of model parameters that the $\mathrm{A_{II}}$ branch is approached dynamically. This strongly suggests that this class of solutions is stable under FLRW fluctuations (although a complete scan of the parameter space is still missing) and thus of potential phenomenological interest.

3.5.4 Parameter space

Within the scaling class, we derive different bounds on $\bar{\lambda}$ that ensure the theoretical consistency of the system. This in turn narrows down the relevant region in parameter space that should be considered when looking for phenomenologically interesting solutions. In

[39] The bound depends on H and hence varies throughout the evolution. The physical reason is that the gravitational energy related to the Hubble expansion on the brane also contributes to the deficit angle.

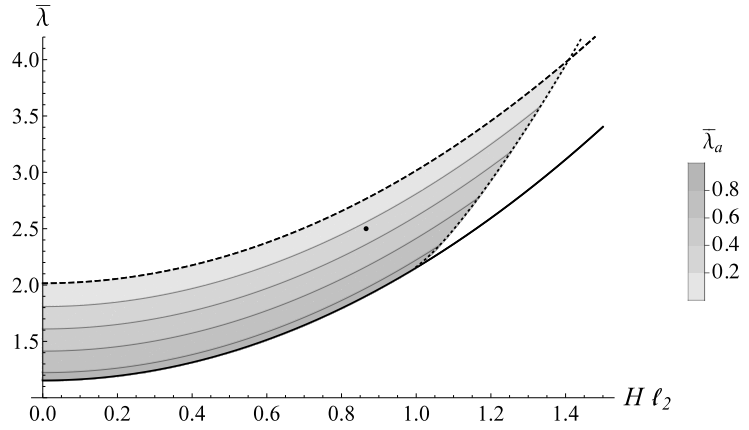

Figure 3.18: Super-critical parameter plot for $HR = 0.05$. Each point within the shaded region corresponds to a unique $\mathrm{A_{II}}$ solution with $\lambda_a \geq 0$ and a consistently stabilized compact brane dimension. The solutions of type $\mathrm{B_{II}}$ are all close to the lower border (solid line). The black dot is the attractor for the initial configuration (3.111).

fact, there are three bounds, which are all depicted in Fig. 3.18, defining a consistent super-critical parameter regime (shaded region). From (3.99) and (3.101) it is clear that for fixed $H\ell_2$, HR and $\bar{\lambda}$ the scaling solution is uniquely determined (up to the choice of branch). Therefore, each point within the shaded region corresponds to a single, theoretically consistent scaling solution. Let us now discuss the three bounds in turn:

1. The super-critical bound (3.27) defines the solid line (demarcating the critical from the super-critical region), it simplifies to

$$\bar{\lambda} \geq H^2\ell_2^2 + 3HR + \check{\gamma}_{\mathrm{II}}\,, \tag{3.113}$$

   where $\check{\gamma}_{\mathrm{II}} \equiv 3HR/\check{v}_{\mathrm{II}} = 1 + \mathcal{O}\left[(HR)^2\right]$ due to (3.105). Under the assumption $v < 1$ (a massive brane cannot propagate with the speed of light or even faster) and by using (3.101), it can be shown that the bound is always fulfilled for scaling solutions.

2. We exclude the possibility of having a negative tension of the second brane,[40] explicitly we demand $\bar{\lambda}_a \geq 0$. For branch $\mathrm{A_{II}}$, this translates via (3.99) and (3.101) to the upper bound

$$\begin{aligned} \bar{\lambda} &\leq H^2\ell_2^2 + 2\check{\gamma}_{\mathrm{II}} \\ &= H^2\ell_2^2 + 2 + \mathcal{O}\left[(HR)^2\right] \end{aligned} \tag{3.114}$$

   where the second line follows from (3.105). It is depicted by the dashed line. If the bound is saturated, the exterior axis is regular, i.e. the conical singularity vanishes,

[40] Negative tension branes are believed to cause unacceptable instabilities [124].

and the system consists of a single (super-critical) brane. Each point in the shaded region corresponds to a certain value of λ_a (determined by the second equation in (3.99) and indicated by the contour lines). $\bar{\lambda}_a$ decreases towards larger values of $\bar{\lambda}$ until it eventually becomes zero when $\bar{\lambda}$ hits the upper bound (3.114). As an aside, we also find that $\bar{\lambda}_a < 1$, irrespective of λ. In other words, the second brane is always sub-critical.

On the other hand, the discussion does not apply to the $\mathrm{B_{II}}$ branch, which is almost insensitive to λ_a. To be precise, by using (3.108b), we see that solutions of type $\mathrm{B_{II}}$ satisfy the bound (3.113) up to small corrections of order $\mathcal{O}\left[(HR)^7\right]$. As a result, irrespective of the value of λ_a, these solutions are confined to an extremely small band of width $\sim HR/10$ at the bottom of the shaded region in Fig. 3.18 (and hence are completely covered by the thickness of the solid line).[41]

3. We demand the stabilization of the compact brane dimensions to be physically consistent. In other words, the equation of state for the angular pressure has to fulfill

$$p_\phi/\rho \equiv p_\phi/\lambda \geq -1\,. \tag{3.115}$$

The bound is saturated on the dotted line in parameter space. It was inferred from (3.101) and (3.103) numerically. Effectively, it limits the shaded region to the right. Analytically, we derive

$$H\ell_2 \leq 1 + \mathcal{O}(HR) \tag{3.116}$$

as a sufficient condition for having a working stabilization.

We have seen that the requirement of having a second brane with positive tension together with a consistently stabilized compact brane dimension leads to a finite region in parameter space. In the case of the $\mathrm{A_{II}}$ branch, it is given by the shaded region in Fig. 3.18; correspondingly, $\bar{\lambda}_a$ decreases when $\bar{\lambda}$ is increased, in accordance with (3.110a). On the other hand, as follows from (3.110b), solutions of type $\mathrm{B_{II}}$ depend on $\bar{\lambda}_a$ only weakly. As a consequence, these solutions are represented by a very small stripe above the super-criticality line.

3.5.5 Phenomenology

Here, we briefly comment on the phenomenological prospects of the scaling solutions. In that context, the crucial question is whether the model admits a consistent 4D regime on observationally relevant scales. In fact, there are two logical possibilities (that are independently realized by the two branches):

[41] We conjecture that this is the reason why these solutions have a much smaller attractor regime (if approached at all).

1. If the extra space volume, set by the scale L_B, is of order R (which holds true for the branch $A_{\rm II}$, cf. Sec. 4.2), the EFT requirement $HR \ll 1$ implies that we are always in a 4D regime irrespective of the scale r_c, which thus remains rather unconstrained.[42] The reason is that even if the bulk gravity term dominates, it yields a 4D regime due to the microscopically small compactification scale L_B (as follows from dimensional reduction, cf. Sec. 1.5). In that case, the phenomenological prospects are obviously good as we could always choose r_c (and hence ℓ_2) such that we are within the consistent regime in Fig. 3.18.[43]

2. If there is a large hierarchy $L_B \gtrsim r_c \gg R$ (which can be realized for the branch $B_{\rm II}$, cf. Sec. 4.2), we encounter the crossover behavior typical for the BIG construction. In that case, we have to ask whether (3.116) is compatible with having a working 4D regime, i.e. with $Hr_c \gg 1$. We can use the upper bound on r_c derived in the sub-critical analysis in Chap. 2 as a proxy in order to arrive at a first (and somewhat naive) assessment. To be specific, we found in (2.129) that $r_c = \nu\ell_2^2/(3R)$ with $\nu < 1$.[44] This in turn allows us to rewrite (3.116) as

$$Hr_c < \frac{\nu}{3HR}\,, \tag{3.117}$$

   which is compatible with having a 4D regime provided $\nu/HR \gg 1$. In fact, for $\nu \sim 1$ this is trivially fulfilled because it simply translates to the requirement that the hierarchy between the Hubble length and the microscopic scale R is huge. Of course, this only shows that there is the possibility of having a working 4D regime (after all, ν could be much smaller than 1).

To settle these phenomenological questions more rigorously, it is not sufficient to solely consider a pure tension brane but other matter components have to be taken into account, too. Only that way, a standard 4D evolution of H can be identified. Alternatively, a linear super-critical analysis could be performed, similar to the sub-critical one in Chap. 2, to derive an expression for the crossover scale. Although we do not see any principle obstacles, we leave this—probably tedious—analysis for future work. After all, we have seen that both scaling solutions are not able to address the CC problem.

3.6 Discussion

We conclude this chapter by giving a short summary of all solutions considered so far. To that end, we provide in Fig. 3.19 a parameter plot which combines our results for the full range of $\bar{\lambda}$ (including the sub-critical and the super-critical regime). Let us discuss the

[42] Here, r_c is defined as the scale above which the bulk gravity term starts to dominate (compared to the BIG term).

[43] So far it is not clear whether a microscopically small extra space would lead to other phenomenological problems.

[44] The precise value of ν in the sub-critical case depends on the tension as well as ℓ_2.

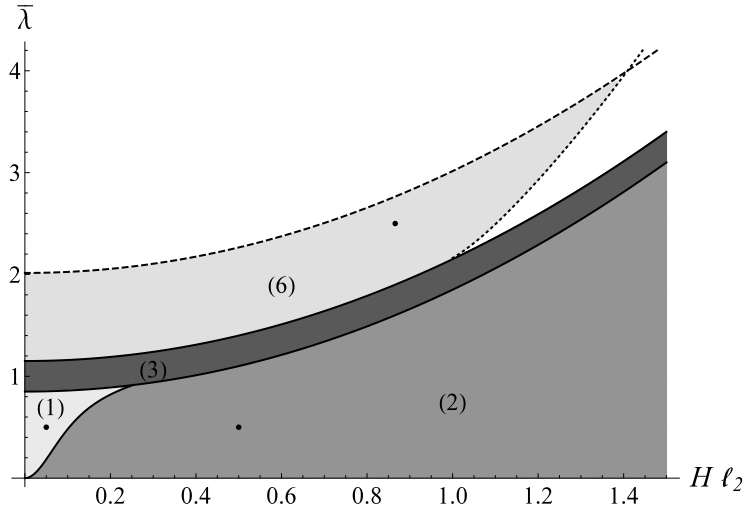

Figure 3.19: Comprehensive parameter plot for $HR = 0.05$. Each region corresponds to a certain class of solutions: (1) degravitating solutions, (2) super-accelerating solutions, (3) critical solutions, (6) (compact) scaling solutions. Above the dashed line $\bar{\lambda}_a$ becomes negative. Beyond the dotted line the compact brane dimension can no longer be stabilized. The black dots correspond to our numerical examples.

different solutions in turn:

1. *Degravitating solutions (1):* For $(H\ell_2)^2 < 3\,|H|\,R/2$ and a large enough (sub-critical) tension, we find stable solutions approaching the static deficit angle geometry. This constitutes an example of dynamical degravitation: Independent of its precise value, the gravitational impact of λ is absorbed into a conical bulk geometry, invisible to a brane observer. In other words, changes in λ are accounted for by a change in the deficit angle, mediated by ER waves. Albeit conceptually interesting, these solutions are not compatible with having a 4D regime, which would be required to reproduce the success of 4D GR in describing the expansion history of our universe. More precisely, a necessary condition for stability is $Hr_c < 1$, whereas a 4D regime would require $Hr_c \gg 1$.

2. *Super-accelerating solutions (2):* For $(H\ell_2)^2 > 3\,|H|\,R/2$ or too small values of the (sub-critical) tension, the solution develops a pathological behavior: Hubble grows unbounded, the effective 6D energy density becomes negative and the compact brane dimension can no longer be stabilized (at least not by physical matter). We dismiss these solutions as being physically inconsistent. We also showed that the instability can be traced back to a ghost mode that was revealed in the linear analysis in Chap. 2. This is similar to the self-accelerating branch of the DGP model which also suffers from a ghost instability.

3. *Critical solutions (3):* Within this regime, the ER coordinate $\hat{r}$, as defined in (3.10),

becomes time-like. We did not further investigate this regime. The reason is that it degenerates to a single line in parameter space in the (physically relevant) limit $HR \to 0$. Realizing a critical solution would therefore require an a priori tuning of the value of λ, which is considered unacceptable with regard to our purposes.

4. *Scaling solutions (4):* For a super-critical value of the tension, the extra space compactifies and thus closes in a second axis with tension λ_a. By solving the full bulk-brane system analytically, we were able to derive two types of scaling solutions that correspond to a constant expansion rate $H \neq 0$. The requirement of $\lambda_a > 0$ (dashed line) and a consistent ring stabilization (dotted line) leaves a finite window in parameter space that might still be phenomenologically viable. We did not further pursue that direction because these solutions cannot help with the CC problem: Although they lead to a certain amount of constant (and hence trivial) degravitation, they do not provide a dynamical mechanism which would be needed to adapt to changes in the vacuum energy throughout the cosmic evolution. As a result, the original tuning problem persists within this class of solutions.

Finally, let us comment on future prospects of the model.

First, as already mentioned, it still might be interesting to explore the phenomenological potential of the scaling solutions. In general, the super-critical 6D BIG model might provide an interesting playground for consistent modifications of 4D GR. As a first step, an analysis of other types of matter (including radiation and dust) would be in order to further identify (and constrain) the modified regime. After all, in the case of a pure tension source, the modification was simply given by a constant shift.

A second direction of future research is provided by higher-codimensional generalizations with $n > 2$. Following the reasoning of Chap. 2, we conjecture that these models are free of any ghost instabilities as long as a large enough brane tension is included. We can use dimensional reasoning to derive a first guess for a modified Friedmann equation:[45]

$$\lambda - 3M_{\rm Pl}^2 H^2 = N \times M_D^{2+n} H^{2-n} \quad (n = \text{no. of codimensions})\,, \tag{3.118}$$

where N is an order one coefficient. For $n = 1$, the equation correctly reproduces the two branches of the DGP model (cf. Eq. (3.1) for $\mathcal{C} = 0$ and identify $N \equiv \pm 6$). With regard to this thesis, the case $n = 2$ is of particular interest and indeed matches both scaling relations (3.110), derived in the super-critical case (we identify $N \equiv 4\pi$ and set $\lambda_a = 0$ for branch $\mathrm{A_{II}}$ and $N \equiv 2\pi$ for branch $\mathrm{B_{II}}$). We consider this agreement a clear indication for the correctness of (3.118).

It is now instructive to explore $n \geq 3$. In that case, a rigorous derivation of the above equation is still missing. However, there is a clear indication for the existence of a solution with $H \neq 0$: In [89] it was shown that the assumption $H = 0$ leads to a naked singularity in the bulk provided $n \geq 3$. This can be understood as an artifact of over-constraining the system; accordingly, the pathology can be cured by allowing $H \neq 0$. Of course, this

[45] This form was first proposed, yet not rigorously proven, in [66] for $n > 2$.

reasoning is not sufficient to derive (3.118); in the best case, we can use the equation as a proxy to infer the potential of higher-dimensional constructions. To be precise, it admits approximate solutions with $H^{n-2} \propto 1/\lambda$ (for a sufficiently large λ the $M_{\rm Pl}^2 H^2$ term can be neglected for this class of solutions), offering thus an efficient way of creating a small curvature from a large tension [66]. We consider this an exciting opportunity for finding technically natural and viable cosmologies. To prove (3.118) though, an explicit solution is needed. We are confident that by applying our solving techniques, it will be possible to finally settle the potential of BIG models as solutions to the CC problem.

Chapter 4

LED: Extra space as a cigar

Note: This chapter is inspired by a publication together with Robert Schneider [132], where a super-critical cosmic string in 4D is investigated. Here, the ideas are generalized to 6D and a similar but new class of solutions (so far unpublished) is discovered and studied.

In six-dimensional GR, a three-brane with tension λ is known to produce a static, locally flat bulk with a wedge removed, corresponding to the direct generalization of the cosmic string geometry in 4D [166, 88, 96].[1] If λ exceeds the critical value $2\pi M_6^4$, the exterior becomes compact, ending in a second brane with tension λ_a. Explicit solutions were solely known in the static case for which $\lambda_a \equiv 4\pi M_6^4 - \lambda$, cf. Eq. (3.90) and [115, 140, 22]. In other words, both tensions have to fulfill a parameter constraint, which implies that the static solution cannot solve the CC problem. It is then obvious to ask what happens if the constraint is violated. A first answer was given in Chap. 3 for the super-critical BIG model as well as in [64] in the case of a domain wall localized on a DGP brane:[2] The brane (or domain wall) geometry is no longer static but expands at a constant rate H. We were able to derive a new class of 4D maximally symmetric solutions that exactly solve the bulk-brane system and lead to a compact extra space. While we studied these scaling solutions as potential vacua of the BIG model, they are also interesting in their own right. The reason is that, as a result of the compactness of the extra space, they offer a natural mechanism to restore 4D GR in a certain regime. In other words, we do not have to rely on the existence of an induced gravity term to recover a 4D Newtonian scaling law.[3] We are thus interested in a particular realization of the ADD model [13, 9, 14] as introduced in Sec. 1.5. Assuming the bulk size is set by the scale L_B, the gravitational potential then shows 4D behavior for distances $\gg L_B$ while it gets modified on length scales close to

[1] There is also a second solution, normally referred to as "Kasner" or "Melvin" branch [111, 45]. Due to its unphysical properties, demonstrated in Sec. 3.2.5, we will not further discuss it.

[2] Another indication is provided by a cosmic string in 4D. Here, it was found that the axial and transverse string directions expand once the tension exceeds $\sim 1.6 \times 2\pi M_{\rm Pl}^2$. This was shown by numerically solving the (super-critical) Nielsen-Olesen vortex [44, 48].

[3] Of course, from an EFT point of view, the BIG term is unavoidable. However, the crucial point is that in the BIG model, the induced gravity term is a necessary ingredient to create a 4D gravity regime, which in turn demands that the coefficient $M_{\rm Pl}$ in (2.1) is phenomenologically large. Here, we assume that it is set by the bulk gravity scale, and hence, compared to the tension term, relatively suppressed by a factor $1/M_6^2$; thus, we can simply neglect it.

(or below) L_B due to the presence of massive KK modes (in accordance with Eq. (1.27) in the introductory discussion of Sec. 1.5). To be specific, post-Cavendish experiments allow the extra space to be as large as $L_B \sim 100\,\mu$m. The aim of this chapter is to study the phenomenological potential of the compact, super-critical setup, termed *cigar model*, without the presence of an induced gravity term.

First, we will see that the extra space volume (set by the scale L_B) and the transverse size of the super-critical brane (set by the scale R) are closely related. In fact, for a generic choice of model parameters, both scales are of the same order.[4] This is not surprising since the brane, which we again describe as a ring of circumference $2\pi R$, defines a slice of the bulk cigar exactly at the point where it is thickest.[5] However, due to the braneworld paradigm, the SM should be confined on a microscopically thin brane, set by the TeV scale, instead of the 10 meV [$\sim 1/(100\mu\text{m})$] scale; otherwise, we would expect to see the effect of the extra space in collider experiments. To circumvent that problem, we use the sub-critical brane (at the other end of the bulk) to host the SM fields.[6] That second brane can be microscopically thin and we do not need to worry about observable consequences of R being close to the millimeter scale. To put it differently, the only purpose of the super-critical brane consists in compactifying the extra space.

The action reads

$$\mathcal{S} = \mathcal{S}^{(6)}_{\text{EH}}[\boldsymbol{g}_6] + \int\limits_{\mathcal{M}_4\times\mathcal{S}_1} \mathrm{d}^5\tilde{x}\,\sqrt{-\tilde{g}}\left[-\tilde{\lambda} + \mathcal{L}_{\text{stab}}\right] + \int\limits_{\mathcal{M}_4} \mathrm{d}^4x\,\sqrt{-g}\left[-\lambda_a + \mathcal{L}_{\text{m}}\right]\,, \tag{4.1}$$

where the first term is the 6D Einstein-Hilbert action defined in (C1) for $D = 6$. The 5D integral describes the super-critical brane (with compact dimension of size $2\pi R$); correspondingly, $\lambda \equiv 2\pi R\tilde{\lambda} > 2\pi M_6^4$, where M_6 as usual denotes the bulk gravity scale. $\mathcal{L}_{\text{stab}}$ represents a sector that stabilizes the compact brane dimension; effectively it leads to a (localized) pressure p_ϕ in angular direction. A possible microscopic realization was discussed in Sec. 2.4.3 [cf. Eq. (2.118)]. The 4D integral stands for the second sub-critical brane with tension $\lambda_a < 2\pi M_6^4$ and additional localized matter fields. Since we limit the discussion to a pure tension brane, which only implies a conical singularity, we do not need to regularize it. Let us summarize the main characteristics of the model, thereby discriminating it from the BIG proposal:

- A super-critical brane (with additional ring dimension of size $2\pi R$) deforms the bulk into a cigar. Then, a 4D regime is realized due to the compactness of the extra space (as opposed to an induced gravity term on the brane).
- The SM matter fields are assumed to be situated at a second sub-critical bane of microscopic width. In fact, we will describe it as a delta defect of vanishing thickness.

[4] It should be stressed though that by tuning the model parameters an arbitrary hierarchy between R and L_B can be realized.

[5] The spacetime is visualized by its embedding diagram in Fig. 4.2.

[6] Alternatively, we could demand the extra space to be microscopically small. However, then we would leave the class of LED models that we intend to study here.

This is the main difference to the super-critical BIG setup discussed before, where the SM is assumed to be confined on the super-critical brane (which then demands an a priori tuning to realize a sufficiently large hierarchy $R \ll L_B$).

- In contrast to the BIG model, the cigar setup constitutes a UV modification of GR. Correspondingly, the theory enters a 6D regime at small distances below $L_B \sim 100\,\mu$m. On the other hand, in the BIG case the modification kicks in at large distances r_c (a phenomenologically motivated choice would be $\sim 1/H_0$).

To develop a better understanding of the origin of the super-critical scenario, we will first discuss in Sec. 4.1 whether a super-critical tension can be realized as the final stage of a cylindrical collapse (like a black hole emerges from a spherical collapse). To that end, we will discuss a theorem by Thorne [11], implying a negative answer. While this is no principle obstruction to the braneworld construction we have in mind, it shows that the super-critical brane must either have formed at an earlier—for instance stringy— quantum phase or simply existed forever.[7] Moreover, this discussion proves on very general grounds that super-criticality (in the case of an axially symmetric system) necessarily leads to a closure of the extra space in a second (sub-critical) axis, in accordance with our findings in Sec. 3.5.1. Next, in Sec. 4.2, we review the scaling solutions found previously as possible vacua of the super-critical BIG setup. To be precise, we re-express them in terms of co-moving coordinates. This in turn provides us with a clear geometrical interpretation: The super-critical brane deforms the bulk into a static cigar while both branes expand at constant rates H and H_a. We also derive an expression for the extra space volume, which turns out to be crucial for the phenomenology of (4.1).

A first stability analysis is performed in Sec. 4.3. We find that at least one of the two branches is stable under FLRW fluctuations. Moreover, the pressure needed to stabilize the super-critical brane may be realized by physical matter. Interestingly, we show that the cigar solution found here is equivalent to a vacuum solution of 6D GR discussed in [90].[8] The difference is that we were able to match them to an explicit core model (given by a super-critical ring-shaped brane). To our knowledge this has not been achieved before. It allows us to express all integration constants in terms of model parameters; in particular, we find an analytic relation between the Hubble parameter and the tension on both branes. This in turn admits a discussion of the model's prospects with respect to the CC problem, which is provided in Sec. 4.4. We conclude with a brief summary of our findings in Sec. 4.4.2.

As in the DGP case, we will work in polar coordinates (r, ϕ), to be precise $x^A = (x^\mu, r, \phi)$, and make the metric ansatz (3.3) reflecting the axial symmetry of the setup.

[7] This observation, though, prevents the formation of super-critical cosmic strings in 4D—at least within classical GR [132].

[8] In 5D these solutions have been used by Witten to demonstrate the instability of the KK vacuum (which decays into a "bubble of nothing") [171].

4.1 Thorne's theorem in 6D

The physical relevance of super-critical strings crucially depends on whether these solutions can be reached dynamically. A tentative creation mechanism could be realized by a cylindrical collapse describing the transition of a sub-critical to a super-critical cylindrical shell. At first sight, the physical picture is convincing: the 5D localized energy density grows when the circumference of the brane shrinks, thus driving the system towards criticality.

To make this statement more precise, let us derive how the energy density depends on R. For the moment, we assume that R is not constant, which motivates the definition of a radial Hubble parameter

$$H_R := \frac{\mathrm{d}R}{\mathrm{d}\tau}/R\,. \tag{4.2}$$

The covariant conservation of the induced energy momentum tensor $\tilde{\mathbf{T}}$ then implies a generalized version of the energy conservation equation (3.18),

$$\frac{\mathrm{d}\tilde{\rho}}{\mathrm{d}\tau} + 3H\,(\tilde{\rho} + \tilde{p}) + H_R\,(\tilde{\rho} + \tilde{p}_\phi) = 0\,, \tag{4.3}$$

where $\tilde{\rho} = \rho/(2\pi R)$, $\tilde{p} = p/(2\pi R)$ and $\tilde{p}_\phi = p_\phi/(2\pi R)$ are the 5D energy and momentum densities [cf. Def. (3.2)]. For the question of criticality the 4D energy density (instead of its 5D counterpart) is the crucial quantity—at least in the static case where the deficit angle $\delta = \lambda/M_6^4$ is determined by $\lambda \equiv \rho$. From the above equation we readily derive its time dependence expressed in terms of the brane and angular scale factors $a(\tau)$ and $R(\tau)$,

$$\rho = \rho_i \left(\frac{a}{a_i}\right)^{-3(1+w)} \left(\frac{R}{R_i}\right)^{-w_\phi}\,. \tag{4.4}$$

This expressions shows that for $w_\phi > 0$, for instance a shell of radiation, the 4D energy grows with shrinking R. We would therefore expect that at some point during a collapse (if it takes place) the 4D energy density ρ exceeds the critical value $\rho^{\downarrow}_{\mathrm{crit}}$, defined in 3.25, thus causing the system to enter first the critical and subsequently the super-critical phase. However, there are two possible obstacles to that reasoning:

1. According to (4.4), an expansion in axial direction ($H > 0$) can overcompensate the effect of a radial collapse ($H_R < 0$).

2. It is not clear whether the system undergoes a full collapse at all, instead it could bounce or at least approach some constant value of R asymptotically.

Finding an answer would require to solve the dynamics of the whole system without angular stabilization. While our numerical approach would in principle allow for such a study, we will use some high level arguments instead. They were first provided by Thorn in [11], where it was showed that a transition to a critical or super-critical brane, starting from sub-critical configuration, is dynamically forbidden due to Einstein's equations. Translated

to the formal language of Sec. 3.2.1, this amounts to the statement

$$D^+ \not\to D^- \,, \tag{4.5}$$

where D^+ and D^- denote the classification of the exterior spacetime according to Tab. 3.1.

In order to show this explicitly, we study a vacuum region with whole-cylinder symmetry and reintroduce coordinates for which the line element is of the form (3.3) [instead of the ER form (3.11)]. In other words, we restore the function $W(t,r)$ fulfilling the free 1D wave equation (3.4a). From Tab. 3.1 it is clear that a change of character is always attended by a change of sign of the functions W'_+ or W'_- defined in (3.8). As W'_+ or W'_- depend on $t+r$ and $t-r$, they are constant along incoming and outgoing null-rays, respectively. This in turn implies that a character change can *only* occur across a null-surface. For definiteness, we consider an outgoing null-ray ($\mathrm{d}t - \mathrm{d}r = 0$). Along that ray the character can change within the subgroups

$$\{D^+, D^\downarrow, D^{+\downarrow}\}, \qquad \{D^-, D^\uparrow, D^{-\uparrow}\}, \qquad \{D^{+\uparrow}, D^{-\downarrow}, D^\times\}\,.$$

Similarly, for an incoming null-ray ($\mathrm{d}t + \mathrm{d}r = 0$) changes within

$$\{D^+, D^\uparrow, D^{+\uparrow}\}, \qquad \{D^-, D^\downarrow, D^{-\downarrow}\}, \qquad \{D^{+\downarrow}, D^{-\uparrow}, D^\times\}$$

are admissible. In particular, this shows that there is no incoming or outgoing null-ray connecting a D^+ with a D^- spacetime region. This proves the claim (4.5), since in the exterior of the brane a transition between D^+ and D^- could only take place across a future (or past) directed null-surface which in turn would imply a transition along an incoming (or outgoing) null-ray in contradiction to the previous statement.

For the sake of completeness, let us work out a further restriction on the allowed transitions: According to the focusing theorem for null geodesics [11, 125], $\mathrm{d}^2W/\mathrm{d}\sigma^2 \leq 0$ with σ the affine parameter along the null geodesic. This means that both functions W'_+ or W'_- cannot increase along a null-ray[9]. For example, within the first set this leaves only a single possibility, given by

$$D^+ \to D^{+\downarrow} \to D^\downarrow\,. \tag{4.6}$$

Finally, the totality of possible transitions (including those along others than null-ray trajectories) is visualized in Fig. 4.1.

From these results we can draw another important conclusion about the exterior of a super-critical brane, viz a D^- spacetime: It always contains an axis. To be precise, there is a time-like trajectory $r_a(t)$, implicitly defined by

$$W(t,r)|_{r=r_a(t)} \stackrel{!}{=} 0\,, \tag{4.7}$$

which describes the position of a (in general singular) symmetry axis. To prove this, consider again an outgoing null-ray starting at the brane. Since the spacetime classification

[9]The derivation of this theorem uses Einstein's equations together with the strong energy condition.

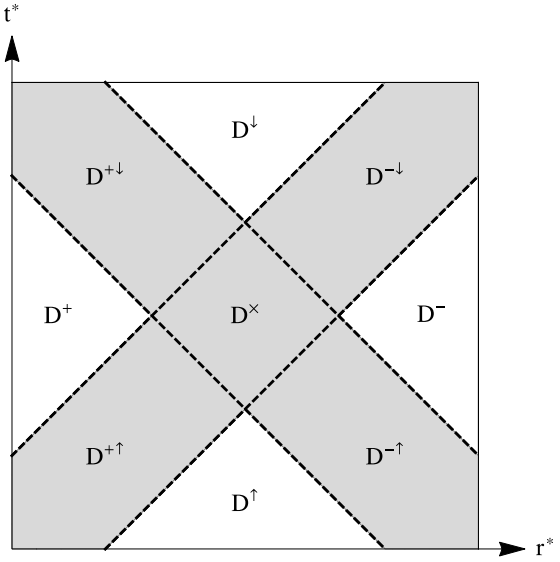

Figure 4.1: The diagram depicts all possible character changes of a vacuum region [132]. They can be read off by following incoming or outgoing time-like or light-like geodesics. Note that here $t \equiv t^*$ and $r \equiv r^*$.

is D^-, $W'_+ < 0$. Therefore, due to the focusing theorem, W_+ decreases at a constant or even growing rate along the null-ray, whereas W^- is simply constant. As a consequence, we will eventually hit the point where $W \equiv W^+ + W^- = 0$, corresponding to an axis. In the static example we have already discussed the presence of this "second" axis which also exhibits a conical singularity (cf. Fig 2.2c). The important point is that this singularity is part of the manifold as it can be reached by a light-like geodesic.

In summary, Thorn's theorem (generalized to 6D) proves that a super-critical brane cannot emerge dynamically from a sub-critical one within a consistent theory of GR. Moreover, for an already existing super-critical brane the exterior space necessarily contains a second axis. A priori, it is not clear whether this axis will be singular. In particular, it can host a conical singularity, corresponding to a brane of tension λ_a. In fact, the scaling solutions of Sec. 3.5.1 provide an explicit example: There, we found both solutions with vanishing and non-vanishing λ_a. In general, i.e. for non-scaling solutions, the singularity can be avoided by choosing appropriate initial conditions, provided ρ_i is not too large.[10]

Before turning to explicit solutions of the setup, let us discuss the significance of our results for cosmic strings in 4D. First note that even though we are mostly interested in six dimensions, the previous discussion was totally general. In particular, it can be applied to cosmic strings in 4D. Their formation is normally assumed to take place in the early universe, say at the GUT scale, and thus in a regime where we would generically expect a 4D tension of order $\lambda/M_{\rm Pl}^4 \sim 10^{-6}$ which is of course vastly sub-critical. Moreover, in light of Thorn's theorem, there is little hope to create super-critical strings by means of some

[10]For a pure tension brane the bound is given by (3.114) with $\ell_2 = 0$ and $\rho_i = \lambda$.

collapse mechanism[11]. This clearly limits the physical relevance of any potential super-critical solution in the case of 4D GR. The story is of course different for extra-dimensional setups. In that case, we are agnostic about the precise formation process of the brane; in particular, it could have taken place at some early epoch outside the regime of validity of 6D GR, say within a stringy context. For our purposes, it is thus sufficient to have some consistent solution of the super-critical setup (albeit we are ignorant about its formation process).

4.2 Scaling solutions revisited

In this section, we develop a more rigorous geometrical picture of the scaling solutions discussed in Sec. 3.5.1. Specifically, by introducing co-moving coordinates, we are able to make contact to known vacuum solutions of Einstein's equations that have been used in 5D in a famous work by Witten [171] to show the instability of the KK vacuum. Later, those solutions were also generalized to higher dimensions in [90]. They turn out to be particularly useful to visualize the bulk geometry.

On a technical level, the new achievement of our work is to match those solutions to an actual core model, which in turn allows us to express all integration constants in terms of physical model parameters. In particular, we are now able to infer the physical significance of those solutions for extra-dimensional model building.

Our starting point is the scaling solution in ER coordinates $(t, r, \boldsymbol{x}, \phi)$ presented in (3.98). We introduce new coordinates[12] $(\bar{t}, \bar{r})$ defined as

$$\bar{t} = \frac{L}{3} \ln\left(\frac{3L^3\, t}{\left(1-\bar{\lambda}_a\right) r_+^4} \sqrt{1-x^2} \right) \,, \tag{4.8a}$$

$$\bar{r} = \frac{r_+}{2^{1/3}} \left(1 + \frac{1}{\sqrt{1-x^2}} \right)^{1/3} \,, \tag{4.8b}$$

where L is an arbitrary length scale that can be adjusted by appropriately shifting and rescaling $\bar{t}$, and $x = r/t$ is the scaling variable first defined in (3.94). In these new coordinates (3.98) becomes

$$\mathrm{d}s^2_{(\mathrm{ext})} = \frac{\bar{r}^2}{L^2}\left(-\mathrm{d}\bar{t}^2 + \mathrm{e}^{2\bar{t}/L}\mathrm{d}\boldsymbol{x}^2\right) + \left[1-\left(\frac{r_+}{\bar{r}}\right)^3\right]^{-1} \mathrm{d}\bar{r}^2 + \frac{4}{9} r_+^2 \left(1-\bar{\lambda}_a\right)^2 \left[1-\left(\frac{r_+}{\bar{r}}\right)^3\right] \mathrm{d}\phi^2 \,, \tag{4.9}$$

[11] So far it is not clear whether their formation through a quantum-mechanical tunneling process would lead to phenomenologically relevant effects.

[12] For simplicity, we limit ourselves to an explicit discussion of the exterior coordinate patch, keeping in mind that all transformations can be applied to the interior coordinates, too.

where r_+ denotes the position of the (second) axis and is given by

$$r_+ = \frac{3R}{1-\bar{\lambda}_a}\frac{\left(1+\sqrt{1-v^2}\right)}{2v}\,. \tag{4.10}$$

By using the transformations (4.8), it is straightforward to show that the brane sits at the constant coordinate position

$$\bar{r}_0 = \frac{3R}{1-\bar{\lambda}_a}\frac{1}{v\,\mathrm{h}(v)}\,, \tag{4.11}$$

which suggests the term *co-moving coordinates*. The function $\mathrm{h}(v)$ is defined in (3.100). The coordinate range of $\bar{r}$ is fixed to $(r_+, \bar{r}_0]$.

The only time dependence is due to a dS-like expansion in axial direction described by the $\mathrm{d}\boldsymbol{x}^2$ part of the line element. By choosing $L = \bar{r}_0$ we can easily identify the on-brane Hubble parameter as $H = 1/\bar{r}_0$ ($\equiv 1/L$). As a simple consistency check, note that with these definitions (4.11) exactly reproduces the second equation in (3.99).

The interior line element $\mathrm{d}s^2_{(\mathrm{int})}$ (characterized correspondingly by $\check{r}_+$ and $L = 1/H$) can be obtained by formally replacing $(r_+, v, \bar{\lambda}_a) \to (\check{r}_+, \check{v}, 0)$ in (4.9) and (4.10). As a result, the interior and exterior geometry is fully determined by the three integration constants r_+, $\check{r}_+$ and H. Since we have already solved the equivalent system in ER coordinates, the algorithm for finding a solution is evident: For a given choice of model parameters R, $\bar{\lambda}$ and $\bar{\lambda}_a$ we solve the algebraic equations (3.99) and (3.101) with $\ell_2 = 0$. For the sake of completeness,

$$3HR = \check{v}\,\mathrm{h}(\check{v})\,, \tag{4.12a}$$

$$3HR = v\,\mathrm{h}(v)\left(1-\bar{\lambda}_a\right)\,, \tag{4.12b}$$

$$3HR = \left(\frac{1}{\check{v}}+\frac{1}{v}\right)^{-1}\bar{\lambda}\,, \tag{4.12c}$$

$$3H_aR = \frac{2v}{1+\sqrt{1-v^2}}\left(1-\bar{\lambda}_a\right)\,, \tag{4.12d}$$

where $\mathrm{h}(v)$ is defined in (3.100) and the last equation follows from (4.10) when we identify the Hubble parameter at the second axis according to $H_a = 1/r_+$. The four equations determine the four integration constants H, H_a, v and $\check{v}$, which via (4.10) can be translated to the corresponding values for r_+ and $\check{r}_+$ in co-moving coordinates. Thus, we have established a link between the bulk integration constants and a specific core model (characterized by $\bar{\lambda}$, $\bar{\lambda}_a$ and R only). This in turn allows us to infer the model's potential with respect to the CC problem (as done in Sec. 4.4.1).

As advertised, the co-moving coordinates admit a simple picture of the geometry. The deviation of the bulk geometry from the static (conical) geometry (3.49) is solely controlled by the parameter v: While the geometry is close to a cone (or to Minkowski space for $\lambda_a = 0$) for small v, it becomes cigar shaped when v approaches one. This behavior is

visualized by the embedding diagrams in Fig. 4.2.

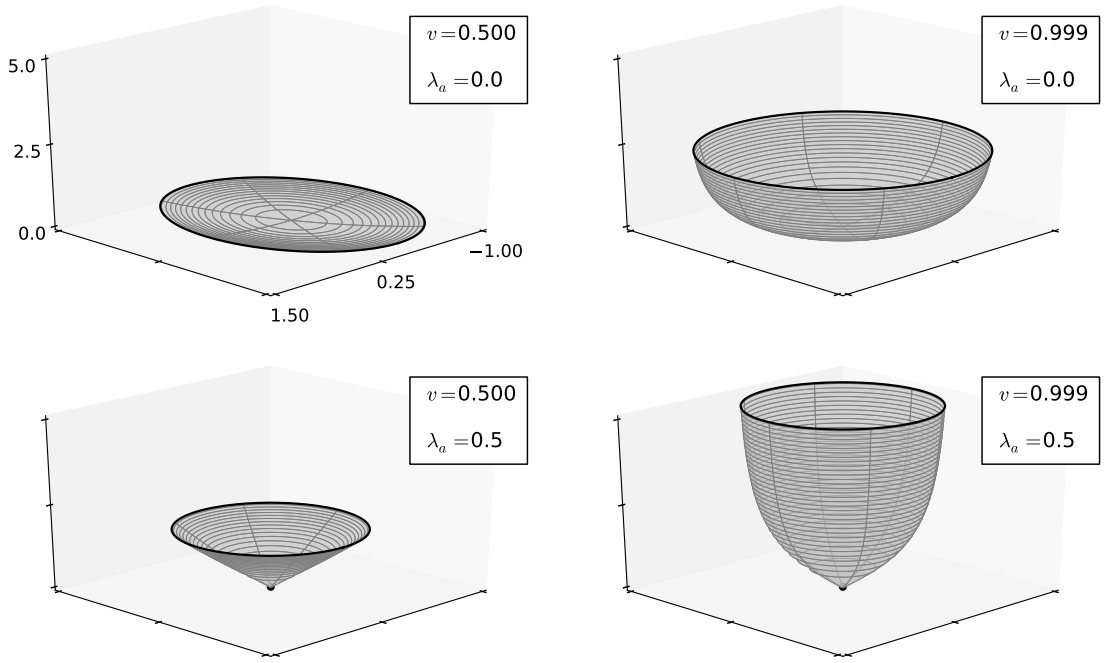

Figure 4.2: Embedding picture of (4.9) (in units of R). While the first row depicts an exterior with regular axis, there is a conical singularity—representing our universe—in the second row (black dot). The larger the parameter v, the more the space is deformed into a cigar. The black ring is the super-critical brane (with compact ring dimension of size $2\pi R$). The interior spacetime is omitted (it would correspond to an almost flat cap).

To show this more explicitly, let us derive the near-flat regime. To that end, we introduce a new radial coordinate

$$\hat{r} = \frac{2}{3}\sqrt{r_+ \bar{r}\left[1 - \left(\frac{r_+}{\bar{r}}\right)^3\right]}\,, \tag{4.13}$$

with range $(0, \hat{r}(\bar{r}_0)]$. By using (4.10) and (4.11) and assuming $v \ll 1$, we can easily derive that[13] $\hat{r}/r_+ \leq v \ll 1$; this in turn admits an approximate expression for the line element,

[13] A short numerical evaluation yields that the first inequality is in fact true for $v \lesssim 0.99$.

which now evaluates to

$$\mathrm{d}s^2_{(\mathrm{ext})} = \left[1+\frac{3}{2}\left(\frac{\hat{r}}{r_+}\right)^2\right]\left(-\mathrm{d}\bar{t}^2+\mathrm{e}^{2\bar{t}/r_+}\,\mathrm{d}\boldsymbol{x}^2\right) + \left[1+\frac{15}{8}\left(\frac{\hat{r}}{r_+}\right)^2\right]\mathrm{d}\hat{r}^2 + \left[1+\frac{3}{2}\left(\frac{\hat{r}}{r_+}\right)^2\right]\left(1-\bar{\lambda}_a\right)^2\hat{r}^2\mathrm{d}\phi^2 + \mathcal{O}\left[(\hat{r}/r_+)^3\right], \quad (4.14)$$

and thus demonstrates that the exterior is indeed given by the conical geometry (1.14) at leading order in v (or $\hat{r}/r_+$ equivalently).

Yet, for large values of v the expansion breaks down and we best stick to the full solution in (4.9). Due to (4.11), $\bar{r}_0 \to \infty$ for $v \to 1$, meaning that the brane is pushed to infinity as measured by $\bar{r}$. When we start at the axis and move towards the brane, $\bar{r} \to \infty$, and hence $(1-r_+/\bar{r}) \to 1$. This means that by approaching the brane the circumference of the extra space tends towards a constant corresponding to a cylindrical embedding geometry. This leads to the before mentioned cigar shaped extra dimension.

To further solidify the above picture, we can calculate the extra-dimensional volume which follows from (4.9),

$$\begin{aligned} V_{\mathrm{ext}} :&= \frac{4\pi}{3}r_+\left(1-\bar{\lambda}_a\right)\int_{r_+}^{\bar{r}_0}\mathrm{d}\bar{r} \\ &= \frac{\pi R^2}{1-\bar{\lambda}_a}\,\frac{3\left(1+\sqrt{1-v^2}\right)^2}{v^2}\left[\left(\frac{1+\sqrt{1-v^2}}{2\sqrt{1-v^2}}\right)^{1/3}-1\right], \end{aligned} \quad (4.15)$$

where (4.10) and (4.11) were used to derive the final expression. It is straightforward to check that in the limit $v \to 0$ the correct flat space result $\pi R^2/(1-\bar{\lambda}_a)$ is approached.[14] On the other hand, in the limit $v \to 1$ the volume diverges, which corresponds to an infinitely long cylinder. In other words, if the integration constant v and the second tensions $\bar{\lambda}_a$ are not chosen close to one, $V_{\mathrm{ext}} \sim R^2$, which implies that R can no longer be a microscopic scale (otherwise the extra dimensions would not be large which is important though to address the hierarchy problem, cf. Sec. 1.5). This is the reason why we confine the SM matter fields on the sub-critical brane (which is of microscopic size $1/M_6$). That way, we avoid any phenomenological problems that would certainly occur when matter "sees" a large fifth dimension of size $R \lesssim 100\,\mu$m (as would be the case if the SM was localized on the super-critical brane and v was not tuned close to one).

The geometric picture developed above applies to both the interior and exterior space. Note that the limiting cases discussed here, correspond to the two branches $\mathrm{A_{II}}$ and $\mathrm{B_{II}}$, previously defined in Sec. 3.5.2 (subject to $\ell_2 = 0$). To be precise, if the *exterior* is close to flat (or conical) space ($v \ll 1$), the solution is of type $\mathrm{A_{II}}$, and of type $\mathrm{B_{II}}$ otherwise ($1-v \ll 1$). On the other hand, the *interior* is always close to flat space ($\check{v} \ll 1$). In

[14] Note that this was also observed for V_{int} by using the ER coordinates [see Eq. (3.109)]. However, there it was not possible to find an analytic expression valid for all $\check{v}$.

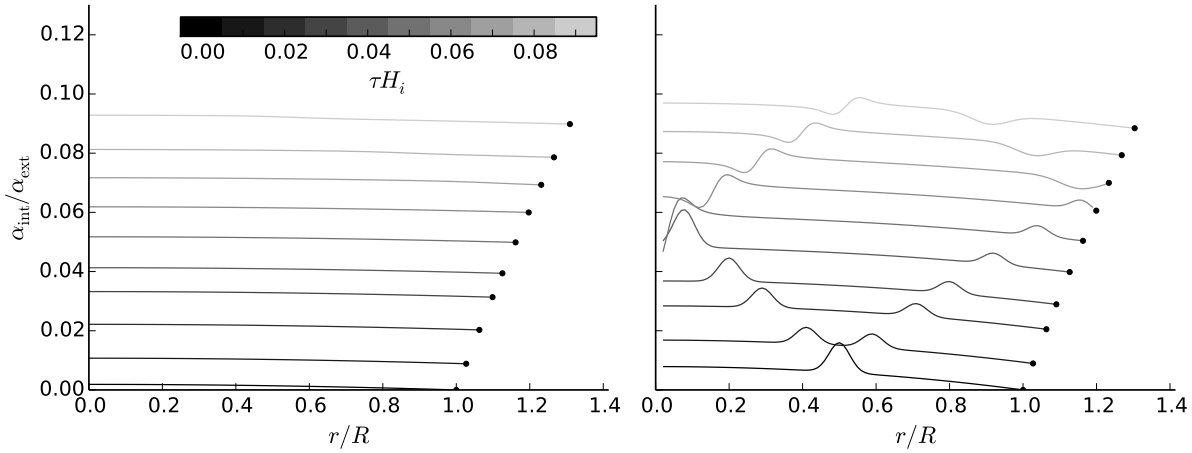

Figure 4.3: Radial profile of $\breve{\alpha}$ ($\equiv \alpha_{\rm int}$; left) and α ($\equiv \alpha_{\rm ext}$; right) at different times for parameters (4.16). The interior profiles are given by the scaling solution (3.98) evaluated at different times. The exterior profiles are dominated by ER waves which are washed out successively. The dotes indicate the position of the brane.

geometrical terms, the branch $\mathrm{A_{II}}$ describes a slightly curved cone in the exterior that is glued (alongside the super-critical brane/ring) to an almost flat interior, whereas $\mathrm{B_{II}}$ yields a cigar shaped extra space (cf. Fig. 4.2).

4.3 Stability

Before studying the naturalness of (4.1), let us briefly discuss the stability of the scaling solution (4.9). To that end, we will employ once again our numerical implementation, introduced in Sec. 3.3. When choosing initial conditions in the BIG case in Sec. 3.3.1, we used a quadratic profile for the metric function α, which hence strongly deviated from the scaling solution (but allowed us to dial the desired value of λ_a). In order to check the stability, we now take a slightly different route and consider a small perturbation of the analytic scaling profile in the exterior, defined in (3.98).[15] Of course, we could also use the quadratic profile function to arrive at the same conclusion. Though, it is instructive to employ this slightly different method here.

The main effect of this initial perturbation is to change the value of the tension $\bar{\lambda}_a \equiv 1 - \mathrm{e}^{-\eta_a}$ (as compared to the scaling expectation). Its value is obtained by numerically integrating the constraint (3.30b).[16] Specifically, for our numerical example the model

[15]For definiteness, we add a Gaussian profile of width $R/25$ and amplitude $R/5$ centered around $r = R/2$.
[16]Note that $\bar{\lambda}_a$ is constant throughout the time evolution since $\partial_t \eta|_a = 0$ due to (3.30c).

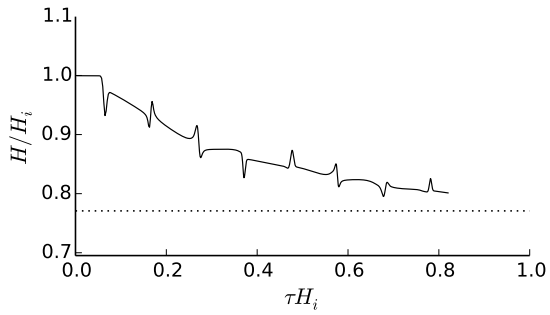

(a) The Hubble parameter decreases. The oscillations correspond to ER waves propagating between the two branes.

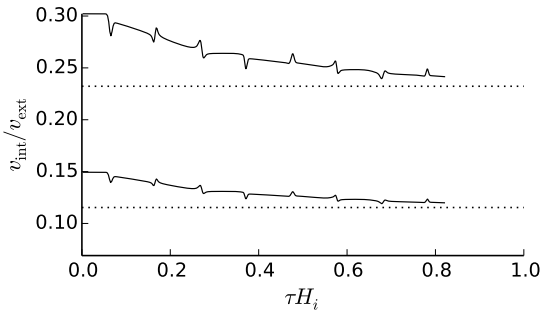

(b) The upper line depicts the exterior coordinate velocity ($v_{\rm ext} \equiv v$) and the lower one the interior velocity ($v_{\rm int} \equiv \check{v}$). They are both significantly below the speed of light.

Figure 4.4: The system approaches the $\mathrm{A_{II}}$ scaling values (dotted lines), specified in (4.17a). Parameters as defined in (4.16).

parameters are[17]

$$H_i R = \frac{1}{20}\,, \qquad \bar{\lambda} = \frac{3}{2}\,, \qquad \bar{\lambda}_a \approx 0.51\,. \tag{4.16}$$

The corresponding scaling prediction that follows from this and (4.12) is

$$H/H_i \approx 0.77\,, \qquad v \approx 0.23\,, \qquad \check{v} \approx 0.12 \qquad (\text{branch } \mathrm{A_{II}})\,, \tag{4.17a}$$
$$H/H_i \approx 3.08\,, \qquad v \approx 0.998\,, \qquad \check{v} \approx 0.45 \qquad (\text{branch } \mathrm{B_{II}})\,. \tag{4.17b}$$

Provided we are in the attractor regime of either $A_{\rm II}$ or $B_{\rm II}$, we expect the system to approach the respective value. Since we slightly perturbed a solution of type $A_{\rm II}$, it is plausible that this branch is approached (instead of $B_{\rm II}$).

To visualize the dynamics, we depict the $\check{\alpha}$ and α profiles in Fig. 4.3 for different times (somewhat close to initial time). First, we find that the interior spacetime is almost insensitive to the presence of the perturbation. On the other hand, in the exterior, the initial perturbation splits into two wave packets that move between the brane and the exterior axis (at $r = 0$). The two of them are washed out gradually as the system evolves. Correspondingly, the Hubble parameter and brane coordinate velocities settle to their scaling predictions (4.17a), depicted as a dotted line in Fig. 4.4a and Fig. 4.4b, respectively.[18] The kinks are caused by the bulk waves, hitting the brane periodically. Correspondingly, the first kink is associated with the profile at time $\tau H_i = 0.07$ in Fig. 4.3.

This discussion shows that the $A_{\rm II}$ scaling solutions are indeed stable under FLRW

[17] For completeness, the step size for integration is $\check{\epsilon} = 2 \times R/10^3$ and $\epsilon = R/10^3$ in the interior and exterior, respectively.

[18] Instead of H, we also could have used H_a to show that the system converges to the scaling solution.

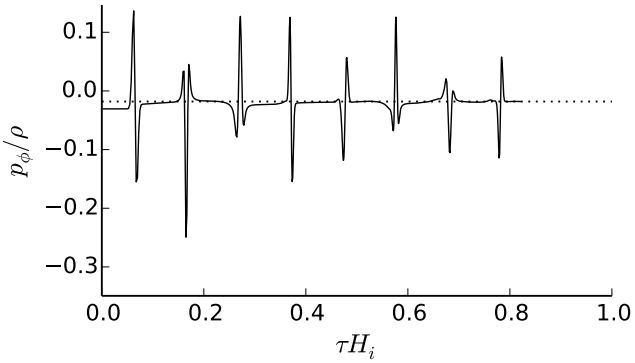

Figure 4.5: The stabilization sector corresponds to physical matter as the equation of state parameter is above -1. Parameters as in (4.16). The scaling prediction, derived from (3.103) (subject to $\ell_2 = 0$), is represented by the dotted line.

fluctuations. This is good news, because in principle they might represent the (final) de Sitter stage of a phenomenologically viable expansion history. To settle their status more rigorously, other types of matter should be considered, too. We leave that question for future research, though.

We still have to check whether the stabilization can be achieved by physical matter, i.e. preserves the NEC. To that end, we plot in Fig. 4.5 the equation of state parameter for the angular pressure and find that it is always above -1, indeed corresponding to physical matter.

Let us finally comment on the second branch B_{II}. On a formal level, it corresponds to large coordinate velocities of the brane; specifically, $v > 2\sqrt{2}/3 \approx 0.94$ [which is defined as the maximum of $\mathrm{h}(v)$ in (3.100)]. However, this makes the numerical study difficult, as an initial perturbation placed in the exterior only very slowly approaches the brane (because it recedes almost with the speed of light), which in turn necessitates many integration steps, thus increasing the numerical error. Therefore, we refrain from a final statement about that branch. Yet, it seems conceivable that further numerical studies can clarify its status.

4.4 Discussion

As this thesis has its focus on the CC problem, we will provide an extensive discussion of the tuning issue. In particular, we ask whether this new type of model, which employs supercriticality (instead of a flux quantization) to compactify the extra space, can circumvent Weinberg's tuning argument. We then conclude by sketching possible future prospects of the model.

4.4.1 Tuning

Analog to the discussion of the compact prototype model (1.29), we quantify the amount of tuning needed to obtain a phenomenologically viable Hubble expansion and extra space volume. In that context, is is crucial to note that a 4D brane observer who lives on the second brane (which hosts the SM sector) measures H_a instead of H. Correspondingly, the phenomenological bound (1.2) has to be applied to H_a. Moreover, $V_{\rm ext}$ is demanded to fulfill the upper bound (1.28) (adding $V_{\rm int}$ would not change the order of magnitude estimates).

We start by evaluating (4.12d) for the limiting cases $v \ll 1$ and $(1-v) \ll 1$, corresponding to branch $\mathrm{A_{II}}$ and $\mathrm{B_{II}}$, respectively; to be precise,

$$9H_a^2R^2 \approx \begin{cases} 4\left(1-\bar\lambda_a\right)^2 & [\text{for} \quad (1-v) \ll 1 \,|\, \text{branch}\, B_{\rm II}]\,, \\ \\ 6\left(1-\bar\lambda_a\right)\left(\bar\lambda+\bar\lambda_a-2\right) & [\text{for} \quad v \ll 1 \,|\, \text{branch}\, A_{\rm II}]\,. \end{cases} \tag{4.18}$$

Here, the first line is obtained from (4.12d) by taking the leading order in $(1-v)$, whereas the second line uses an expansion of (4.12a) (up to order $\check v$) and another one of (4.12b) (up to order v^3) as well as (4.12c).[19] We also solved the system (4.12) numerically with the result depicted in Fig. 4.6 by the solid line. The branch $\mathrm{A_{II}}$ corresponds to the line below the black dot and $\mathrm{B_{II}}$ to the one above. Both segments can be parametrized by v with the respective intervals $(v_*, 0]$ and $(1, v_*]$, where $v_* := 2\sqrt{2}/3$ corresponds to the branch point (indicated as a dot). The dashed and dotted line represent the estimates (4.18). As expected, they approach the numerical result in the limit $v \to 1$ and $v \to 0$, respectively. In particular, we see that they can be used as proxy functions, provided we are only interested in order of magnitude estimates.

Phenomenology requires the Hubble length $1/H_a$ to be much larger than the size of the extra space (which is constrained to be below a hundred microns due to post-Cavendish experiments), specifically $H_a^2 V_{\rm ext} \lesssim 10^{-66}$ (cf. bound (1.33) and its derivation). Moreover, a short inspection of (4.15) yields $\pi R^2 \leq V_{\rm ext}(1-\bar\lambda_a)$, which together with the phenomenological bound implies an upper limit on the left side of (4.18),

$$9H_a^2R^2 \lesssim 10^{-66}\left(1-\bar\lambda_a\right)\,. \tag{4.19}$$

The factor $(1-\bar\lambda_a)$ cancels with the corresponding factors on the right side of (4.18). First, we see from Fig. 4.6 that branch $B_{\rm II}$ does not admit a hierarchically small H_aR. The reason is that for a generic choice of $\bar\lambda$, the factor $1-\bar\lambda_a$ has to be of order one (in fact, the smallest possible value corresponds to the branch point at v_*).[20] Thus, we focus on the remaining branch $A_{\rm II}$. Here, we find that $(\bar\lambda+\bar\lambda_a-2)$ has to be tuned to zero with a

[19] Note that there is always a regime for which $v \gg \check v$, hence justifying the double expansion.

[20] This conclusion could only be avoided if $\bar\lambda - b_{\rm II} \ll 1$, which is a tuning condition on $\bar\lambda$. But then we would still need to dial $1-\bar\lambda_a \ll 1$.

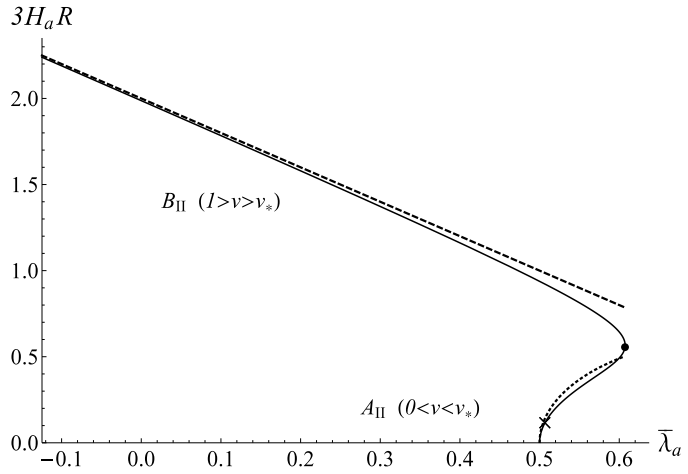

Figure 4.6: Numerical solution of (4.12) for $\bar{\lambda} = 1.5$. The dashed and dotted line correspond to both estimates in (4.18); they approach the numerical result (solid line) in the respective limits $v \to 1$ (for branch $B_{\rm II}$) and $v \to 0$ (for branch $A_{\rm II}$). Here, $\times$ depicts the attractor (4.17a) of our numerical example. The black dot is the branch point.

precision of 66 decimal places to meet the phenomenological requirements. On the other hand, if we choose all model parameters of order M_6, (4.18) implies $H_a^2 V_{\rm ext} \gtrsim 1$, which is of course vastly incompatible with the phenomenological bound.

As a result, we exactly reproduce the tuning (or phenomenological) problem encountered in our prototype model in Sec. 1.5.2. As we will exemplify for yet another model in Sec. 6, this conclusion seems to be inevitable whenever the extra dimension is compact. There, we go a step further and conjecture that from a 4D perspective this is just a manifestation of Weinberg's argument (cf. Sec. 1.2.2).

4.4.2 Summary

Let us conclude by stating our main result. We presented a mechanism for creating a 4D de Sitter vacuum on a brane in two codimensions. It relies on a pure tension brane that consists of three infinite and one additional compact dimension. Since the tension exceeds its critical value, the bulk becomes cigar-shaped and closes in another axis, which in general hosts a second, sub-critical brane. Accordingly, the setup contains two branes, a super-critical one (which sets the size of one of the two compact bulk dimensions) and a sub-critical one (which is of microscopic size). The latter is identified as a candidate for our universe. The corresponding solution generalizes the well-known conical geometry as defined in (3.49) to non-vanishing values of Hubble.

There are two branches, one ($A_{\rm II}$) characterized by a somewhat flatter bulk geometry and another one ($B_{\rm II}$) corresponding to a more accentuated cigar shape. The former turns out to have a finite basin of attraction and might describe the final de Sitter stage of a

phenomenologically viable cosmic expansion. We still lack a final statement about the stability of the latter branch. Without doubt, it possesses a smaller basin of attraction.

We find for both branches that they cannot address the CC problem. Without tuning the brane tension λ_a, the bulk volume is of cosmological scale and hence certainly incompatible with the phenomenological bounds.[21] As we will see for yet another extra space construction in Chap. 6, the volume problem is typical for compact models.

To further assess the phenomenological status of the model, the following questions should be addressed:

- How do other types of matter influence the expansion of the brane (or cosmic evolution equivalently)? In particular, one should ask whether a phenomenologically viable Hubble expansion is possible.
- Does the B_{II} branch admit a finite attractor regime?
- Are the solutions stable under general fluctuations (so far this was shown for FLRW symmetries only)?

Finally, let us note that the same setup was recently discussed in 4D as describing an inflating cosmic string [132]. The physics are primarily the same with the only difference that there the scaling solution in the exterior was only realized asymptotically. To be precise, instead of approaching $v = \mathrm{const} < 1$ [observed here for parameters (4.16)], $v \to 1$. In geometrical terms, this implies a bulk and brane geometry that is not static; instead, the cigar grows in size and the expansion rate of the brane approaches a constant value (corresponding to the hypothetical brane velocity $v = 1$). Correspondingly, the 4D model only admits a quasi de Sitter geometry on the brane. We do not have a final physical explanation for that difference. So far, it looks like a higher-dimensional accident, yet a welcome one.

[21] Equivalently, it can be rephrased as saying that the 4D curvature is way too large provided the volume fulfills its phenomenological bound (1.28).

Chapter 5

BIG: Extra space as a cylinder

Note: The major part of this chapter is a verbatim reproduction of a publication together with Robert Schneider [131].

Instead of considering two infinite (or two compact) extra dimensions, the idea of the present chapter is to investigate one compact and one infinite extra dimension. To be specific, the infinite extra dimension of the five-dimensional DGP model is supplemented with another (microscopically small) compact dimension around which the brane is wrapped, hence implying that the brane itself has an additional compact dimension. In an embedding picture, the bulk corresponds to an infinitely long cylinder (cf. Fig. 5.1a). Consequently, the model is topologically different from the previously discussed six-dimensional models (cf. Fig. 5.1b). First, there is no distinction between an interior and exterior space; instead, there is a reflection symmetry at the brane position. Second, the codimension-two setup is not recovered by sending the brane circumference to zero (rather the DGP configuration is approached); in other words, the brane is a codimension-one object on a fundamental level.

This hybrid model serves as a simple prototype for systems that have both infinite as well as compact extra dimensions. Due to the induced Einstein-Hilbert term and the compactness of the additional brane dimension, there is a 4D gravity regime at small distances. Moreover, the model introduces an important physical feature, which is generically expected to influence the cosmology of braneworld setups with more than five dimensions, namely the emission of gravitational waves into the bulk (cf. the discussion in Sec. 3.2.6). Yet, it is still simple enough to admit analytic solutions, which greatly simplifies the discussion of its physical characteristics. The cosmologies we will find turn out to have some very intriguing properties, giving (at least) two *a posteriori* motivations:

1. The model provides a new degravitation mechanism at the full nonlinear level, which—albeit being ruled out observationally in this particular case —can be considered a proof of principle. This might also serve as an inspiration to come up with other similar (and hopefully phenomenologically viable) models that are able to degravitate the CC.

2. It yields a potentially interesting late time-modification of the DGP cosmology. As will be explained below, this is due to a breakdown of the modulus stabilization of the

compact extra dimension. Therefore, this mechanism might be relevant for all other higher-dimensional theories with stabilized compact extra dimension, and it might open the door to a novel class of consistent GR competitor theories which could be put to the test on cosmologically relevant scales.

We will investigate the cosmology of this model by deriving a set of modified Friedmann equations describing the curvature evolution on the brane. To that end, we assume that the metric and the localized energy momentum tensor possess 4D FLRW symmetries. Compared to the DGP model, a new dynamical feature is the existence of bulk gravitational waves. Similar to the cosmic string cosmology discussed in Chap. 3, the only emitter of gravitational waves is the brane itself, and the physical requirement of having no incoming bulk waves has to be imposed. While this was only possible by means of a non-local criterion in the case of the cosmic string universe [cf. Eq. (3.52)], the advantage of the setup at hand is that there is a local "outgoing wave condition" for plane waves, which makes it possible to derive a closed system of modified Friedmann equations valid on the brane. This in turn admits an analytic discussion of the corresponding cosmology. Let us again stress that this is opposed to the codimension-two setup which could only be studied by solving the full bulk-brane system numerically.

Since we are interested in curvature quantities that can be inferred by an on-brane observer, the aim of Sec. 5.1 is to find a closed system of ordinary differential equations (ODEs) for the induced metric on the brane. To that end, we derive the matching conditions across the brane in Sec. 5.1.3. Like in the codimension-two setup, these equations do not yet constitute a closed system. As discussed extensively in Sec. 3.2.6, this is related to the existence of bulk gravitational waves: in general, incoming waves will affect the curvature evolution on the brane. As mentioned before, we thus have to implement a differential condition that excludes incoming waves—in accordance with a source-free bulk. Following our previous results on this topic, published in [97], this can be achieved in a coordinate independent way by employing the Weyl tensor, provided the bulk has certain symmetries.[1] This convenient technique is reviewed and successfully applied in Sec. 5.2. That way, we arrive in Sec. 5.3 at a closed system of ODEs. We then further constrain the solution space by excluding any static curvature component in the bulk, which in turn eliminates one integration constant and yields the modified Friedmann equations in their final form. In Sec. 5.4 we consider two different classes of solutions:

1. Of particular *physical* interest are solutions for which the compact dimension is stabilized. As usual, this can be achieved by some underlying stabilization mechanism which is effectively implemented by tuning the azimuthal pressure p_ϕ. In this case, we exactly reproduce the DGP equations. Therefore, these solutions correspond to the trivial embedding of the DGP solutions in the higher-dimensional space. Moreover, bulk waves are absent for these solutions which is in accordance with the DGP result for which the brane is embedded in a static bulk. However, we find that for a

[1] In particular, this method could not be applied to the cosmic string universe in Chap. 3 as it corresponds to a cylindrically symmetric bulk spacetime which does not admit a local "outgoing wave condition".

tension dominated brane source, the stabilization can no longer be realized by means of physical matter. More specifically, the corresponding equation of state parameter would need to be $w_\phi \leq -4/3$ which signals a violation of the Null Energy Condition. Therefore, it is argued that the size of the compact dimension starts to evolve for late times when the brane enters the regime of tension domination and all other matter components have thinned out sufficiently. In general, the non-trivial dynamics of the compact direction leads to a modification of the standard 4D Friedmann evolution which is different from the DGP case. A more quantitative statement requires a microscopic description of the stabilization mechanism and is left for future work.

2. Of particular *conceptual* interest are solutions with an expanding or collapsing compact dimension. As an exemplary case, we discuss $p_\phi = 0$. In the pure tension case, we find analytic solutions for which the Hubble parameter, describing the evolution of the three non-compact brane directions, vanishes. Thus, an effective 4D brane observer will measure a vanishing curvature despite the presence of a 4D spacetime homogeneous energy source. We also solve the equations numerically for a non-vanishing initial Hubble parameter and find that the degravitating solution is an attractor. This is an important result of this chapter, since it constitutes another stable and dynamical example of the degravitation proposal at the fully non-linear level. Compared to the degravitating cosmic string solutions discussed in Sec. 3.4.1.1, we do not have to rely on complicated numerics to solve for the (time dependent) extra-dimensional profile of the metric functions. Instead, we are able to find a set of local on-brane evolution equations governing the dynamics of the two scale factors—one related to the three infinite and the other one to the compact brane dimension(s). As they constitute a closed system of two ODEs (instead of PDEs), this significantly simplifies the study of the on-brane cosmology. As an analytic byproduct, we also obtain the full bulk profiles.

   By comparing both degravitating solutions, we find that the physical mechanism differs in the two scenarios: For the cosmic string, the effect of the CC is to curve the transverse spatial dimensions into a cone, whereas here, it is the temporal curvature (i.e. expansion) in the compact extra dimension which absorbs λ. However, without proposing a microscopic model for the angular pressure component, it is not yet clear whether the choice $p_\phi = 0$ implies an unwanted fine-tuning. Thus, a final assessment on the model's potential to address the CC problem still has to be found.

   Since the degravitating solution is not compatible with a stabilized compact dimension, there are observable effects related to the corresponding size modulus. The existence of such a scalar degree of freedom during all cosmological epochs questions the phenomenological viability of the model since, generically, it leads to deviations from a standard 4D behavior. To demonstrate this explicitly, we perform a supernova fit which clearly shows that the degravitating solution with $p_\phi = 0$ is ruled out.

We conclude in Sec. 5.5 by pointing out possible directions of future research.

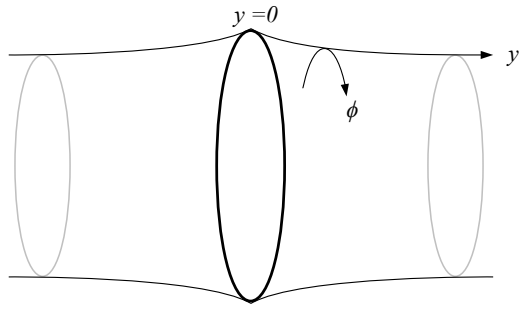

(a) *Cylindrical geometry:* there is no symmetry axis, and it is natural to assume reflection symmetry around $y = 0$.

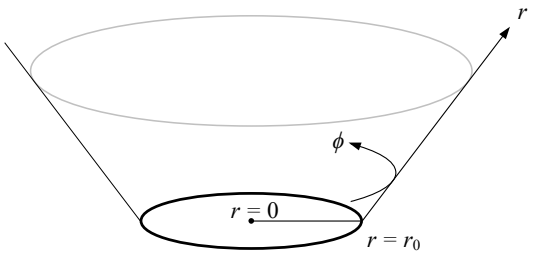

(b) *Radial geometry:* $r = 0$ is the symmetry axis and the brane can create a defect angle in the exterior. There is no reflection symmetry around $r = r_0$ in this case.

Figure 5.1: Illustration of two possible bulk geometries that could locally be described by the same metric ansatz, but are topologically different [131]. In this work, we are considering the cylindrical topology (a), see also Sec. 5.3.4. Only the two extra dimensions are drawn, embedded into a fictitious three-dimensional space. The 5D brane is located at $y = 0$ and $r = r_0$ ($\equiv R$), respectively.

5.1 The ring setup

We are considering a model in which the brane has five dimensions—the four infinite spacetime dimensions we see in low energy physics, plus one compact (spatial) dimension of microscopic size $2\pi R$. The bulk, on the other hand, has one additional infinite dimension and thus is six-dimensional (cf. Fig. 5.1a). This should not be confused with a model with two infinite extra dimensions with the codimension-two brane regularized by blowing it up to a circle of radius R, which is topologically different (cf. Fig. 5.1b).

The corresponding action reads

$$\mathcal{S} = \mathcal{S}^{(6)}_{\mathrm{EH}}[\boldsymbol{g}_6] + \int\limits_{\mathcal{M}_4\times\mathcal{S}_1} \mathrm{d}^5\tilde{x}\,\sqrt{-\tilde{g}}\left[\frac{\tilde{M}^3}{2}\tilde{\mathcal{R}} - \tilde{\lambda} + \mathcal{L}_{\mathrm{stab}} + \mathcal{L}_{\mathrm{m}}\right] , \tag{5.1}$$

where the first term is the 6D Einstein-Hilbert action (defined in (C1) for $D = 6$) and the integral describes all brane induced contributions; in particular, $\tilde{\boldsymbol{R}}$ is the 5D Ricci scalar constructed with $\tilde{\boldsymbol{g}}$, and $\mathcal{L}_{\mathrm{m}}$ collectively denotes additional matter fields. $\mathcal{L}_{\mathrm{stab}}$ describes a sector that stabilizes the compact brane dimension such that $R = \mathrm{const}$.[2] Correspondingly, by dimensional reduction, the mass scale $\tilde{M}$ is related to the four-dimensional Planck mass by $M^2_{\mathrm{Pl}} \equiv 2\pi R\tilde{M}^3$ and the 5D brane tension $\tilde{\lambda}$ to its 4D counterpart by $\lambda \equiv 2\pi R\tilde{\lambda}$. The last term in (5.1) denotes the matter part of the action that is strictly localized on the

[2] In this chapter, we will also consider the case for which the compact brane dimension is no stabilized, and hence $R(t)$ is a function of time.

brane.

Given the symmetries of the system, it is most convenient to work in coordinates $X^A =: (t, x^i, y, \phi)$ where $\phi \in [0, 2\pi)$ labels the compact brane dimension.

5.1.1 Gaussian normal coordinates

We are looking for a classical background geometry which is independent of the compact extra-dimensional coordinate ϕ, as well as homogeneous and isotropic (and for simplicity spatially flat) in the three spatial brane dimensions, labeled by the coordinates x^i. The most general metric ansatz can thus be written as

$$\mathrm{d}s^2 = -\mathrm{e}^{2n(t,y)}\mathrm{d}t^2 + \mathrm{e}^{2f(t,y)}\mathrm{d}t\,\mathrm{d}y + \mathrm{e}^{2a(t,y)}\delta_{ij}\mathrm{d}x^i\mathrm{d}x^j + \mathrm{e}^{2b(t,y)}\,\mathrm{d}y^2 + \mathrm{e}^{2c(t,y)}\,\mathrm{d}\phi^2\ , \tag{5.2}$$

where y is the coordinate corresponding to the infinite extra dimension. The brane's position in extra-space will then in general be given by a worldline of the form $(t, y_0(t))$. To make the junction conditions as simple as possible, however, it is convenient to introduce *Gaussian normal coordinates* (cf. [125, 158]): the new radial coordinate (which we will call y again) is defined to be the proper distance along space-like geodesics perpendicular to the brane. This is always possible (at least locally; the geodesics can in principle cross at some finite distance away from the brane, which would lead to a coordinate singularity at that point), and implies that:

- the brane is located at the fixed coordinate $y = 0$;
- the metric now takes the form[3]

$$\mathrm{d}s^2 = \mathrm{d}y^2 + \sum_{x^A \neq y} g_{AB}\,\mathrm{d}x^A\mathrm{d}x^B \tag{5.3a}$$

$$= -\mathrm{e}^{2n(t,y)}\mathrm{d}t^2 + \mathrm{e}^{2a(t,y)}\delta_{ij}\mathrm{d}x^i\mathrm{d}x^j + \mathrm{d}y^2 + \mathrm{e}^{2c(t,y)}\mathrm{d}\phi^2\ ; \tag{5.3b}$$

- the brane coordinates can be trivially identified through $\tilde{x}^\alpha := X^\alpha \equiv (t, x^i, \phi)$ (this further implies that $\tilde{g}_{\alpha\beta} = g_{D\alpha\beta}$).

In Gaussian normal coordinates, implementing Israel's junction conditions [100, 101] is equivalent to inserting delta function terms into Einstein's field equations. The complete set of equations of motion can thus be written as

$$M_6^4 G^{(6)}_{AB} = \delta(y)\delta^a_A\delta^b_B\left(\tilde{T}_{\alpha\beta} - \tilde{M}^3\,\tilde{G}_{\alpha\beta}\right)\ . \tag{5.4}$$

Here, $\tilde{\boldsymbol{T}}$ is the 5D energy momentum tensor localized on the brane. The most general form compatible with the symmetries of our setup that it can take is

$$\tilde{\boldsymbol{T}} = \mathrm{diag}\left(-\tilde{\rho},\, \tilde{p},\, \tilde{p},\, \tilde{p},\, \tilde{p}_\phi\right)\ . \tag{5.5}$$

[3] By a slight abuse of notation, we use the same names for the coordinates and functions as before.

The pressure component in angular direction ϕ can be used to stabilize the brane circumference. We will come back to this point later. Again, note that (5.4) is equivalent to the system (2.6) and (2.9).

For an observer living on the brane, only the intrinsic brane curvature can be directly inferred from gravitational or cosmological measurements. Thus, it would be extremely useful to derive the modified Friedmann equations stemming from (5.4) which describe the evolution of the scale factor on the brane, but without having to solve for the full bulk geometry. Therefore, one of the main purposes of this paper consists in deriving a closed system for the variables $a_0(t) := a(t,0)$, $c_0(t) := c(t,0)$ and $n_0(t) := n(t,0)$ which are evaluated at the position of the brane $y = 0$.

In fact, we can already make our lives a bit easier by employing the residual gauge freedom of (5.3), viz. a redefinition of the time coordinate t at the position of the brane, to set $n_0 \equiv 0$. As a result, the induced metric that a brane observer can measure is given by

$$\mathrm{d}s_5^2 = -\mathrm{d}t^2 + \mathrm{e}^{2a_0(t)}\delta_{ij}\mathrm{d}x^i\mathrm{d}x^j + \mathrm{e}^{2c_0(t)}\mathrm{d}\phi^2\,, \tag{5.6}$$

and we would like to determine the two unknown functions $a_0(t)$ and $c_0(t)$ for any given matter source.

5.1.2 Bulk-brane system

In order to illustrate the basic properties of the system (5.4), let us write down Einstein's field equations explicitly. Inserting (5.3) into (5.4) results in five independent equations for the functions $n(t,y)$, $a(t,y)$ and $c(t,y)$:

$$(tt): \quad \mathrm{e}^{-2n}\left(-3\dot{a}^2 - 3\dot{a}\dot{c}\right) + 6a'^2 + 3a'c' + c'^2 + 3a'' + c'' = -\frac{\delta(y)}{M_6^4}\,\tilde{\rho}_{\text{eff}} \tag{5.7a}$$

$$(ii): \quad \mathrm{e}^{-2n}\left(-3\dot{a}^2 - 2\dot{a}\dot{c} - \dot{c}^2 + 2\dot{a}\dot{n} + \dot{c}\dot{n} - 2\ddot{a} - \ddot{c}\right) \tag{5.7b}$$
$$+ 3a'^2 + 2a'c' + c'^2 + 2a'n' + c'n' + n'^2 + 2a'' + c'' + n'' = \frac{\delta(y)}{M_6^4}\,\tilde{p}_{\text{eff}}$$

$$(\phi\phi)-(yy): \quad \mathrm{e}^{-2n}\left(3\dot{a}\dot{c} + \dot{c}^2 - \dot{c}\dot{n} + \ddot{c}\right) \tag{5.7c}$$
$$+ 3a'^2 - 3a'c' - c'n' + n'^2 + 3a'' + n'' = \frac{\delta(y)}{M_6^4}\,\tilde{p}_{\phi,\text{eff}}$$

$$(yy): \quad \mathrm{e}^{-2n}\left(-6\dot{a}^2 - 3\dot{a}\dot{c} - \dot{c}^2 + 3\dot{a}\dot{n} + \dot{c}\dot{n} - 3\ddot{a} - \ddot{c}\right) \tag{5.7d}$$
$$+ 3a'^2 + 3a'c' + 3a'n' + c'n' = 0$$

$$(ty): \quad \mathrm{e}^{-2n}\left(3a'\dot{a} - 3n'\dot{a} + c'\dot{c} - n'\dot{c} + 3\dot{a}' + \dot{c}'\right) = 0 \tag{5.7e}$$

Here, a dot is shorthand notation for the partial derivative ∂/∂_t, and a prime denotes ∂/∂_y. Furthermore, we employ a notation in which all the brane induced terms are absorbed in modified expressions for the pressures and the energy density. This is useful because many

of the general statements in this paper do not depend on the existence of the brane induced gravity term and would therefore equally apply in a setup where only a perfect fluid source is localized on the brane. Specifically,

$$\tilde{\rho}_{\text{eff}} := \tilde{\rho} - 3\tilde{M}^3 \left(H_a^2 + H_a H_c\right) , \tag{5.8a}$$

$$\tilde{p}_{\text{eff}} := \tilde{p} + \tilde{M}^3 \left(2\dot{H}_a + \dot{H}_c + 3H_a^2 + H_c^2 + 2H_a H_c\right) , \tag{5.8b}$$

$$\tilde{p}_{\phi,\text{eff}} := \tilde{p}_\phi + 3\tilde{M}^3 \left(\dot{H}_a + 2H_a^2\right) . \tag{5.8c}$$

Here we also introduced the two "Hubble" parameters associated with the on-brane metric (5.6), $H_a := \dot{a}_0$ and $H_c := \dot{c}_0$, measuring the expansion rate in x^i and ϕ direction, respectively.

5.1.3 On-brane equations

In the general case, equations (5.7) constitute a complicated system of PDEs. However, we are only interested in the on-brane dynamics, i.e. in the dynamics of the variables evaluated at $y = 0$. The idea is to extract this information from the system without knowing the detailed y-profile of the metric functions.

But we then have to face the question of how to deal with the y-derivatives of the metric functions in (5.7). The appearance of the delta functions will introduce a non-regular behavior of the solution in y-direction at the position of the brane. In fact, the only possibility to create the delta functions consists in assuming that terms with two y-derivatives themselves contain a part that is proportional to a delta function, so that we can write

$$a'' = \hat{a}'' + \delta(y)\,[a'] , \tag{5.9a}$$

$$c'' = \hat{c}'' + \delta(y)\,[c'] , \tag{5.9b}$$

$$n'' = \hat{n}'' + \delta(y)\,[n'] , \tag{5.9c}$$

where $\hat{a}''$, $\hat{c}''$ and $\hat{n}''$ do not contain any further delta function contributions. The squared brackets denote the *jump* of the first derivative of the corresponding quantity across the brane,

$$[f] := f(t, 0^+) - f(t, 0^-) , \tag{5.10}$$

where f is an arbitrary function of t and y.[4] This allows us to match all delta function

[4]For notational convenience, we omit the subscript "disc" introduced in (2.10).

parts of the equations (5.7), yielding the following *junction conditions*:

$$(tt): \qquad 3\,[a'] + [c'] = -\frac{1}{M_6^4}\,\tilde{\rho}_{\text{eff}} \tag{5.11a}$$

$$(ii): \qquad 2\,[a'] + [c'] + [n'] = \frac{1}{M_6^4}\,\tilde{p}_{\text{eff}} \tag{5.11b}$$

$$(\phi\phi): \qquad 3\,[a'] + [n'] = \frac{1}{M_6^4}\,\tilde{p}_{\phi,\text{eff}} \tag{5.11c}$$

The (yy) and (ty) equations do not contain any delta functions.[5] Solving (5.11) for the jumps yields

$$[a'] = \frac{1}{4M_6^4}\left(\tilde{p}_{\phi,\text{eff}} - \tilde{p}_{\text{eff}} - \tilde{\rho}_{\text{eff}}\right)\,, \tag{5.12a}$$

$$[c'] = \frac{1}{4M_6^4}\left(3\tilde{p}_{\text{eff}} - 3\tilde{p}_{\phi,\text{eff}} - \tilde{\rho}_{\text{eff}}\right)\,, \tag{5.12b}$$

$$[n'] = \frac{1}{4M_6^4}\left(\tilde{p}_{\phi,\text{eff}} + 3\tilde{p}_{\text{eff}} + 3\tilde{\rho}_{\text{eff}}\right)\,. \tag{5.12c}$$

There is more information that can be extract from the system (5.7) in a small vicinity of the brane. As the metric functions themselves are allowed to have a kink at the position of the brane, the first y-derivatives (a', b' and n'), as well as the non-distributional parts of the second y-derivatives ($\hat{a}''$, $\hat{b}''$ and $\hat{n}''$) posses a discontinuity at the position of the brane. It is fully characterized by the jump, as defined in (5.10), as well as the *mean* across the brane,

$$\langle f\rangle := \frac{f(t,0^+) + f(t,0^-)}{2}\,. \tag{5.13}$$

Thus, in order to derive further on-brane equations, we simply have to calculate the jump and the mean of each equation in the system (5.7). In fact, these are all the on-brane equations that can be extracted from the full set of Einstein equations. Since there are terms that are quadratic in the discontinuous functions, we use the relations

$$[fg] = [f]\,\langle g\rangle + [g]\,\langle f\rangle \qquad \text{and} \qquad \langle fg\rangle = \langle f\rangle\langle g\rangle + \frac{1}{4}\,[f]\,[g]\,, \tag{5.14}$$

which hold for any arbitrary functions $f(y)$ and $g(y)$. By that procedure the five PDEs are reduced to a system of ten ODEs in the variable t. Since the (tt), (ii) and $(\phi\phi)$ components of the Einstein equations are second order in y-derivatives, they yield six equations which can be used to solve for $[f'']$ and $\langle f''\rangle$ with $f \in \{a, n, c\}$. The (yy) and (ty) components, which are both first order in y-derivatives, yield the remaining four equations:

[5] Note that this set of equations is equivalent to Israel's junction conditions (2.9).

$$[yy]:\ 3\,[a']\Big(2\langle a'\rangle+\langle c'\rangle+\langle n'\rangle\Big)+[c']\Big(3\langle a'\rangle+\langle n'\rangle\Big)+[n']\Big(3\langle a'\rangle+\langle c'\rangle\Big)=0\,, \tag{5.15a}$$

$$\langle yy\rangle:\ \frac{3}{4}\,[a']\Big([a']+[c']+[n']\Big)+\frac{1}{4}\,[c']\,[n']+3\langle a'\rangle\Big(\langle a'\rangle+\langle c'\rangle+\langle n'\rangle\Big)+\langle c'\rangle\langle n'\rangle \tag{5.15b}$$
$$-6H_a^2-3H_aH_c-H_c^2-3\dot{H}_a-\dot{H}_c=0\,,$$

$$[ty]:\ 3H_a\Big([a']-[n']\Big)+H_c\Big([c']-[n']\Big)+3[\dot{a'}]+[\dot{c'}]=0\,, \tag{5.15c}$$

$$\langle ty\rangle:\ 3H_a\Big(\langle a'\rangle-\langle n'\rangle\Big)+H_c\Big(\langle c'\rangle-\langle n'\rangle\Big)+3\langle\dot{a'}\rangle+\langle\dot{n'}\rangle=0 \tag{5.15d}$$

It is straightforward to check that after inserting (5.12) in equation (5.15c), it becomes

$$\dot{\tilde{\rho}}+3H_a\,(\tilde{\rho}+\tilde{p})+H_c\,(\tilde{\rho}+\tilde{p}_\phi)=0\,. \tag{5.16}$$

This is nothing but the t-component (which due to the symmetries is the only non-trivial one) of the covariant conservation of the energy momentum tensor as defined in (5.5), $\tilde{\boldsymbol{\nabla}}\tilde{\boldsymbol{T}}=0$. Note that the brane induced gravity terms dropped out in (5.16) due to the Bianchi identity.

Let us now discuss the system (5.15) of ODEs qualitatively. Since $[a']$, $[c']$ and $[n']$ can be expressed by virtue of (5.8) and (5.12) in terms of a_0 and c_0 (and their time-derivatives), this constitutes a system of *four* second order differential equations (with respect to t) for the *six* unknown functions $\langle a'\rangle, \langle c'\rangle, \langle n'\rangle, a_0, c_0$ and ρ. (The pressure functions $\tilde{p}$ and $\tilde{p}_\phi$ are not independent since they are linked to $\tilde{\rho}$ via an equation of state.) Consequently, the system is not closed and does not allow to determine the on-brane evolution in a deterministic way by simply fixing certain initial values at the position of the brane.

There is a very simple physical explanation for this failure (already encountered in the case of the cosmic string universe in Chap. 3): The evolution on the brane strongly depends on the wave content in the bulk. One can prepare gravitational waves (nonlinear wave solutions of the vacuum Einstein equations) in the bulk at some initial moment of time t_i. These waves will propagate towards the brane and eventually affect the on-brane evolution. In parlance of differential equations this is equivalent to fixing certain initial conditions on a space-like hypersurface in the bulk, i.e. $h(t_i,y)=f_h(y)$ as well as $\dot{h}(t_i,y)=g_h(y)$ for $h\in\{a,c,n\}$, subject to the constraints (5.7a) and (5.7e). The whole evolution in the bulk *and* on the brane is then uniquely determined by the system of PDEs (5.7). Of course, in general the on-brane evolution will depend on $f_h(y)$ and $g_h(y)$ with $y\neq 0$ and it is not sufficient to fix initial values only at the position of the brane.

However, there is one prominent exception. For codimension one, which is the DGP model, this approach allows to derive a closed on-brane system [51]. One might wonder why this is possible because also in this case the brane-evolution should be influenced by the absorption of bulk waves. The solution to this puzzle is quite simple: In Sec. 5.2.2 we confirm that in this particular setup the Einstein equations do not allow for wave solutions in the bulk that are compatible with the symmetries of the system. Thus, in this case the

evolution is uniquely determined (up to one arbitrary constant of integration corresponding to a *static* curved bulk geometry [51]) by fixing initial values solely at the position of the brane. This can also be understood as a consequence of a generalization of Birkhoff's theorem to geometries with planar symmetry [162].

5.2 Interlude: Interpretation of the Weyl tensor

Now the question is whether it is still possible, by making some assumptions about the bulk geometry (but without solving for it), to arrive at a closed system of ODEs for the on-brane evolution. Since we are dealing with an empty bulk, a necessary condition we would like to impose is the absence of incoming gravitational waves from the bulk. As just argued, such incoming waves are the reason that the on-brane system is not closed. Therefore, we expect that imposing an "outgoing wave condition" will yield a closed system. This expectation is also consistent with the number of equations, because excluding incoming waves from the bulk on both sides of the brane would add two more equations to the system (5.15), which is exactly the number that is needed to get a closed system.

Let us from now on simplify the analysis by assuming a reflection symmetry $y \mapsto -y$ around the brane. For an empty bulk and the topology we are interested in, this assumption is quite natural. Regarding the on-brane system (5.15), it amounts to setting all mean values to zero. Consequently, equations (5.15a) and (5.15d) are satisfied identically. Recalling that (5.15c) is equivalent to the energy conservation equation (5.16) that allows to determine ρ, only equation (5.15a) is left, which now reduces to

$$\frac{3}{4}\,[a']\left([a']+[c']+[n']\right)+\frac{1}{4}\,[c']\,[n']-3\dot{H}_a-\dot{H}_c-6H_a^2-3H_aH_c-H_c^2=0\,. \tag{5.17}$$

The remaining variables are a_0 and c_0, so the system is still under-determined, as expected. Due to the y-symmetry, an outgoing wave condition would now only add one equation and should thus again yield a closed system.

The gravitational wave content of a metric is encoded in the Weyl tensor. In order to formulate an outgoing wave condition, it is therefore natural to ask whether the Weyl tensor can be decomposed in such a way that certain components can be identified as incoming or outgoing waves. And indeed, it is possible—at least in certain situations—to find such a decomposition of the Weyl tensor. To be specific, it can be obtained by looking at the geodesic deviation the waves cause for nearby freely falling test particles. This was first done in four spacetime dimensions by Szekeres [160] and more recently generalized to arbitrary dimensions by Podolsky and Svarc [144]. The result is that the Weyl tensor can be decomposed into components corresponding to transverse and longitudinal, outgoing and incoming gravitational waves, as well as Newton-like parts.

Note that it was recently realized [97] that this interpretation is in fact not applicable to cylindrical geometries. More precisely, it was shown that in four-dimensional geometries with whole-cylinder symmetry, static configurations give rise to non-vanishing wave-like field components, and correspondingly, dynamic ER waves can not be separated

into incoming and outgoing parts by this procedure. In our setup, however, the expected gravitational waves are plane waves, for which the decomposition of the Weyl tensor was confirmed in [97] to work perfectly well.

5.2.1 Gravitational compass

We will now briefly review the aforementioned decomposition of the Weyl tensor in D spacetime dimensions [160, 144], and then apply it to the concrete metric that we are interested in. In this section, capital Latin indices $A, B, \ldots$ denote D-dimensional spacetime indices and small Latin indices $a, b, \ldots$ correspond to the D tetrad indices (as opposed to the definition in Tab. 1); D-dimensional vectors are written in boldface.

First, one considers a time-like geodesic with unit tangent vector $\mathbf{t}$ and chooses an orthonormal space-like vector $\mathbf{x}$, which will correspond to the direction of wave-propagation. These two vectors are combined into two null vectors

$$\mathbf{k} := \frac{1}{\sqrt{2}}(\mathbf{t} + \mathbf{x}), \qquad \mathbf{l} := \frac{1}{\sqrt{2}}(\mathbf{t} - \mathbf{x}), \tag{5.18}$$

and complemented with $D-2$ further orthonormal vectors $\mathbf{m}_p$ ($p = 2, \ldots, D-1$) to form a real null tetrad, or *mixed tetrad*[6]

$$\mathbf{m}_a = (\mathbf{m}_0, \mathbf{m}_1, \mathbf{m}_p) := (\mathbf{k}, \mathbf{l}, \mathbf{m}_p). \tag{5.19}$$

The indices $\{p, q, \ldots\}$ correspond to the $D-2$ space-like tetrad components and have the range $(2, \ldots, D-1)$. By construction, these tetrad vectors now satisfy the quasi orthonormality relations

$$\mathbf{k}\cdot\mathbf{k} = \mathbf{l}\cdot\mathbf{l} = 0, \qquad \mathbf{k}\cdot\mathbf{l} = -1 \tag{5.20a}$$

$$\mathbf{m}_p\cdot\mathbf{k} = \mathbf{m}_p\cdot\mathbf{l} = 0, \qquad \mathbf{m}_p\cdot\mathbf{m}_q = \delta_{pq}. \tag{5.20b}$$

This frame is useful because certain components of the Weyl tensor[7] in this frame,

$$C_{abcd} = C_{ABCD}\, m_a^A m_b^B m_c^C m_d^D, \tag{5.21}$$

can be given a physical interpretation by looking at the geodesic deviation they induce for nearby freely falling test particles. For instance, the term $\Omega_{pq} := C_{0p0q}$ will deform a sphere of test particles lying in the hyperplane orthogonal to $\mathbf{x}$ into an ellipsoid in this hyperplane and is therefore interpreted as a transverse gravitational wave component. The result is summarized in Table 5.1. However, note that this interpretation fails in certain cases [97],

[6] In 4D, it is possible to construct a complete null tetrad by taking complex combinations of the space-like vectors [160]. But this is not necessary, and does not work for odd numbers of dimensions.

[7] The Weyl tensor is defined as the traceless part of the Riemann tensor, i.e. $C_{ABCD} := R_{ABCD} - \frac{2}{D-2}\left(R_{A[C}g_{B]D} - R_{B[C}g_{D]A}\right) + \frac{2}{(D-1)(D-2)} R\, g_{A[C}g_{D]B}$.

as already mentioned. The components

$$C_{0pqr}, C_{pqrs}, C_{01pq} \text{ and } C_{1pqr}, \tag{5.22}$$

which do not appear in this list, have no effect on the geodesic deviation at linear order and are thus not observable at this level.

Component	Name	Identities	Interpretation
C_{0p0q}	Ω_{pq}	$\Omega_{pq} = \Omega_{qp}$ $\Omega^p{}_p = 0$	Transverse gravitational wave propagating in the direction $-\mathbf{x}$
C_{010p}	Ψ_p		Longitudinal gravitational wave propagating in the direction $-\mathbf{x}$
C_{0101} C_{0p1q}	Φ Φ_{pq}	$\Phi + \Phi^p{}_p = 0$	Newton-like part of the gravitational field
C_{101p}	Ψ'_p		Longitudinal gravitational wave propagating in the direction $+\mathbf{x}$
C_{1p1q}	Ω'_{pq}	$\Omega'_{pq} = \Omega'_{qp}$ $\Omega'^p{}_p = 0$	Transverse gravitational wave propagating in the direction $+\mathbf{x}$

Table 5.1: The standard interpretation [160, 144] of the components of the Weyl tensor. The indices $(0, 1, p)$ correspond to the mixed tetrad indices as in equation (5.19), and the notation for the individual components follows [59]. The listed identities follow directly from the symmetries and tracelessness of the Weyl tensor. For cases where the given interpretation fails, see [97].

5.2.2 Digression: DGP model

Before we investigate the six-dimensional scenario, let us first take a look at the 5D case, i.e. the DGP model. The five-dimensional metric describing a cosmological evolution on the brane can be written in the form

$$\mathrm{d}s^2 = -\mathrm{e}^{2n(t,y)}\mathrm{d}t^2 + \mathrm{e}^{2a(t,y)}\delta_{ij}\mathrm{d}x^i\mathrm{d}x^j + \mathrm{d}y^2. \tag{5.23}$$

One obvious choice of a mixed tetrad associated with this metric is[8]

$$\mathbf{k} = \frac{1}{\sqrt{2}}\left(\mathrm{e}^{-n}\boldsymbol{\partial}_t + \boldsymbol{\partial}_y\right), \quad \mathbf{l} = \frac{1}{\sqrt{2}}\left(\mathrm{e}^{-n}\boldsymbol{\partial}_t - \boldsymbol{\partial}_y\right), \quad \mathbf{m}_i = \mathrm{e}^{-a}\boldsymbol{\partial}_i, \tag{5.24}$$

where we chose $\mathbf{x} = \boldsymbol{\partial}_y$, which is the spatial direction perpendicular to the brane. However, there is a problem with this choice of tetrad: For the interpretation discussed above to apply, the time-like vector must be tangent to a geodesic. But $\mathrm{e}^{-n}\boldsymbol{\partial}_t$ is in general *not*

[8]Note that from now on the index range for $\{i, j, \ldots\}$ should be understood to be $(2, 3, 4)$ in order to be consistent with the index range for the tetrad components.

parallel transported along its integral curves, so the frame (5.24) can actually not be used. However, since the metric (5.23) admits the Killing vectors $\mathbf{m}_i$, it is clear that there are geodesics with tangent vectors of the form $\mathbf{t} = f\boldsymbol{\partial}_t + g\boldsymbol{\partial}_y$ with some functions $f(t,y), g(t,y)$. The various orthonormality relations among the vectors then imply that the resulting null vectors will have the form $\alpha^{\pm 1}\left[\mathrm{e}^{-n}\boldsymbol{\partial}_t \pm \boldsymbol{\partial}_y\right]$ with some function $\alpha(t,y)$. Therefore, the Weyl components in the frame (5.24), will only differ from the ones for which the physical interpretation was derived by some overall (nonzero) factors. But since the main purpose is to set some of those components equal to zero, we do not care about those factors and will thus use the frame (5.24) in the following.

Having established the frame, it is now straightforward to compute the various Weyl components. It turns out that *all of the wave components vanish identically*:

$$\Omega_{ij} = \Psi_i = 0 = \Omega'_{ij} = \Psi'_i. \tag{5.25}$$

This means that the symmetries we assumed (3D isotropy and homogeneity) do not admit any propagating waves in the case of one extra dimension.[9] The only non-vanishing components are the Newton-like fields. Due to the symmetry and the traceless condition they are not all independent. In fact, there is only one independent component:

$$\Phi = 3\left(a'^2 - \mathrm{e}^{-2n}\dot{a}^2\right), \qquad \Phi_{ij} = -\frac{1}{3}\Phi\,\delta_{ij}. \tag{5.26}$$

Note that this term was simplified by using the vacuum Einstein equations to eliminate all second y-derivatives as well as the second t-derivative of a.

(For completeness, it should be mentioned that there are also some non-vanishing Weyl components in the non-observable sector (5.22). They are given by

$$C_{ijkl} = -\frac{1}{3}\Phi\left(\delta_{ik}\delta_{jl} - \delta_{jk}\delta_{il}\right), \tag{5.27}$$

so they contain no further independent components. Their appearance follows from the Newton-like terms (5.26) by the traceless condition $C^i{}_{jik} = C_{0j1k} + C_{1j0k} = \Phi_{jk} + \Phi_{kj}$.)

The impossibility of gravitational waves in the bulk is an important feature, which is special to the codimension-one case. It implies that one can find a closed system of ODEs governing the on-brane evolution, without making any further assumptions about the bulk geometry. If bulk waves were possible, one could always prepare initial conditions in the bulk which could propagate towards the brane, leading to any arbitrary on-brane evolution. This is in agreement with the results of [20, 51], where it was shown that the bulk Einstein field equations, together with the brane matching conditions suffice to derive a unique 4D modified Friedmann equation, containing only one arbitrary constant $\mathcal{C}$. In fact, our findings show why this program was possible at all. Furthermore, $\mathcal{C}$ vanishes

[9] This can also be seen from the well known fact that there is a generalized version of Birkhoff's theorem to geometries with planar symmetry [162].

if and only if the Newton term Φ (and thus the Weyl tensor) is zero, confirming the physical interpretation of the constant as the Levi-Civita curvature parameter [113] (or the Schwarzschild mass parameter for non-vanishing spatial curvature [51]) in accordance with the discussion of Sec. 5.2.2. Finally, taking the mean of $\Phi = 0$ together with the junction condition readily yields (after assuming $\langle a' \rangle = 0$ due to symmetry)

$$H_a = -\frac{\epsilon}{6M_5^3}\rho_{\text{eff}} \equiv -\frac{\epsilon}{6M_5^3}\left(\rho - 3M_{\text{Pl}}^2 H_a^2\right), \tag{5.28}$$

which is exactly the modified Friedmann equation (3.1) with $\mathcal{C} = 0$, and $\epsilon = \pm 1$ chooses the branch.

5.3 Modified Friedmann equations

5.3.1 Excluding incoming waves

Let us now come back to the case of two extra dimensions, where the metric in Gaussian normal coordinates reads

$$\mathrm{d}s^2 = -\mathrm{e}^{2n(t,y)}\mathrm{d}t^2 + \mathrm{e}^{2a(t,y)}\delta_{ij}\mathrm{d}x^i\mathrm{d}x^j + \mathrm{d}y^2 + \mathrm{e}^{2c(t,y)}\mathrm{d}\phi^2. \tag{5.29}$$

The mixed orthonormal tetrad for this metric is

$$\mathbf{k} = \frac{1}{\sqrt{2}}\left(\mathrm{e}^{-n}\boldsymbol{\partial}_t + \boldsymbol{\partial}_y\right), \quad \mathbf{l} = \frac{1}{\sqrt{2}}\left(\mathrm{e}^{-n}\boldsymbol{\partial}_t - \boldsymbol{\partial}_y\right), \quad \mathbf{m}_i = \mathrm{e}^{-a}\boldsymbol{\partial}_i, \quad \mathbf{m}_\phi = \mathrm{e}^{-c}\boldsymbol{\partial}_\phi. \tag{5.30}$$

Again, the physical interpretation of Sec. 5.2.1 does not directly apply to this frame, because $\mathrm{e}^{-n}\boldsymbol{\partial}_t$ is not tangent to a geodesic. But repeating the reasoning of Sec. 5.2.2, one finds that this will only change the corresponding Weyl components by overall factors, which we are not interested in anyway. The straightforward calculation then gives:

$$\Omega_{ij} = \Omega^{(\mathrm{L})}\delta_{ij}, \qquad \Omega_{\phi\phi} = -3\Omega^{(\mathrm{L})}, \qquad \Omega_{i\phi} = 0 \tag{5.31a}$$

$$\Psi_i = 0 \tag{5.31b}$$

$$\Phi_{ij} = \Phi^{(x)}\delta_{ij}, \qquad \Phi_{\phi\phi} = \Phi^{(\phi)} \qquad \Phi = -3\Phi^{(x)} - \Phi^{(\phi)} \tag{5.31c}$$

$$\Psi_i' = 0 \tag{5.31d}$$

$$\Omega_{ij}' = \Omega^{(\mathrm{R})}\delta_{ij}, \qquad \Omega_{\phi\phi}' = -3\Omega^{(\mathrm{R})}, \qquad \Omega_{i\phi}' = 0 \tag{5.31e}$$

with

$$\Omega^{(\mathrm{L})} = -\frac{a'c'}{2} - \frac{c'n'}{3} - \frac{\mathrm{e}^{-n}}{4}\left(a'\dot{a} - c'\dot{c} - n'\dot{a} + n'\dot{c} + \dot{a}' - \dot{c}'\right) + \frac{\mathrm{e}^{-2n}}{6}\left(3\dot{a}\dot{c} + 2\dot{c}^2 - 2\dot{c}\dot{n} + 2\ddot{c}\right) \tag{5.32a}$$

$$\Phi^{(x)} = -a'^2 - \frac{a'c'}{2} + \frac{\mathrm{e}^{-2n}}{2}\left(2\dot{a}^2 + \dot{a}\dot{c}\right) \tag{5.32b}$$

$$\Phi^{(\phi)} = \frac{3}{2}\left(-a'c' + \mathrm{e}^{-2n}\dot{a}\dot{c}\right) \tag{5.32c}$$

$$\Omega^{(\mathrm{R})} = -\frac{a'c'}{2} - \frac{c'n'}{3} + \frac{\mathrm{e}^{-n}}{4}\left(a'\dot{a} - c'\dot{c} - n'\dot{a} + n'\dot{c} + \dot{a}' - \dot{c}'\right) + \frac{\mathrm{e}^{-2n}}{6}\left(3\dot{a}\dot{c} + 2\dot{c}^2 - 2\dot{c}\dot{n} + 2\ddot{c}\right) \tag{5.32d}$$

which were again simplified by using the vacuum Einstein equations to eliminate all second y-derivatives as well as the second t-derivative of a.

(As in 5D, there are also some non-zero Weyl components in the class of terms (5.22). But again, they do not contain any new independent terms, and their appearance is required by the traceless conditions of the Weyl tensor.)

So in a six-dimensional geometry with (spatially flat) 3D isotropy and homogeneity on the brane as well as rotational symmetry around the compact extra dimension, the Weyl tensor is completely characterized by the four components (5.32). According to the standard interpretation, they correspond to left-moving (i.e. propagating in direction $-\mathbf{y}$) gravitational waves $\Omega^{(\mathrm{L})}$, to two independent Newton-like field components $\Phi^{(x)}, \Phi^{(\phi)}$, and to right-moving gravitational waves $\Omega^{(\mathrm{R})}$. As an aside, note that the appearance of wave-terms is only possible because the ϕ-direction is different from the x-directions in (5.29), reducing the symmetries of the metric. If one had set $c = a$ in this ansatz, the wave parts would have vanished identically, as in the 5D case.

As already mentioned, we expect the interpretation of the Weyl components to be correct in our set-up. Therefore, to exclude incoming bulk waves, we set $\Omega^{(\mathrm{L})}(y > 0) = 0$ and $\Omega^{(\mathrm{R})}(y < 0) = 0$. To convert these conditions into on-brane equations, we simply take the limit $y \to 0^+$ and $y \to 0^-$, respectively. Due to the $\mathbb{Z}_2$-symmetry, this yields one further on-brane equation:

$$[a'][c'] + \frac{2}{3}[c'][n'] + H_a\left([a'] - [n']\right) - H_c\left([c'] - [n']\right) + [\dot{a}'] - [\dot{c}'] - \frac{4}{3}\left(2\dot{H}_c + 3H_aH_c + 2H_c^2\right) = 0 \tag{5.33}$$

After using (5.12) to eliminate all the jumps, the two equations (5.17) and (5.33) indeed constitute a closed on-brane system of ODEs that in principle allows to solve for $a_0(t)$ and $c_0(t)$. Note that it is second order in both a_0 and c_0, and so one has to specify four initial conditions. However, we expect at least one of these constants (or some combination of them) to correspond to a parameter measuring the constant curvature of the bulk geometry. This also happens in the DGP case, with the (technical) difference that there the second

order ODE can be integrated once analytically, in which case the corresponding constant of integration turns out to be the Levi-Civita parameter $\mathcal{C}$ of the bulk geometry. The subsequent analysis of cosmological solutions is then usually simplified by setting $\mathcal{C} = 0$.

In the case at hand, an analytic integration of the ODEs does not seem feasible. However, the decomposition of the Weyl tensor still allows to identify the Newton-like parts of the bulk gravitational field, viz. (5.32b) and (5.32c). Therefore, setting them to zero should be analogous to setting $\mathcal{C} = 0$ in the DGP case. One might worry that this could add an additional independent on-brane equation thus leading to an over-determined system. However, as we will show now, this is not the case.

5.3.2 Zero Newton-like bulk fields

We will now assume that the bulk gravitational field does not contain any Newton-like components,

$$\Phi^{(x)} = 0, \quad \Phi^{(\phi)} = 0 \qquad\qquad (y \neq 0)\,. \tag{5.34}$$

Due to the mirror symmetry[10] in y, these conditions add two on-brane equations, which can be brought into the following form:

$$2H_a = \sigma\,[a']\,, \tag{5.35a}$$
$$2H_c = \sigma\,[c']\,, \tag{5.35b}$$

where $\sigma = \pm 1$. (Note that in deriving (5.35b), we divided by H_a, so for a static solution this equation would be absent.) Without making any assumptions about the wave components, for the moment, there are now three on-brane equations: (5.17), (5.35a) and (5.35b). However, it turns out that after using (5.35) in (5.17), it becomes identical to (5.15c) and thus to the energy conservation equation (5.16). *As a result, the two equations* (5.35) *constitute a consistent, closed system of ODEs for* $a_0(t)$ *and* $c_0(t)$.

This is rather surprising, because so far we have not made any assumptions about the wave content in the bulk, so a priori incoming waves could still be possible. Nonetheless, we arrived at a closed on-brane system. How can this be possible? To answer this question, let us evaluate the wave components of the Weyl tensor at the brane position, using the relations (5.35) [as well as (5.15c)]:

$$\Omega^{(\mathrm{R})}(0^+) = \Omega^{(\mathrm{L})}(0^-) = (1-\sigma)\Omega(t) \tag{5.36a}$$
$$\Omega^{(\mathrm{R})}(0^-) = \Omega^{(\mathrm{L})}(0^+) = (1+\sigma)\Omega(t) \tag{5.36b}$$
$$\Omega(t) := \frac{H_a\left(\dot{H}_c + H_c^2\right) - H_c\left(\dot{H}_a + H_a^2\right)}{3H_a + H_c} \tag{5.36c}$$

[10] Without assuming this symmetry, it turns out that the jumps of (5.34) together with (5.15a) imply — if $[a']\,, [c'] \neq 0$, which would otherwise yield $\tilde{\rho} = 0$ — that all the means have to vanish. In other words, zero Newton-like field components can only be achieved for (locally) symmetric configurations.

This shows that in the branch $\sigma = -1$ there are only waves propagating away from the brane, while the branch $\sigma = +1$ only allows for waves traveling towards the brane. Therefore, the absence of Newton-like field components implies that there are either purely incoming or purely outgoing waves, which allowed to arrive at the closed system (5.35).

We choose the $\sigma = -1$ branch, because we do not want any incoming bulk waves. After using (5.12), the modified Friedmann equations for this branch become

$$H_a = \frac{1}{8M_6^4}\left(\tilde{\rho}_{\text{eff}} + \tilde{p}_{\text{eff}} - \tilde{p}_{\phi,\text{eff}}\right) , \tag{5.37a}$$

$$H_c = \frac{1}{8M_6^4}\left(\tilde{\rho}_{\text{eff}} - 3\tilde{p}_{\text{eff}} + 3\tilde{p}_{\phi,\text{eff}}\right) . \tag{5.37b}$$

Since the outgoing wave components vanish, all solutions of these equations are contained in the larger class of solutions to the system discussed in the previous section. But they correspond only to those solutions for which the initial conditions are compatible with vanishing Newton-like field components. In that sense they are analogous to the $\mathcal{C} = 0$ solutions in the DGP model. However, while $\mathcal{C} = 0$ in the DGP case implies a completely flat bulk spacetime, here the situation is different because the geometry still allows for outgoing gravitational waves.

As already discussed, without setting the Newton-like components to zero the system of ODEs is second order for both a_0 and c_0. Now we see that — without the brane induced gravity terms — the system (5.37) is first order for both variables, so only two initial conditions need to be specified, and the "Newton = 0" solutions correspond to a two-dimensional subspace of the four-dimensional parameter space of initial conditions characterizing the most general outgoing wave solutions. The brane induced gravity terms, however, reintroduce second t-derivatives. But they only enter via the combination $\left(\dot{H}_a - \dot{H}_c\right)$, so there is one constraint left, and the number of required initial values equals three. Explicitly, the two modified Friedmann equations can for instance be written as:

$$\boxed{\begin{aligned} 3H_a + H_c &= \frac{1}{2M_6^4}\left[\tilde{\rho} - 3\tilde{M}^3\left(H_a^2 + H_a H_c\right)\right] , && \text{(5.38a)} \\ H_c &= \frac{1}{8M_6^4}\left[\rho - 3\tilde{p} + 3\tilde{p}_\phi + 3\tilde{M}^3\left(\dot{H}_a - \dot{H}_c + 2H_a^2 - 3H_a H_c - H_c^2\right)\right] && \text{(5.38b)} \end{aligned}}$$

As will be shown in the next section, the assumption (5.34) even allows to solve for the whole bulk geometry, confirming the picture of gravitational waves propagating off the brane into one infinite extra dimension, thus justifying the Weyl component procedure.

5.3.3 Analytic bulk profiles

In the appendix of [131], we provided a derivation of the full bulk solution under the assumption of vanishing Newton terms. Let us here simply state the result.

As a starting point, we take the functions $a_0(t)$ and $c_0(t)$, obtained by integrating (5.38) after choosing initial conditions as well as specific equations of state for the on-brane matter content. To present the bulk solution, we use new coordinates [for convenience still denoted by $X^A = (t, x^i, y, \phi)$]; in fact, they are equivalent to the ones used in the case of an axial symmetric system [cf. Eq. (3.3)]. Specifically, the metric reads

$$\mathrm{d}s^2 = \mathrm{e}^{2(\eta-3\alpha)}\left(-\mathrm{d}t^2 + \mathrm{d}y^2\right) + \mathrm{e}^{2\alpha}\delta_{ij}\mathrm{d}x^i\mathrm{d}x^j + \mathrm{e}^{-6\alpha}W^2\mathrm{d}\phi^2, \tag{5.39}$$

where η, α and W take the form

$$\alpha(t,y) = a_0(t-|y|)\,, \tag{5.40a}$$
$$W(t,y) = W_0(t-|y|)\,, \tag{5.40b}$$
$$\eta(t,y) = 3a_0(t+|y|) - \bar{\eta}(t+|y|) + \bar{\eta}(t-|y|)\,. \tag{5.40c}$$

The functions W_0 and $\bar{\eta}$ are then obtained by solving the system

$$\log W_0 = c_0 + 3a_0\,, \tag{5.41}$$
$$2\dot{\bar{\eta}} = \frac{\ddot{W}_0}{\dot{W}_0} + 12\frac{\dot{W}_0}{W_0}\dot{a}_0^2\,. \tag{5.42}$$

Thus, the bulk solution is fully determined once $\bar{\eta}$ is obtained by simply integrating the last equation (the corresponding initial condition is no physical choice as it simply corresponds to the freedom of rescaling (t, r) by a constant). The above solution already suggests that the bulk geometry is fully characterized by gravitational waves. In fact, α and W are outgoing plane waves. The solution for η still looks puzzling as it also contains terms that naively might be interpreted as incoming waves, e.g. $a_0(t+|y|)$. After all, we expended a lot of effort to exclude these contributions. However, so far it is not clear whether they are just coordinate artifacts and thus do not correspond to any observable effects. Fortunately, with the Weyl tensor, we have a tool at our disposal which admits a clear, and hence coordinate independent, statement. An evaluation of its (transverse wave) components yields:

$$\Omega^{(\mathrm{R})}(t,y) = \begin{cases} 0 & (y<0) \\ 2\left[\ddot{\alpha}_0(t-y) + 7\dot{\alpha}_0(t-y)^2 - 2\dot{\alpha}_0(t-y)\dot{\eta}_{\mathrm{out}>}(t-y)\right] & (y>0) \end{cases} \tag{5.43a}$$
$$\Omega^{(\mathrm{L})}(t,y) = \begin{cases} 2\left[\ddot{\alpha}_0(t+y) + 7\dot{\alpha}_0(t+y)^2 - 2\dot{\alpha}_0(t+y)\dot{\eta}_{\mathrm{out}>}(t+y)\right] & (y<0) \\ 0 & (y>0) \end{cases} \tag{5.43b}$$

This nicely confirms two things. First, there are no incoming wave components. In fact, they have been excluded by construction when deriving (5.40). And second, the nonzero components indeed represent outgoing plane waves because they only depend on $(t-|y|)$ [instead of $(t+|y|)$]. Both observations therefore constitute an important consistency check of our general approach. Moreover, from this we also learn that the outgoing waves are not mere coordinate artifacts, rather they can be observed by measuring the acceleration

of test particles as described in Sec. 5.2.1.

5.3.4 Cosmic string versus cosmic ring

The ansatz (5.29) is formally the same that would be used for a radially symmetric spacetime, with y taking the role of a radial coordinate as depicted in Fig. 5.1b. It could therefore be used for a model in which the brane is a codimension-two object living in two infinite extra dimensions. If the brane is regularized by blowing it up to a circle of finite radius, then also the action would formally take the same form as here in (5.1). After all, this is precisely the model we studied previously in Chap. 3. Thus, the aim of this section is to draw a clear distinction between both scenarios.

Let us stress that the solution derived here does not correspond to a codimension-two setup, but rather to the cylindrical embedding geometry depicted in Fig. 5.1a.[11] This can be seen in different ways: First of all, there is in general no axis—a place where $c = 0$—in our spacetime, as would be necessary for an axial symmetric geometry.[12] Furthermore, even if there were an axis, say, located at some $y_\mathrm{a} < 0$, then due to the mirror symmetry there would also be an axis at $-y_\mathrm{a} > 0$. More generally, the mirror symmetry is incompatible with a distinction between an interior and exterior region (as would be required in the codimension two setup). (Note that we did not need to enforce the mirror symmetry by hand, it already followed from the assumption of zero Newton-like Weyl components.) Finally, the full bulk solution that was presented in the last section explicitly shows that the spacetime describes plane waves, consistent with the one infinite (and one compact) extra dimension that we are modeling, but inconsistent with a codimension two picture in which we would expect cylindrical waves.

One also has to keep in mind that while the interpretation of the Weyl components works for planar symmetry, it fails for cylindrical geometries [97]. Hence, the outgoing wave criterion, which was rightfully used here in Sec. 5.3.1 to derive a closed on-brane system, could not be used for the codimension-two case. In fact, one cannot expect to be able to derive a closed on-brane system in that case, because there is no local outgoing wave criterion for cylindrical waves, already at the linear level. Therefore, in the codimension two system one has to deal with PDEs (i.e. the full set of Einstein equations) instead of simple ODEs, which is much more difficult to solve as we have seen in Chap. 3.

5.4 Cosmology

In this section, we discuss two types of cosmologies. One corresponding to a stabilized angular dimension and another one for which the stabilization is absent. While the first solution reproduces the DGP cosmology, the second one features a new type of degravitation mechanism.

[11] Note that in the present case the symmetry axis is not part of the manifold.

[12] This should not be confused with the axis that arises due to the embedding as it is not part of the physical manifold.

5.4.1 4D Friedmann on the ring

As already mentioned, the on-brane equations need to be supplemented with equations of state for both $\tilde{p}$ and $\tilde{p}_\phi$. For the former we shall assume a linear equation of state of the form $\tilde{p} = w\tilde{\rho}$, with some constant w. The latter, on the other hand, could for instance be used to stabilize the compact extra dimension. Let us now investigate the consequences of this scenario.

Stabilization means that we set $H_c = 0$. The azimuthal pressure $\tilde{p}_\phi$ that is needed to achieve this, can be read off from equation (5.38b) and allows to infer the corresponding equation of state

$$w_\phi := \frac{\tilde{p}_\phi}{\tilde{\rho}} = \frac{-1+3w}{2} - \frac{1+w}{2\sqrt{1+\chi}} + \frac{4}{3\chi}\left(\sqrt{1+\chi}-1\right) , \tag{5.44}$$

where $\chi := \tilde{M}^3\tilde{\rho}/(3M_6^8)$. For a pure 4D CC source ($w = -1$) this equation together with $\chi \geq 0$ implies $w_\phi \leq -\frac{4}{3}$. This shows that a stabilization requires unphysical matter leading to a violation of the NEC. For dust and radiation though, we find $w_\phi \geq -1$ and $w_\phi \geq -\frac{2}{3}$, respectively. Therefore, it is possible to implement a stabilization in these two cases by means of physical matter. In other words, the assumption of having a stabilized angular direction is only possible during a radiation or dust dominated epoch but no longer during a subsequent CC dominated epoch.

The corresponding evolution of $a_0(t)$ is determined by (5.38a), which now takes the form

$$3H_a = \frac{1}{2M_6^4}\left(\tilde{\rho} - 3\tilde{M}^3 H_a^2\right) . \tag{5.45}$$

It turns out that (5.45) is exactly the same modified Friedmann equation as in the DGP case (5.28). This can be seen by dimensionally reducing the brane induced energy density and Planck masses according to

$$\tilde{\rho} = \frac{\rho}{2\pi R}, \qquad \tilde{M}^3 = \frac{M_{\mathrm{Pl}}^2}{2\pi R}, \qquad M_6^4 = \frac{M_5^3}{2\pi R} , \tag{5.46}$$

where $R := \exp(c_0)$ (so that $2\pi R$ is the physical circumference of the compact extra dimension). The crossover is identified as $r_{c,1} := M_{\mathrm{Pl}}^2/(2M_5^3)$ in accordance with Sec. 2.2.1.

To be more precise, it is the *normal branch* of the DGP cosmology. The *self-accelerated branch* would be recovered by taking the $c_0 = \text{const}$ limit of the "incoming wave" solution ($\sigma = -1$). However, (5.36) immediately shows that the assumption $H_c = 0$ also implies that the wave components vanish, and the solution is in fact Riemann-flat. But then the result that we reproduced the DGP equation can physically be understood because the only difference to the DGP case is the addition of one trivial compact extra dimension to the geometry, which does not take part in the dynamics of the model at all.

Note that this "DGP branch/propagation direction" correspondence could serve as a physically justified criterion for dismissing the self-accelerated branch of the DGP cosmology, if one is willing to view this branch as a limiting case of one additional, approximately

constant, compact extra dimension, because in that case it would correspond to incoming bulk waves incompatible with a source-free bulk. As an aside note that the same observation was made on a linear level by studying the DGP brane-to-brane propagator in Sec. 2.2.1.

Form a phenomenological perspective, these solutions are promising because for early times ($H_a r_{c,1} \gg 1$) they reproduce the standard Friedmann evolution in analogy with the DGP model. However, for late times ($H_a r_{c,1} \lesssim 1$) there are two sources of modification. First, the bulk term, i.e. the left side of (5.45), starts to dominate. This effect alone would lead to a modification which is not different from the one in the DGP model. But there is a second modification due to the fact that the compact dimension cannot be stabilized once the evolution enters the tension (or CC) dominated epoch. The dynamics of the corresponding size modulus, described by H_c, as well as the presence of emitted bulk waves will affect the evolution significantly. Of course, in order to investigate this effect, it is necessary to resolve the stabilization mechanism dynamically. This could be done along the lines of Sec. 2.4.3 where a scalar field, living on the brane, winds around the compact dimension in order to stabilize it. This approach is beyond the scope of the present work and requires further study.

5.4.2 Degravitating a tension on the ring

There are of course other possible solutions in the class of (5.38), for which the size of the compact extra dimension is not stabilized at all, and which imply a different evolution of a_0. These solutions generically contain waves that are emitted into the bulk. As a specific representative of this class of solutions, we will consider the case of vanishing azimuthal pressure, $\tilde{p}_\phi = 0$. In that case, the energy conservation (5.16) implies that $\tilde{\rho}$ scales like

$$\tilde{\rho} \propto \mathrm{e}^{-3(1+w)a_0 - c_0} \,. \tag{5.47}$$

Hence, the dimensionally reduced 4D energy density scales like

$$\rho \equiv 2\pi R(t)\, \tilde{\rho} \propto \mathrm{e}^{c_0} \tilde{\rho} \propto \mathrm{e}^{-3(1+w)a_0} \,, \tag{5.48}$$

that is, exactly like in standard 4D GR without any extra dimensions. In particular, choosing $w = -1$ then implies that ρ is constant, in accordance with the interpretation of a 4D CC. This makes the choice $\tilde{p}_\phi = 0$ very special and can be viewed as a motivation for studying it. In fact, it is the only choice—apart from the stabilized scenario $H_c = 0$—which achieves this.

Denoting initial values by a subscript i, we need to specify $\tilde{\rho}_\mathrm{i}$, $a_{0\mathrm{i}}$, $c_{0\mathrm{i}}$ and e.g. $H_{a\mathrm{i}}$, in which case $H_{c\mathrm{i}}$ is determined by the constraint (5.38a). We can, however, without loss of generality[13], assume $a_{0\mathrm{i}} = c_{0\mathrm{i}} = 0$. The solutions for a_0 and c_0 are then uniquely determined by (5.38) for any given choice of $H_{a\mathrm{i}}$, $\check{\rho} := \tilde{\rho}_\mathrm{i}/M_6^4$ and $\check{r}_c := M_5^3/(2M_6^4)$.

Since the size of the compact dimension is not stabilized, we do not expect to have a

[13]The general solutions are obtained by substituting $a_0(t) \to a_0(t) + a_{0\mathrm{i}}$ and $c_0(t) \to c_0(t) + c_{0\mathrm{i}}$.

pure 4D regime for this solution. More precisely, in the regime where the brane induced term dominates, the corresponding size modulus $c_0(t)$ affects the gravitational dynamics in a non-trivial way. This can be seen directly from (5.38), where only for $H_c = 0$ the equations would take the standard Friedmann form in the limit $M_6 \to 0$.

Let us first focus on pure dust ($w = 0$) and pure tension ($w = -1$) solutions, before we discuss the general fluid containing both components and its phenomenological viability.

5.4.2.1 Pure dust

For $\tilde{p} = \tilde{p}_\phi = 0$, there exist exact solutions with $a_0(t) = c_0(t)$, satisfying

$$H_a = \frac{1}{8}\check{\rho}_{\rm dust}\, \mathrm{e}^{-4a_0} - \frac{3}{2}\check{r}_c\, H_a^2\,. \tag{5.49}$$

This is equivalent (apart from numerical factors) to the DGP modified Friedmann equation, sourced by radiation. The existence of this class of solutions can easily be understood because by setting $a = c$, the metric ansatz (5.6) can equally well describe a $(4+1)$-dimensional, spatially homogeneous and isotropic brane of one codimension. Thus, it is the straightforward generalization of the usual 4/5D DGP model to a 5/6D "DGP" setup. (In fact, this class of solutions could be extended to $\tilde{p} = \tilde{p}_\phi \neq 0$, with $\tilde{\rho}_{\rm dust} \propto \mathrm{e}^{-4(1+w)a_0}$.) Furthermore, in this case the wave components (5.36) vanish and the brane is thus embedded in a flat bulk geometry.

In this class of solutions, the initial conditions satisfy $H_{a\rm i} = H_{c\rm i}$. For $H_{a\rm i} \neq H_{c\rm i}$ the evolution will differ from the exact $a_0 = c_0$ one. But it turns out that it is an attractor solution, i.e. for late times the $a_0 = c_0$ solution is approached for generic initial conditions. This is shown in Fig. 5.2a, where some numerical solutions for H_a (dotted) and H_c (dashed) are plotted for fixed $\check{r}_c = 0.1L$ and $\check{\rho}_{\rm dust}L = 46/5$ but different $H_{a\rm i}$ (and thus different $H_{c\rm i}$ according to the constraint).[14] The solid line corresponds to $H_{a\rm i} = H_{c\rm i}$, and therefore $a_0 = c_0$ for all times. Note that while no gravitational waves are emitted into the bulk for the attractor solution, there are non-zero wave components (approaching zero as $t \to \infty$) for all other solutions.

5.4.2.2 Pure cosmological constant

For $\tilde{p} = -\tilde{\rho}_\lambda$ and $\tilde{p}_\phi = 0$, there are exact solutions of (5.38) with

$$a_0 = 0 \qquad \text{and} \qquad c_0 = \log(1 + \frac{\check{\rho}_\lambda}{2}t)\,. \tag{5.50}$$

So in this case the expansion is solely in angular (or ring) direction. From a 4D point of view, this can be viewed as a realization of the degravitation mechanism (cf. Sec.1.3), because the Hubble parameter in $\boldsymbol{x}$-direction is zero, despite the presence of an effective

[14] The parameters $\check{r}_c$ and $\check{\rho}$ are chosen such that $H_{ai} = H_{ci}$ holds iff $H_{ai} = 1$. L is an arbitrary length scale.

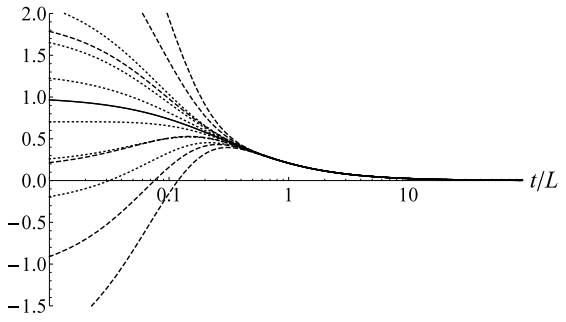

(a) Dust source ($w = 0$): The ring and brane expansion dynamics are identical for the attractor, corresponding to a 5/6D "DGP" regime.

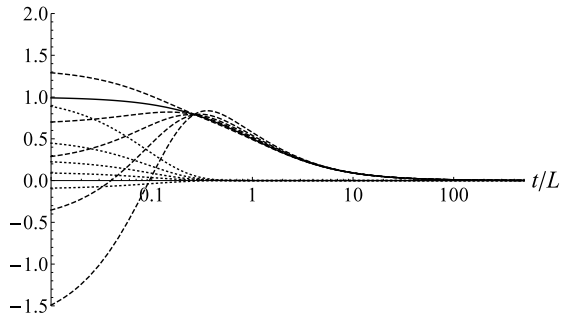

(b) CC source ($w = -1$): The attractor solution features degravitation because H_a is zero despite the presence of a CC.

Figure 5.2: The Hubble parameters H_a (dotted) and H_c (dashed) for different initial conditions generically approach the attractor solutions (solid lines). Time and the Hubble parameters are measured in units of an arbitrary (but fixed) length scale L.

4D CC ($= 2\pi R(t)\tilde{\rho}_\lambda = \text{const}$). Again, one can verify that these are attractor solutions, as can be seen from Fig. 5.2b. The dotted and dashed lines show numerical results for H_a and H_c, respectively, again for $\check{r}_c = 0.1L$ and $\check{\rho}_\lambda L = 46/5$ and different $H_{a\mathrm{i}}$ (as well as $H_{c\mathrm{i}}$). They asymptotically approach the solid lines, corresponding to the exact solution (5.50). As with the dust solutions, the outgoing wave components vanish for the attractor solutions, but are non-zero for the other solutions.

5.4.2.3 Dust and cosmological constant

For a fluid containing both dust and a CC, the solutions can in general only be obtained numerically. Since the dust contribution to $\tilde{\rho}$ falls off faster than that due to the CC, the late time asymptotic is that of the degravitating attractor (5.50). Depending on the other parameters, there can also be an intermediate regime in which the solution behaves like the $a_0 = c_0$ attractor. These attractor solutions are clearly not capable of explaining the evolution history of the universe as we observe it. But it is possible to have solutions that are far away from the attractors for early times, which might in principle still be in accordance with cosmological observations. However, a numerical analysis shows that the past evolution is never close to the standard 4D ΛCDM evolution. In Fig. 5.3, the scale factor e^{a_0} are plotted for various parameters. The black dashed line is the scale factor for standard ΛCDM with $\Omega_\Lambda = 0.72$. The crossover $\check{r}_c$ has the greatest impact on the evolution of e^{a_0}, while $\check{\rho}_{\mathrm{dust}}$ and $\check{\rho}_\lambda$ mainly influence e^{c_0} (which is not depicted). We find that the closest one can get to the standard 4D evolution is in the limit $\check{r}_c \to \infty$, in which case the behavior of e^{a_0} is practically insensitive to the parameters $\check{\rho}_{\mathrm{dust}}$ and $\check{\rho}_\lambda$.

There is a peculiarity related to the angular scale factor: if either $\check{\rho}_{\mathrm{dust}}$ or $\check{\rho}_\lambda$ is chosen

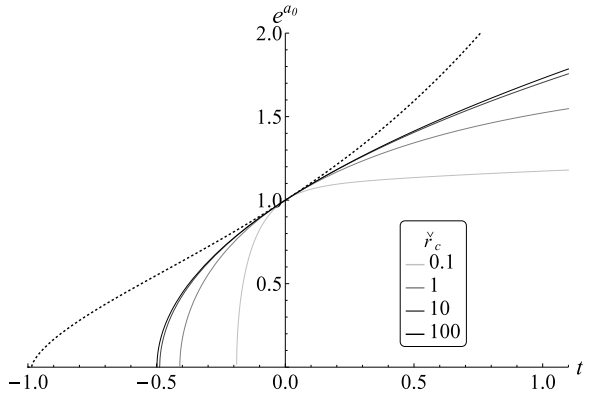

(a) The expansion history is always different from ΛCDM, it is closest though for $\check{r}_c \to \infty$. Here, we chose $\check{\rho}_\lambda = \check{\rho}_{\rm dust} = 1$; however, a different choice would not alter the qualitative outcome.

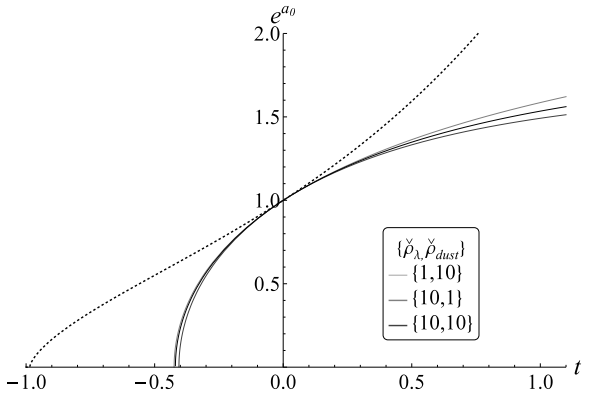

(b) Provided $\check{r}_c$ is large enough, the expansion history is almost insensitive to changes in $\check{\rho}_\lambda$ and $\check{\rho}_{\rm dust}$ (which predominantly affect e^{c_0}).

Figure 5.3: The scale factor e^{a_0} for various choices of parameters; the dashed black lines show the scale factor for a standard ΛCDM cosmology with $\Omega_\Lambda = 0.72$. All dimensionful quantities are measured in units of $H_{a\rm i}$.

too large, e^{c_0} becomes zero even before[15] the Big Bang in x-direction is reached, i.e. before $e^{a_0} = 0$. Thus, Fig. 5.3 only shows cases in which $\check{\rho}_{\rm dust}$ and $\check{\rho}_\lambda$ are small enough so that e^{c_0} turns around before it reaches zero, leading to a Kasner-like behavior close to the singularity (specifically, $e^{c_0} \to \infty$ for $e^{a_0} \to 0$). Hence, it is not possible to get much closer to the standard evolution (by further increasing $\check{\rho}_{\rm dust}$ or $\check{\rho}_\lambda$) than shown in these plots.

In summary, the closest one can get to the standard 4D evolution is in the limit $\check{r}_c \to \infty$, in which case the behavior of e^{a_0} is practically insensitive to the parameters $\check{\rho}_{\rm dust}$ and $\check{\rho}_\lambda$. However, even in this limit the evolution is very different from 4D ΛCDM. A corresponding supernova-fit[16] to the Union 2.1 data set [143] is shown in Fig. 5.4, and clearly rules out the $\tilde{p}_\phi = 0$ model.

5.5 Discussion

In this work the DGP model was generalized by introducing an additional compact brane dimension. Assuming 4D FRW symmetries on the brane, the cosmology of this setup was investigated. Subsequently, a closed system of modified Friedmann equations describing the brane curvature evolution was derived. This was achieved by excluding any incoming gravitational waves as required by a source-free bulk. To that end, an "outgoing wave criterion" based on a certain decomposition of the Weyl tensor was employed. Two physically

[15] We are looking backwards in time, so by "before" we mean larger t here.

[16] The fit does not converge but tends towards $r_c \to \infty$, thus becoming insensitive to $\bar{\rho}_{\rm dust}$ and $\bar{\rho}_{\rm cc}$, and approaching the form shown in the plot.

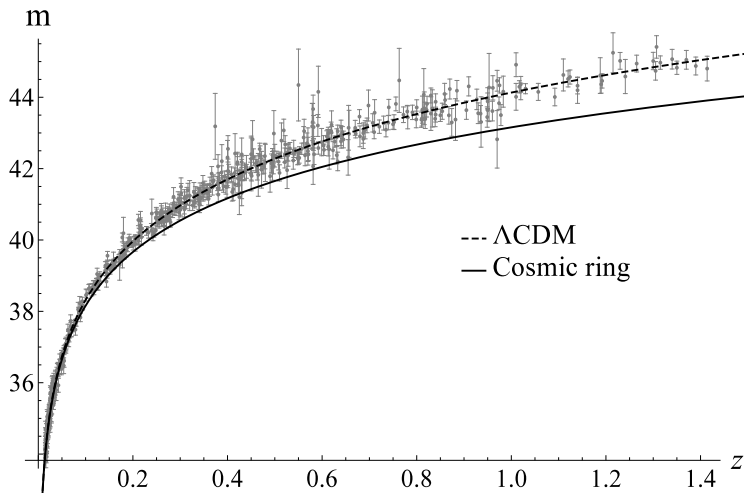

Figure 5.4: Magnitudes of the Union 2.1 SNe as function of redshift, together with the ΛCDM best fit ($\Omega_\Lambda = 0.72$). The dashed line is the best fit obtained for the modified Friedmann equations (5.38) with $\tilde{p}_\phi = 0$ and two fluid components ($w = 0$ and $w = -1$).

distinct realizations of this setup were considered:

1. *The compact brane direction is stabilized by introducing a non-trivial pressure $\tilde{p}_\phi$ in angular direction.* The corresponding cosmological solutions are equivalent to the DGP solutions and correspond to a static bulk geometry.

2. *The brane is allowed to freely expand or collapse in angular direction by setting $\tilde{p}_\phi = 0$.* In this case, the brane generically acts as an emitter of 1D gravitational waves. Moreover, these solutions dynamically degravitate a 4D CC at the full nonlinear level.

Subsequently, the phenomenological viability of the model was discussed. The first class of solutions reproduces the DGP phenomenology provided the compact dimension is sufficiently stabilized. In particular, there is a standard 4D Friedmann regime which makes these solutions phenomenologically interesting. As a future direction, it might be interesting to resolve the stabilization mechanism dynamically by introducing additional fields. This could be achieved along the lines of Sec. 2.4.3 where a Scherk-Schwarz like mechanism [157] was employed to stabilize the compact dimension. From our analysis it can already be anticipated that such a stabilization breaks down for a tension dominated stress-energy on the brane. This implies corrections to the DGP and standard Friedmann predictions at late times which would give rise to a new phenomenology. The second class is ruled out due to the non-trivial angular dynamics, incompatible with a 4D regime, which can be inferred from supernova observations. Therefore, the significance of these solutions is of purely conceptual nature as they provide an analytical realization of the degravitation mechanism at the nonlinear level. In that context, it would be interesting to further investigate the linearized theory according to which the effective 4D graviton

is a resonance, i.e. an infinite superposition of massive graviton states. This approach might illustrate how the degravitation mechanism can be incorporated in the 4D theory of a resonant graviton in a consistent and dynamical way. Moreover, it should be checked whether the choice $\tilde{p}_\phi = 0$ can be achieved in a technically natural way.

Let us finally comment on Weinberg's no-go theorem, reviewed in Sec. 1.2.2. It states on very general grounds that a fine-tuning cannot be avoided in any local 4D theory with a finite number of fields. In addition, the lesson we learned from our previous investigations—in particular of the compact prototype model (1.29) and the cigar model (4.1)—was that the tuning persists in higher-dimensional models provided the extra space is compact. This can be explained at least qualitatively: Due to the compactness of the extra space, the bulk fields can be decomposed into a tower of massive modes (so-called KK modes) which, in a low energy EFT, can be integrated out to yield a local 4D theory to which Weinberg's theorem is applicable again. The main benefit of the present model is to elucidate how this conclusion can be avoided by considering infinite volume extra dimensions. First note that in this case the above argument, based on integrating out KK modes, is not valid because the theory is intrinsically higher-dimensional. In other words, integrating out the extra dimensions results in a nonlocal theory of gravity to which the theorem cannot be applied anymore [66, 12]. In that context, it is instructive to consider the modified Friedmann equation (5.38a). Removing the infinite dimension is realized by sending $M_6 \to 0$, which simply corresponds to replacing (5.38a) by

$$\tilde{\rho} = 3\tilde{M}^3 \left(H_a^2 + H_a H_c \right) \ . \tag{5.51}$$

Then, by demanding $H_a = 0$, the equation implies that also $\tilde{\rho}$ ($\equiv \tilde{\rho}_\lambda$) has to be tuned to zero. To be more specific, the amount of tuning to realize a phenomenologically viable H_a would not be any less than in standard GR. Thus, there is no dynamical adjustment or, equivalently, degravitation at work, as we expected for a model with only one microscopically small extra dimension. If, on the other hand, we restore the infinite dimension, (5.38a) admits a solution, viz. (5.50), with an arbitrary value of $\lambda \equiv 2\pi R \rho_\lambda$ and vanishing H_a. This means that, in accordance with the degravitation idea, the whole gravitational effect of a 4D CC is absorbed by the extrinsic curvature contribution of the infinite dimension. In fact, it is a purely temporal curvature effect, describing the expansion of the compact extra dimension measured by H_c. This makes the mechanism especially interesting because it is different to the one discussed in the case of the cosmic string universe in Chap. 3 where the effect of λ is to curve the transverse spatial dimensions into a cone. Note, however, that it is not clear whether the choice $\tilde{p}_\phi = 0$, which was made for the degravitating solution, corresponds to yet another fine-tuning. In other words, we do not know whether there exists a dynamical mechanism to ensure a vanishing azimuthal pressure. From a conceptual point of view, this is a pressing issue that requires further investigations.

In summary, we presented a degravitation mechanism for which the CC drives the expansion of one compact brane dimension instead of the three infinite spatial dimensions our apparent universe is made of. The presence of an infinite size extra dimension provides the (potential) loophole to Weinberg's theorem.

Chapter 6

SLED: Extra space as a rugby ball

Note: This chapter is based on two publication together with Robert Schneider [133, 134]. The major part of Sec. 6.2 is a verbatim reproduction of a corresponding section in [134].

In this chapter, we present a different extra-dimensional model that is based on two large, viz. sub-millimeter sized, compact extra dimensions, which have the topology of a rugby ball. It is referred to as the *supersymmetric large extra dimensions* (SLED) model, and attempts to solve the CC problem by embedding the brane into a scale invariant (SI) bulk. The aim of the present chapter is to reassess this claim carefully. In particular, we ask whether it is indeed possible to avoid any tuning of model parameters without compromising the phenomenological viability of the model. As we have seen by studying other compact models in Sec. 1.5.2 and Sec. 4, this is the difficult part, which normally fails due to Weinberg's no-go argument, reviewed in Sec. 1.2.2. Let us start here by giving a brief historic introduction to the SLED model. To that end, we distinguish between three stages that best exemplify its evolution:

1. The gravitational sector was first described by 6D GR [43, 112, 38, 127, 47]. A Maxwell flux that wraps around one of the compact dimensions is used to stabilize the bulk, which closes in two microscopically thin three-branes. In fact, this is exactly the prototype (1.29) studied in the introduction. So let us simply summarize its main deficiencies. Even though the model allows for 4D flat solutions, it does not help with the CC problem because, due to a flux quantization condition, a parameter constraint has to be imposed on the brane tension (cf. Eq. (1.32), as well as [82, 128, 137]). A violation would lead to a non-vanishing 4D curvature. In particular, the system is not able to readjust after a change in the brane tension, as would occur during a phase transition in the early universe. As a result, the tension has to be fine-tuned to achieve a value of the 4D curvature that is compatible with observations. Therefore, as it stands, the model does not feature a dynamical adjustment mechanism, and thus the tuning problem is as severe as it was in 4D Einstein gravity. Moreover, there is a second shortcoming related to the size of the extra dimensions. To be precise, the bulk CC has to be chosen hierarchically small to make sure that the volume fulfills its phenomenological bound.

2. In a second stage, the bulk gravity sector was promoted to supergravity,[1] thereby giving rise to the SLED model [156, 6, 24, 25]. On a technical level, the model is extended by the dilaton as a new scalar degree of freedom. The bulk theory is (as a consequence of supersymmetry) classically SI, which implies a flat dilaton direction in field space and a vanishing bulk CC. Again, the model admits 4D flat solutions, however, the tuning problem caused by the flux quantization condition persists, albeit in a slightly different way [167]: Its violation would lift the flat dilaton direction, thus leading to an intolerable run-away behavior (instead of creating a de Sitter phase on the brane). In other words, the tuning here is needed to preserve the flat dilaton direction (cf. the discussion in Sec. 1.2.2). This does not come as a surprise because from a 4D point of view it is the classical SI which ensures the flat brane geometry, making hence Weinberg's general no-go argument applicable again.

3. In the third and last stage, a *brane-localized flux* (BLF) term was added to the Maxwell sector of the theory [33, 34, 35]. This term, which should be included anyhow if the theory is treated as an EFT, constitutes a potential source of SI breaking. The hope was that it would lift the degeneracy in field space (through an explicit breaking of SI) while preserving a flat on-brane geometry. Correspondingly, the flux quantization condition—instead of imposing a parameter constraint on the tension—would fix the field value of the dilaton (at the brane).

In this chapter, we will focus on the SLED proposal in its final form, featuring the BLF term. Our analysis is guided by three main questions. We present them here in turn and give a short summary of our corresponding answers.

What is the condition for exact 4D flatness?

First, to answer that question it is sufficient to study the thin brane setup, as done in Sec. 6.1. To be precise, we make a 4D maximally symmetric ansatz and describe the transverse profile of the brane by means of a two-dimensional delta function. That way, we derive the desired condition: *Only a SI dilaton-brane coupling ensures 4D flatness.* This is one of the central results of this chapter. In particular, we find that the dilaton has to couple to the BLF (and thus to the brane) in a nontrivial way to preserve SI. This contradicts a former analysis with BLF term in [33, 34]. There, it was claimed that 4D flatness is ensured only if the BLF term does not couple to the dilaton (which corresponds to an explicitly broken SI). We discuss the origin of the mismatch.

Can the 4D flat solutions avoid Weinberg's no-go theorem?

By slightly generalizing the so-called GGP[2] solution to incorporate the effect of a BLF, we find a negative answer (see Sec. 6.1.5). The reason is that, due to SI, the dilation drops

[1] Specifically, it is is the Nishino-Szegin chiral gauged supergravity theory [150, 138].

[2] GGP stands for Gibbens, Gueven and Pope; in [83] they found an explicit 4D flat solution of the SLED setup in its original form, i.e. without BLF.

out of the flux quantization condition, which then becomes a pure parameter constraint on the brane tension; we refer to it as the GGP constraint. In fact, the (constant) value of the dilaton is not determined by any of the field equations, which corresponds to saying that there is a flat direction in field space. It could be lifted by violating the constraint, which would lead to an intolerable run-away behavior. This is the same observation Weinberg made when trying to devise a 4D adjustment mechanism to cancel the CC. In other words, our findings are the 6D manifestation of Weinberg's arguments.

What is the condition for a phenomenologically viable 4D de Sitter solution?

While the previous results make a statement about the (non-)existence of a natural 4D Minkowski vacuum, they also raise concerns about the radiative stability of 4D de Sitter solutions. Before arriving at a final statement, we have to derive the condition under which a phenomenologically viable 4D de Sitter geometry can be realized. In that context, we identify two independent contributions to the 4D curvature: First, an explicit breaking of SI on the brane, which can be modeled by coupling the dilaton either to the brane tension or the BLF. In fact, the tension-dilaton coupling is generated by quantum loops if the brane matter fields break SI. Second, a finite transverse brane width ℓ,[3] which breaks SI on the brane (depending on the construction this happens either explicitly or spontaneously). The crucial point is that both contributions should be included in a realistic setup. We study the corresponding SI breaking thick brane setup in Sec. 6.2. As our main result, we obtain an expression for how the 4D curvature $\bar{\mathcal{R}}$ scales with the extra space volume V. Provided the parameter values are generically set by the 6D Planck scale, we find that the contribution related to the transverse size ℓ is most problematic,

$$M_6^2 \bar{\mathcal{R}} \sim \left(M_6^2 \ell^2\right) V^{-2} + \text{'dilaton coupling'}, \tag{6.1}$$

where we skipped further contributions due to the SI breaking dilaton coupling.[4] This scaling law implies that a large extra space volume leads to a small curvature. Since, there are phenomenological bounds on both quantities, we derive the necessary condition,

$$M_6 \ell \lesssim 10^{-18} \,, \tag{6.2}$$

that needs to be fulfilled to comply with observations. In other words, the transverse size of the brane has to be hierarchically small compared to the 6D Planck length (alternatively, it would also be possible to tune the brane tension with an even higher precision). We consider this a very problematic condition because it is not clear in which way such a hierarchy could be protected against radiative corrections.

What amount of tuning is needed to fulfill the phenomenological bounds?

[3] Note that ℓ corresponds to R used in previous chapters.

[4] The latter contributions are less problematic as they can be chosen to be stronger suppressed with V.

If we accept the hierarchy (6.2), we have to ask whether at least the other model parameters can be chosen generically. Unfortunately, we show in Sec. 6.3 that this is not possible. In fact, we are able to pin down the necessary amount of tuning: The model parameters have to fulfill the GGP constraint with a relative precision of 10^{-64} in order to admit a phenomenologically viable solution (alternatively, this can be traded against another tuning of the same size). This is certainly not any better than the tuning problem we started with in the first place.

Let us summarize the main technical aspects of our approach. As explained in Sec. 6.1.2, a key ingredient is the addition of a counter term to the action. It is necessary (and sufficient) to dispose of divergences which arise due to the BLF, and which were missed in previous studies. Note that the same subtraction scheme was confirmed recently in [28] by using an explicit UV model. The corresponding renormalized theory is the starting point of our analysis. We consider it as an effective field theory valid for energies above the fundamental bulk scale M_6. This program allows us to make quantitative predictions without resolving any of the microscopic details of the brane. In fact, we use two different methods to describe the brane: First, in Sec. 6.1, we model it as an infinitely thin object by using two-dimensional delta functions, and second, in Sec. 6.2, we promote it to a ring of circumference ℓ.[5] This twofold approach allows for a complementary picture of the system, as well as different consistency checks. Moreover, as mentioned before, introducing a thickness is physically required (and correspondingly the thin brane setup should be understood as an over-idealization).

As usual, to stabilize the thick brane, we have to introduce an angular pressure that points in the direction of the ring. To check the consistency of this particular construction, we study the thin brane limit in Sec. 6.2.3. We find that, in order to be compatible with the delta function results, the pressure has to vanish. Physically, this makes sense because there is no direction an angular pressure could act in for an infinitely thin brane. By studying different brane-dilaton couplings, we are able to explicitly confirm that expectation. This also allows us to address recent concerns brought up in [31] about the consistency of the thin brane (or delta function) analysis. Specifically, we present a loophole in the argumentation of [31] and explicitly show under which conditions the thin brane description is sufficient.

As explained before, the main result of our analysis is a relation between the 4D curvature and the extra space volume, see (6.1). This result is obtained in two different ways: First, in Sec. 6.1 and 6.2 by making certain assumptions about properties of the bulk solution, which in general cannot be derived analytically. And second, in Sec. 6.3, without relying on any assumptions, by solving the whole bulk-brane system numerically. This is particularly convenient in the ring regularization because the only effect of the brane is to introduce kinks in the bulk profiles, which are then determined by Israel's junction conditions [100, 101]. By using these two independent approaches, we are able to cross-check our results. In addition, the numerical analysis enables us estimate the amount of tuning necessary to fulfill the phenomenological bounds.

[5] Note that this is the same technique as used for the BIG model; for further details we thus refer the reader to Sec. 2.1.

Let us also note that the same setup was recently investigated in [29]. There, the idea was to integrate out the extra dimensions to obtain an effective 4D description. Here instead, we solve the full extra-dimensional system. In that sense, the two approaches are complementary, yet different. In particular, we agree with [29] that it is possible to have a parametrically large volume without the need of tuning. However, as opposed to [29], we also show that this is only possible by either introducing a further tuning or violating the phenomenological bound on the 4D curvature.

6.1 Thin brane setup

The approach presented in this section is based on the idealized picture of having an infinitely thin brane. Correspondingly, the localization of fields on the brane is modeled by two-dimensional delta functions. It is clear that a more realistic description requires the brane to have some intrinsic transverse size ℓ. If, however, we are interested in low energy questions that take place on much larger length scales, we expect the thin brane description to provide the correct physical answers—at least at leading order. According to the EFT paradigm, corrections should be organized in a power series of ℓ. We will confirm this expectation by studying the thick brane setup in Sec. 6.2.

Moreover, while the thin brane approach perfectly captures the (leading) physics of the SI setup, we will see that the SI breaking case suffers from divergent field values at the position of the codimension-two brane (like the electric field of a charged string, which diverges logarithmically) and hence requires some sort of regularization. This is conveniently realized by introducing a thick brane.

In summary, the thin approach provides a convenient way of studying the SI setup. In particular, it allows to find fully consistent 4D flat solutions, and provides an extra-dimensional perspective on Weinberg's tuning argument. Subsequent considerations about the phenomenological potential of the model (which require to include both a brane width and a breaking of SI) are postponed to Sec. 6.2.

6.1.1 The delta action

We start by briefly reviewing the SLED model introduced in [33]. A priori, the field content comprises the 6D metric $\boldsymbol{g}_6$, a Maxwell field $\boldsymbol{A}$, which stabilizes the compact bulk dimensions, and the dilaton ϕ, which renders the bulk theory scale invariant.

Its action decomposes into two parts,

$$\mathcal{S} = \mathcal{S}_{\text{bulk}} + \mathcal{S}_{\text{branes}} \,, \tag{6.3}$$

where the bulk contribution reads

$$\mathcal{S}_{\text{bulk}} = -\int \mathrm{d}^6X\sqrt{-g_6}\left\{\frac{1}{2\kappa^2}\left[\mathcal{R}_6 + (\nabla_M\phi)(\nabla^M\phi)\right] + \frac{1}{4}\mathrm{e}^{-\phi}F_{MN}F^{MN} + \frac{2e^2}{\kappa^4}\mathrm{e}^{\phi}\right\}, \tag{6.4}$$

with $\kappa \equiv 1/M_6^2$ and e the gravitational and U(1) coupling constants, respectively. The 6D Ricci scalar $\mathcal{R}_6$ is built from the 6D metric $\boldsymbol{g}_6$, and $\boldsymbol{F} \equiv \mathrm{d}\boldsymbol{A}$.[6] The brane contributions are

$$\mathcal{S}_{\text{branes}} = -\sum_b \int \mathrm{d}^4x\sqrt{-g}\left\{\mathcal{T}_b(\phi) - \frac{1}{2}\mathcal{A}_b(\phi)\epsilon_{mn}F^{mn}\right\}, \tag{6.5}$$

where the index $b \in \{+,-\}$ runs over both branes situated at the north (+) and south (−) pole of the compact space. The 4D brane tension is denoted by $\mathcal{T}_b(\phi)$. The second term controlled by $\mathcal{A}_b(\phi)$ describes the localized flux on the brane. In general, both terms are allowed to have arbitrary dilaton dependences. It is straightforward to check that the brane action preserves SI if and only if

$$\mathcal{T}_b(\phi) \equiv \lambda = \text{const} \qquad \text{and} \qquad \mathcal{A}_b(\phi) \propto \mathrm{e}^{-\phi}. \tag{6.6}$$

To be precise, under a metric rescaling with a (constant) factor ζ, $\mathrm{e}^{\phi} \mapsto \zeta^{-1}\,\mathrm{e}^{\phi}$, implying that the bulk action only transforms with a (constant) global factor, $\mathcal{S}_{\text{bulk}} \mapsto \zeta^2\mathcal{S}_{\text{bulk}}$. This is equivalent to the statement that the bulk equations of motion are scale invariant.

Of major importance for the proposed mechanism is the presence of the BLF term. Depending on its dilaton dependence, it admits a controlled breaking of SI. Then, the claim (which we are going to reassess) was that this can be done in a way which preserves the 4D flatness on the brane.

In the first step, we discuss the Maxwell, dilaton and gravity sector one by one. To that end, we assume a maximally symmetric on-brane geometry, as well as a rotational symmetry in the extra space, thus leading to the ansatz

$$\mathrm{d}s^2 = W^2(\rho)\,\bar{g}_{\mu\nu}\mathrm{d}x^\mu\mathrm{d}x^\nu + \mathrm{d}\rho^2 + B^2(\rho)\mathrm{d}\theta^2, \tag{6.7a}$$

$$A = A_\theta(\rho)\mathrm{d}\theta, \tag{6.7b}$$

$$\phi = \phi(\rho), \tag{6.7c}$$

where $\bar{\boldsymbol{g}}$ ($:= \boldsymbol{g}/W^2$) is 4D maximally symmetric and thus fully characterized by its constant 4D Ricci scalar $\bar{\mathcal{R}}$. We use corresponding bulk coordinates $X^A = (x^\mu, \rho, \theta)$.

6.1.2 Renormalized action

We start by considering the Maxwell part of the theory. The ansatz (6.7b) corresponds to a topologically nontrivial solution for which the electromagnetic field winds around the compact space. Physically, this stabilizes the volume of the extra dimension because the amount of (quantized) flux is conserved. As we will see, it is possible to integrate out the Maxwell field to obtain a theory of the metric and the dilaton field only.

[6] In this chapter, we use a different convention for the Ricci tensor, which now contains an additional minus sign compared to (C1).

The Maxwell Lagrangian after introducing a two-dimensional delta function $\delta^{(2)}(y)$ reads

$$\mathcal{L}_F = -\sqrt{-g}\,\frac{1}{4}\mathrm{e}^{-\phi}F^2 + \frac{1}{2}\sum_b \sqrt{-g_4}\mathcal{A}_b(\phi)\,\epsilon_{mn}F^{mn}\,\delta^{(2)}(y-y_b)\,, \tag{6.8}$$

where $F^2 \equiv F_{MN}F^{MN}$. The field equations are readily found,

$$\partial_M\left[\sqrt{-g}\,\mathrm{e}^{-\phi}F^{MN} - \sqrt{-g_4}\,\delta^M_m\delta^N_n\sum_b \mathcal{A}_b(\phi)\epsilon^{mn}\delta^{(2)}(y-y_b)\right] = 0\,. \tag{6.9}$$

With the above winding ansatz (6.7b), this equation can be integrated, thus yielding the field strength[7]

$$F_{\rho\theta} = \mathrm{e}^{\phi}B\left[\frac{Q}{W^4} + \sum_b \frac{\delta(\rho-\rho_b)}{2\pi B}\mathcal{A}_b(\phi)\right], \tag{6.10}$$

with Q the corresponding constant of integration. Its value is fixed due to flux quantization [151, 34], which in fact is a condition on the total flux $\Phi_{\text{tot}} := \int \mathrm{d}\rho\,\mathrm{d}\theta\,F_{\rho\theta}$ of the system, and reads explicitly

$$\Phi_{\text{tot}} := 2\pi Q\int \mathrm{d}\rho\,\frac{\mathrm{e}^{\phi}B}{W^4} + \sum_b\left[\mathcal{A}_b(\phi)\mathrm{e}^{\phi}\right]_{\rho=\rho_b} \overset{!}{=} \frac{2\pi n}{\tilde{e}} \qquad (n\in\mathbb{N})\,. \tag{6.11}$$

This equation can be derived by integrating the Maxwell field from both poles and demanding that its value at the equator is unique up to a U(1) gauge transformation[8]. We will refer to it as the *flux quantization condition* (FQC).

At this point, we encounter a problem with the Maxwell solution (6.10) that is caused by the term $\propto \delta(\rho-\rho_b)$. Plugging the solution back into the Lagrangian (6.8) leads to a divergent contribution to the action. Specifically, the F^2 term, also sourcing the Einstein and dilaton equations, contains a part where the delta function is squared, hence leading to an infinite factor $\propto \delta(0)$. This term has to be understood as a consequence of the (over-)idealized thin brane description. Let us stress that this peculiarity was missed in previous investigations [33, 34, 27]). To consistently dispose of that divergence, we introduce a renormalized action. To be precise, we introduce a counter term into the action that cancels the divergent part. Physically, this is motivated by the fact that we expect a consistent and hence finite EFT to exist. Otherwise, we would need to specify the UV theory in order to answer low energy questions. Even though this would be a logical possibility, it would be very unsatisfactory from a physical point of view, and could certainly not help with the naturalness problem we want to address.

The counter term can be derived by plugging the solution (6.10) back into the action, yielding

$$\mathcal{S}_F|_{\text{sol}} = -\frac{1}{2}\int \mathrm{d}^6X\sqrt{-g}\,\mathrm{e}^{\phi}\frac{Q^2}{W^8} + \mathcal{S}_{\text{div}}\,, \tag{6.12}$$

[7] According to our conventions, and the ansatz (6.7), $\epsilon^{\rho\theta} = 1/B$, and $\delta^{(2)}(y) = \delta(\rho)/(2\pi)$.

[8] As was pointed out in [33], in general the U(1) gauge coupling $\tilde{e}$ can be different from e.

where the last term is the divergent contribution

$$\mathcal{S}_{\text{div}} = \frac{1}{2}\sum_b \int \mathrm{d}^4x\sqrt{-g_4}\,\frac{\delta^{(2)}(0)}{\sqrt{g_2}}\mathrm{e}^{\phi}\mathcal{A}_b(\phi)^2\,. \tag{6.13}$$

Thus, to obtain a finite action, we introduce a counter term that exactly cancels $\mathcal{S}_{\text{div}}$; specifically, we work with a renormalized action,

$$\mathcal{S}_{\text{ren}} := \mathcal{S} - \mathcal{S}_{\text{div}}\,. \tag{6.14}$$

Let us stress that $\mathcal{S}_{\text{div}}$ is a 4D scalar and as such qualifies as a legitimate brane action. As the term does not contain A_M, the Maxwell sector is not affected, in particular, the solution (6.10) is not changed (otherwise, it would not be clear whether the new solution would introduce another divergence). It will enter the Einstein equations differently from a tension due to the metric factor $1/\sqrt{g_2}$. As a consequence, the BLF term does not source the gravitational equations directly but only indirectly via the dilaton sector.

Beside its correct symmetries, there are also several a posteriori justifications of the proposed renormalization scheme:

- After including a single counter term, the theory can be solved consistently. In other words, the renormalized theory $\mathcal{S}_{\text{ren}}$ is an explicit realization of the SLED model with BLF term that still admits a consistent thin brane description, as opposed to the original action.
- We reproduce the results of [30], where a concrete UV model was used to microscopically resolve the BLF contribution. (This was first done in a model without dilation and later also applied to the full SLED setup [28].)
- Our final results obtained in the renormalized delta approach are in line with the naive expectation: A fully SI theory, corresponding to couplings (6.6), implies a vanishing 4D curvature.

In order to obtain an explicit expression for the counter term, the Maxwell sector had to be solved for a specific coordinate choice. Therefore, in the renormalized action (6.14) the Maxwell field has already been integrated out. The resulting Einstein-dilaton theory is discussed in the following.

6.1.3 Einstein-dilaton system

The corresponding system of vacuum field equations (valid away from the branes) consists of the dilaton equation

$$-\frac{1}{\kappa^2}\frac{1}{BW^4}\left(BW^4\phi'\right)' = \frac{\mathrm{e}^{\phi}}{2}\left(\frac{Q^2}{W^8}-\frac{4e^2}{\kappa^4}\right) - \sum_b \frac{\delta_b}{2\pi B}\left\{\mathcal{T}_b'(\phi) - \frac{Q}{W^4}\mathrm{e}^{\phi}\left[\mathcal{A}_b'(\phi)+\mathcal{A}_b(\phi)\right]\right\}\,, \tag{6.15}$$

and the $\binom{\mu}{\nu}$, $\binom{\rho}{\rho}$ and $\binom{\theta}{\theta}$ components of Einstein's field equations,

$$-\frac{1}{\kappa^2}\left(\frac{\bar{\mathcal{R}}}{4W^2}+3\frac{W''}{W}+\frac{B''}{B}+3\frac{W'^2}{W^2}+3\frac{W'B'}{WB}+\frac{1}{2}\phi'^2\right)=\frac{\mathrm{e}^{\phi}}{2}\left(\frac{Q^2}{W^8}+\frac{4e^2}{\kappa^4}\right)+\sum_b\frac{\delta_b}{2\pi B}\mathcal{T}_b(\phi)\,, \tag{6.16a}$$

$$\frac{1}{\kappa^2}\left(\frac{\bar{\mathcal{R}}}{2W^2}+6\frac{W'^2}{W^2}+4\frac{W'B'}{WB}-\frac{1}{2}\phi'^2\right)=\frac{\mathrm{e}^{\phi}}{2}\left(\frac{Q^2}{W^8}-\frac{4e^2}{\kappa^4}\right)\,, \tag{6.16b}$$

$$\frac{1}{\kappa^2}\left(\frac{\bar{\mathcal{R}}}{2W^2}+4\frac{W''}{W}+6\frac{W'^2}{W^2}+\frac{1}{2}\phi'^2\right)=\frac{\mathrm{e}^{\phi}}{2}\left(\frac{Q^2}{W^8}-\frac{4e^2}{\kappa^4}\right)\,. \tag{6.16c}$$

The parameter Q is the Maxwell integration constant introduced in (6.10). Eq. (6.16b) is of first order and we will refer to it as the radial Einstein constraint. In fact, only two of the above four equations are independent: As a consequence of Bianchi's identities, differentiating the Einstein constraint with respect to ρ yields a linear superposition of the remaining equations.

As mentioned earlier, only the 4D tension $\mathcal{T}_b$—and not the BLF term $\mathcal{A}_b$—is sourcing the gravitational equations. On the other hand, the gravitational effect of the BLF term is mediated by the dilaton (which couples to gravity) via the localized source contribution to (6.15).

For later reference, we consider the difference of the $\binom{\rho}{\rho}$ and $\binom{\theta}{\theta}$ equation; it reads

$$\frac{W''}{W}-\frac{W'B'}{WB}+\frac{1}{4}\phi'^2=0\,, \tag{6.17}$$

showing that a nontrivial dilaton profile implies a warped geometry. In other words, a warping needs to be included when we want to make statements about a generic dilaton profile.

Let us note that neither the $\binom{\rho}{\rho}$ nor the $\binom{\theta}{\theta}$ Einstein equation obtains a localized source contribution, which could in turn be interpreted as a radial and angular pressure component, respectively. This is not surprising as for a codimension-two object there is no physically meaningful notion of an intrinsic radial or angular pressure because there is no direction these two components could act in. We will discuss this aspect, recently brought up in [31], in more detail in Sec. 6.2.3, in the context of the thick brane setup.

Integrating the dilaton equation over an infinitesimally small disc covering one of the axes and using Stokes' theorem yields the boundary condition for ϕ. For W and B the same is achieved by taking appropriate combinations of the Einstein equations. Explicitly,

we find

$$[B\phi']_{\rho=\rho_b} = \frac{\kappa^2}{2\pi}\mathcal{C}_b, \tag{6.18a}$$

$$\left[B(W^4)'\right]_{\rho=\rho_b} = 0, \tag{6.18b}$$

$$[B']_{\rho=\rho_b} = 1 - \frac{\kappa^2}{2\pi}\left[\mathcal{T}_b(\phi)\right]_{\rho=\rho_b}\,, \tag{6.18c}$$

where deviations from SI are measured by the (ϕ-dependent) quantity

$$\mathcal{C}_b := \left\{\mathcal{T}_b'(\phi) - \frac{Q}{W^4}\mathrm{e}^{\phi}\left[\mathcal{A}_b'(\phi) + \mathcal{A}_b(\phi)\right]\right\}_{\rho=\rho_b}\,. \tag{6.19}$$

Eq. (6.18a) implies a vanishing ρ-derivative of the dilaton at the brane in the SI case. On the other hand, for non SI couplings, we expect $\phi'|_{\rho=\rho_b}$ to be non-vanishing (or even to diverge due to the vanishing of B). We will further study this case in the thick brane analysis in Sec. 6.2.

6.1.4 4D curvature

In order to assess the potential of the SI model with respect to the CC problem, we look for an explicit expression of $\bar{\mathcal{R}}$. This in turn enables us to infer the conditions under which this quantity is vanishing (or small enough to be compatible with observations).

We take an appropriate linear combination of (6.16b), (6.16c) and (6.15),

$$BW^2\bar{\mathcal{R}} = -2\left[BW^4\left(\phi + 2\ln W\right)'\right]'\,. \tag{6.20}$$

Integrating this equation over the whole extra space, i.e. the vacuum region between the north and south pole, yields

$$V\bar{\mathcal{R}} = 4\pi\sum_b\left[BW^4\left(\phi + 2\ln W\right)'\right]_{\rho=\rho_b}\,, \tag{6.21}$$

where the extra-dimensional (2D) volume was defined as

$$V := 2\pi\int \mathrm{d}\rho\, BW^2 = \int \mathrm{d}^2y\,\sqrt{g_2}\,W^2\,. \tag{6.22}$$

Using the matching equation (6.18b), we obtain

$$V\bar{\mathcal{R}} = 4\pi\sum_b\left[BW^4\phi'\right]_{\rho=\rho_b}\,, \tag{6.23}$$

which shows that the dilaton derivative at the brane controls the 4D curvature. In particular, a trivial dilaton profile implies a vanishing of $\bar{\mathcal{R}}$. This was also observed in [6], yet in [33, 34, 27] the wrong conclusion was drawn that only dilaton independent brane couplings

($\mathcal{A}_b' = \mathcal{T}_b' = 0$) could lead to a vanishing of ϕ' at the brane and hence to $\bar{\mathcal{R}} = 0$.[9] However, this leaves aside the fact that the dilaton is also sourced by the bulk Maxwell field. To be precise, the F^2 term in the bulk action (6.4) leads to an additional $\delta^{(2)}$-contribution in (6.15), given by the $\mathcal{A}_b$ term. As a result, even for vanishing brane-dilaton coupling $\mathcal{A}_b' = 0$ the dilaton can have a nontrivial profile close to the brane [as follows from (6.18a) together with (6.19)], hence implying $\bar{\mathcal{R}} \neq 0$.

By using (6.18a), we can express the 4D curvature completely in terms of the dilaton-brane couplings,

$$V\bar{\mathcal{R}} = 2\kappa^2 \sum_b W_b^4 \mathcal{C}_b \,. \tag{6.24}$$

This formula is one important result of our analysis as it shows that only a SI coupling guarantees a vanishing $\bar{\mathcal{R}}$. This is not very surprising because $\bar{\mathcal{R}} \neq 0$ requires some scale to appear in the theory to set its size, which however is not compatible with having a SI theory.[10]

6.1.5 Scale invariant couplings

At first sight, the SI case ($\mathcal{C}_b = 0$) looks very promising with respect to the CC problem because the brane tension (or CC equivalently) is shielded from the brane observer, who only "sees" a 4D Minkowski vacuum. However, this comes at the price of introducing yet another tuning problem, which is caused by the FQC (6.11). While this is already known for the model without BLF [167], we show it here for the present theory including a BLF term.[11] Explicitly, this is achieved by employing known solutions of the SI setup, first derived in [83] and henceforth referred to as the GGP solutions. They include the effect of a nontrivial warping and are given by

$$\mathrm{d}s^2 = W^2(\xi)\left[\eta_{\mu\nu}\mathrm{d}x^\mu \mathrm{d}x^\nu + \mathrm{e}^{-\phi_0}\frac{\kappa^2}{4e^2}\left(\mathrm{d}\xi^2 + \frac{\alpha_+\alpha_-}{W^8(\xi)}\sin^2(\xi)\mathrm{d}\theta^2\right)\right], \tag{6.25a}$$

$$\phi(\xi) = \phi_0 - 2\ln W(\xi)\,, \tag{6.25b}$$

with

$$W^4(\xi) = \cosh(v) - \sinh(v)\cos(\xi)\,, \quad \text{where} \quad v := \frac{1}{2}\ln\left(\frac{\alpha_+}{\alpha_-}\right) \tag{6.25c}$$

Here, the integration constants $\alpha_\pm$, describing the conical defects caused by the two branes, are determined by imposing appropriate boundary conditions at the south and north pole,

[9] Technically, the error was caused by using the dilaton boundary condition from Ref. [18], which is only applicable in the case without BLF.

[10] In principle, V would be a candidate for such a scale but, as we will see, it is determined by the dilaton field value, which, due to SI, can be chosen freely.

[11] Let us stress though that in the meantime the same result was obtained in a different analysis in [30].

respectively,

$$\alpha_\pm = 1 - \frac{\kappa^2}{2\pi}\mathcal{T}_\pm \,. \tag{6.26}$$

A map $\xi(\rho)$ relating the two radial coordinates ξ and ρ, as respectively defined in (6.7) and (6.25), can be found by solving

$$\frac{\kappa\, \mathrm{e}^{-\phi_0/2}}{2e} W(\xi)\, \xi' - 1 = 0 \tag{6.27}$$

subject to the boundary conditions $\xi_+ = 0$ and $\xi_- = \pi$. An important observation is that the integration constant ϕ_0 is not fixed. In fact, it corresponds to a flat direction in field space, the existence of which is a result of SI. Its value determines the extra space volume via

$$V_{\mathrm{GGP}} = \frac{\kappa^2}{e^2}\pi\sqrt{\alpha_+\alpha_-}\, \mathrm{e}^{-\phi_0} \,. \tag{6.28}$$

Within this class of solutions the Maxwell integration constant is readily found, $Q = 2e/\kappa^2$. Using this and (6.25) to evaluate the FQC (6.11), we derive

$$\frac{\sqrt{\alpha_+\alpha_-}}{e} + \frac{1}{2\pi}\sum_b \Phi_b = \frac{n}{\tilde{e}} \,, \tag{6.29}$$

which can be read as a parameter relation on the brane tensions via $\alpha_\pm$. In other words, having a vanishing 4D curvature requires to tune the model parameters. Technically, the reason is that, due to SI, ϕ_0 drops out of (6.11), making this equation a parameter constraint (as all other integration constants have already been determined). The only effect of the BLF is to introduce the second term on the left side of (6.29) which cannot avoid the tuning problem (as was originally intended).

In summary, the 4D flat solutions in the SI case cannot help with the CC problem because they do not exist for a *generic* choice of model parameters. In fact, if the tuning is violated, the system no longer admits a static solution, hence implying an unwanted run-away behavior (which is incompatible with a Minkowski geometry on the brane). This is just the 6D version of Weinberg's famous no-go argument, reviewed in Sec. 1.2.2.

6.1.6 Non scale invariant couplings

It is clear that phenomenology requires a non-vanishing (albeit small) value of $\bar{\mathcal{R}}$. While the previous results exclude the possibility of having a natural 4D Minkowski vacuum, strictly speaking, this does not exclude the possibility of realizing a de Sitter geometry on the brane in a technically natural way.

From (6.24) together with (6.19), we see that the 4D curvature needs not to vanish in the case of non SI couplings. This motivates to further explore the possibility of slightly breaking SI to realize a non-vanishing 4D curvature. However, in this case it is more

difficult to arrive at a quantitative statement because $\mathcal{C}_b(\bar{\phi})$ explicitly depends on the dilaton field. Thus, as opposed to the SI case, determining $\bar{\mathcal{R}}$ requires to derive the value of the dilaton field at the brane position. Since bulk fields generically diverge at the position of a codimension-two brane, the final answer cannot be found within the delta setup. Instead, the system has to be regularized in a consistent way, which will be discussed in the next section.

6.2 Thick brane setup

6.2.1 Ring regularization

In order to avoid any singularities and potential ambiguities of the (non SI) delta brane setup, the authors in [30, 28] introduced a specific UV model describing the brane as a vortex of finite width in extra space. We will instead use a different and technically simpler way of regularizing the system, in which the delta brane is replaced by a ring of circumference ℓ [142, 32].[12] We assume the microscopic details of the regularization to be irrelevant for the low energy questions we want to study.

For simplicity, the brane at the south pole is chosen to be a pure tension brane without dilaton coupling, for which no regularization is required as it only leads to a conical defect of size

$$\alpha_- = 1 - \frac{\kappa^2}{2\pi}\mathcal{T}_- \,. \tag{6.30}$$

The northern brane, which breaks SI, is regularized and now sits near the north pole at the coordinate position ρ_+, corresponding to a proper circumference $\ell \equiv 2\pi B_+ > 0$.[13] Figure 6.1 depicts the regularized bulk geometry for $\mathcal{T}_\pm = 0$, physically corresponding to the absence of both branes, as well as for the exemplary parameter choice (6.54) supplemented with $\tau = 0$. The interior of the ring (dark) is almost flat, whereas the exterior (bright) is strongly curved. For the trivial parameter choice, the geometry corresponds to a two-sphere, the size of which is set by ϕ_+ according to (6.28). On the other hand, in the presence of non-vanishing brane tensions, the two-sphere gets deformed into a teardrop shape. The conical singularity at the south pole is clearly visible. The important point is that the interior of the brane/ring at the north pole contains a regular axis in both cases,[14] hence signaling a working regularization.

Since the delta function $\delta_+ \equiv \delta(\rho - \rho_+)$ is now localized at the position of the finite width ring, the regularized equations of motion are formally identical to those presented

[12] Note that even though it is not obvious how the BLF term could be consistently adapted to the 5D brane in a covariant way at the level of the action, introducing the regularization after the Maxwell field has been solved for is straightforward. (In any case, the BLF term will in the end not be crucial for our main conclusions.)

[13] Here and henceforth, evaluation at $\rho = \rho_0$, ρ_+ and ρ_- will be denoted by subscripts "0", "+" and "−", respectively.

[14] The position of the axis at the north pole is denoted by ρ_0 ($< \rho_+$). We can perform a shift of the ρ coordinate such that $\rho_0 = 0$.

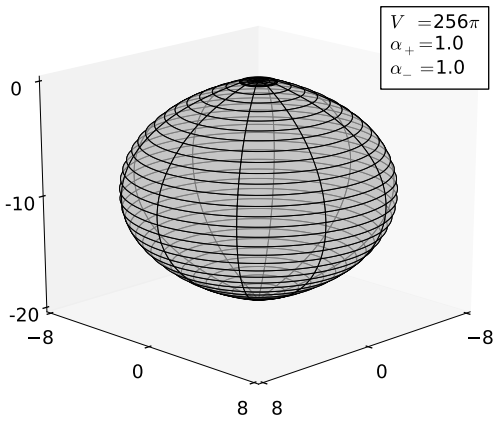

(a) Regularized two-sphere corresponding to a SI setup with vanishing tension on both branes.

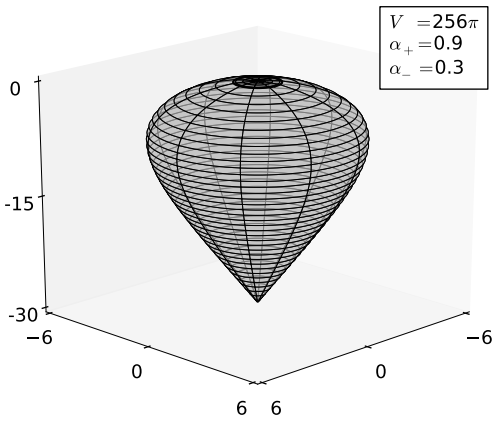

(b) Deformed two-sphere for parameters (6.54) with SI choice $\tau = 0$. The conical singularity at the south pole is caused by the brane tension.

Figure 6.1: Embedding picture of two numerical solutions with $V = 256\,\pi$ (in units of the bulk Planck scale κ). The regularized northern brane (which in general breaks SI) is represented by the black ring, separating the interior (dark) from the exterior region.

in Sec. 6.1, apart from one crucial further modification: In order to prevent the ring from collapsing, it is necessary to introduce an angular pressure component, i.e. to add the term

$$\frac{\delta_+}{2\pi B_+}\, p_\theta \tag{6.31}$$

to the right hand side of the $\binom{\theta}{\theta}$ Einstein equation (6.16c). A possible way of modeling such a stabilization microscopically was first given in [157] and later also applied to the SLED model [32]: The idea is to introduce a localized scalar field that winds around the compact brane dimension and is subject to nontrivial matching conditions. In fact, we could use the microscopic mechanism introduced in Sec. 2.4.3. As a result, shrinking the extra dimensions causes the related field energy to increase, hence implying a stable configuration with finite ring size. By integrating out the scalar field, it was explicitly shown in [32] that it contributes to the (ϕ-dependent) tension on the brane and leads to a pressure in angular direction. The tension shift can be taken care of by an appropriate renormalization, and the whole stabilizing sector is then solely characterized by an angular pressure component p_θ. Thus, without loss of generality, we will work with the renormalized theory. As argued in [32], the value of p_θ needed to stabilize the ring can be inferred from the Einstein equations.

The junction conditions across the brane can be readily derived and read[15]

$$[B\phi']_{\text{disc}} = \frac{\kappa^2}{2\pi}\mathcal{C}_+ \,, \tag{6.32a}$$

$$4[B(\ln W)']_{\text{disc}} = \frac{\kappa^2}{2\pi}\, p_\theta \,, \tag{6.32b}$$

$$[B']_{\text{disc}} = -\frac{\kappa^2}{2\pi}\left[\mathcal{T}_+(\phi) + \frac{3}{4}\, p_\theta\right]_{\rho=\rho_+} \,, \tag{6.32c}$$

where we introduced [like in (2.10)] the notation

$$[f]_{\text{disc}} := \lim_{\epsilon\to 0}\left[f(\rho_+ + \epsilon) - f(\rho_+ - \epsilon)\right] \,, \tag{6.33}$$

for any function $f(\rho)$.

Furthermore, we have to impose appropriate boundary conditions at both axes. Since the north pole is regularized, the corresponding axis (at coordinate position $\rho = 0$) is required to be elementary flat, i.e.

$$\phi_0' = 0 \,, \qquad W_0' = 0 \,, \qquad B_0' = 1 \,, \qquad B_0 = 0 \,. \tag{6.34}$$

In general, the unregularized south pole (at coordinate position $\rho = \rho_-$) features a conical singularity characterized by

$$\phi_-' = 0 \,, \qquad W_-' = 0 \,, \qquad B_-' = -\alpha_- \,, \qquad B_- = 0 \,. \tag{6.35}$$

Note that only three of the four boundary conditions at each axis are independent, due to the radial Einstein constraint (6.16b). Let us now count the total number of integration constants originating from the dilaton-Einstein system: There are two second order and one first order equation, leading to a total of five a priori undetermined integration constants. In addition, there is one integration constant included in the metric ansatz (6.7a), namely $\bar{\mathcal{R}}$. All of them are fixed by imposing the six independent boundary conditions stated above. The closed system for ϕ, W and B is thus given by the off-brane ($\rho \neq \rho_b$) equations (6.15) and (6.16), the junction conditions across the ring (6.32) and the boundary conditions (6.34) and (6.35) at the north and south pole, respectively.

After fixing the above boundary conditions, we are left with a one-parameter family of solutions, parametrized by the integration constant Q, arising from the Maxwell sector. However, it cannot be chosen freely, because it contributes to the total flux Φ_{tot}, which is subject to the flux quantization condition (6.11).

[15]For convenience, here and throughout the rest of Sec. 6.2, we set $W_+ = 1$, which is always possible by a (rigid) rescaling of the 4D coordinates.

6.2.2 4D curvature

The 4D curvature is crucial in studying the phenomenological viability of the model, so let us again derive its relation to the brane couplings, but now for the regularized model. Repeating the derivation that led to (6.24) in the thin brane setup, and taking into account (6.31), we now find

$$V\bar{\mathcal{R}} = \kappa^2 \left(2\mathcal{C}_+ + p_\theta\right) . \tag{6.36}$$

We see that the regularized expression is only modified by the last term proportional to p_θ. Next, we will also express p_θ in terms of the brane couplings in the thin brane limit.

6.2.3 Angular pressure and thin brane limit

The aim of this section is to explicitly check whether the above relations are compatible with the delta results of Sec. 6.1, and to gain further intuition about the regularized system and its stabilization. This will in turn allow us to narrow down physically interesting dilaton couplings.

Whether the brane looks point-like to a good approximation is determined by the hierarchy between brane and bulk size, i.e. by the dimensionless ratio $\epsilon := \ell^2/V$. Thus, the delta limit corresponds to $\epsilon \to 0$, and can be realized by letting $\ell \to 0$ and/or $V \to \infty$. In this work, we will keep ℓ fixed at a value not smaller than the bulk Planck length,[16] and let V become large.

Let us first check whether the matching conditions (6.32) are compatible with the delta results (6.18) in the limit $\epsilon \to 0$. Since the geometry is close to flat space in the vicinity of the regularized axis, we assume[17]

$$\lim_{\rho \nearrow \rho_+} \phi' = \mathcal{O}(\epsilon) , \qquad \lim_{\rho \nearrow \rho_+} W' = \mathcal{O}(\epsilon) , \qquad \lim_{\rho \nearrow \rho_+} B' = 1 + \mathcal{O}(\epsilon) . \tag{6.37}$$

In that case, Eq. (6.32a) indeed reduces to the dilaton boundary condition (6.18a) as $\epsilon \to 0$. On the other hand, Eqs. (6.32b) and (6.32c) show that the boundary conditions for W and B are again modified by a term proportional to p_θ. This was also observed in [32]. At this point several remarks are in order:

- The delta results are recovered if and only if $\lim_{\epsilon \to 0} p_\theta = 0$.
- The occurrence of p_θ is expected, and a mere consequence of regularizing the setup as a ring. It has the clear physical interpretation as the angular pressure that is needed to stabilize the compact dimension.
- From a physical perspective, there is no understanding of an angular pressure for an infinitely thin object. As a result, we expect the pressure to vanish whenever there is a large hierarchy between the bulk size V and the regularization scale ℓ. This

[16] Specifically, we will set $\rho_+ = \sqrt{\kappa}$ in the numerical examples below, corresponding to $\ell \approx 2\pi\sqrt{\kappa}$.
[17] These assumptions will be verified numerically in Sec. 6.3.1.3.

expectation is in accordance with the above observation that for $p_\theta \to 0$ all results of the delta analysis are recovered. Our present analysis allows to go beyond physical expectations and to explicitly take the thin brane limit.

- For the physically relevant class of exponential couplings (which admit a small 4D curvature and a large bulk volume), we will confirm the above expectation by showing $\lim_{V\to\infty} p_\theta = 0$. This result also confirms the correctness of the delta approach within this class of couplings. While it is possible to construct examples in which $p_\theta \nrightarrow 0$, these are typically plagued by some sort of pathology, like a runaway behavior or a diverging brane energy (cf. Sec. 6.2.4). Again, this is not very surprising, as there is no meaningful notion of a point-like angular pressure.

- The authors of [31] instead argued that p_θ should be nonzero for SI breaking delta branes. We comment on this in Sec. 6.3.1.4.

We will now derive an expression for p_θ in terms of the dilaton coupling. This in turn enables us to identify and discuss those couplings that are compatible with the delta description. As we will see, these are also just the ones that lead to small $\bar{\mathcal{R}}$.

As pointed out in [32], an expression for p_θ can be found by evaluating the radial Einstein constraint (6.16b) in the limit $\rho \searrow \rho_+$:

$$3\left(\kappa^2 p_\theta\right)^2 - 8\left(2\pi - \kappa^2\mathcal{T}_+\right)\kappa^2 p_\theta + 4\kappa^4\,\mathcal{C}_+^2 \\ - \epsilon\, 4V\bar{\mathcal{R}} + \epsilon\, 4\kappa^2 V \mathrm{e}^{\phi_+}\left(Q^2 - \frac{4e^2}{\kappa^4}\right) = \mathcal{O}(\epsilon)\,, \quad (6.38)$$

where we used (6.37) and (6.32) to express the radial derivatives through the brane fields. The terms in the second line are suppressed by ϵ and can be neglected in the delta limit. Solving for p_θ, we find

$$\kappa^2 p_\theta = \frac{4}{3}\left\{\left(2\pi - \kappa^2\mathcal{T}_+\right) \pm \sqrt{\left(2\pi - \kappa^2\mathcal{T}_+\right)^2 - \frac{3}{4}\kappa^4\,\mathcal{C}_+^2}\right\} + \mathcal{O}(\epsilon) \quad (6.39)$$

where the branch was chosen such that the delta result $p_\theta = 0$ is recovered for SI couplings in the limit $\epsilon \to 0$.[18] For vanishing BLF this coincides with the result derived in [32]. An important observation from the above equation is that for finite ϵ and SI couplings in general[19] $p_\theta = \mathcal{O}(\epsilon) \neq 0$. The physical reason is that introducing a brane width in general requires a stabilizing angular pressure.

[18] Note that we only consider *sub-critical* tensions $\mathcal{T}_+ < 2\pi/\kappa^2$.

[19] There is a special class of SI solutions with $W' = 0$ (no warping), $Q = 2e/\kappa^2$ and $\bar{\mathcal{R}} = 0$ for which $p_\theta = 0$ as an exact result even for $\epsilon \neq 0$. Physically, these solutions correspond to the regularized rugby ball setup. However, with respect to the CC problem this class is of no interest as it requires to unacceptably tune the relative size of both tensions.

The requirement of being close to SI can be made more precise by defining a near SI regime according to

$$\kappa^2 \mathcal{C}_+ \ll 1\,. \tag{6.40}$$

This in turn leads to an approximate expression for the stabilizing pressure,

$$p_\theta = \frac{\kappa^2}{4\pi}\left(1 - \frac{\kappa^2 \mathcal{T}_+}{2\pi}\right)^{-1} \mathcal{C}_+^2 + \mathcal{O}(\epsilon) + \mathcal{O}(\mathcal{C}_+^4)\,. \tag{6.41}$$

After inserting this into the formula for $\bar{\mathcal{R}}$ in (6.36), we arrive at

$$\boxed{V\bar{\mathcal{R}} = 2\kappa^2\,\mathcal{C}_+ + \frac{1}{4\pi}\left(1 - \frac{\kappa^2 \mathcal{T}_+}{2\pi}\right)^{-1} \kappa^4\,\mathcal{C}_+^2 + \mathcal{O}(\epsilon) + \mathcal{O}(\mathcal{C}_+^4)}\,. \tag{6.42}$$

By comparing to its delta counterpart (6.24), we find two small corrections:

(i) a term quadratic in $\mathcal{C}_+$ and hence suppressed (in the near SI regime) relative to the leading linear term;

(ii) generic order ϵ contributions caused by the finite brane width.

Which of the two dominates depends on the details of the dilaton coupling. Later, we will find that both possibilities can be realized.

In summary, we have shown that the delta result for $\bar{\mathcal{R}}$ receives two corrections which are small in the near SI regime (which we intend to study) and for a large hierarchy between the brane size and extra space volume.

6.2.4 Modeling near scale invariance

As expected, the near SI regime is of superior phenomenological importance as it leads to parametrically small values of the 4D curvature due to (6.42). We look for a dilaton coupling which allows to keep the SI breaking effects small without introducing an a priori hierarchy of the coupling parameters. In principle, this can be realized by using exponential couplings [30, 29], i.e.

$$\mathcal{T}_+(\phi) = \lambda_+ + \tau\,\mathrm{e}^{\gamma\phi} \qquad \text{and} \qquad \mathcal{A}_+(\phi) = \Phi_+ \mathrm{e}^{-\phi}\,, \tag{6.43}$$

with ϕ-independent (and SI) tension λ and constant parameters γ, τ and Φ_+. For τ and $\gamma \neq 0$ the tension term breaks SI explicitly. We see that even for (a naturally) large τ, the SI breaking given by $\mathcal{T}'_+$ becomes small when ϕ_+ is sufficiently negative. This makes the exponential couplings interesting with respect to the CC problem.

By contrast, the BLF term preserves SI. Technically, we could have introduced the SI

breaking also via the BLF term, which would lead to the same outcome.[20] However, it should be noted that it is physically more imperative to include a SI breaking tension as we expect loops of localized brane matter, which in general breaks SI,[21] to contribute to τ. In other words, there is no obvious way of having τ small without imposing a fine-tuning. As a consequence, when looking for natural solutions, we have to consider a ϕ-dependent tension with generic coefficient τ. On the other hand, in the case of the BLF term, it depends on the details of the matter theory whether we expect loop corrections to Φ_+. Following the discussion in [29], if the matter fields are not coupled directly to the Maxwell sector, there might be a chance of keeping SI breaking contributions to $\mathcal{A}_+$ small. In any case, including a breaking via the BLF term would, due to (6.42), yield an additional contribution to $\bar{\mathcal{R}}$ and, as we will see, would make it even more difficult to comply with the observational constraints.

With these couplings we find

$$\mathcal{C}_+ = \tau\gamma\, \mathrm{e}^{\gamma\,\phi_+}\,, \tag{6.44}$$

leading to an angular pressure

$$p_\theta = \frac{\kappa^2}{4\pi\alpha_+}\left(\tau\gamma \mathrm{e}^{\gamma\phi_+}\right)^2 + \mathcal{O}(\epsilon) + \mathcal{O}(\mathcal{C}_+^3)\,, \tag{6.45}$$

where $\alpha_+ := 1 - \frac{\kappa^2}{2\pi}\lambda_+$. The numerical analysis we conduct in this work (cf. Sec. 6.3) will show that the volume obeys

$$V = V_{\mathrm{GGP}}\left[1 + \mathcal{O}(\epsilon)\right], \qquad \text{with} \qquad V_{\mathrm{GGP}} := \frac{\kappa^2}{e^2}\pi\alpha_+ \mathrm{e}^{-\phi_+}\,, \tag{6.46}$$

where we identified ϕ_+ in (6.28) and used the fact that, there, W_0 is rescaled by a constant factor. This implies

$$p_\theta \propto \begin{cases} V^{-2\gamma} & (\text{for } 0 < \gamma < 1/2) \\ V^{-1} & (\text{for } \gamma = 0 \text{ or } \gamma > 1/2) \end{cases}, \tag{6.47}$$

asymptotically for $V/\kappa \gg 1$. The second line follows from the observation that for $\gamma > 1/2$ the first expression in (6.45) becomes sub-dominant compared to the $\mathcal{O}(\epsilon)$ contribution. The case $\gamma = 0$ is special as it corresponds to a SI coupling, where SI is only broken by the regularization. From (6.45) it is clear that it is not continuously connected to $\gamma \neq 0$ because the first term vanishes identically (irrespective of the value of V). In both cases,

[20] In fact, we checked this explicitly. The reason is that the terms $\mathcal{T}_+'$ and $(\mathrm{e}^{\phi}\mathcal{A}_+)'$ (which lead to SI breaking if non-vanishing) always occur in the combination (6.19), so technically it makes no difference which of the two mediates the SI breaking.

[21] A SI matter theory would lead to observational problems: As argued in [36, 29], this would imply a direct coupling between brane matter and ϕ, corresponding to an additional (Brans-Dicke like) force of gravitational strength. This is clearly ruled out by solar system observations [170] unless a mechanism is included to shield the dilaton fluctuations inside the solar system. A complete study of this case is thus beyond the scope of our present work.

$\gamma = 0$ and $\gamma > 1/2$, the exponent saturates to the constant value -1.

The above formula allows us to discuss the consistency of the delta limit. We distinguish two cases:

1. For $\gamma \geq 0$, increasing the volume of the compact space leads to a decreasing angular pressure. In other words, when we make the hierarchy between transverse brane size and bulk volume large, the angular pressure tends to zero in accordance with the physical expectation. Moreover, in this limit the SI case is approached (since $\mathcal{C}_+ \propto \gamma V^{-\gamma} \to 0$), which renders the above approximations more and more accurate. As an aside, note that this observation, i.e. the concurrency of p_θ being small and having a small amount of SI breaking, is the loophole to the objections raised in [31]. We discuss this more extensively in Sec. 6.3.1.4.

2. For $\gamma < 0$ the situation is different: If $\tau > 0$, the system eventually hits a point (just before it becomes super-critical) where (6.39) yields no real solution for p_θ anymore, indicating a runaway behavior. Therefore, a discussion of that case requires the inclusion of a general time dependence of the fields which is beyond the scope of this work.

   On the other hand, if $\tau < 0$, there are static solutions for which p_θ grows as V is increased due to (6.39). This is related to the observation that the system gets driven away from SI ($\mathcal{C}_+ \to \infty$). As a result, the 4D curvature $\bar{\mathcal{R}}$ cannot be kept under control for a phenomenologically large V unless the coefficient τ is tuned to be extremely small. Moreover, the tension tends to $-\infty$ in this case which strongly questions the physical consistency of these solutions [124]. So this case is not interesting, neither phenomenologically nor with respect to the tuning issue.

In summary, the exponential coupling with $\gamma \geq 0$ is of particular interest, as it allows to be close to SI, which is important to make the 4D curvature parametrically small. This is achieved by considering a sufficiently large bulk volume. Other types of couplings (including monomial and exponential ones with $\gamma < 0$) either lead to a runaway behavior or are incompatible with being close to SI (if the coefficient is not tuned to be small). The above discussion also shows that the physically relevant class of couplings is compatible with the delta description because p_θ (or any hidden metric dependence of the delta function as argued in [31]) vanishes for $V \to \infty$.

6.2.5 Phenomenology

We have singled out the exponential tension-dilaton coupling (6.43) as the phenomenologically relevant one, since its contribution to the 4D curvature can be made arbitrarily small. Let us now discuss whether this can lead to phenomenologically viable solutions.

At the present stage, there are two main phenomenological inputs the model has to comply with:

1. In models with large extra dimensions the weakness of 4D gravity is a result of the large extra dimensions. This is possible because the 4D Planck mass is given, via dimensional reduction, by [29]

$$M_{\rm Pl}^2 = \frac{V}{\kappa^2}\,. \tag{6.48}$$

   Given present tests of the gravitational inverse square-law [107] (see [4] for a review), the upper bound on the size of the extra dimensions is of order a few ten microns. Then, (6.48) implies that the bulk gravity scale $\kappa^{-1/2}$ is not allowed to be significantly below ~ 10 TeV, which translates to the upper bound

$$\frac{V}{\kappa} \lesssim 10^{28}\,. \tag{6.49}$$

2. The observed value of the 4D curvature measured in Planck units is notoriously small, viz. [2]

$$\frac{\bar{\mathcal{R}}}{M_{\rm Pl}^2} \sim 10^{-120}\,. \tag{6.50}$$

   According to our sign conventions, observations would also require a negative sign of $\bar{\mathcal{R}}$. Here, we use the weaker constraint (6.50), demanding the absolute value of $\bar{\mathcal{R}}$ to have the correct order of magnitude. In fact, a sign sensitive discussion would not alter the tuning issue we are actually interested in (but it would make the discussion more involved).

Let us now study whether the model is compatible with both requirements. For convenience, we will set $\kappa = 1$, i.e. here and henceforth dimensionful quantities are all measured in units of the bulk gravity scale.

We now make use of our central formula (6.42) which permits to express the 4D curvature in terms of the extra space volume. Using (6.44), (6.46) as well as (6.48), we then find that the leading contribution is

$$\frac{\bar{\mathcal{R}}}{M_{\rm Pl}^2} = N_1 V^{-(2+\gamma)} + N_2 V^{-3}\,, \tag{6.51}$$

where N_i are dimensionless coefficients, with

$$N_1 = 2\tau\gamma\left(\frac{\pi\alpha_+}{e^2}\right)^{\gamma} \qquad \text{and} \qquad N_2 = \eta\ell^2\,. \tag{6.52}$$

The constant of proportionality η is due to the unknown coefficient of the $\mathcal{O}(\epsilon)$ term in (6.42). It is a function of all model parameters, including α_+ and τ. Generically, we expect it to be ~ 1. While at this point, it is merely a reasonable expectation, this will also

be confirmed by the numerical solutions discussed in Sec. 6.3, which allow us to explicitly calculate the coefficient. The relation (6.51) is one of the main results of this work. The two phenomenological bounds above then require

$$N_1 \times 10^{-28(2+\gamma)} + N_2 \times 10^{-84} \lesssim 10^{-120}\,. \tag{6.53}$$

One way how this could in principle be fulfilled is by assuming a cancellation of the two terms. However, this would only be achieved by tuning the parameters γ and τ very accurately. Therefore, we dismiss this possibility and demand both terms to fulfill the bound separately. From (6.52), we know that the first term vanishes identically for a SI coupling ($\tau\gamma = 0$). If SI is broken, it could only comply with the bound without tuning N_1 if $\gamma \gtrsim 2.3$.[22] The second term, though, is more problematic: it implies that $N_2 \lesssim 10^{-36}$ (otherwise, for $N_2 \sim 1$, (6.51) implies that $\bar{\mathcal{R}}$ could only be sufficiently small if V exceeds its phenomenological bound by 12 orders of magnitude). However, for generic values of the brane tension, we expect $\eta \sim 1$, which will be explicitly confirmed in Sec. 6.3. In this case, the bound could only be fulfilled if the brane width ℓ is ~ 18 orders of magnitude smaller than the bulk Planck length. Not only would this again correspond to introducing an a priori hierarchy by hand, but also question the applicability of a classical analysis.

On the other hand, if ℓ is not below the Planck length, the only alternative is to tune the brane tension to make η sufficiently small. For instance, let us consider the (trivial) limit where all brane parameters are sent to zero, explicitly $\{\lambda_+, \lambda_-, \Phi_+, \tau\} \to 0$, corresponding to a physical situation where both branes are absent and accordingly full SI is restored.[23] In that case, the system uniquely approaches the GGP solution, characterized by a vanishing 4D curvature [83]. And indeed, due to (6.51), this is only possible if $\eta \to 0$. As several dimensionful parameters (including the tensions) have been set to zero by hand, it should be clear that this corresponds to an unacceptable tuning. This also agrees with the result of [133] where it was shown that a vanishing 4D curvature is only guaranteed by SI (for which the above limit is a special case); however, it was also shown that this is only possible at the price of introducing a parameter constraint. Therefore, we arrive at the following conclusion:

> *If we do not allow the model parameters to be fine-tuned or to introduce large hierarchies, the model is ruled out phenomenologically. Either the 4D curvature or the size of the extra dimensions would be too large to be compatible with observations.*

Before concluding this sections, let us summarize the assumptions that went into this result:

1. The interior profiles are close to their flat space estimates with corrections $\mathcal{O}(\epsilon)$, cf. Eq. (6.37).

[22] In Sec. 6.3, however, we will uncover yet another fine-tuning (imposed by flux quantization) which could only be avoided if $\gamma \ll 1$.

[23] More general, we could also consider a situation without warping to realize $\eta = 0$; however, this would correspond to the same tuning.

2. The (relative) difference between V and $V_{\rm GGP}$ is assumed to vanish in the thin brane limit, cf. Eq. (6.46).

3. The coefficient η in (6.52) is at least of order unity.

They are all quite reasonable, and will indeed all be explicitly confirmed by our numerical analysis. Moreover, the numerical treatment will allow us to infer the amount of tuning (due to flux quantization) that is required to get a sufficiently small 4D curvature (albeit corresponding to a too large V).

6.3 Numerical results

To further solidify the analytical picture, we solved the whole system—consisting of the bulk equations (6.15), (6.16), the matching (6.32) as well as the boundary (6.34), (6.35) conditions—numerically. Before presenting our results, let us briefly sketch the algorithm.

As explained before in the non SI case, the solution is completely fixed once the boundary conditions for B and ϕ, as well as the flux quantization condition (6.11) is imposed. On a technical level, a difficulty occurs when we start the integration at the north pole because this requires to specify the three integration constants $(\bar{\mathcal{R}}, Q, \phi_0)$, which are only implicitly determined by the two boundary conditions at the south pole (viz. $B'_- = -\alpha_-$ and $\phi'_- = 0$) and the quantization condition on $\Phi_{\rm tot}$. This problem can be resolved by using a standard shooting method: First, we make a random choice for the integration constants which allows us to integrate[24] the equations down to the south pole. In general, the resulting solution violates both the flux and the boundary conditions. Second, these violations are minimized by using a root finding algorithm that varies the integration constants; once converged, it yields the correct values for $(\bar{\mathcal{R}}, Q, \phi_0)$.

In the first part of this section, we check the consistency of our regularization by taking the thin brane limit. This in turn enables us to confirm the assumptions made in the last section. In the second part, we infer the amount of tuning necessary to keep the 4D curvature or the volume within its phenomenological bound.

6.3.1 Consistency of the thin brane limit

The key question of our study is whether the model allows for technically natural solutions that are compatible with the observed 4D curvature. To answer that question, we should thus restrain from including any a priori hierarchies into the action that are unstable under radiative corrections. In fact, we will follow a rather conservative approach and assume that all model parameters take generic values set by the bulk gravity scale κ (which is of order TeV). We make the specific (but arbitrary) choice

$$e = 1\,, \qquad \rho_+ = 1\,, \qquad \Phi_+ = -0.6\,, \qquad \alpha_+ = 0.9 \qquad \text{and} \qquad \alpha_- = 0.25\,, \tag{6.54}$$

[24] We use the Runge-Kutta-Fehlberg algorithm (implemented in Python) to find the numerical solution [79].

where we again used units for which $\kappa = 1$. Of course, we checked that different values would not alter the results, provided they do not involve a specific tuning.[25] The gauge coupling parameter $\tilde{e}$ enters merely through the flux quantization, motivating hence the definition

$$\mathcal{N} := \frac{2\pi n}{\tilde{e}}\,. \tag{6.55}$$

We will use this parameter [which equals the total flux due to (6.11)] as a dial to realize any desired value of the extra space volume V (or the 4D curvature $\bar{\mathcal{R}}$).[26] After specifying the ϕ-dependence of the tension term in (6.43) by setting

$$\tau = 0.7 \times 2\pi \qquad \text{and} \qquad \gamma = 0.2\,, \tag{6.56}$$

the solution is uniquely determined.

6.3.1.1 Numerical profiles

To get a first idea of the regularized system, we depict the ρ-profiles for B, W and Φ as well as their first derivatives in Fig. 6.2 for three different values of V (corresponding to three different choices of $\mathcal{N}$). First, we find that the system is sufficiently regular because ϕ' and W' vanish at the south pole. Only B' is non-vanishing which implies a conical singularity, as expected. Due to the presence of localized matter, all derivatives have a finite discontinuity at the brane position. With regard to the interior profiles, the larger we choose the hierarchy between brane size and extra space volume, the flatter the geometry gets. This already confirms one of the assumptions used in the last section on a qualitative level. Since we did not tune both tensions to be cloth to each other, the solution is warped.

In summary, we have successfully solved the regularized setup because the profiles are all finite and in line with the physical expectation.

6.3.1.2 GGP asymptotics

Let us now check whether the GGP solutions are correctly reproduced in the thin brane limit. This constitutes an important consistency check of both the ring regularization and the numerical solver. To be compatible with SI, we switch off the explicit dilaton-tension coupling by setting $\tau = 0$. Now, the idea is to increase V (by dialing $\mathcal{N}$) while keeping all other model parameters fixed. In order to see whether the GGP solutions are approached, we use three different measures that are all supposed to vanish in this limit:

1. The 4D curvature $\bar{\mathcal{R}}$,

[25] For example, if both tensions are chosen very close to each other, the warping disappears and the solution shows a qualitatively different behavior. However, this type of tuning is exactly what we want to avoid as it would introduce just another (at least potential) naturalness problem.

[26] To which extend this constitutes a tuning of model parameters is discussed in Sec. 6.3.2 extensively.

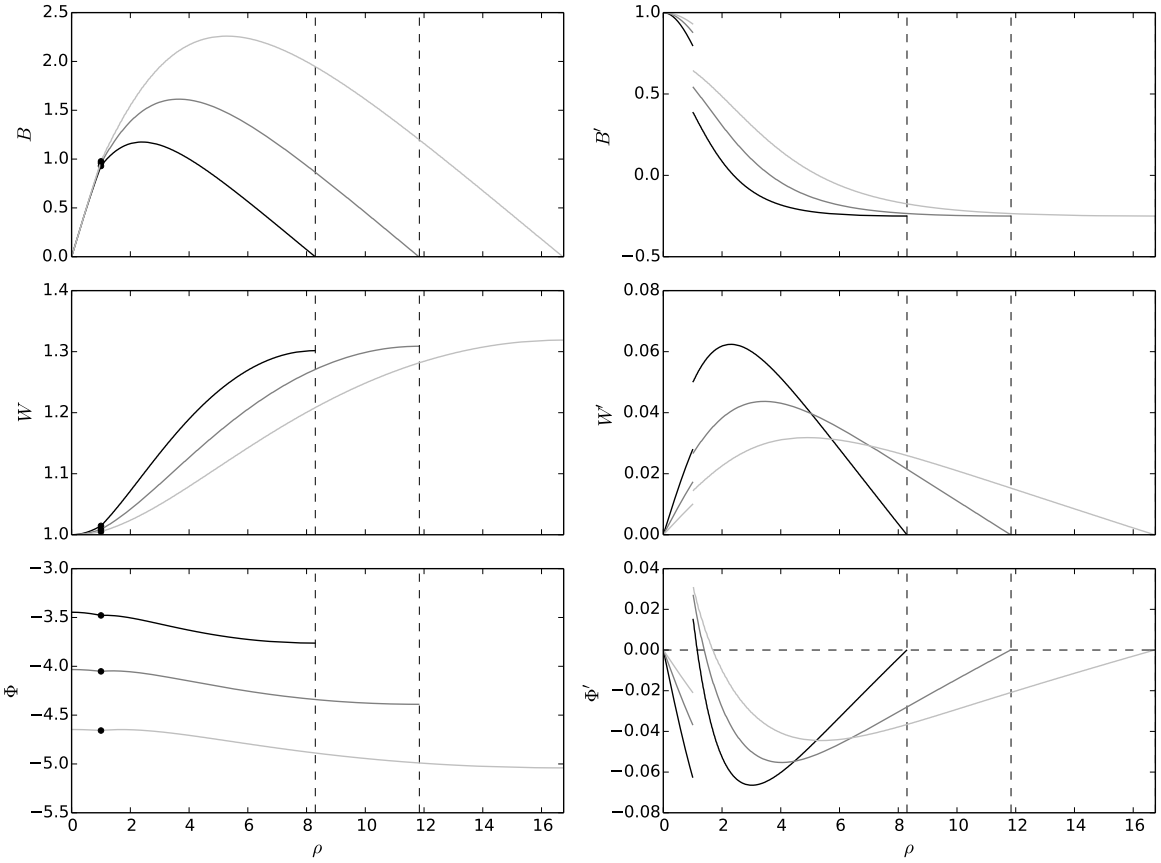

Figure 6.2: Numerical solutions for parameter values (6.54) and (6.56) with $V = 16\pi$ (black), $V = 32\pi$ (dark gray) and $V = 64\pi$ (light gray). The black dot highlights the brane position. The solutions are regular at both axes (see 2nd column), except for a conical singularity at the south pole, i.e. $B'_+ \neq 0$. For a larger volume, the interior profiles are closer to the flat space expectation.

2. the relative deviation of the extra space volume from its GGP value (6.46),

$$\delta V/V := (V_{\text{GGP}} - V)/V\,, \tag{6.57}$$

3. and likewise, the deviation of the total flux from its GGP value (6.29),

$$\delta\Phi := \Phi_{\text{GGP}} - \Phi_{\text{tot}}\,, \qquad \text{with} \qquad \Phi_{\text{GGP}} := \frac{2\pi}{e}\sqrt{\alpha_+\alpha_-} + \Phi_+\,. \tag{6.58}$$

For the parameter choice (6.54) our numerical results are shown in Fig. 6.3. We find that all of the above quantities vanish in the thin brane limit. The corresponding power laws are inferred numerically. The result for $\bar{\mathcal{R}}$ coincides with the scaling found in (6.51) (after using $M_{\text{Pl}} = V$ and setting $N_1 = 0$), which hence confirms our analytical analysis. In

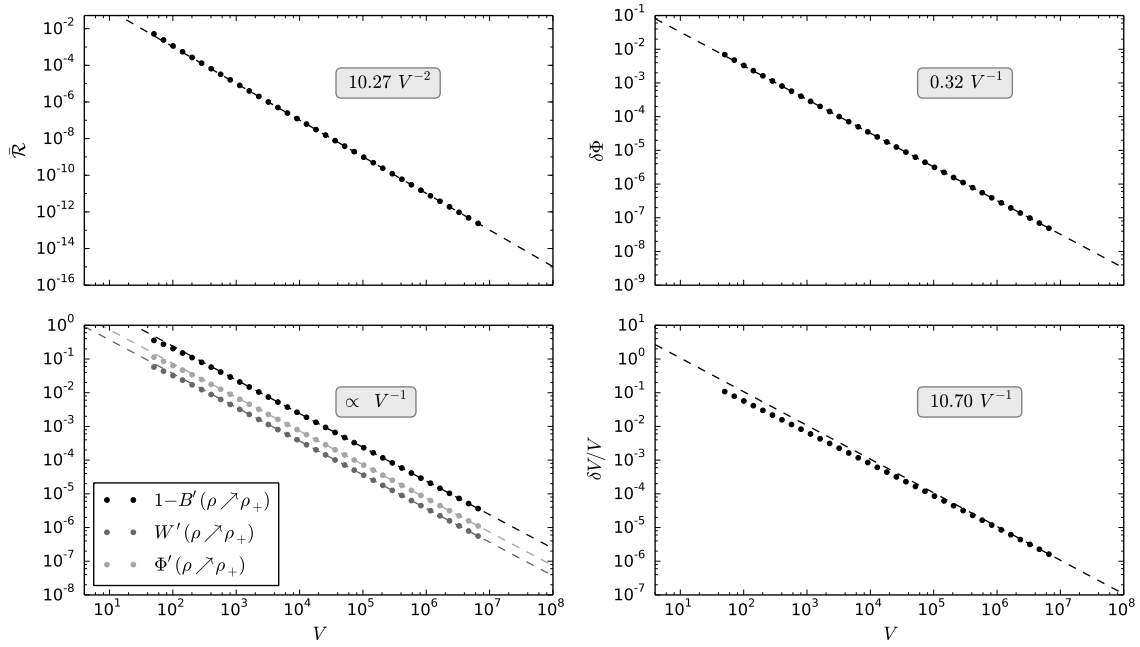

Figure 6.3: Results of the thin brane limit for a SI dilaton coupling ($\tau = 0$) and parameter values (6.54). Different dots corresponds to solutions with different V (and hence $\mathcal{N}$). The dashed lines are the analytically expected power laws with fitted coefficient. We find that $\bar{\mathcal{R}}$, $\delta\Phi$ and $\delta V/V$ vanish in agreement with the GGP expectation. Moreover, we confirm all analytic assumptions: The ρ-derivatives approach their flat space values like $1/V$, $\delta V/V \to 0$ and the coefficient in (6.52) is $N_2 \approx 10.27$.

particular, this shows that the dominant contribution to $\bar{\mathcal{R}}$ (for SI couplings) is indeed of order ϵ ($\propto 1/V$).

6.3.1.3 Approximation control

Our numerical results also enable us to check the validity of the assumptions made in Sec. 6.2. First, by fitting the values of B', W' and Φ' (evaluated in the limit $\rho \nearrow \rho_+$) as a function of V, we find that deviations of the interior profile from its flat space version are of order ϵ, in accordance with (6.37). Second, the extra space volume approaches its GGP value (6.46), which follows from $\delta V/V \to 0$. Third, the coefficient N_2 turns out to be of order one (or above), which was crucial for the phenomenological discussion in Sec. 6.2.5 to be applicable. As a result, all assumptions are verified numerically, at least for SI couplings.[27]

In that context, let us also discuss to which extend the scaling laws depicted in Fig. 6.3 and the size of N_2 are generic predictions. By running our numerics for different model

[27]We checked their validity also for several couplings with $\tau \neq 0$.

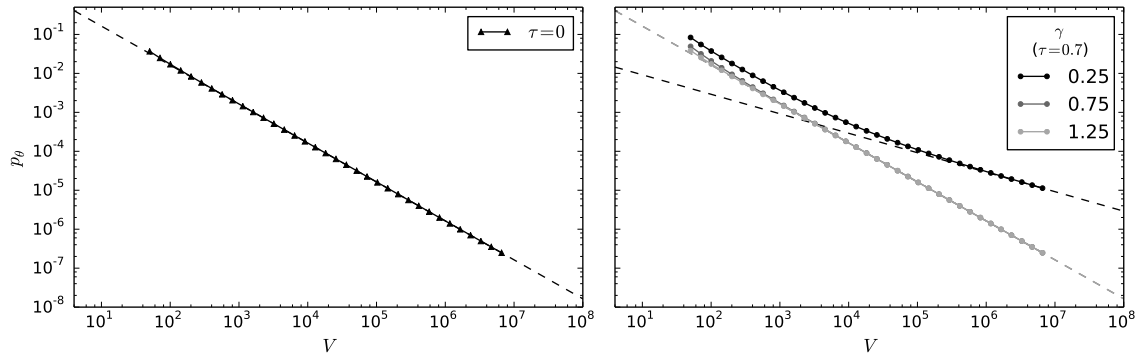

Figure 6.4: Pressure in angular direction as a function of V for SI ($\tau = 0$) and SI breaking ($\tau \neq 0$) dilaton coupling. Parameter values as in (6.54). Dashed lines correspond to the analytic expectation (6.47). We see that in all cases p_θ vanishes in the thin brane limit.

parameters, we find that the scalings are indeed independent of the precise value of the tensions and the parameter e (which can be absorbed into a constant shift of ϕ and a rescaling of Q). In contrast, the coefficient N_2 does dependent on the microscopic size of the brane $\ell \approx 2\pi\rho_+$. Explicitly, we reproduce the quadratic dependence in (6.52). As mentioned before, the assumption $\ell \gtrsim 1$ is thus central to our analysis. However, whether all parameters (including $\mathcal{N}$ which we have not considered so far) can be chosen independent from each other or whether they have to fulfill some parameter constraint is a different question that will be addressed in Sec. 6.3.2.

6.3.1.4 Angular pressure

In a physically sensible setup, the angular pressure has to vanish in the thin brane limit. We put a lot of emphasis on this issue in our analytic discussion in Sec.6.2.3. Now, we have the means to check whether this is indeed the case—at least for exponential couplings. Our results are depicted in Fig. 6.4 for SI ($\tau = 0$) as well as SI breaking ($\tau \neq 0$) dilaton-tension couplings. In both cases, we find that the pressure is vanishing as expected, and we reproduce the analytically derived scaling (6.47), which corresponds to the dashed lines.

This context seems suitable for addressing the issues raised in the analysis of [31]. There the authors objected to the use of two-dimensional delta functions for describing an infinitely thin brane (as we did in Sec. 6.1). They argued that this approach would miss an additional angular metric dependence of a codimension-two source that is not captured by delta functions. More precisely, they allowed for a hidden metric dependence of the delta function, parametrized as

$$\frac{\partial\delta^{(2)}(y)}{\partial g_{\theta\theta}} =: C\,\frac{\delta^{(2)}(y)}{g_{\theta\theta}}\,, \tag{6.59}$$

which leads to an additional localized source term in the $(\theta\theta)$ Einstein equation. Them, the value of C can be inferred from the $(\rho\rho)$ Einstein equation, specifically,

$$\mathcal{T}_+ C \simeq -\frac{\kappa^2}{8\pi}\left(1-\frac{\kappa^2\mathcal{T}_+}{2\pi}\right)^{-1}\mathcal{T}_+'^2\,, \tag{6.60}$$

where we neglected higher order terms in $\mathcal{T}_+'$ and set $\Phi_+ = 0$ for simplicity. For $\mathcal{T}_+' \neq 0$, which corresponds to a breaking of SI, this equation implies $C \neq 0$. For SI couplings, we get $C = 0$, proving the absence of any additional metric dependence. In other words, two-dimensional delta functions seem insufficient for describing the system in the non SI case (for which $\mathcal{T}_+' = 0$ is not guaranteed).

With that said, we arrive at a puzzle: The constant C is equivalent to an angular pressure. Specifically, by comparing with (6.41), we identify $\lim_{\epsilon\to 0} p_\theta \equiv -2\mathcal{T}_+(\phi)C$. Thus, the statement of [31] can be rephrased as saying that an infinitely thin brane can have an angular pressure in the non SI case. From a physical perspective this is surprising as for a point like object there is no direction the pressure could act in. Moreover, for the special choice of an exponential dilation-tension coupling, we have explicitly seen that $p_\theta \to 0$ in the thin brane limit.

However, there is a loophole to the above argumentation because the right side of (6.60) depends on ϕ_+ through $\mathcal{T}_+(\phi)$. Consequently, without knowing its value we cannot say whether $C \neq 0$ is realized for any configuration. In fact, it is possible that ϕ_+ is always such that the right side vanishes (corresponding to the SI point). In that case, it would be impossible to break SI on a codimension-two brane—at least for a 4D maximally symmetric setup, as was assumed here.[28] Proving this hypothesis requires to solve the whole bulk-brane system to obtain the radial profiles of all functions.

This is exactly what we did in our work by studying the thick brane setup for the relevant class of exponential brane-dilaton couplings, cf. (6.43). We found that for $\gamma > 0$, p_θ, and hence also C, go to zero (as a consequence of $\phi_+ \to -\infty$) when the codimension-two case is approached. Thus, the loophole is indeed realized for exponential couplings. We checked it also for several monomial couplings like the linear one, $\mathcal{T}_+(\phi) \propto \phi$. Of course, we could not investigate all possible couplings but, based on our previous findings, we conjecture that they either lead to $C \to 0$ in the thin brane limit or come with some sort of pathology (like the runaway for $\gamma < 0$ as discussed in Sec. 6.2.4).

At this point, let us stress that it was mandatory to solve the whole system to answer that question unambiguously. In particular, solving only the equations close to one brane is insufficient as for example the value of p_θ crucially depends on the boundary conditions at the south pole.

[28] A plausible possibility would be that SI breaking solutions always show a run-away behavior, which would be incompatible with 4D maximal symmetry. Answering that question was beyond the scope of our work.

6.3.2 Tuning estimates

The scaling law (6.51) (albeit incompatible with observational bounds for a sizable brane width) illustrates in which way models with large extra dimensions might address the CC problem: There is an inverse scaling relation between $\bar{\mathcal{R}}$ and V, thus, a large extra-dimensional volume creates a small 4D curvature. In this section, we discuss whether this mechanism is realized for generic model parameters or implies a specific tuning among them. In that context, let us stress that we do not calculate loop contributions, so it is not clear whether a certain tuning might be protected against quantum corrections. However, our analysis is able to pin down the bounds those corrections would need to fulfill in order not to spoil the classical tuning.

It turns out that $\delta\Phi$ is a convenient measure for the amount of tuning a certain solution requires. Using the flux quantization condition (6.11), the definition (6.58) implies

$$\delta\Phi = \frac{2\pi}{e}\sqrt{\alpha_+\alpha_-} + \Phi_+ - \frac{2\pi n}{\tilde{e}}\,, \tag{6.61}$$

which is a relation among model parameters only. In other words, the value of $\delta\Phi$ quantifies to which extend λ_+, λ_-, Φ_+, e and $\tilde{e}$ have to be tuned to achieve a certain value of $\bar{\mathcal{R}}$ (or V).

6.3.2.1 Scale invariant dilaton coupling

Let us first consider SI brane-dilaton couplings, i.e. $\tau = 0$. As depicted in Fig. 6.3, we find the following relation

$$\delta\Phi \sim V^{-1} \sim \left(\frac{\bar{\mathcal{R}}}{M_{\rm Pl}^2}\right)^{1/3} \sim 10^{-40}\,, \tag{6.62}$$

where we used $M_{\rm Pl}^2 = V$. Therefore, the parameters in (6.62) have to be tuned up to (at least) 40 decimal places to comply with the phenomenological bound on $\bar{\mathcal{R}}$ (following the discussion in Sec. 6.2.5 this would violate the bound on V by 12 orders of magnitude). This is certainly not any better than the tuning problem we started with. On the other hand, we still need to tune 28 decimal places to realize the largest V that is compatible with observation (but then $\bar{\mathcal{R}}/M_{\rm Pl}^2$ would be 36 orders of magnitude larger than the observed value).

6.3.2.2 Scale invariance breaking dilaton coupling

Let us know check whether there is some improvement for SI breaking couplings, i.e. $\tau \neq 0$. In that case, the outcome crucially depends on the value of γ. The scaling of $\bar{\mathcal{R}}$ and V with $\delta\Phi$ is depicted in Fig. 6.5. From this we can infer the empirical scaling law

$$\bar{\mathcal{R}} \propto \begin{cases} \delta\Phi^{1+1/\gamma} \\ \delta\Phi^2 \end{cases}, \qquad V \propto \begin{cases} \delta\Phi^{-1/\gamma} & (\text{for } 0<\gamma<1) \\ \delta\Phi^{-1} & (\text{for } 1<\gamma) \end{cases}. \tag{6.63}$$

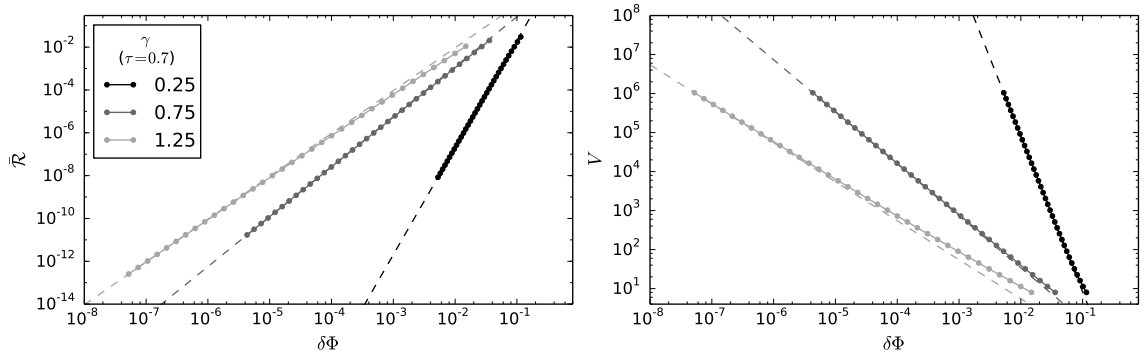

Figure 6.5: Tuning precision, quantized by $\delta\Phi$, needed to obtain a certain value of $\bar{\mathcal{R}}$ or V. Parameter values as in (6.54). The dashed lines are numerically inferred power laws valid for $\delta\Phi \ll 1$. In general, a small 4D curvature or large extra space volume requires a high tuning precision (corresponding to a small $\delta\Phi$). Remarkably, we find that for smaller values of γ less tuning is needed.

The first important observation is that our analytical results are fully confirmed. More precisely, by eliminating $\delta\Phi$ we get

$$\bar{\mathcal{R}} \propto \begin{cases} V^{-(1+\gamma)} \\ V^{-2} \end{cases}, \tag{6.64}$$

which indeed describes the asymptotic scaling of (6.51) (after using $M_{\rm Pl} = V$). This provides the final confirmation of the phenomenological discussion in Sec. 6.2.5.

For $\gamma > 1$ we get the same (asymptotic) scaling as in the previously discussed case with SI coupling $\tau = 0$, hence the same tuning problem arises. On the contrary, for $\gamma < 1$ the situation turns out to be more favorable. A phenomenologically small $\bar{\mathcal{R}}$ can now be realized by choosing γ small enough (instead of $\delta\Phi$). To see this, consider the observational constraint

$$\delta\Phi^{1+2/\gamma} \sim \frac{\bar{\mathcal{R}}}{M_{\rm Pl}^2} \sim 10^{-120}\,. \tag{6.65}$$

It can be satisfied by choosing $\delta\Phi \sim 0.1$ and $\gamma \sim 1/60$, which are both not hierarchically small numbers. In that case, due to (6.63), the extra space volume becomes extremely large $V \sim 10^{60}$. Alternatively, we could also choose $\gamma \sim 1/28$ which would lead to a viable volume, but then $\bar{\mathcal{R}}$ would exceed its observed value by 63 orders of magnitude.

First, this is remarkable because both a hierarchically small curvature and large volume are realized without the need of tuning any model parameters, which is indeed a conceptually interesting feature of the setup. On the downside, choosing $\gamma < 1$ leads to a worsening of the phenomenological problems.

At this point it worth noting that a similar result was obtained before in [29]; there it was

found that it is possible to realize a phenomenologically large volume without the need of any tuning. However, here we go a step further and reveal the (ominous) phenomenological consequences.

Finally, we can ask what tuning is necessary for a solution *to be* phenomenologically viable. In that case, we actually identify two independent tuning problems:

1. According to the discussion below equation (6.50), either ℓ has to be $\sim$ 18 orders of magnitude below the 6D Planck length[29] or its coefficient has to be tuned close to zero, $\eta \sim 10^{-36}$.

2. If we demand $N_1 \sim 1$, $\gamma \gtrsim 2.3$ due to (6.50). In that case, we read off from (6.65) the tremendous tuning $\delta\Phi \sim 10^{-64}$. If on the other hand we demand $\delta\Phi \sim 0.1$ in order to avoid the particular tuning (6.61), we have to choose $N_1 \sim 10^{-63}$, which is yet another unacceptable tuning.[30]

6.4 Discussion

Our analysis constitutes an extensive discussion of the SLED proposal. We investigate both the thin and thick brane setup, and provide a complete and consistent physical picture that takes into account the brane's backreaction to the bulk geometry. In this work, we followed a two step approach:

1. To infer the model's potential with respect to the CC problem, we looked for 4D flat solutions that do not rely on a tuning of model parameters.

2. To infer its phenomenological potential, we studied 4D de Sitter solutions. In particular, we asked under which conditions the observational bounds on the curvature scale and the extra-dimensional volume can be fulfilled.

According to claims in the literature, [33, 34, 27], the first step has already been achieved. Specifically, it was assumed that the absence of a brane-dilaton coupling ($\mathcal{A}_b' = \mathcal{T}_b' = 0$) implies a trivial dilaton profile, and hence via (6.23) a vanishing 4D curvature. In that case, the BLF term would lead to an explicit breaking of SI, which was assumed to be the key to resolve the tuning problem that is normally caused by the FQC (6.11). The reason is that in the non SI case, Eq. (6.11) fixes the value of ϕ_+, instead of constraining the model parameters. The conclusion therefore was that 4D flatness can be achieved for a generic choice of model parameters, which would exactly correspond to the type of solution we were looking for. However, we showed that the above reasoning was based on a wrong boundary condition for the dilaton. Using the corrected version (6.15) (which takes into account how the Maxwell field backreacts on the dilaton sector) leads to a different conclusion:

[29] We consider this a special type of tuning because ℓ has to be very close to zero. It is not clear whether such a hierarchy is respected by quantum corrections.

[30] This follows from (6.63), when we assume that the scaling of V with $\delta\Phi$ is not affected by N_1.

Only a SI brane-dilaton coupling ensures a vanishing 4D curvature.

This is bad news because it leads to a tuning on model parameters (6.29), as expected in the SI case. Recently, this was also confirmed in an explicit UV model [28].

This result casts doubts on the models capacity to solve the CC problem. Nevertheless, it was not clear whether the same conclusion holds in the more realistic case of a 4D de Sitter geometry on the brane. In other words, one might have the hope that the tuning disappears if a non-vanishing curvature on the brane is taken into account. Moreover, the generalized approach offered the possibility to test the phenomenological viability of the model. Accordingly, in the second step, we identified two sources contributing to $\bar{\mathcal{R}}$, both of which have to be included in a realistic setup: First, a dilaton-tension coupling, which is induced by quantum lops of localized matter fields (provided the SM sector breaks SI), and second, a finite, microscopic brane width ℓ, which also constitutes a convenient regularization of the system. Both contributions lead to a breaking of SI (either explicitly or implicitly). On a technical level, we considered an exponential dilaton-tension coupling (which has the advantage of being suppressed for a large extra space volume V) and a well-known ring regularization (which is the most minimal way of introducing a brane width).

We then found an analytic relation between two specific 4D observables on the brane, the curvature scale $\bar{\mathcal{R}}$ and the KK mass scale $V^{-1/2}$, which in turn allowed us to confront the model with the two corresponding phenomenological bounds. The relation was derived in two (independent) ways: First, fully analytically by making certain reasonable assumptions about the solution of the full system, and second, by integrating the equations numerically from the north to the south pole. Provided all parameter values are generically set by the 6D Planck mass, we find that the two bounds cannot be fulfilled simultaneously (in one case V exceeds its bound by 12 orders of magnitude, in the other case $\bar{\mathcal{R}}$ is 36 orders of magnitude too large). This negative conclusion would only be avoided if ℓ was hierarchically small compared to the 6D Planck length (or the brane tensions were tuned with extremely high precision). However, we consider this a physically problematic scenario because it is questionable whether such a hierarchy would be protected from loop corrections. Neither is it clear whether quantum gravity effects should be taken into account to describe a sub-Planckian brane size.

Independent of the model's phenomenological potential, we investigated the tuning issue. We found that the rigid relation in the SI case, viz. (6.29), can indeed be relaxed if SI is broken. We quantified the amount of tuning that is still needed to achieve a certain value of $\bar{\mathcal{R}}$ (or V). The good news is that, in agreement with the findings in [29], the tuning can be avoided either for $\bar{\mathcal{R}}$ or V by choosing the γ parameter, which characterizes the brane-dilaton coupling, small enough. On the downside, it cannot be avoided for both quantities at the same time. In fact, the phenomenological problems become even worse, unless yet another tuning (on N_1) is imposed.

In summary, we either violate the phenomenological bounds by many orders of magnitude or we have to deal with a tremendous tuning of model parameters. For the moment, this is the biggest challenge to the SLED proposal.

Our discussion relies on the expectation that the model parameters take generic values set by the bulk gravity scale. This choice makes sure that no unnatural hierarchies are introduced by hand and hence is physically sensible when addressing the CC problem. In principle, it might be possible, though rather unlikely, that this assumption can be relaxed in a technically natural way, i.e. without being spoiled by quantum corrections. A definite statement would require to calculate loop contributions for an explicit brane matter model, and is thus beyond the scope of the present work. Rather, our analysis was able to pin down the bounds radiative corrections would need to fulfill in order not to spoil the classically required tuning.

Bibliography

[1] Abbott, B. P., et al. Observation of Gravitational Waves from a Binary Black Hole Merger. *Phys. Rev. Lett. 116*, 6 (2016), 061102.

[2] Ade, P. A. R., et al. Planck 2013 results. XVI. Cosmological parameters. *Astron. Astrophys. 571* (2014), A16.

[3] Ade, P. A. R., et al. Planck 2015 results. XIII. Cosmological parameters. *ArXiv e-prints* (2015).

[4] Adelberger, E. G., Heckel, B. R., and Nelson, A. E. Tests of the gravitational inverse square law. *Ann. Rev. Nucl. Part. Sci. 53* (2003), 77–121.

[5] Afshordi, N., Geshnizjani, G., and Khoury, J. Do observations offer evidence for cosmological-scale extra dimensions? *JCAP 0908* (2009), 030.

[6] Aghababaie, Y., Burgess, C. P., Parameswaran, S. L., and Quevedo, F. Towards a naturally small cosmological constant from branes in 6-D supergravity. *Nucl. Phys. B 680* (2004), 389–414.

[7] Akhmedov, E. K. Vacuum energy and relativistic invariance. *ArXiv High Energy Physics - Theory e-prints* (2002).

[8] Amundsen, P. A., and Grøn, O. General static plane-symmetric solutions of the Einstein-Maxwell equations. *Phys. Rev. D 27* (Apr 1983), 1731–1739.

[9] Antoniadis, I., Arkani-Hamed, N., Dimopoulos, S., and Dvali, G. R. New dimensions at a millimeter to a Fermi and superstrings at a TeV. *Phys. Lett. B 436* (1998), 257–263.

[10] Antoniadis, I., Minasian, R., and Vanhove, P. Noncompact Calabi-Yau manifolds and localized gravity. *Nucl. Phys. B 648* (2003), 69–93.

[11] Apostolatos, T. A., and Thorne, K. S. Rotation halts cylindrical, relativistic gravitational collapse. *Phys. Rev. D 46* (Sep 1992), 2435–2444.

[12] Arkani-Hamed, N., Dimopoulos, S., Dvali, G., and Gabadadze, G. Non-local modification of gravity and the cosmological constant problem. *ArXiv High Energy Physics - Theory e-prints* (2002).

[13] Arkani-Hamed, N., Dimopoulos, S., and Dvali, G. R. The Hierarchy problem and new dimensions at a millimeter. *Phys. Lett. B 429* (1998), 263–272.

[14] Arkani-Hamed, N., Dimopoulos, S., and Dvali, G. R. Phenomenology, astrophysics and cosmology of theories with submillimeter dimensions and TeV scale quantum gravity. *Phys. Rev. D 59* (1999), 086004.

[15] Arkani-Hamed, N., Dimopoulos, S., Dvali, G. R., and Kaloper, N. Infinitely large new dimensions. *Phys. Rev. Lett. 84* (2000), 586–589.

[16] Arkani-Hamed, N., Dimopoulos, S., Kaloper, N., and Sundrum, R. A Small cosmological constant from a large extra dimension. *Phys. Lett. B 480* (2000), 193–199.

[17] Arnowitt, R. L., Deser, S., and Misner, C. W. The Dynamics of general relativity. *Gen.Rel.Grav. 40* (2008), 1997–2027.

[18] Bayntun, A., Burgess, C. P., and van Nierop, L. Codimension-2 Brane-Bulk Matching: Examples from Six and Ten Dimensions. *New J. Phys. 12* (2010), 075015.

[19] Berkhahn, F., Hofmann, S., and Niedermann, F. Brane Induced Gravity: From a No-Go to a No-Ghost Theorem. *Phys. Rev. D 86* (2012), 124022.

[20] Binetruy, P., Deffayet, C., Ellwanger, U., and Langlois, D. Brane cosmological evolution in a bulk with cosmological constant. *Phys. Lett. B 477* (2000), 285–291.

[21] Binetruy, P., Deffayet, C., and Langlois, D. Nonconventional cosmology from a brane universe. *Nucl. Phys. B 565* (2000), 269–287.

[22] Blanco-Pillado, J. J., Reina, B., Sousa, K., and Urrestilla, J. Supermassive Cosmic String Compactifications. *JCAP 1406* (2014), 001.

[23] Burgess, C. P. Quantum gravity in everyday life: General relativity as an effective field theory. *Living Rev. Rel. 7* (2004), 5–56.

[24] Burgess, C. P. Supersymmetric large extra dimensions and the cosmological constant: An Update. *Annals Phys. 313* (2004), 283–401.

[25] Burgess, C. P. Towards a natural theory of dark energy: Supersymmetric large extra dimensions. *AIP Conf. Proc. 743* (2005), 417–449. [,417(2004)].

[26] Burgess, C. P. Introduction to Effective Field Theory. *Ann. Rev. Nucl. Part. Sci. 57* (2007), 329–362.

[27] Burgess, C. P. The Cosmological Constant Problem: Why it's hard to get Dark Energy from Micro-physics. In *100e Ecole d'Ete de Physique: Post-Planck Cosmology Les Houches, France, July 8-August 2, 2013* (2015), pp. 149–197.

[28] Burgess, C. P., Diener, R., and Williams, M. EFT for Vortices with Dilaton-dependent Localized Flux. *JHEP 11* (2015), 054.

[29] Burgess, C. P., Diener, R., and Williams, M. Self-Tuning at Large (Distances): 4D Description of Runaway Dilaton Capture. *JHEP 10* (2015), 177.

[30] Burgess, C. P., Diener, R., and Williams, M. The Gravity of Dark Vortices: Effective Field Theory for Branes and Strings Carrying Localized Flux. *JHEP 11* (2015), 049.

[31] Burgess, C. P., Diener, R., and Williams, M. A problem with δ-functions: stress-energy constraints on bulk-brane matching (with comments on arXiv:1508.01124). *JHEP 01* (2016), 017.

[32] Burgess, C. P., Hoover, D., de Rham, C., and Tasinato, G. Effective Field Theories and Matching for Codimension-2 Branes. *JHEP 03* (2009), 124.

[33] Burgess, C. P., and van Nierop, L. Large Dimensions and Small Curvatures from Supersymmetric Brane Back-reaction. *JHEP 04* (2011), 078.

[34] Burgess, C. P., and van Nierop, L. Technically Natural Cosmological Constant From Supersymmetric 6D Brane Backreaction. *Phys. Dark Univ. 2* (2013), 1–16.

[35] Burgess, C. P., van Nierop, L., and Williams, M. Distributed SUSY breaking: dark energy, Newton's law and the LHC. *JHEP 07* (2014), 034.

[36] Burgess, C. P., van Nierop, L., and Williams, M. Gravitational Forces on a Codimension-2 Brane. *JHEP 04* (2014), 032.

[37] Capper, D. M. On Quantum Corrections to the Graviton Propagator. *Nuovo Cim. A25* (1975), 29.

[38] Carroll, S. M., and Guica, M. M. Sidestepping the cosmological constant with football shaped extra dimensions. *ArXiv High Energy Physics - Theory e-prints* (2003).

[39] Cavendish, H. Experiments to Determine the Density of the Earth. By Henry Cavendish, Esq. F. R. S. and A. S. *Philosophical Transactions of the Royal Society of London 88* (1798), 469–526.

[40] Charmousis, C., Copeland, E. J., Padilla, A., and Saffin, P. M. General second order scalar-tensor theory, self tuning, and the Fab Four. *Phys. Rev. Lett. 108* (2012), 051101.

[41] Charmousis, C., Emparan, R., and Gregory, R. Selfgravity of brane worlds: A New hierarchy twist. *JHEP 0105* (2001), 026.

[42] Charmousis, C., Gregory, R., Kaloper, N., and Padilla, A. DGP Specteroscopy. *JHEP 0610* (2006), 066.

[43] Chen, J.-W., Luty, M. A., and Ponton, E. A Critical cosmological constant from millimeter extra dimensions. *JHEP 09* (2000), 012.

[44] Cho, I. Inflation and nonsingular space-times of cosmic strings. *Phys. Rev. D 58* (1998), 103509.

[45] Christensen, M., Larsen, A. L., and Verbin, Y. Complete classification of the string - like solutions of the gravitating Abelian Higgs model. *Phys. Rev. 60* (1999), 125012.

[46] Clifton, T., Ferreira, P. G., Padilla, A., and Skordis, C. Modified Gravity and Cosmology. *Phys. Rept. 513* (2012), 1–189.

[47] Cline, J. M., Descheneau, J., Giovannini, M., and Vinet, J. Cosmology of codimension two brane worlds. *JHEP 06* (2003), 048.

[48] de Laix, A. A., Trodden, M., and Vachaspati, T. Topological inflation with multiple winding. *Phys. Rev.D 57* (1998), 7186–7191.

[49] de Rham, C. Massive Gravity. *Living Rev.Rel. 17* (2014), 7.

[50] de Rham, C., Hofmann, S., Khoury, J., and Tolley, A. J. Cascading Gravity and Degravitation. *JCAP 0802* (2008), 011.

[51] Deffayet, C. Cosmology on a brane in Minkowski bulk. *Phys. Lett. B 502* (2001), 199–208.

[52] Deffayet, C., Dvali, G. R., and Gabadadze, G. Accelerated universe from gravity leaking to extra dimensions. *Phys. Rev. D 65* (2002), 044023.

[53] Deffayet, C., Dvali, G. R., Gabadadze, G., and Vainshtein, A. I. Nonperturbative continuity in graviton mass versus perturbative discontinuity. *Phys. Rev. D 65* (2002), 044026.

[54] Dirac, P. A. *Lectures on quantum mechanics*. Dover Publications, 2001.

[55] Donoghue, J. F. General relativity as an effective field theory: The leading quantum corrections. *Phys. Rev. D 50* (1994), 3874–3888.

[56] Donoghue, J. F. Leading quantum correction to the Newtonian potential. *Phys. Rev. Lett. 72* (1994), 2996–2999.

[57] Donoghue, J. F. Introduction to the effective field theory description of gravity. In *Advanced School on Effective Theories Almunecar, Spain, June 25-July 1, 1995* (1995).

[58] Dubovsky, S. L., and Rubakov, V. A. Brane-induced gravity in more than one extra dimension: Violation of equivalence principle and ghost. *Phys. Rev. D 67* (May 2003), 104014.

[59] Durkee, M., Pravda, V., Pravdova, A., and Reall, H. S. Generalization of the Geroch-Held-Penrose formalism to higher dimensions. *Class. Quant. Grav. 27* (2010), 215010.

[60] Dvali, G. Predictive Power of Strong Coupling in Theories with Large Distance Modified Gravity. *New J. Phys. 8* (2006), 326.

[61] Dvali, G., and Gabadadze, G. Gravity on a brane in infinite volume extra space. *Phys. Rev. D 63* (2001), 065007.

[62] Dvali, G., Gabadadze, G., Hou, X.-r., and Sefusatti, E. Seesaw modification of gravity. *Phys. Rev. D 67* (2003), 044019.

[63] Dvali, G., Gabadadze, G., and Porrati, M. 4-D gravity on a brane in 5-D Minkowski space. *Phys. Lett. B 485* (2000), 208–214.

[64] Dvali, G., Gabadadze, G., Pujolas, O., and Rahman, R. Domain Walls As Probes Of Gravity. *Phys. Rev.D 75* (2007), 124013.

[65] Dvali, G., Gabadadze, G., and Shifman, M. Diluting Cosmological Constant via Large Distance Modification of Gravity. In *Continuous Advances in QCD 2002* (Dec. 2002), K. A. Olive, M. A. Shifman, and M. B. Voloshin, Eds., pp. 566–581.

[66] Dvali, G., Gabadadze, G., and Shifman, M. Diluting cosmological constant in infinite volume extra dimensions. *Phys. Rev. D 67* (2003), 044020.

[67] Dvali, G., and Gomez, C. Quantum Compositeness of Gravity: Black Holes, AdS and Inflation. *JCAP 1401* (2014), 023.

[68] Dvali, G., and Gomez, C. Quantum Exclusion of Positive Cosmological Constant? *Annalen Phys. 528* (2016), 68–73.

[69] Dvali, G., Gruzinov, A., and Zaldarriaga, M. The Accelerated universe and the moon. *Phys. Rev. D 68* (2003), 024012.

[70] Dvali, G., Hofmann, S., and Khoury, J. Degravitation of the cosmological constant and graviton width. *Phys. Rev. D 76* (2007), 084006.

[71] Dvali, G. R. Cosmological constant and Fermi-Bose degeneracy. *ArXiv e-prints* (2000).

[72] Dvali, G. R., Gabadadze, G., Kolanovic, M., and Nitti, F. Scales of gravity. *Phys. Rev. D 65* (2002), 024031.

[73] Dvali, G. R., Gabadadze, G., and Porrati, M. Metastable gravitons and infinite volume extra dimensions. *Phys. Lett. B 484* (2000), 112–118.

[74] Echeverria, F. Gravitational collapse of an infinite, cylindrical dust shell. *Phys. Rev. D 47* (1993), 2271–2282.

[75] Eglseer, L., Niedermann, F., and Schneider, R. Brane induced gravity: Ghosts and naturalness. *Phys. Rev. D 92* (2015), 084029.

[76] Einstein, A. Die Grundlage der allgemeinen Relativitätstheorie. *Annalen der Physik 354* (1916), 769–822.

[77] Einstein, A. HAMILTONsches Prinzip und allgemeine Relativitätstheorie. *Sitzungsberichte der Königlich Preußischen Akademie der Wissenschaften (Berlin), Seite 1111-1116.* (1916), 1111–1116.

[78] Einstein, A., and Rosen, N. On Gravitational waves. *J. Franklin Inst. 223* (1937), 43–54.

[79] Fehlberg, E. Classical fourth- and lower order runge-kutta formulas with stepsize control and their application to heat transfer problems. *Computing 6*, 1 (1970), 61–71.

[80] Fierz, M., and Pauli, W. On relativistic wave equations for particles of arbitrary spin in an electromagnetic field. *Proc. Roy. Soc. Lond. A173* (1939), 211–232.

[81] Franceschini, R., Giardino, P. P., Giudice, G. F., Lodone, P., and Strumia, A. LHC bounds on large extra dimensions. *JHEP 05* (2011), 092.

[82] Garriga, J., and Porrati, M. Football shaped extra dimensions and the absence of self-tuning. *JHEP 08* (2004), 028.

[83] Gibbons, G. W., Gueven, R., and Pope, C. N. 3-branes and uniqueness of the Salam-Sezgin vacuum. *Phys. Lett. B 595* (2004), 498–504.

[84] Giudice, G. F., Rattazzi, R., and Wells, J. D. Quantum gravity and extra dimensions at high-energy colliders. *Nucl. Phys. B 544* (1999), 3–38.

[85] Giudice, G. F., and Strumia, A. Constraints on extra dimensional theories from virtual graviton exchange. *Nucl. Phys. B 663* (2003), 377–393.

[86] Givoli, D. Non-reflecting Boundary Conditions. *J. Comput. Phys. 94*, 1 (May 1991), 1–29.

[87] Gorbunov, D., Koyama, K., and Sibiryakov, S. More on ghosts in DGP model. *Phys. Rev. D 73* (2006), 044016.

[88] Gott, III, J. R. Gravitational lensing effects of vacuum strings: Exact solutions. *Astrophys. J. 288* (1985), 422–427.

[89] Gregory, R. Cosmic p-branes. *Nucl. Phys. B 467* (1996), 159–182.

[90] Gregory, R. Inflating p-branes. *JHEP 06* (2003), 041.

[91] Gregory, R., Kaloper, N., Myers, R. C., and Padilla, A. A New perspective on DGP gravity. *JHEP 0710* (2007), 069.

[92] Gruending, L., Hofmann, S., Mueller, S., and Rug, T. Probing the Constituent Structure of Black Holes. *JHEP 05* (2015), 047.

[93] Gruzinov, A. On the graviton mass. *New Astron. 10* (2005), 311–314.

[94] Hassan, S., Hofmann, S., and von Strauss, M. Brane Induced Gravity, its Ghost and the Cosmological Constant Problem. *JCAP 1101* (2011), 020.

[95] Hilbert, D. *Gesammelte Abhandlungen: Band III: Analysis · Grundlagen der Mathematik Physik · Verschiedenes Lebensgeschichte*. Springer Berlin Heidelberg, Berlin, Heidelberg, 1970, ch. Die Grundlagen der Physik, pp. 258–289.

[96] Hiscock, W. A. Exact Gravitational Field of a String. *Phys. Rev. D 31* (1985), 3288–3290.

[97] Hofmann, S., Niedermann, F., and Schneider, R. Interpretation of the Weyl tensor. *Phys. Rev. D 88* (2013), 064047.

[98] Hofmann, S., and Rug, T. A Quantum Bound-State Description of Black Holes. *Nucl. Phys. B 902* (2016), 302–325.

[99] Hubble, E. A Relation between Distance and Radial Velocity among Extra-Galactic Nebulae. *Proceedings of the National Academy of Science 15* (Mar. 1929), 168–173.

[100] Israel, W. Singular hypersurfaces and thin shells in general relativity. *Il Nuovo Cimento B Series 10 44*, 1 (1966), 1–14.

[101] Israel, W. Singular hypersurfaces and thin shells in general relativity. *Il Nuovo Cimento B Series 10 48*, 2 (1967), 463–463.

[102] Jain, B., and Khoury, J. Cosmological Tests of Gravity. *Annals Phys. 325* (2010), 1479–1516.

[103] Joyce, A., Jain, B., Khoury, J., and Trodden, M. Beyond the cosmological standard model. *Physics Reports 568* (2015), 1 – 98.

[104] Kaloper, N., and Kiley, D. Charting the landscape of modified gravity. *JHEP 0705* (2007), 045.

[105] Kaloper, N., and Padilla, A. Vacuum Energy Sequestering: The Framework and Its Cosmological Consequences. *Phys. Rev. D 90* (2014), 084023.

[106] Kaluza, T. On the Problem of Unity in Physics. *Sitzungsber. ss. Akad. Wiss. Berlin (Math. Phys.) 1921* (1921), 966–972.

[107] Kapner, D., Cook, T., Adelberger, E., Gundlach, J., Heckel, B. R., et al. Tests of the gravitational inverse-square law below the dark-energy length scale. *Phys. Rev. Lett. 98* (2007), 021101.

[108] Klein, O. Quantum Theory and Five-Dimensional Theory of Relativity. (In German and English). *Z. Phys. 37* (1926), 895–906. [Surveys High Energ. Phys.5,241(1986)].

[109] Kowalski, M., et al. Improved Cosmological Constraints from New, Old and Combined Supernova Datasets. *Astrophys. J. 686* (2008), 749–778.

[110] Koyama, K. Are there ghosts in the self-accelerating brane universe? *Phys. Rev. D 72* (2005), 123511.

[111] Laguna, P., and Garfinkle, D. Space-time of Supermassive U(1) Gauge Cosmic Strings. *Phys. Rev. D 40* (1989), 1011–1016.

[112] Leblond, F., Myers, R. C., and Winters, D. J. Consistency conditions for brane worlds in arbitrary dimensions. *JHEP 07* (2001), 031.

[113] Levi-Civita, T. ds^2 *einstein*iani in campi *newton*iani. V: Il sottocaso B_2: Soluzioni longitudinali ($\xi = 0$). *Rom. Acc. L. Rend. (5) 27*, 2 (1918), 240–248.

[114] Levi-Civita, T. *Rend. Acc. Lincei 28* (1919), 101.

[115] Linet, B. On the supermassive U(1) gauge cosmic strings. *Class.Quant.Grav. 7* (1990), L75–L79.

[116] Lombriser, L., Hu, W., Fang, W., and Seljak, U. Cosmological Constraints on DGP Braneworld Gravity with Brane Tension. *Phys. Rev. D 80* (2009), 063536.

[117] Lue, A. Global structure of Deffayet (Dvali-Gabadadze-Porrati) cosmologies. *Phys. Rev. D 67* (2003), 064004.

[118] Lue, A. The phenomenology of Dvali-Gabadadze-Porrati cosmologies. *Physics Reports 423*, 1 (2006), 1 – 48.

[119] Lue, A., Scoccimarro, R., and Starkman, G. D. Probing Newton's constant on vast scales: DGP gravity, cosmic acceleration and large scale structure. *Phys. Rev. D 69* (2004), 124015.

[120] Lue, A., and Starkman, G. Gravitational leakage into extra dimensions: Probing dark energy using local gravity. *Phys. Rev. D 67* (2003), 064002.

[121] Luty, M. A., Porrati, M., and Rattazzi, R. Strong interactions and stability in the DGP model. *JHEP 0309* (2003), 029.

[122] Maartens, R., and Koyama, K. Brane-World Gravity. *Living Rev. Rel. 13* (2010), 5.

[123] Marder, L. Gravitational Waves in General Relativity. I. Cylindrical Waves. *Proceedings of the Royal Society of London. Series A, Mathematical and Physical Sciences 244*, 1239 (1958), 524–537.

[124] Marolf, D., and Trodden, M. Black holes and instabilities of negative tension branes. *Phys. Rev. D 64* (2001), 065019.

[125] Misner, C. W., Thorne, K. S., and Wheeler, J. A. *Gravitation.* W. H. Freeman and Company, New York, 1973.

[126] Narlikar, J. V., and Padmanabhan, T. *Gravity, Gauge Theories and Quantum Cosmology*, vol. 11. Springer Netherlands, 1986.

[127] Navarro, I. Codimension two compactifications and the cosmological constant problem. *JCAP 0309* (2003), 004.

[128] Navarro, I. Spheres, deficit angles and the cosmological constant. *Class. Quant. Grav. 20* (2003), 3603–3612.

[129] Navarro, I., and Santiago, J. Gravity on codimension 2 brane worlds. *JHEP 0502* (2005), 007.

[130] Nicolis, A., and Rattazzi, R. Classical and quantum consistency of the DGP model. *JHEP 0406* (2004), 059.

[131] Niedermann, F., and Schneider, R. Cosmology on a cosmic ring. *JCAP 1503*, 03 (2015), 050.

[132] Niedermann, F., and Schneider, R. Radially stabilized inflating cosmic strings. *Phys. Rev. D 91* (2015), 064010.

[133] Niedermann, F., and Schneider, R. Fine-tuning with brane-localized flux in 6D supergravity. *JHEP 02* (2016), 025.

[134] Niedermann, F., and Schneider, R. SLED phenomenology: curvature vs. volume. *JHEP 03* (2016), 130.

[135] Niedermann, F., Schneider, R., Hofmann, S., and Khoury, J. Universe as a cosmic string. *Phys. Rev. D 91* (2015), 024002.

[136] Nielsen, H. B., and Olesen, P. Vortex Line Models for Dual Strings. *Nucl. Phys. B 61* (1973), 45–61.

[137] Nilles, H.-P., Papazoglou, A., and Tasinato, G. Selftuning and its footprints. *Nucl. Phys. B 677* (2004), 405–429.

[138] Nishino, H., and Sezgin, E. The Complete $N = 2$, $d = 6$ Supergravity With Matter and Yang-Mills Couplings. *Nucl. Phys. B 278* (1986), 353–379.

[139] Nordtvedt, K. Lunar laser ranging: A Comprehensive probe of postNewtonian gravity. In *Villa Mondragone International School of Gravitation and Cosmology: From the Hubble Length to the Planck Length Monte Porzio Catone, Rome, Italy, September 6-10, 2002* (2003).

[140] Ortiz, M. E. A New look at supermassive cosmic strings. *Phys. Rev. D 43* (1991), 2521–2526.

[141] Padilla, A. A Short review of 'DGP specteroscopy'. *J. Phys. A40* (2007), 6827–6834.

[142] Peloso, M., Sorbo, L., and Tasinato, G. Standard 4-D gravity on a brane in six dimensional flux compactifications. *Phys. Rev. D 73* (2006), 104025.

[143] Perlmutter, S., et al. Supernova Cosmology Project. `http://supernova.lbl.gov/Union/`, July 2012.

[144] Podolsky, J., and Svarc, R. Interpreting spacetimes of any dimension using geodesic deviation. *Phys. Rev. D 85* (2012), 044057.

[145] Polchinski, J. Tasi lectures on D-branes. In *Fields, strings and duality. Proceedings, Summer School, Theoretical Advanced Study Institute in Elementary Particle Physics, TASI'96, Boulder, USA, June 2-28, 1996* (1996), pp. 293–356.

[146] Porrati, M. Fully covariant van Dam-Veltman-Zakharov discontinuity, and absence thereof. *Phys. Lett. B 534* (2002), 209–215.

[147] Press, W. H., Teukolsky, S. A., Vetterling, W. T., and Flannery, B. P. *Numerical Recipes in C: The Art of Scientific Computing*, 2 ed. Cambridge University Press, New York, NY, USA, 1992.

[148] Randall, L., and Sundrum, R. A Large mass hierarchy from a small extra dimension. *Phys. Rev. Lett. 83* (1999), 3370–3373.

[149] Randall, L., and Sundrum, R. An Alternative to compactification. *Phys. Rev. Lett. 83* (1999), 4690–4693.

[150] Randjbar-Daemi, S., Salam, A., Sezgin, E., and Strathdee, J. A. An Anomaly Free Model in Six-Dimensions. *Phys. Lett. B 151* (1985), 351–356.

[151] Randjbar-Daemi, S., Salam, A., and Strathdee, J. Spontaneous compactification in six-dimensional Einstein-Maxwell theory. *Nucl. Phys. B 214*, 3 (1983), 491 – 512.

[152] Rattazzi, R. Cargese lectures on extra-dimensions. In *Particle physics and cosmology: The interface. Proceedings, NATO Advanced Study Institute, School, Cargese, France, August 4-16, 2003* (2003), pp. 461–517.

[153] Rubakov, V., and Shaposhnikov, M. Do We Live Inside a Domain Wall? *Phys. Lett. B 125* (1983), 136–138.

[154] Rubakov, V., and Shaposhnikov, M. Extra Space-Time Dimensions: Towards a Solution to the Cosmological Constant Problem. *Phys. Lett. B 125* (1983), 139.

[155] Rubakov, V. A. Strong coupling in brane induced gravity in five-dimensions. *ArXiv High Energy Physics - Theory e-prints* (2003).

[156] Salam, A., and Sezgin, E. Chiral compactification on Minkowski $\times S^2$ of $N = 2$ Einstein-Maxwell supergravity in six dimensions. *Phys. Lett. B 147*, 1 (1984), 47 – 51.

[157] Scherk, J., and Schwarz, J. H. Spontaneous Breaking of Supersymmetry Through Dimensional Reduction. *Phys. Lett. B 82* (1979), 60.

[158] Stephani, H., Kramer, D., MacCallum, M., Hoenselaers, C., and Herlt, E. *Exact Solutions of Einstein's Field Equations*. Cambridge University Press, Cambridge, England, 2003.

[159] Stueckelberg, E. C. G. Die Wechselwirkungskräfte in der Elektrodynamik und in der Feldtheorie der Kernkräfte. Teil I. *Helv. Phys. Acta 11* (1938), 225–244.

[160] Szekeres, P. The Gravitational compass. *J. Math. Phys. 6* (1965), 1387–1391.

[161] 't Hooft, G. Naturalness, chiral symmetry, and spontaneous chiral symmetry breaking. *NATO Sci. Ser. B 59* (1980), 135.

[162] Taub, A. H. Empty Space-Times Admitting a Three Parameter Group of Motions. *Annals of Mathematics 53*, 3 (1951), 472–490.

[163] Thorne, K. S. Energy of Infinitely Long, Cylindrically Symmetric Systems in General Relativity. *Phys. Rev. 138* (Apr 1965), B251–B266.

[164] Vainshtein, A. I. To the problem of nonvanishing gravitation mass. *Phys. Lett. B 39* (1972), 393–394.

[165] van Dam, H., and Veltman, M. J. G. Massive and massless Yang-Mills and gravitational fields. *Nucl. Phys. B 22* (1970), 397–411.

[166] Vilenkin, A. Gravitational Field of Vacuum Domain Walls and Strings. *Phys. Rev. D 23* (1981), 852–857.

[167] Vinet, J., and Cline, J. M. Codimension-two branes in six-dimensional supergravity and the cosmological constant problem. *Phys. Rev. D 71* (2005), 064011.

[168] Weinberg, S. The Cosmological Constant Problem. *Rev.Mod.Phys. 61* (1989), 1–23.

[169] Weinberg, S. *The quantum theory of fields. Vol. 2: Modern applications*. Cambridge University Press, 2013.

[170] Will, C. M. The Confrontation between general relativity and experiment. *Living Rev. Rel. 9* (2006), 3.

[171] Witten, E. Instability of the Kaluza-Klein vacuum. *Nucl. Phys. B 195*, 3 (1982), 481 – 492.

[172] Zakharov, V. I. Linearized gravitation theory and the graviton mass. *JETP Lett. 12* (1970), 312. [Pisma Zh. Eksp. Teor. Fiz.12,447(1970)].

[173] Zel'dovich, Y. B. Cosmological Constant and Elementary Particles. *JETP Lett. 6* (1967), 316. [Pisma Zh. Eksp. Teor. Fiz.6,883(1967)].

[174] Zel'dovich, Ya. B., Krasinski, A., and Zeldovich, Ya. B. The Cosmological constant and the theory of elementary particles. *Sov. Phys. Usp. 11* (1968), 381–393. [Usp. Fiz. Nauk95,209(1968)].

Acknowledgments

I thank my supervisor Stefan Hofmann for being an outstanding mentor throughout the last years. Our countless discussions about physics were a constant source of inspiration and motivation, which made this thesis possible. I learned a lot from his ability to single out the meaningful theoretical questions and to pursue them without being hampered by any form of conventionalism. He also helped me to keep my spirits up whenever things turned out to be difficult—both on a research and personal level. I will miss our epic lunch break at the "Lo" during which many questions of large scale importance were addressed.

I also want to thank my second supervisor Gia Dvali for his strong support he dedicated to my research. His deep understanding of physics that he shared with us at many different occasions was an inspiring and valuable contribution to my work. Furthermore, I express my gratitude to Dorothee Schaile and Jochen Weller for taking part in my PhD committee.

A major part of this thesis originated from discussions with my collaborator Robert Schneider. Whenever we worked together on braneworlds, gravitational waves or any other topic—usually related to general relativity—we were able to finally arrive at a deeper understanding. That way, we went through the whole range of experiences research involves: We had difficult moments when yet another idea resolved into nothing, but also many joyful ones when something worked out. For this I am very grateful. I am also indebted to my collaborator and fellow student Felix Berkhahn for the great time we had in doing physics and for an exceptionally fruitful collaboration. I will preserve the memory to countless valuable moments of almost a decade of physics.

I am particularly grateful to Justin Khoury who supported my research during a very critical phase. He came up with many new ideas and valuable insights, which in turn propelled the cosmological analysis of the BIG model to a higher rank. A visit to his institute proved particularly fruitful in that context. I also want to thank Cliff Burgess for hosting me at the Perimeter Institute. The many discussion I had with him, Ross Diener and Matt Williams sharpened my understanding of compact braneworld models.

My gratitude also goes to my colleagues at the LMU, in particular Michael Kopp, Tehseen Rug, Cora Uhlemann, Sophia Müller, Ludwig Eglseer, Daniel Flassig, Nico Wintergerst, Marc Schneider, Parvin Moyassari, Cristiano Germani, Thomas Haugg and Florian Kühnel for many interesting and stimulating discussions. They made the LMU a great place to work at. I also want to thank Herta Wiesbeck-Yonis for her administational support. Furthermore, I acknowledge the financial support from TRR 33 "The Dark Universe" and the DFG cluster of excellence "Origin and Structure of the Universe".

Finally, my girlfriend Lena receives my most personal thanks. Her great support, her unlimited patience and her way of setting things into perspective were crucial to accomplish this work.